Sorption behaviour of heavy metals on a dithizone-impregnated polymer resin

by

ANDRé RONALD LEE SPIES

Thesis submitted in fulfilment of the requirements for the degree

Doctor of Philosophy: Chemistry

Faculty of Applied Sciences
(Bellville)

Cape Peninsula University of Technology

Supervisor: Dr F Wewers
Co-supervisor: Prof T N van der Walt

September 2020

DECLARATION

I, André Ronald Lee Spies, declare that the contents of this thesis represent my own unaided work, and that the thesis has not previously been submitted for academic examination towards any qualification. Furthermore, it represents my own opinions and not necessarily those of the Cape Peninsula University of Technology.

_____ _____

Signed **Date**

ABSTRACT

Amberchrom CG-300m, a styrene acrylic ester polymer resin, was studied for the first time as sorbent for metal ion sorption in a solid-phase extraction system. The polymer sorbent was modified via impregnation with dithizone, a chelating ligand, to improve its efficiency and selectivity. The loading capacity of the resin is 3.2 mg dithizone per gram of sorbent. The physico-chemical characterisation of the sorbent before and after impregnation was done by Scanning Electron Microscopy and Fourier Transform Infrared Spectroscopy. Surface morphology studies show a significant decrease in resin pore size after impregnation. The appearance of a broad band at around 1360 cm^{-1} in the FTIR spectrum of the impregnated resin signifies the introduction of the thiol functional group of dithizone into the resin backbone.

This study reports on the sorption behaviour of ten (10) heavy metal ions – Ag^{+}, Bi^{3+}, Cd^{2+}, Co^{2+}, Cu^{2+}, In^{3+}, Mn^{2+}, Ni^{2+}, Pb^{2+} and Zn^{2+} – onto the dithizone-impregnated resin. The sorption behaviour of the metal ions was studied in batch and column experiments. The sorption parameters investigated were initial metal ion concentration, pH, *V*/*m* ratio, time and temperature. Sorption generally increased with initial concentration and pH, but most metals hydrolysed at higher pH, even in the presence of the tartrate ion. Cu (pH < 5.5), Ag (pH < 3) and Bi (pH < 2) were sorbed quantitatively (> 95 %) in moderate to strongly acidic medium. Mn(II) was sparsely sorbed in the pH range 4.57 – 8.54. Most metals were quantitatively sorbed at low initial concentration. However, Ag and Bi were quantitatively sorbed at relatively high initial concentration of 4.104 mg/L and 3.30 mg/L, respectively. Sorption capacity of the metal ions studied decreased in the order: $Ag^{+} > Bi^{3+} > Pb^{2+} > Co^{2+} > Cu^{2+} > Zn^{2+} > Ni^{2+} > Cd^{2+} > Mn^{2+}$.

Ag^{+} and Bi^{3+} were completely sorbed in the temperature range 283 K – 298 K. Thermodynamics of Mn sorption was rendered futile as it remained unsorbed in the same temperature range. Positive values of ΔH^{0} suggest sorption of Cd, Co, Cu, Pb and Ni was endothermic, whereas Zn was the only metal whose sorption was exothermic ($\Delta H^{0} < 0$). ΔH values were in the range 25 – 60 kJ suggesting sorption of heavy metal ions onto the impregnated resin could be attributed to a physico-chemical sorption process, rather than pure physi- or chemisorption. Apart from Ni, sorption was favourable over the entire temperature range ($\Delta G^{0} < 0$); sorption of Zn was favourable at $T > 288$ K only. The positive ΔS^{0} values associated with sorption of all metals (except Zn) meant sorption was accompanied by increased disorder at the solid/liquid interface.

The efficiency and reliability of the dynamic method viz-à-viz the static method was undeniable, and quantitatively proven by kinetic studies of Pb. Sorption kinetics during all column experiments was sufficiently fast so that steady-state approximation was established within the first three min.

Langmuir, Freundlich, Temkin and Dubinin-Rudeshkivich sorption isotherms were investigated at 294 K. Except for Cu, the Langmuir isotherm provided the best fit to sorption data. Temkin, Langmuir and Freundlich isotherms modelled sorption of Cu best ($r^2 > 0.9990$). The Freundlich isotherm proved a credible model for sorption of all metals except Cd.

Sorption of all metal ions followed pseudo-second order reaction kinetics. Sorption of Cu onto dry, impregnated resin followed pseudo-first order kinetics though. Diffusion kinetics was successfully modelled by Weber-Morris and Homogeneous Particle Diffusion models. Weber-Morris plots indicate sorption of all metal ions were controlled by both pore and film diffusion mechanisms. Cu(II) and Co(II) diffusion were seemingly independent of resin pore size.

The dithizone-impregnated resin was successfully applied to the qualitative separation of Cd^{2+}-Sn^{4+}, Mn^{2+}-Co^{2+}-Ni^{2+} and Bi^{3+}-Pb^{2+} ion mixtures. Separation was achieved quantitatively within 5 min.

ACKNOWLEDGEMENTS

I wish to thank:

- The Source of Life, through Whom all things were created.
- My parents for their sacrifices, unconditional love, and unwavering belief in me.
- My supervisor, Dr Francois Wewers, for your constructive criticism, attention to detail and thorough “interrogation” of scientific arguments.
- My co-supervisor, Professor Nico van der Walt, for your guidance and introducing me to the fascinating world of Ion Exchange. Thank you for allowing me the freedom to explore and express myself in my research activities.
- The giants on whose shoulders I stood (and will forever stand), from where I caught a glimpse of the vast land of scientific knowledge.
- Family, colleagues and friends for support and encouragement.
- Ayesha, for your support and doing the proofreading of the final manuscript.

The financial assistance of the National Research Foundation under the grant no. 110866 is acknowledged and appreciated. Opinions expressed in this thesis and the conclusions arrived at, are those of the author, and are not necessarily to be attributed to the National Research Foundation.

DEDICATION

To my late mother (Mamma)

ABBREVIATIONS AND ACRONYMS

ACG300m-H_2Dz:	Amberchrom® CG-300m-dithizone
BEC:	Background equivalent concentration
CFSE:	Crystal field splitting energy
DFT:	Density functional theory
DHET	Department of Higher Education and Training
EIR:	Extractant impregnated resin
EXFAS:	Extended X-ray absorption fine structure
FEG-SEM:	Field emission gun scanning electron microscope
FFPS:	Field flow preconcentration system
FTIR:	Fourier-transform infrared
HPCIC:	High performance chelation ion chromatography
HPDM:	Homogeneous particle diffusion model
ICP-OES:	Inductively coupled plasma optical emission spectroscopy
IEC:	Ion-exchange chromatography
LET:	Linear energy transfer
LOD:	Limit of detection
LOQ:	Limit of quantification
NRF	National Research Foundation
PF:	Preconcentration factor
PFO:	Pseudo-first order
PS-DVB:	Polystyrene-divinylbenzene
PSO:	Pseudo-second order
RP-HPLC:	Reverse phase high performance liquid chromatography
Rpm:	Revolutions per minute
RSD:	Relative standard deviation
S-DVB:	Styrene-divinylbenzene
SEM:	Scanning electron microscope
SIR:	Solvent impregnated resin
SPE:	Solid phase extraction
SPM:	Shell progressive model
SX:	Solvent extraction
TGA:	Thermogravimetric analysis
UV-Vis:	Ultraviolet-visible

TABLE OF CONTENTS

CHAPTER 5

Results and discussion

LIST of FIGURES:

LIST of TABLES

APPENDICES

CHAPTER 1

Introduction

1.1 Background to the study

The performance of any separation system depends mainly on two factors, namely separation *efficiency* and separation *selectivity*. *Efficiency* is related to the chemical and physical properties[1] of the separation media (resin particle size, sorption capacity of the resin, porosity of the resin, sorption kinetics, nature and chemistry of functional groups, oxidation state of analyte species and sorbent dosage) as well as the separation conditions (pH, flow rate, column length, sample volume, eluent choice and temperature). *Selectivity* is predominantly associated with the sorption mechanism and depends on the interactions between the sorbate and sorbent[2].

It is easier to manipulate separation efficiency than separation selectivity. To achieve maximum separation selectivity, *all* possible interactions between sorbent and sorbate need to be considered. These interactions include weak interactions (such as Van der Waals forces, induction, and dispersion) as well as higher energy interactions (such as hydrogen bonding, π-π interactions and coordinate bonding). Chelation, one type of sorbate-sorbent interaction that provides a significantly higher degree of separation selectivity, involves coordinate bonding. It has been widely employed in traditional technologies such as solvent extraction to concentrate, quantify and separate metal ions (Netserenko *et al.*, 2011). Typically, during solvent extraction, an extractant that forms stable chelates with the metal ions is added to the organic phase. Metals are subsequently separated based on the stability constants of their respective complexes. 1,5-diphenylthiocarbazone (dithizone) is an example of a chelating agent that forms stable complexes with about twenty heavy metal ions.

The latest separation technologies include membrane separation, electrodialysis, cloud point extraction and solid-phase extraction (Tiwari *et al.*, 2016; Saha *et al.*, 2004). Of these techniques, solid-phase extraction (SPE) is ostensibly most efficient as it combines the characteristics of ion-exchange with solvent extraction. SPE gained increasing popularity because of its fast, simple, and direct application to micro-litre volumes without any sample loss, higher preconcentration factor, rapid phase separation, time, and cost efficiency.

[1] Hereafter the term “physicochemical” will be used to refer to physical and chemical properties jointly.
[2] The term “sorbent” will hereafter be used interchangeably with “substrate”, “support” or “solid phase”.

In SPE systems, the solid phase is normally activated, or modified, to enhance its selectivity. The most efficient SPE systems have been demonstrated using sorbents with chelating groups immobilised at the external surface and inside the pores of micro-particles of organic polymers. These chelating resins are more selective due to multiple interactions (ion exchange, chelation, and physical adsorption) between the sorbent and sorbate.

Over the years, many solid phase supports have been recommended as sorbents. Among these are silica gel, pore glass, cellulose powder, polyurethane foam, naphthalene, activated carbon and hydrophobic macroporous resins. Styrene divinylbenzene (S-DVB) copolymer has proven an outstanding solid phase because of its high surface area, uniform pore size, good sorbent properties and durability. Amberlite® XAD® resins (XAD-2, XAD-4, XAD-7, XAD-16, XAD-1180 and XAD-2000) are examples of S-DVBs that were proven useful as solid phase in SPE systems. The Amberchrom® line of styrenic polymeric resins (Amberchrom® CG-71, CG-161, CG-300 and CG-1000) are smaller particle versions of Amberlite® XAD® sorbent resins, designed for higher performance purifications that are not possible with the larger XAD resins. Amberchrom® resins are chemically, mechanically and physically stable, resistant to microbial attack, and dimensionally stable to changes in pH and ionic strength (Sigma-Aldrich Co., 1997).

As stated earlier, the solid phase in SPE systems is modified to enhance its selectivity. There are primarily two methodologies by which the solid phase support can be modified: the extractant can be attached to the support through (i) chemical bonding or (ii) physical sorption (*impregnation*). Covalent linking of complexing molecules to a polymeric material is difficult, expensive and requires extensive research on the chemistry involved. Impregnation, on the other hand, is convenient, effective, and economical. Currently, considerable research is being conducted into the synthesis of new and more selective chelating extractants for their incorporation into new polymer substrates, each effectively producing a new chelating resin with unique selectivity. Published research can be classified into any of the following types of studies:

i) introduction of new chelating groups into a commercially available organo-polymer substrate and subsequent characterisation of selectivity;
ii) covalent linking or impregnation of a single type of chelating group onto a variety of organo-polymer substrates; and
iii) characterisation of one type of chelating group bonded to the same matrix via different synthetic routes (not applicable to SIRs).

Chelating resins have been studied for their use in various applications such as trace metal analysis, chemical catalysis, hydrometallurgy, nuclear waste, and wastewater treatment.

They have also been productive in radiochemistry to isolate and purify daughter isotopes formed as by-products during particle bombardment of the parent analogues. The latter application is critical in nuclear medicine where there is an ever-increasing demand for radionuclides for both diagnostic and therapeutic purposes in cancer treatment. In this regard, the alpha-emitting radionuclide ^{212}Bi and its parent ^{212}Pb are ideal candidates due to their relatively short half-lives (Despotopulos, 2018). Radiopharmaceuticals labelled with ^{117m}Sn have promising application in the palliative treatment of painful metastases in bone cancers. Maslov *et al.* (2011) produced no-carrier-added (nca) Sn-117m via the ^{116}Cd(α,3n)^{117m}Sn synthesis route. ^{67}Cu ($t_{1/2} = 61.83\,\mathrm{h}$) is another therapeutically important nuclide; it has previously been separated from zinc target material (Dolley *et al*., 2006; Dolley & van der Walt, 2014).

1.2 Problem statement

1,5-diphenylthiocarbazone ($C_{13}H_{12}N_4S$) is commonly known as “dithizone”. It has two potentially dissociable hydrogen atoms, and its formula is conveniently abbreviated as H_2Dz. The suitability of dithizone as chelating agent and its efficiency in the preconcentration and separation of various metals have been widely investigated. According to Chwastowska *et al.* (2008), chelating reagents with thiol groups (such as dithizone) are used frequently in solid phase extraction for separation of heavy metals because they form stable complexes with these metals through coordination via the *S,N* donor atoms. Research on the use of dithizone in SPE systems is limited to *extraction* and/or *separation* of a few heavy metals. Very little has been reported on the sorption *mechanisms* of these heavy metals onto dithizone modified sorbents. A survey of literature also showed that studies on polymeric resins modified with dithizone are less prolific than those reporting on the use of bio-sorbents and other less conventional substrates. Studies on the Amberchrom® CG-300m-dithizone (ACG300m-H_2Dz) extraction system have barely, if at all, been documented.

1.3 Study objectives

As stated in Section 1.1, the selectivity of any separation system is largely dependent on the sorption *mechanism*. This study focused on the sorption mechanisms of ten (10) heavy metal ions – Ag^{+}, Bi^{3+}, Cd^{2+}, Co^{2+}, Cu^{2+}, In^{3+}, Mn^{2+}, Ni^{2+}, Pb^{2+} and Zn^{2+} – onto the ACG300m-H_2Dz SPE system. The main objectives of the research were as follows:

- optimise the parameters for impregnation of Amberchrom® CG-300m with dithizone;
- characterise, using FTIR spectroscopy and SEM imaging, the sorbent before and after impregnation;

- establish optimal parameters (pH, initial metal ion concentration, volume-to-mass ratio, time, and temperature); maximise sorption capacity; evaluate the mathematical model (Langmuir, Freundlich, Temkin or Dubinin-Radushkevich isotherm) that best fits sorption equilibrium data; and determine the sorption capacity of the sorbent for each metal ion under investigation;
- assess whether sorption follows pseudo-first order or pseudo-second order kinetics; ascertain if sorption is controlled by pore or film diffusion by applying Weber-Morris and Homogeneous Particle Diffusion (HPD) models to sorption data; and establish whether sorption occurs via chemical or physical processes, or a combination of both;
- apply the Amberchrom® CG-300m-H_2Dz SPE system to the qualitative separation of selected binary/ternary cation mixtures (Cd^{2+}-Sn^{4+}, Bi^{3+}-Pb^{2+} and Co^{2+}-Ni^{2+}-Mn^{2+}), using the column method.

1.4 Methodology

The same method employed by Dolley and Van der Walt (2014) to impregnate Amberlite® XAD-8 polymer resin with dithizone was used to impregnate Amberchrom® CG-300m. According to this method, dithizone is dissolved in an aqueous solution of NaOH and agitated in slurry form with the resin. When equilibrium is reached, the dithizonate anions that have penetrated the resin pores are titrated back to their neutral (dithizone) state by slow addition of concentrated HCl. This method is preferred over other impregnation methods because it is simple, fast and does not employ toxic organic solvents that need to be disposed of.

Optimal conditions for dithizone impregnation of Amberchrom® CG-300m were determined by investigating experimental parameters akin to those in similar studies. The loading capacity of the resin was determined by stripping the trapped dithizone from known amounts of impregnated resin with chloroform, and measuring the absorbance of dithizone in the eluate at λ = 605 nm (Jenway 7305 spectrophotometer; 10 mm quartz cell). A calibration curve was constructed to determine the dithizone concentration in the eluate.

Characterisation of the resin before and after impregnation was done using Fourier-Transform Infrared (FTIR) spectroscopy and Scanning Electron Microscope (SEM) imaging.

The sorption and kinetic behaviour of ten heavy metals onto ACG300m-H_2Dz were investigated by the batch and column method. Sorption data was applied to various isotherm and kinetic models to determine which model best fits the experimental data.

Langmuir, *Freundlich*, *Temkin, Dubinin-Radushkevich*, *Weber-Morris, HPDM, SPM, Lagergren pseudo-first order* and *Ho & McKay pseudo-second order* are typical mathematical models that were applied to experimental data to gain insight into the sorption mechanisms of the metal ions. The temperature dependence of sorption was described by common thermodynamic parameters such as $\Delta G°$, $\Delta H°$ and $\Delta S°$. An optimised extraction system was applied under dynamic conditions (column method) to separate a selection of binary (Bi^{3+}-Pb^{2+}; Cd^{2+}-Sn^{4+}) and ternary (Co^{2+}-Mn^{2+}-Ni^{2+}) synthetic metal ion mixtures. In all experiments, Inductively Coupled Plasma Optical Emission Spectroscopy (ICP-OES) was used to quantify metal ion content.

Although the research undertaken was largely quantitative in nature, its primary focus was not merely collecting and reporting data. Instead, the interpretation of data collected is considered critical to a deeper understanding of the scientific principles that underpin the sorption of heavy metals onto a dithizone-impregnated substrate.

1.5 Delimitations

Several mathematical models can be used to predict the mechanisms of various sorption systems. In a review of the applications of sorption isotherms, Ayawei *et al.* (2017) discussed at least 27 of these models. The models chosen in this project to describe sorption equilibrium, diffusion and reaction kinetics were those commonly used in similar studies.

Ten heavy metal ions were selected for investigation of their sorption behaviour onto ACG300m-H_2Dz. Heavy metals were selected based on proximity in the periodic table, which is usually associated with similar chemical properties that make chemical separation difficult.

Investigating both efficiency and selectivity of a newly developed separation system would be quite ambitious; this study investigated and report on the *selectivity* of the ACG300m-H_2Dz SPE system only.

A study on any SPE system would not be complete if its application to analyte separation is not validated. Therefore, the separation of a selection of metal ions was investigated. However, this study (separation) was of a qualitative nature; it was not the aim to investigate and maximise parameters that would ensure the most efficient separation.

CHAPTER 2

Solid phase extraction systems

This chapter deals mainly with solid phase extraction (SPE) as opposed to solvent extraction (SX). Distinguishing features of both procedures are highlighted, and a case is argued for solid phase extraction as the preferred method for the preconcentration, determination and separation of heavy metals. Modification of a solid substrate is a salient feature of SPE systems. Focus of this chapter is on impregnation as type of modification.

2.1 Introduction

Ongoing research into the recovery, preconcentration and separation of trace metals aims to substitute traditional separation techniques with modern technologies. Among traditional methods are fractional crystallisation, co-precipitation, solvent extraction, and ion-exchange. Solvent extraction (SX) has been widely applied in hydrometallurgical and wastewater treatment processes (Juang & Su, 1992). Solvent extraction (also called liquid-liquid extraction) involves the vigorous shaking of two immiscible solvents, normally water and an organic solvent. Either solvent contains the metal ion to be extracted. The metal ion is extracted from the aqueous phase into the organic phase, which ideally contains a suitable, complexing molecule or extractant to create a neutral hydrophobic complex. The metal ion distributes itself between the two solvents based on its relative solubility in both solvents and the stability of the formed complex. Solvent extraction, however, suffers from the following drawbacks:

- labour intensiveness;
- large scale use of organic solvents and associated problems related to waste disposal;
- vigorous mixing of the phases followed by gravity settling of the mixed phases;
- third phase formation; and
- significant environmental impact from the possible loss of extractant during extraction.

SPE has emerged as alternative technique to solvent extraction as it overcomes these drawbacks. It is based on the modification of a solid support with an extractant that has selectivity towards certain metals. Since the extractants are normally in liquid form, the system functions essentially as a solid-supported solvent-extraction system. Metal ions are typically transferred from the aqueous phase to active sites of the modified solid phase (Dave *et al.*, 2010).

SPE offers the following advantages over the SX technique:

- simplicity of equipment and operation;
- high selectivity, recovery, and enrichment factor;
- short analysis time;
- low consumption of harmful (chlorinated) organic solvents; and
- repeated use of the polymeric sorbent for numerous cycles without significant loss of its metal extraction capacity.

The use of ligands to modify polymer resins, combines the selectivity of a ligand with the ease of separation, porosity, large surface area, stability, and durability of a polymer resin. Macroporous organic polymers are ideal supports because of their high surface area, good mechanical stability, and flow characteristics (Cortina *et al*., 1997). SPE therefore combines the high selectivity of extractants with the efficiency and operational simplicity of solid ion-exchange technology. The impregnated extractant can exhibit strong affinity for the polymeric matrix, yet it behaves as if in the liquid state (Warshawsky, 1981; Cortina & Miralles, 1997).

Two methodologies are adopted for preparation of the solid phase, namely (i) physical impregnation of a suitable, selective ligand onto the surface and inside the pores of the solid support and (ii) chemical immobilisation (via covalent binding) of a reagent to the solid support structure. A polymeric substrate modified via chemical immobilisation has a three-dimensional distribution of ligands within the polymer particles. This morphology limits their application in column chromatography primarily due to low diffusion rates of ions within the stationary phase. SIRs allow the use of efficient complexing ligands whose immobilisation through chemical bonding would otherwise be difficult or impossible. For this reason, interest in the development of Solvent Impregnated Resins (SIRs) has intensified over the last 40 years.

2.2 Solvent-impregnated resins

Impregnation of polymeric resins gives rise to the formation of *Solvent Impregnated Resins* (SIRs) or *Extractant Impregnated Resins* (EIRs). Warshawsky (1971) and Grinstead (1971) pioneered the concept, synthesis, and applications of solvent impregnated resins. SIRs are tailor made for specific applications and have high selectivity efficiency as it combines characteristics of ion-exchange with liquid-liquid extraction. SIRs can therefore be considered as a particular case of liquid-liquid extraction (Strikovsky *et al.*, 1996). They are particulate sorbents that have higher sorption capacity than classical sorbents because the whole pore volume is utilised rather than the pore surface (Kabay *et al*., 2010).

Ideally, an SIR should exhibit the following characteristics:

- The extractant must be a liquid or retained in the liquid state (by the addition of a diluent).
- The extractant should have a strong affinity towards the matrix.
- Both the extractant and diluent should have minimal solubility in water or in the aqueous phase used.
- The polymeric support should be fully expanded during the impregnation process and remain so.

Early research on SIRs was confined to identifying support-solvent-extractant combinations.

Of the many extractants commercially available, organophosphorous compounds are by far the most prolific extractants used in SIRs. Juang & Chen (1997) described *organophosphorous compounds* as extractants of choice due to their chemical stability, extremely low aqueous solubility and high distribution ratios and selectivity of metals. A wide range of commercially available metal-specific liquid extractants have previously been used to impregnate porous, polymeric supports for the (i) chromatographic separation of toxic elements, (ii) extraction of rare and valuable metals, (iii) radio-analytical separations; and (iv) purification of wet process phosphoric acid. These applications are documented extensively in published literature and are discussed later.

Over the years, many supports have been suggested as sorbents – among these are silica gel, pore glass, cellulose powder, polyurethane foam, naphthalene, activated carbon and hydrophobic macroporous resins. The latter are ideal supports as they have high surface area, good mechanical stability, good flow characteristics and low solvent swelling during the impregnation process. The Amberlite XAD resins (XAD-2, XAD-4, XAD-7, XAD-16, XAD-1180 and XAD-2000) fulfil all these requirements (Saha *et al*., 2004) and have therefore been employed extensively as supports for SIRs. Amberchrom® resins (CG-71, CG-161, CG-300 and CG-1000) are smaller particle versions of Amberlite® XAD® sorbent resins, designed for higher performance purifications that are not possible with the larger XAD resins. For example, Amberchrom CG-161 was shown to provide greater resolution of a dye mixture than Amberlite XAD-16. Amberchrom® resins are chemically, mechanically and physically stable, resistant to microbial attack and dimensionally stable to changes in pH and ionic strength (Sigma-Aldrich Co., 1997).

The following sections deal with impregnation as the preferred synthesis method of SIRs. Synthesis methods and parameters that affect impregnation are discussed, along with the advantages and disadvantages of SIRs.

2.3 Impregnation

Impregnation involves immobilisation of a selective, complexing ligand (normally in liquid form) on a solid support that would otherwise be difficult or impossible to achieve via chemical functionalisation (covalent linking) (Warshawsky, 1971). The ligand, when impregnated into the support, maintains its ability to form complexes selectively with metal ions. The selectivity of the impregnated substrate is based upon the conditional stability constants of the formed complexes. The efficiency of separation of metal ions adsorbed onto the solid substrate depends on the rate at which metal ion complexes are formed and dissociated. This in turn depends on several factors, namely the:

- nature of the functional group associated with the extractant;
- concentration and nature of competing ligands within the bulk solution;
- pH of the sorbate medium;
- form of the metal ions in solution;
- conformation and surface structure of the adsorbed ligand layer(s); and
- stability of the ligand layer(s).

2.3.1 Impregnation methods

Cortina & Warshawsky (1997) postulated that the impregnation of a solvent onto the hydrophobic internal surface of a macroporous, neutral polymer substrate proceeded via a combination of two mechanisms: (i) attraction between alkyl chains and/or aromatic rings of ligands in the solvent structure and those of the resin backbone; and (ii) the subsequent physical entrapment of the ligands within the pores of the resin beads. To prepare the 'ideal' SIR, the impregnation method should meet the following requirements:

- the impregnation method should not destroy the properties of the extractant or the polymer;
- the polymer support should have good mechanical stability; and
- the supporting structure should be chemically inert so that the extractant does not react with it.

Methods used to functionalise solid supports via impregnation are simple – these are the: (i) dry method; (ii) wet method; (iii) modifier addition method; and (iv) dynamic column method. All these methods have the same mechanism of impregnation (Jeřábek *et al*., 1996) – during impregnation, the extractant fills the pore space from the smallest pore to pores of larger size. The dry method is the most widely used impregnation method. In the dry method, a solution containing the extractant is contacted with the polymer; the excess solvent is subsequently removed by slow evaporation under vacuum, leaving the impregnated sorbent behind.

[In the case of a hydrophobic polymer support, it is necessary to add to the diluent a small quantity (5 – 15 %) of an appropriate organic modifier to 'wet' the stationary phase surface. Care should be taken, however, that the impregnated extractant does not leach into the organic modifier]. The impregnated resin is subsequently washed several times with various aqueous solutions of varying pH to remove unstable portions of adsorbed ligand and eliminate ligand bleed.

2.3.2 Impregnation parameters

Jones *et al.* (1993) studied impregnation procedures involving Xylenol Orange (XO) and neutral PS-DVB resins and achieved stable ligand loadings of ±53 mg per gram of resin. They could, however, not reproduce these results in subsequent experiments, obtaining loadings of between 17 and 28 mg only. This prompted further investigations into factors influencing impregnation, focusing on *pH* and *ligand concentration* (Jones *et al*., 1996). In their earlier work, XO was impregnated at pH values ranging between 6.0 and 8.5 and ligand concentration of 0.2 %. Adjusting the pH to 5 and ligand concentration to 0.5 % increased the ligand loading to 39 mg. While studying the extraction of Cr(III) using Cyanex 272, Mendoza *et al.* (2000) validated the work of Jones and his co-workers by showing that the efficiency of the sorption process increased with an increase in extractant concentration.

Rovira *et al.* (1998) determined that the impregnation of a resin with an extractant was independent of the resin-particle size. Previously, Jeřábek *et al.* (1996) investigated the relationship between the impregnation process and polymer support morphology. They used two macroporous resins, Amberlite XAD-2 (pore diameter = 90 Å) and Amberlite XAD-4 (pore diameter = 50 Å) and two microporous sorbents prepared by hyper-crosslinking of swollen chloro-methylated styrene-divinylbenzene copolymers. Their results showed that sorption of the extractant di-(2-ethylhexyl) thiophosphoric acid (DEHTPA) onto the macroporous resins started only at a certain critical concentration of DEHTPA in solution. This critical concentration was preceded by an induction interval where no observable sorption occurred. The induction interval was absent in the sorption of the microporous polymers. They concluded that a relationship existed between the diameter of pores in the polymer beads and the critical concentration of DEHTPA – when impregnating a resin, the extractant sequentially fills the pores from the smallest to the largest (up to ±10 nm), after which surface sorption becomes the dominant force.

Table 2.1: Specific area of polymer carriers and the SIR obtained during the sorption isotherm determinations of DEHTPA from methanol (adapted from Jeřábek *et al*., 1996)

	Surface area (m^2/g)		Corresponding DEHTPA loading (g/g)
	Starting carrier	SIR	
Amberlite XAD-2	340	31	0.23
Amberlite XAD-4	804	5	0.64

The substantial changes in surface area (Table 2.1) due to DEHTPA loading confirmed the hypothesis that sorption proceeded via a pore-filling mechanism. Similar investigations were undertaken by Paull & Jones (1996) who used PS-DVB substrates of varying particle and pore size to investigate the effect of resin structure (notably surface area and porosity) on the degree of xylenol orange (XO) loading. The results showed a significant increase in ligand loading with resins of smaller pore size (10-30 nm) as compared to resins of larger pore size (up to 400 nm). They attributed their findings to the larger surface area of resins with smaller pore size, arguing that the smaller spaces contributed to the increased loading through the possible physical trapping of the ligand molecules inside the pores. The results of this study are shown in Table 2.2.

Table 2.2: Loadings of xylenol orange on neutral PS-DVB resins of varying particle and pore size (Paull & Jones, 1996)

Pore size (nm)	Surface Area (m^2/g)	Particle size (μm)	Amount impregnated (mg ligand/g resin)
Polymer laboratories PLRP-S resin			
400	139	10	21
100	267	10	21
30	384	10	31
10	414	10	31
Dionex macroporous neutral resin			
30	60	7.0	22
12	470	8.8	25

Their studies also revealed that impregnated Dionex neutral resins had lower ligand loadings than PLRP-S, although the trend of increased loading with decreasing pore size was still evident. These results corroborated the findings of Jeřábek *et al*. (1996).

Shaw *et al.* (2003) developed a new approach to improve the ligand impregnation of polymer resins. They impregnated a neutral PS-DVB resin with the chelating dye aurin tricarboxylic acid (ATA) in batch experiments, using ultra-sonic agitation of the loose resin in a buffered solution of the ligand. The study determined that ultra-sonication during batch impregnation experiments led to an almost fourfold increase in the number of sites available for chelation (13.2 % versus 3.9 %). In addition, they varied the ligand concentration to force more dye particles onto the stationary phase surface (0.1 – 0.4 %) and increased the methanol content from 0 % to 30 %. Finally, the pH was increased from three to seven to optimise the dye-solubility in solution. The optimal loading parameters established were as follows: 2 % ATA solution, 10 % methanol and pH = 5.

In a similar study (Paull & Jones, 1996) the effective capacity of resins impregnated with various metallochromic chelating ligands (dyes) was evaluated by sorption of Zn^{2+} from an aqueous buffer solution (pH = 8) onto the hydrophobic, neutral PS-DVB Dionex resin. Results of this study are presented in Table 2.3. A large percentage of the impregnated dyes were unable to complex with the Zn^{2+} ions, suggesting that the loading capacity was dependent on the type and structure of the impregnated dye.

Table 2.3: Metallochromic ligand total loading and effective capacity on hydrophobic neutral 8.8 μm PS-DVB resin (Dionex) (Paull & Jones, 1996)

Metallochromic Ligand	Amount impregnated (μmol ligand·g^{-1}resin)	Capacity (μmol Zn^{2+}· g^{-1} impregnated resin)	Effective capacity (%)
XO	33	10	30
SXO	29	-	-
MTB	48	13	27
PP	157	22	14
GCR	99	7	7
CAS	35	3	9
CAL	28	5	18
PAR	396	19	5
OII	111	2	2
SPPH	36	1	3

Nesterenko *et al.* (2011) cite a study that compared the overall ligand loading and effective capacity (mmol Cu^{2+} per gram of resin) of various polystyrene-based resins impregnated with 4-(2-pyridylazo)-resorcinol (PAR). The resins used were Amberlite IRA 904, a strong basic anion exchange PS-DVB resin with exchange capacity of 0.7 $meq \cdot g^{-1}$; Amberlite XAD-2, a neutral macroporous PS-DVB resin; Purolite MN100, a weak base anion exchange hyper-crosslinked PS-DVB resin; and Purolite MN200, a neutral hyper cross-linked polystyrene resin. The study reported lowest total loadings for the anion exchangers, with Amberlite IRA 904 showing a 4.4 % effective capacity. Amberlite XAD-2 exhibited the highest ligand loading, but an effective capacity of only 7.9 %. Purolite MN200 demonstrated a high overall ligand loading (0.2 mmol PAR per gram of resin) and an almost quantitative effective capacity of 0.147 mmol Cu^{2+} per gram of resin (95.3 %). The authors concluded that the high loading and effective capacity shown for the impregnated MN200 resin could be attributed to its well-developed microporous structure and large surface area (1000 – 500 $m^2 \cdot g^{-1}$).

In studies elsewhere, Saha *et al.* (2004) investigated the removal of Cr(IV) from aqueous solution using Amberlite XAD-7 impregnated with Aliquat 336 (tricaprylmethylammonium chloride), establishing a linear relationship between the impregnation ratio (grams of Aliquat 336 per gram Amberlite XAD-7) and the change in weight of the resin. There was no saturation plateau up to a ratio of 2 g Aliquat 336/g polymer. They did not, however, investigate impregnation ratios higher than this, citing possible leaching of Aliquat 336 from the SIR at higher ratios. Kabay *et al.* (2003) reported similar observations when they impregnated Diaion HP-20 and HP-2 MG with Aliquat 336. It will be shown later (Chapter 5) that the ACG300m-H_2Dz impregnation ratio also reached no plateau but approached a limit after which leaching of dithizone occurred. Nakamura *et al.* (2009) loaded 0.90 mmol bis(4-cyclohexylcyclohexyl) phosphoric acid (D4DCHPA) per gram Diaion HP2-MG; Shahida *et al.* (2013) achieved optimal loading of 290 mg nalidixic acid (HNA) per gram XAD-4, while Ansari *et al.* (2006) loaded 47 % (w/w) *N*,*N*,*N*',*N*'-tetraoctyl diglycolamide (TODGA) onto Chromosorb-W.

2.3.3 Advantages of solvent-impregnated resins

- SIRs merge the inherent advantages of liquid/liquid extraction and ion-exchange separation with the properties of a conventional polymeric sorbent material. These include:
  (i) specificity and selectivity of readily available extractants; (ii) straightforward mechanism of interaction of metal ions with liquid/liquid extractants; (iii) lack of third phase formation; (iv) possibility of treating unclarified solutions; and (v) adopting a continuous liquid-solid separation process (Kabay *et al.*, 2010).

- The synthesis of SIRs is simple and versatile – various combinations of liquid extractants and polymeric supports can be employed that are tailored for particular ions in solution.
- SIRs have higher sorption capacity – the entire pore volume is utilised as opposed to the pore surface only, as is the case with chemical modification. According to Warshawsky (1981), the interior structure of impregnated supports bears close resemblance to the interior structure of the untreated support. With supports of large diameters (1400 – 2000 Å), the modifying reagents seem to adhere closely to the network structure, leaving free most of the pore volume. In supports with small pore diameters (50 – 90 Å), the reagents partially block the pore (e.g., 2 M DE-HPA on XAD-2 or 1 M hydroxyoxime on XAD-2).
- The stoichiometry of the impregnation process is straightforward – complexing agents can be introduced onto the sorbent in the precise amount, leaving no unreacted remnants of functional groups.
- SIRs are flexible with respect to applications. In the case of chemically functionalised sorbents, specific functional groups must be attached to the support for each specific application.
- SIRs are easy to regenerate.
- The impregnated layer(s) can remain stable in aqueous solutions over a wide range of ionic strength and pH.

2.3.4 Disadvantages of solvent-impregnated resins

- SIRs are inherently unstable due to the gradual leaching of the extractant to the aqueous phase. Even if extractants are highly hydrophobic, they are not completely insoluble in water, causing gradual leakage. This gradual leaking invariably causes a decrease in the amount of extractant immobilised within the SIR, thereby diminishing its sorption capacity towards targeted ions in aqueous solutions. This problem can be solved by (i) removing extractant that is loosely attached to the support and (ii) post-impregnation coating of the SIR beads through the formation of a protective film or membrane on the surface.
- The stabilities and preconcentration abilities may be inferior to those supports to which the reagent has been covalently coupled (Kantipuly *et al.,* 1990).

2.4 Theory of solid phase extraction

The sorption equilibrium in SPE is analogous to that between an aqueous and organic solution and essentially involves four equilibria (Skoog *et al.*, 2004). The first is the distribution of the extractant, HX, between the solid phase and aqueous phase. The second is acid dissociation of HX to give H^+ and X^- ions. The third equilibrium is the complex-formation reaction forming MX_2, and the last is distribution of the chelate between the two phases (Fig. 2.1).

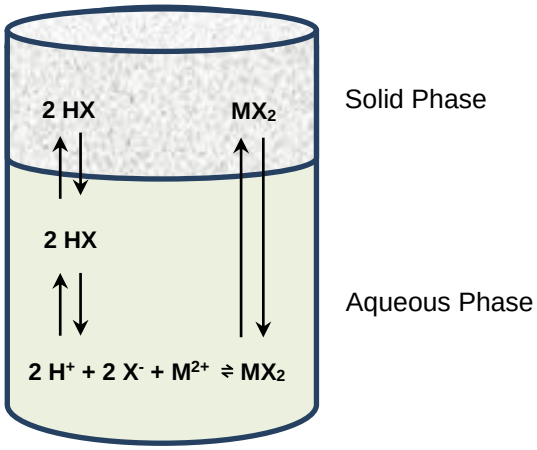

Fig. 2.1: Equilibria in the extraction of an aqueous cation M^{2+} onto a sorbent containing extractant HX (adapted from Skoog *et al.* (2004)

The overall equilibrium is a combination of the equilibria described above:

$$2\ HX_{org} + M^{2+}{}_{aq} \rightleftharpoons MX_{2org} + 2\ H^{+}{}_{aq}$$

The equilibrium constant for this equilibrium is given by the expression:

$$K' = \frac{[MX_2]_{org}[H^+]^2_{aq}}{[HX]^2_{org}[M^{2+}]_{aq}} \qquad (2.1)$$

Assuming $[HX]_{org} >>> [M^{2+}]_{aq}$ = constant:

$$K'[HX]^2_{org} = K = \frac{[MX_2]_{org}[H^+]^2_{aq}}{[M^{2+}]_{aq}} \qquad (2.2)$$

Thus:

$$\frac{[MX_2]_{org}}{[M^{2+}]_{aq}} = \frac{K}{[H^+]^2_{aq}} \qquad (2.3)$$

Eq. (2.3) makes clear that the ratio of concentration of the metal ion in the sorbent and sorbate solution is inversely proportional to the square of the hydrogen ion concentration in the bulk solution.

Thus, the following can be inferred:

- Sorption of metal ions onto the sorbent is pH dependent; and
- Since *K* varies with the metal ion, cations can be separated from another by buffering the aqueous solution appropriately.

In adsorption studies of Cd(II), Pb(II) and Zn(II) onto unmodified and EDTA-modified maize cob, Igwe & Abia (2007) found that the sorption capacities of Zn^{2+} (0.74 Å), Cd^{2+} (0.97 Å) and Pb^{2+} (1.20 Å) increased in the order Pb(II) < Cd(II) < Zn(II). Based on these results, they claimed that sorption capacity increased with decreasing ionic radius. However, in their report the authors dealt with sorption *capacity* and sorption *rate* as if they had similar meanings. They also failed to distinguish between the effects of *diffusion* and *reaction* on the overall sorption rate. The authors concluded that the trend in sorption capacity was related to the trend in hydration energies of the metal ions studied, namely Pb^{2+} (-1480 kJ·mol^{-1}) < Cd^{2+} (-1806 kJ·mol^{-1}) < Zn^{2+} (-2044 kJ·mol^{-1}).

2.4.1 Sorption equilibrium

The removal (*R* %) and sorption capacity of a sorbent for a metal ion can be expressed by described by:

$$q_{\mathrm{e}} = (C_0 - C_{\mathrm{e}}) \times \frac{V}{m} \tag{2.4}$$

$$R\,\% = \left(\frac{C_0 - C_{\mathrm{e}}}{C_0}\right) \times 100\,\% \tag{2.5}$$

[q_e = amount of solute per unit weight of sorbent (mg/g); C_0 = initial concentration (mg·mL^{-1}); C_e concentration of solute remaining in solution at equilibrium; V = volume of the aqueous phase (mL) and m is the mass of the sorbent (g).]

The empirical relationship between q_e and C_e is described by a sorption isotherm. Sorption isotherms are graphical representations that map the distribution of absorbable solute between the liquid and solid phase at various equilibrium concentrations (Chilton *et al.*, 2002). Isotherms provide useful information on the nature of the sorption mechanism, i.e., whether it occurred via chemical reaction (chemisorption) or because of long range, weak van der Waals forces between sorbate species and sorbent (physisorption). *Chemisorption*, also called specific sorption, is limited to monolayer coverage of the sorbent. Chemisorption is irreversible because it involves the formation of strong covalent bonds and high heat of sorption (in the order ~200 kJ/mol).

Physisorption, on the other hand, involves enthalpy values in the order ~20 kJ/mol (Atkins, 1999). Physisorption is affected by factors such as surface area, pore structure and surface chemistry of the sorbent as well as the pH of the sorbate medium. Competing chemical species in the sorbate medium also affect physisorption.

Two-parameter isotherms most used to describe sorption are the Langmuir, Freundlich, Temkin and Dubinin-Radushkevich isotherms. In the following sections, the essential characteristics of each isotherm are discussed briefly.

2.4.1.1 *The Langmuir isotherm*

The Langmuir isotherm, initially designed to describe gas-solid phase sorption, is used to quantify and contrast the sorptive capacity of various sorbents. It describes quantitatively the formation of a monolayer sorbate layer on the outer surface of the sorbent, after which no further sorption occurs. The Langmuir isotherm model is an empirical model based on several assumptions. In the context of this study, it assumes:

- Metal ions can only be adsorbed at a finite number of well-defined localised sites;
- Sorption increases with increasing initial metal ion concentration if the binding sites are not saturated;
- Each site can hold only one ion so that the adsorbed layer is one molecule in thickness (monolayer sorption);
- All sorption sites are energetically equivalent;
- There is no interaction between the sorbed ions.

The Langmuir isotherm can be written in the following linear form:

$$\frac{C_e}{q_e} = \left(\frac{1}{K_L Q_0}\right) + \left(\frac{1}{Q_0}\right) C_e \qquad (2.6)$$

Where:

C_e = equilibrium concentration of sorbate ($mg \cdot L^{-1}$);

Q_0 = maximum monolayer coverage capacity ($mg \cdot g^{-1}$);

q_e = amount of metal ions adsorbed per gram of sorbent at equilibrium ($mg \cdot g^{-1}$);

K_L = Langmuir isotherm constants ($L \cdot mg^{-1}$).

According to Bilba *et al.* (1999), the Q_0-value provides information with respect to the accessibility of the sorption sites within the resin matrix, while K_L reflects the binding strength of the functional groups with metal ions.

It is further noted (Piccin *et al.,* 2011) that the K_L parameter corresponds to the concentration at which the amount of metal ions sorbed is equal to 0.5 Q_0. Doke & Khan (2017) provide further significance of the K_L-value, relating it to a dimensionless constant called the separation factor (R_L):

$$R_L = \frac{1}{1+K_L C_0} \tag{2.7}$$

The value of R_L predicts the favourability of the sorption process at different initial concentrations (C_0) as follows:

$R_L > 1$: unfavourable

$0 < R_L < 1$: favourable

$R_L = 1$: linear

$R_L = 0$: irreversible[3]

At low solute concentration, C_e approaches zero and the Langmuir isotherm is reduced to a linear expression, $q_e = Q_0 \cdot K_L \cdot C_e$. Thus, a plot of q_e vs. C_e produces a straight line with slope $Q_0 \cdot K_L$. The value of the slope $Q_0 \cdot K_L$ is an indicator of the sorption efficiency of the sorbent. In other words, the steeper the isotherm, the more effective the sorbent.

2.4.1.2 *The Freundlich isotherm*

Unlike the Langmuir isotherm, the Freundlich isotherm does not predict the formation of a monolayer and surface coverage of the sorbent surface by the sorbate. The Freundlich isotherm is suitable for a highly heterogeneous surface and a sorption isotherm lacking a plateau (Igwe & Abia*,* 2007), i.e., suggesting multilayer sorption. Although not based on any theoretical background, it provides a mathematical description (over a restricted range of concentration) of the surface heterogeneity and the exponential distribution of active sites and their energies according to Eq. (2.8).

$$q_e = K_F C_e^{1/n} \tag{2.8}$$

[K_F and "n" are constants; $n > 1$]

The logarithmic form of the Freundlich isotherm is more useful, as data fitted to the logarithmic form produces a straight line with intercept log K_F (at $C_e = 0$) and slope $1/n$:

$$\log q_e = \frac{1}{n} \log C_e + \log K_F \tag{2.9}$$

[3] R_L can never equal zero; it can only approach zero

'K_F' represents the sorption capacity (mg·g^{-1}) of the sorbent: the higher the K_F value, the greater the sorption intensity. Values of $^1/_n < 1$ is an indication that sorption is favoured at low concentration, but an increase in the amount sorbed becomes less significant at higher concentration. If '*n*' is in the range 1 < *n* < 10, sorption is favourable. Values of n < 1 suggest sorption of ions onto the sorbent is concentration dependent (Metwally, 2006). If *n* = 1, the distribution of sorbable species between the solid and liquid phase is independent of concentration.

2.4.1.3 *The Temkin isotherm*

The Temkin isotherm is described by Eq. (2.10).

$$q_e = \frac{RT}{b}(ln\, K_T + ln\, C_e) \tag{2.10}$$

[K_T is the equilibrium constant (L·mol^{-1}) corresponding to the maximum binding energy; *b* is related to the sorption heat; *R* is the universal gas constant (8.314 J·K^{-1}·mol^{-1}) and *T* is the absolute temperature (K).]

According to this model, the sorption heat of all ions decreases linearly with increased coverage of the sorbent surface. Sorption is characterised by a uniform distribution of binding energies up to a maximum binding energy (K_T), considering the effects of indirect sorbate-sorbate interactions. The Temkin isotherm is only valid, however, for intermediate range concentrations (Ayawei *et al.,* 2017). Plotting q_e against *ln* C_e yields a straight line of slope *RT*/*b* and intercept (*RT*/b)·*ln* K_T. A value of *RT*/*b* < 20 kJ/mol implies physisorption is the dominant sorption mechanism (Atkins, 1999).

2.4.1.4 *The Dubinin-Radushkevich (D-R) isotherm*

The Dubinin-Radushkevich isotherm model is generally applied to express the sorption mechanism with Gaussian energy distribution onto a heterogeneous surface. It is only suitable for intermediate range of sorbate concentrations and does not predict Henry's laws at low pressure. The D-R equation is an empirical model in which sorption follows a pore-filling mechanism, presuming a multilayer character involving van der Waals forces (physisorption) (Ayawei *et al*., 2017). The D-R isotherm is described by Eq. (2.11).

$$\ln q_e = \ln X_m - \beta\varepsilon^2 \tag{2.11}$$

[X_m = theoretical isotherm saturation capacity (mg/g); β = D-R isotherm constant (mol^2·kJ^{-2});

ε = *RT ln* (1 + 1/C_e) is the Polanyi potential where *R*, *T* and C_e represent the universal gas constant (8.314 J·mol^{-1}·K^{-1}), absolute temperature (K) and sorbate equilibrium concentration (mg/L), respectively.]

An essential characteristic of the Dubinin-Radushkevich isotherm is the mean sorption energy *E,* the energy released per mole of sorbate as it approaches the sorbent from infinite distance in the bulk solution. The value of *E* is applied to differentiate between chemical and physical sorption of metal ions, calculated as follows:

$$E = \frac{1}{\sqrt{-2\beta}} \tag{2.12}$$

A plot of ln q_e versus ε^2 yields a straight line with slope equal to -β. A value of *E* in the range 9 – 16 kJ·mol^{-1} signifies chemisorption as sorption mechanism, whereas *E* < 8 kJ·mol^{-1} suggests physisorption (Memon *et al*., 2006). Another essential feature of the D-R isotherm is its temperature dependence – a plot of log q_e versus ε^2 at different temperatures produces a characteristic curve on which all suitable sorption data lie.

2.5 Sorption kinetics

The kinetic aspects of a sorbent are of great significance if more details are required about its performance and the sorption mechanisms involved. In addition, the scale of a sorption apparatus is based on the kinetic information (Qiu *et al*., 2009). In essence, kinetic analysis reveals the residence time required for completion of the sorption process.

Several mathematical models have been applied to describe the kinetic process of sorption, but they can be broadly classified as sorption *reaction* models and sorption *diffusion* models. According to Ho *et al.* (2000), it is often difficult to characterise the distinction between the two models. Obviously, in an ion-exchanger or chelating resin where metals are removed from aqueous solution via ion exchange or coordinate bonding, chemical reaction is often rapid and not rate controlling. Instead, intra-particle diffusion of the metal ions throughout the pores of the sorbent could be rate controlling.

Citing extensive literature review based on bio-sorbents, Ho and co-workers provide as a very general guideline, that if equilibrium is achieved within three hours, the process is usually kinetically controlled, and above twenty-four hours, it is diffusion controlled. Inbetween the three- and twenty-four-hour period, either mechanism could be rate controlling. Another general guideline is that changes in pH have a greater effect on sorption in reaction-controlled sorption processes. These are, however, qualitative approaches. More appropriate quantitative approaches are discussed later in this section.

Sorption *reaction* models are based on the whole process of sorption (i.e., not considering the diffusion steps only) and assume *ion-exchange reaction* at the interior surfaces that bind pore and capillary spaces. According to the reaction models, pore diffusion is normally rate controlling, especially where the degree of cross-linking is high, and the resin particle is more compact. There are only a few cases in which chemical reactions are the rate controlling steps (Cortina *et al.,* 1998).

Sorption *diffusion* models, on the other hand, are premised on the notion that the exchange of ions between the solid phase support and bulk solution is a heterogeneous mass transfer process that involves various diffusion options: (i) *film diffusion* (i.e. diffusion across the liquid film that surrounds the sorbent particles followed by transfer across the solution/particle interface); (ii) *intra-particle diffusion* (i.e. diffusion of metal ions within the pores of the resin particle and/or along the pore walls) and (iii) *bulk diffusion* or *mass action*, where ions possibly interact with the impregnated extractant molecules on the surface of the substrate. One of these processes normally offers more resistance than the others and is considered the rate-controlling step. Fig. 2.2 is a schematic illustration of the diffusion processes:

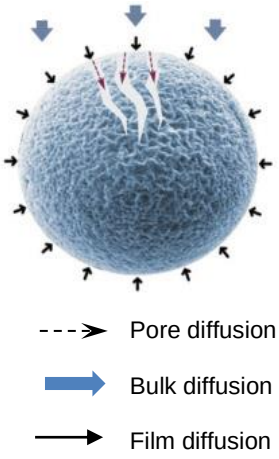

Fig. 2.2: A schematic illustration of the three major types of diffusion processes

Mass transfer in the bulk solution is easily controlled and considered negligible (Kabay *et al.,* 2003). Hence, the other two resistances determine the overall exchange rate. In the analysis of most sorption kinetics, film diffusion is assumed to be rate controlling. However, rigorous stirring of the sorption solution may attenuate the effect of film diffusion, making intra-particle diffusion of the solute sorbed from solution to the sorbent sites the rate-controlling mechanism (Nibou *et al*., 2010). Saha *et al.* (2010) performed kinetic studies “at very vigorous stirring” (440 rpm) to mitigate the influence of film diffusion.

Bilba *et al.* (1999) merely mentioned “vigorous shaking” of samples, while Cortina *et al.* (1998) claimed when convection in the sorbate solution is low it is highly likely that the main resistance to diffusion is found in the liquid phase. Consistent with these hypotheses, Saha *et al.* (2004) also asserted vigorous agitation destroyed film diffusion; they added that when the metal concentration or extractant concentration in the resin increased, diffusion in the pores and consequently the rate of extraction became slow.

2.5.1 Sorption diffusion kinetics

The two kinetic models widely used for describing sorption onto solid ion exchange and chelating resins are the *Homogeneous Particle Diffusion Model (HPDM)* and *Shell Progressive Model (SPM)*. A third model often used is the *Weber-Morris Model*. Pertinent aspects of each model are discussed briefly.

2.5.1.1 *Homogeneous Particle Diffusion Method*

According to this model, the solid particle is surrounded by an external film resisting the mass transfer. Once the solute molecules enter the pores of the solid particle, equilibrium sorption is considered instantaneous, and the adsorbed molecules move by diffusion. Diffusion from an infinite volume of bulk solution into a spherical ion-exchange resin particle could be described by the Nernst-Planck equations (2.13) and (2.14) (Cortina *et al.,* 1998; Saha *et al.,* 2004). If diffusion of ions in the resin phase controls the diffusion process, Eq. (2.13) is used.

$$ln\ (1 - X^2) = -2\ kt \qquad (2.13)$$

[$k = \frac{D_r \pi^2}{r_0^2}$ is the rate constant (s^{-1}), X = fractional attainment (q_t/q_e) of equilibrium or extent of resin conversion; t = time (s); D_r = diffusion coefficient[4] in solid phase ($m^2 \cdot s^{-1}$); r_0 = particle radius (m), assuming spherical geometry.]

This equation was applied by Saha *et al.* (2004, 2000) to study the sorption of heavy metals by SIRs from aqueous solutions. A plot of $ln\ (1 - X^2)$ versus t should produce a straight line passing through the origin with slope “$-2k$” if resin phase (or pore) diffusion is the rate-determining step. If film-diffusion controlled the overall diffusion process, Eq. (2.14) applies, and a plot of $ln\ (1 - X)$ versus t should produce a straight line through the origin with slope “$-k_{li}$”.

[4] D_r, D_p and D_s are used interchangeably, denoting the diffusion coefficient in the resin/pore/solid phase.

$$ln\ (1 - X) = -k_{li}\ t \tag{2.14}$$

[$k_{li} = \frac{3DC}{r_0 \delta C_r}$ is the rate constant for film diffusion (s^{-1}); D = diffusion coefficient in solution phase ($m^2 \cdot s^{-1}$); C = total concentration of both exchanging species (M); δ = liquid film thickness (m); C_r = total concentration of both exchanging species in the ion-exchanger (M).]

Equations (2.13) and (2.14) were used to describe the exchange of Cd^{2+} and Na^{+} ions on chelating and ion-exchange resins (Bilba *et al.*, 1999) and the extraction kinetics of heavy metal ions by Amberlite XAD-2 impregnated resins (Cortina *et al.*, 1998).

In a critical review of sorption kinetic models, Qiu *et al.* (2009) criticized the indiscriminate use of mathematical models to describe sorption *reaction* kinetics and sorption *diffusion* kinetics as if they were the same. They referred to the Homogeneous Solid Diffusion Model (HSDM) as a kinetic diffusion model to quantitatively describe intra-particle diffusion. Accordingly, HSDM describes mass transfer in an amorphous and homogeneous sphere and can be represented by the differential equation,

$$\frac{\partial q}{\partial t} = \frac{D_s}{r^2} \frac{\partial}{\partial r} \left(r^2 \frac{\partial q}{\partial r} \right) \tag{2.15}$$

[D_s is the intra-particle diffusion coefficient, r = radial position and q the sorption quantity of solute in the solid varying with radial position at time t.]

Qiu *et al.* (2009) cite research that reportedly provide a solution to Eq. (2.15), assuming the "infinite bath" case where the spherical resin particle is initially free of solute and the concentration of sorbate on the sorbent surface remains constant with time. A critical element of the solution is the assumption that film resistance is negligible. The solution is then written as follows:

$$\frac{q_t}{q_s} = 1 + \frac{2R}{\pi r} \sum_{n=1}^{\infty} \frac{(-1)^n}{n} \sin \frac{n \pi r}{R} \exp \left(\frac{-D_s n^2 \pi^2 t}{R^2} \right) \tag{2.16}$$

[R is the total particle radius.]

If $\bar{q}$ is defined as the average value of q in a spherical sphere, then it can be represented as follows:

$$\bar{q} = \frac{3}{R^3} \int_0^R q(r)\, r^2\, dr \tag{2.17}$$

[q is the local value of the solid-phase concentration.]

Eq. (2.16) then becomes:

$$\frac{\bar{q}}{q_\infty} = 1 - \frac{6}{\pi^2}\sum_{n=1}^{\infty}\frac{1}{n^2}\exp\left(\frac{-D_s n^2 \pi^2 t}{R^2}\right) \tag{2.18}$$

[q_∞ represents the average concentration in the solid at infinite time.]

Assuming short-time data where the fractional attainment of equilibrium, $X = \frac{\bar{q}}{q_\infty}$ is less than 0.3, Eq. (2.18) becomes:

$$X = 6\left(\frac{D_s}{R^2\pi}\right)^{1/2} t^{1/2} \tag{2.19}$$

If data is recorded over a long time, i.e., $q_e = q_\infty$, the lines representing Eq. (2.18) converge asymptotically over time (Ho *et al*., 2000) so that the higher terms of the summation become small and are negligible. Eq. (2.18) then becomes:

$$ln\,(1 - X) = ln\,\frac{6}{\pi^2} - \left(\frac{D_s \pi^2}{R^2}\right)t \tag{2.20}$$

However, the assumption of constant surface concentration is likely to be violated over a long time so that Eq. (2.20) is only valid in a short time. What is meant by "short time" was not clarified by Qiu and co-workers in their review. Equations (2.19) and (2.20) were later used by Nibou *et al.* (2010) in sorption studies of Zn^{2+} ions onto NaA and NaX zeolites. The researchers reportedly focused their attention on the use of models based on Fick's laws in the analysis of empirical data. Like Qiu *et al.*, they plotted graphs of q_t/q_∞ vs. $t^{1/2}$ and *ln* $(1 - q_t/q_\infty)$ versus t, but differentiated between initial diffusion coefficient, D_i, and final diffusion coefficient, D_f. According to the researchers, the initial diffusion coefficient assumed a particle diffusion mechanism to be rate controlling. The value of D_i was derived from the gradient (p_1) of the initial linear portion of a plot of q_t/q_∞ vs. $t^{1/2}$. They rearranged q_e values at t = 120 min as q_∞ values, and the initial portion of the curve was used typically up to values q_t/q_∞ = 0.4 – 0.6. Thus,

$$p_1 = \frac{6}{r_0}\left(\frac{D_i}{\pi}\right)^{1/2} \tag{2.21}$$

and,

$$D_i = \frac{p_1^2 \pi r_0^2}{36} \tag{2.22}$$

For longer operating times, presumably t > 120 min, and q_t/q_∞ > 0.6, they plotted ln $(1 - q_t/q_\infty)$ versus t (min) and used the gradient (p_2) of this curve to determine the value of the final diffusion coefficient, D_f:

$$p_1 = \frac{D_f}{r_0^2}\pi^2 \tag{2.23}$$

and,

$$D_f = -\frac{p_2 r_0^2}{\pi^2} \tag{2.24}$$

Their statements therefore generally echoed those of Qiu and his co-workers but had their own idiosyncrasies. Nibou *et al.* assumed intensive stirring of the sorptive system where intra-particle diffusion was assumed to be the rate-controlling mechanism. In addition, they did not mention the significance of the second linear portion of the q_t/q_∞ vs. $t^{½}$ graph. Both reports failed to consider the occasion of steady-state approximation, where fractional attainment of equilibrium exceeded X = 0.6, but in very short time.

Doke & Khan (2017) shed more light on the significance of the value of D_s, saying the magnitude of the diffusion coefficient was dependent upon the nature of the sorption process – if the value of D_s is in the range 10^{-6} – 10^{-8} $cm^2 \cdot s^{-1}$, then film diffusion is most likely to control the sorption mechanism. If D_s is in the range 10^{-11} – 10^{-13} $cm^2 \cdot s^{-1}$, then the sorption mechanism is controlled by pore diffusion. However, the two diffusion mechanisms may not always be clearly distinguishable. In their study of Cr(VI) sorption onto activated carbon derived from wood apple shell, the authors obtained values of the film and pore diffusion coefficients in the order 10^{-9} – 10^{-12} $cm^2 \cdot s^{-1}$, ascribing it to the duality of film and pore diffusion.

El-Naggar (2010) and his fellow workers presented arguments similar to Cortina *et al.,* but interpreted the distribution coefficient-values slightly differently. Citing a study, they claimed for physisorption, the value of the effective diffusion coefficient ranges from 10^{-6} to 10^{-9} m^2/s and for chemisorption between 10^{-9} – 10^{-17} m^2/s. Nonetheless, they ascribed the difference in the values of the diffusion coefficients to the fact that in physical sorption, the molecules are weakly bound and migrate with relative ease, whereas for chemisorption, the molecules are strongly bound and mostly localised.

2.5.1.2 *Shell Progressive Model*

Assuming that the resin pores were small and practically impervious to the analyte, the sorption of metal ions could be explained by the *Shell Progressive Model (SPM)*. According to this model, the diffusion and reaction of a liquid extractant counter ion A occur within an outer shell layer of the resin particle and advances towards the centre of the solid particle with the progression of sorption (Bilba *et al.,* 1999).

In this case, Fick's diffusion equation describes the material balance of the counter ion as it penetrates a spherical bead of a partially substituted ion-exchanger. The time-dependence of the degree of conversion (X) is given by the following expressions:

Film diffusion controlled: $$t = \frac{ar_0 C_{so}}{3C_{A0}K_{mA}} X \quad (2.25)$$

[a = stoichiometric coefficient; C_{so} = concentration of solid reactant at the beads unreacted core (M); C_{Ao} = concentration of species A in bulk solution (M); K_{mA} = mass transfer coefficient of species A through the liquid film (ms^{-1}).]

Particle diffusion controlled: $$t = \frac{ar_0^2 C_{so}}{6D_{e,r}C_{A0}}[3-3(1-X)^{2/3}-2X] \quad (2.26)$$

[$D_{e,r}$ = diffusion coefficient in solid phase (m^2s^{-1}).]

Chemical reaction controlled: $$t = \frac{r_0}{k_s C_{A0}}[1-(1-X)^{1/3}] \quad (2.27)$$

[k_s = reaction constant based on surface (ms^{-1}).]

In each of the above cases, the appropriate graphs should be linear and pass through the origin. Often deviation from linearity near the origin can be explained by the fact that at the beginning of the reaction, the thickness of the reacted layer approximates that of the liquid film surrounding the particle; film resistance to ion diffusion then becomes comparable with the resistance offered by the outer surface of the resin particle (Cortina *et al.,* 1998).

Cortina *et al.* (2006) reached several conclusions: (i) pore diffusion was the rate-determining step when working with high metal ion concentrations; (ii) liquid-film diffusion controlled the metal extraction rate at low concentrations of metal ions; and (iii) Fick's law and the shell progressive mechanism generally represented good approaches to the kinetics of Zn, Cu and Cd extraction reactions on impregnated polymer resins. The researchers conceded, though, that a rigorous kinetic model for metal exchange reactions in impregnated resins could not be developed due to the lack of precise information, an observation corroborated by Kabay *et al.* (2003).

In kinetic studies elsewhere, Saha *et al.* (2000) found that the pore-diffusion model fitted the data obtained during sorption of copper and cadmium ions onto thiol containing chelating resins. Bilba *et al.* (1999) could explain the sorption data of cadmium ions onto Purolite S-930 chelating resin by the shell progressive model and showed that the cadmium uptake was particle diffusion controlled.

2.5.1.3 *Weber-Morris model*

The Weber-Morris model has been used successfully in many cases to distinguish between kinetic and diffusion rate control. According to the Weber-Morris model, sorbate uptake varies almost proportionally with $\sqrt{t}$ as opposed to *t*:

$$q_t = K_{ad}\sqrt{t} \tag{2.28}$$

[K_{ad} is the rate constant of intra-particle transport (mg/g·min$^{0.5}$).]

A linear graph of q_t versus $\sqrt{t}$ that passes through the origin implies intra-particle diffusion is the sole rate-determining step. However, the graph may not always pass through the origin as sorption diffusion kinetics may be controlled by film diffusion and pore diffusion simultaneously (Qiu *et al.,* 2009). This assertion was affirmed by Doke & Khan (2017) citing Saha (2010), saying the presence of both diffusion regimes leads to multi-linear plots. Ho *et al.* (2000) cite work done by numerous researchers in which they report that plots of sorption capacity against the square root of time were linear, but the initial curved portions of the graphs might be attributed to boundary layer diffusion effects. Cases where graphs would pass through the origin normally involved rapid stirring in the batch reactor. Furthermore, in cases with sorbents whose pore size were extensive including micro-, meso- and macropores, up to three linear sections have been obtained. Doke & Khan extended Eq. (2.28) by including a constant (*I*) which is related to the boundary layer thickness (mg·g^{-1}), so that it becomes:

$$q_t = K_{ad}\sqrt{t} + I \tag{2.29}$$

2.5.2 Sorption reaction kinetics

Sorption reaction models that attempt to describe chemical reaction kinetics are based on the whole process of sorption and do not consider the diffusion processes outlined above. Equations used to model sorption reaction kinetics include pseudo-first order (PFO) and pseudo-second order (PSO) equations. In both cases, the term *pseudo* was introduced to distinguish kinetic equations based on sorption capacity from solution concentration.

2.5.2.1 *Pseudo-first order (PFO) kinetics*

Lagergren (1898) postulated the first model that related sorption rate to sorption capacity. It has been called 'pseudo-first order' by Ho & McKay (1998a) to distinguish between kinetic equations based on sorption capacity and those based on solution concentration. In differential form, the Lagergren pseudo-first order can be presented as follows:

$$\frac{dq_t}{dt} = k(q_e - q_t) \tag{2.30}$$

After integration and applying boundary conditions $t = 0$ to $t = t$ and $q_t = 0$ to $q_t = q_t$, the integrated form of the Lagergren equation becomes:

$$\log (q_e - q_t) = \log q_e - \frac{k}{2.303}\, t \tag{2.31}$$

[q_e = equilibrium concentration of the sorbed ion (mg·g^{-1}); q_t = concentration of the sorbed ion at time t (s); k is the pseudo-first order rate constant (min^{-1}).]

Eq. (2.31) is valid only for the initial period of sorption (Gulipalli *et al.,* 2011). A plot of log ($q_e - q_t$) against t (min) will produce a straight line with slope $-\frac{k}{2.303}$ and intersects the vertical axis at the value of log q_e. However, the experimental value of q_e generally differs from the value obtained from a plot of log ($q_e - q_t$) against *time* (Ho *et al.,* 2000) because the parameter q_e does not represent the true number of available sites (see Section 5.4). Moreover, Eq. (2.31) is only an approximate solution to the true first order rate mechanism.

2.5.2.2 *Pseudo-second order (PSO) kinetics*

The pseudo-second order model (Ho & McKay, 1998) assumes that sorption supports second order chemisorption according to the rate law:

$$\frac{dq_t}{dt} = k(q_e - q_t)^2 \tag{2.32}$$

The driving force ($q_e - q_t$) of sorption is proportional to the available fraction of active sites (Ho, 2006). For the boundary conditions $t = 0$ to $t = t$ and $q_t = 0$ to $q_t = q_t$, the integrated form of Eq. (2.32) becomes:

$$\frac{t}{q_t} = \frac{1}{h} + \frac{1}{q_e} t \tag{2.33}$$

[The initial sorption rate $h = k_2 q_e^2$ (mg/g·min) and k_2 (g/mg·min^{-1}) is the rate constant of the second order equation.]

Thus, sorption is pseudo-second order if a plot of $\frac{t}{q_t}$ vs. time (t) produces a straight line of which the slope is $\frac{1}{q_e}$ and the vertical axis-intercept is $\frac{1}{h}$. If sorption data fits the pseudo-second order model, it implies that sorption occurs predominantly via chemical reaction (i.e., chemisorption) through sharing or the exchange of electrons between functional groups on the sorbent and metal ions (Ho, 2006). In conclusion, Ho and colleagues reported that the selection of a sorption model was not an easy or obvious choice as the initial rate-controlling mechanism may change throughout the duration of the sorption process. For example, external film diffusion may initially control the sorption process before it gives way to reaction, after which pore diffusion becomes the rate-determining mechanism. To identify the correct sorption model, they propose selecting and testing several models and system variables (e.g., initial concentration, sorbent particle size, solution temperature, solution pH and agitation) over the entire sorption range, from t = 0, until sorption equilibrium is achieved. They claim correlation coefficients between experimental and theoretical data will provide the 'best fit' model, although it has yet to be confirmed by proposing a mechanism appropriate to the sorption model.

2.6 Temperature-dependence of sorption

The free energy of sorption (ΔG^0) is related to the distribution coefficient, K_d, by the classical van't Hoff equation (Saha & Chowdurry, n.d.):

$$\Delta G = -RT \ln K_d \tag{2.34}$$

[K_d = distribution coefficient (q_e/C_e); R = ideal gas constant (8.314 J·K·$^{-1}$·mol^{-1}); T is the absolute temperature (K)].

This relationship can be expressed in differential form as follows:

$$\frac{d \ln K_d}{dt} = \frac{\Delta H^0}{RT^2} \tag{2.35}$$

After integration, Eq. (2.35) becomes:

$$\ln K_d = -\frac{\Delta H^0}{R}\left(\frac{1}{T}\right) + \frac{\Delta S^0}{R} \tag{2.36}$$

[ΔH^0 = change in enthalpy (kJ·mol^{-1}); ΔS^0 = change in entropy (J·mol^{-1})]

Substituting Eqs. (2.34) and (2.36), ΔG^0 can be calculated as follows:

$$\Delta G^0 = \Delta H^0 - T\Delta S^0 \tag{2.37}$$

A plot of ln K_d versus $\left(\frac{1}{T}\right)$ yields a straight line with slope $-\frac{\Delta H^\circ}{R}$ from which the enthalpy (ΔH°) can be calculated. From the intercept of the graph, the value of ΔS° can be determined.

The enthalpy value (ΔH°) can be used to discriminate between physi- and chemisorption as follows – the heat of physisorption is normally in the range 2.1 – 20.9 kJ·mol^{-1}, whereas chemisorption generally falls in the range 80 – 200 kJ·mol^{-1} (Saha & Chowdurry, n.d.). On the other hand, Huang *et al*. (2007) cite work published by von Oepen *et al*. (1991) in which they describe the sorption energy associated with different types of interactions: van der Waals forces (4 – 10 kJ/mol), hydrophobic forces (~5 kJ/mol), hydrogen bonding (2 – 40 kJ/mol), coordination exchange (40 kJ/mol), dipole forces (2 – 29 kJ/mol) and chemical bonding (> 60 kJ/mol). Enthalpy changes for ion-exchange reactions are less than 8.4 kJ/mol.

Negative values of ΔG° indicate spontaneity and feasibility of sorption across the temperature range. As a rule of thumb, a decrease in ΔG° with increasing temperature signifies that sorption is more favourable at higher temperatures. A positive ΔS° value reflects the irreversibility of sorption and affinity of the sorbent towards the sorbate species. It further suggests randomness exhibited by the sorption system at the liquid-solid interface, accompanied by structural changes in the sorption system.

CHAPTER 3

Dithizone as chelating extractant

3.1 Introduction

Wayne E. White (1935) described *dithizone* as a reagent of the first class. Koroleff (1950) described it as a heavy metal reagent *per excellence*. It reacts with various heavy metals to form complexes with distinctive colours ranging from shades of violet to distinct red and orange shades. Given the disadvantages of conventional solvent extraction systems, dithizone has become a ligand of choice in the synthesis of chelating substrates. Its selectivity and sensitivity render it suitable to prepare sorbents for removal and preconcentration of a variety of metal ions.

This chapter provides a theoretical framework on dithizone as an analytical reagent, including an overview of dithizone-based solid phase extraction systems, with emphasis on dithizone-*impregnated* solid phases. Moreover, salient points emanating from research conducted on these systems will be highlighted and gaps revealed by the review identified.

3.2 The chemistry of dithizone

The complete name of dithizone is diphenylthiocarbazone ($C_{13}H_{12}N_4S$), a dark blue-green solid crystalline powder with a melting point of 168 °C and molecular weight, *MW* = 256 g/mol. It is a weak acid, insoluble in cold water but soluble in alkaline media, alcohols, hydrocarbons, and chlorinated hydrocarbons such as chloroform and carbon tetrachloride. It has been widely used in solvent extraction techniques using chloroform and carbon tetrachloride as organic phase.

Dithizone was first synthesized and studied by Emil Fischer but was used as an analytical reagent for the first time by Hellmut Fischer (White, 1935). Fischer, studying metallic dithizonates and their possible applications in analytical chemistry, was the first to report that dithizone existed in two tautomeric forms he referred to as the “keto” and “enol” forms (Fig. 3.1).

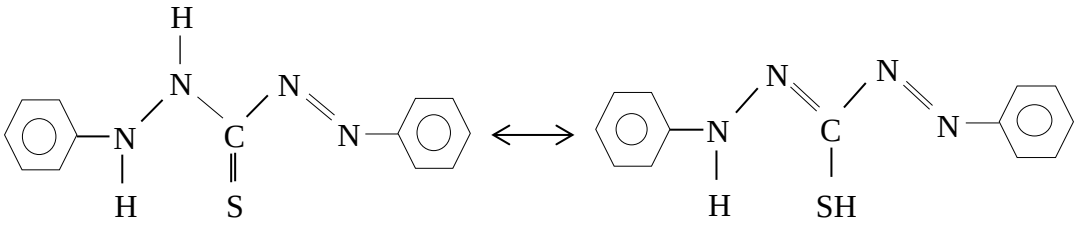

Keto Enol

Fig. 3.1: The two tautomeric forms of dithizone

The keto tautomer is formed predominantly in acid or neutral solution whereas the enol tautomer presents in alkaline solution or where there are insufficient quantities of dithizone.

In accordance with Fischer's findings, Paradkar & Williams (1994) reported that dithizone dissolved in alkaline aqueous media of concentration >20 g/L to form the orange coloured dithizonate ion (HDz^-) according to the following reaction equation (Fig. 3.2):

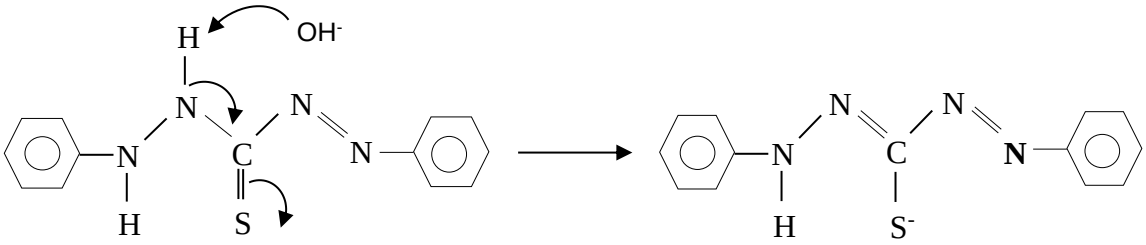

Dithizone (H_2Dz) Dithizonate (HDz^-)

Fig. 3.2: Dithizone forms dithizonate in alkaline medium

Wewers (2012) and Hutton (1980) cited findings that corroborated Fischer's postulate that dithizone existed as a tautomeric equilibrium mixture in organic solvents. Irving presented as evidence two intense absorption bands (*ca*. 450 and 620 nm respectively) in the visible spectrum of dithizone in organic solvents, the thiol form being responsible for the band at shorter wavelength (λ = 450 nm).

However, in their study of dithizone and its oxidation products, von Eschwege *et al.* (2011) used time dependent density functional theory (DFT) to corroborate experimental X-ray crystallography results pointing to the existence of at least six different tautomers (Fig. 3.3).

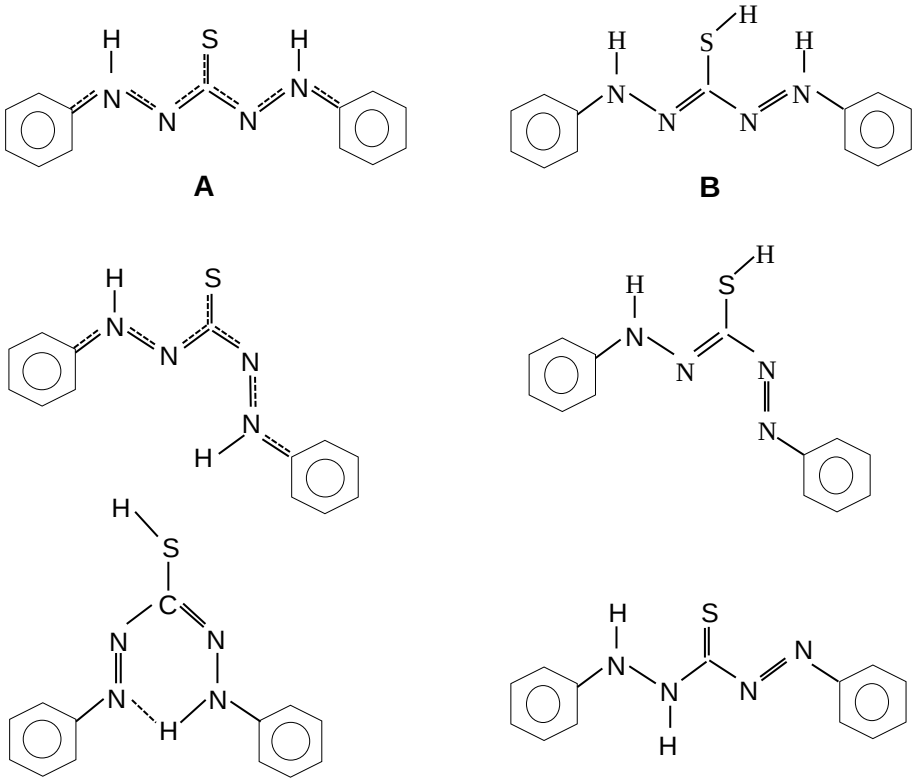

Fig. 3.3: Six tautomers of dithizone discovered by von Eschwege *et al.* using density functional theory (DFT)

The two geometries labelled A and B represent the lowest energy conformations in both solid and gas phase. Von Eschwege *et al.* (2011) cite Hutton (1986) who ascribed the stability of these isomers to the fact that their linear backbone affords them rotation about the conjugated bonds. Yet, A is the computationally favoured geometry (also in solution) as its relative energy is more than 20 $kJ \cdot mol^{-1}$ less than that of B because of π-electron delocalization along the backbone (including the phenyl rings), contributing towards stabilization of the dithizone molecule.

Reaction with divalent metal ions leads to the replacement of H-atoms of either of the imide (-NH) or sulfhydryl group (-SH) (White, 1935). In acid or near neutral media, the metal ion replaces the hydrogen atom of the imide group; in alkaline media, the hydrogen of the sulfhydryl group is replaced. The formulae for the keto and enol forms of divalent metal dithizonates are presented in Fig. 3.4.

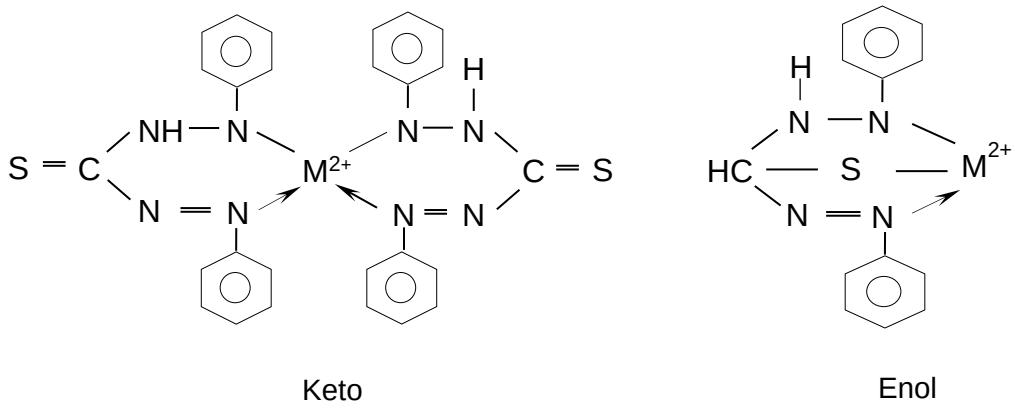

Fig. 3.4: Two tautomeric forms of divalent metal dithizonates

Fischer further postulated that the following equilibrium existed between the keto and enol forms:

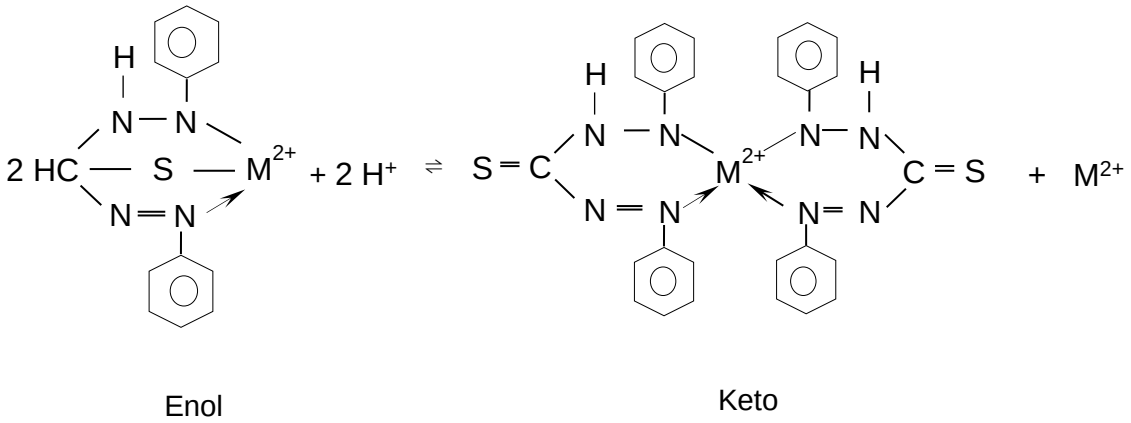

Fig. 3.5: An equilibrium exists between the keto and enol tautomers

Thus, formation of the keto tautomer is favoured by conditions of (i) low pH and/or (ii) low [M^{2+}]. Conversely, reaction conditions of high pH and/or high [M^{2+}] shift the equilibrium towards formation of the enol tautomer.

Dithizone is a bidentate ligand and should therefore provide relatively fast and reversible sorption of metal ions. In cases where a ligand forms stable complexes, acids that are more concentrated are needed to elute the metal ion through protonation of the functional group (Nesterenko *et al*., 2011). Metal ions combine with dithizone to yield coloured complexes that are non-polar and therefore only slightly soluble in water, but soluble in organic solvents. These complexes are classified as either *primary* or *normal* dithizonates.

Primary dithizonates are formed when dithizone reacts with a metal as a monobasic acid anion (HDz^-); they are of the form $M(HDz)_n$, where "M" is a metal ion of charge n^+. Metals that typically form primary dithizonate complexes are Hg(II), Zn(II), Cu(II), Pb(II) and Cd(II). Structural investigations of primary complexes have shown that the metal is bonded to the sulphur atom and co-ordinately bonded to the nitrogen atom (Fig. 3.6).

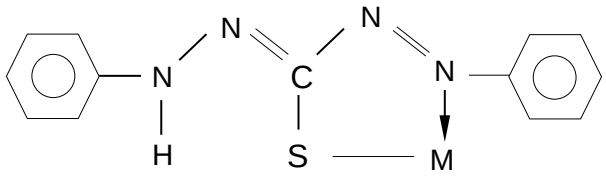

Fig. 3.6: Bonding in primary metal dithizonate complexes

Some metals (M = Cu, Hg, Ag, Pt, Au, Pd) form *secondary* dithizonate complexes which are of the form M_2Dz. Rice *et al*. (2017) describe secondary complexes as of the form $M\text{-}DzH_2$. They claim secondary complexes contain the species in a 1:1 ratio of metal to dithizone and are formed at high metal to ligand concentration or at high pH. The actual nature of secondary complexes remains elusive though.

In one of his most comprehensive papers, Fischer reported on the distinctive reactions of the following metals with dithizone: Cu, Ag, Au, Zn, Cd, Hg, Tl (lower valency), Sn (lower valency), Pb, Bi, Mn (lower valency), Co, Ni, Pd and Pt. Noting the pH dependence of metal sorption, he classified these metals (except for Mn and Pt) into four groups according to their reactions with dithizone:

- Pd, Au, Hg, Ag and Cu react in acid solution;
- Zn is most sensitive to dithizone in a slightly acidic solution (pH = 5.5), but large amounts of Co, Ni, Pb and Cd interfere by causing some coloration;
- In a slightly alkaline solution containing CN^-, the lower valency ions of Sn and Tl, as well as Pb and Bi are reactive; and
- In a strongly alkaline solution containing tartrate ion Co, Ni and Cd are most sensitive to dithizone.

Chwastowska & Kosiarska (1988), however, found that zinc was quantitatively sorbed only in alkaline medium. It should be borne in mind that the latter study was conducted on a SPE system and not SX, as was the case with the study conducted by Fischer. Costa *et al.* (2002) provided a more comprehensive list of metals that reacted with dithizone, reporting that dithizone reacts with 'soft' cations of Mn, Fe, Co, Ni, Cu, Zn, Pd, Ag, Cd, In, Sn, Pt, Au, Hg, Tl, Pb, Bi, Se, Te and Po. The claim of some cations labelled "soft" can be contested though.

Koroleff (1950) cites a study in which it is reported that certain metals reacted with dithizone in one valency only – for example, Fe^{2+}, Sn^{2+} and Pt^{2+} react, whereas their higher oxidation state analogues Fe^{3+}, Sn^{4+} and Pt^{4+} do not.

Horwitt & Cowgill (1937) applied various dithizone methods for the determination of lead to a large variety of materials. They studied, among others, the interference of stannous tin with lead. The researchers reported that Sn(IV) did not interfere with dithizone. Likewise, in the colorimetric determination of lead in beer and brewing materials, Andrews & Stringer (1951) asserted that if potassium cyanide and ammonium citrate were added to the aqueous solution before shaking with the dithizone reagent, only the dithizonates of lead, bismuth, Sn(II) and Tl(II) would pass into the carbon tetrachloride. They concurred with Horwitt & Cowgill that the higher oxidised state of Sn would remain in the aqueous layer along with many other metals that give coloured complexes with dithizone.

3.3 Review of dithizone-based SPE systems

Chwastowska & Kosiarska (1988) reported the anchoring of dithizone on a diazotised styrene-divinyl benzene support, failing to identify the polymer. Here, 10 g of the copolymer was reacted with 2.5 g dithizone in the presence of other reagents. The maximum loading capacity was not reported either. The researchers used this chelating resin for the sorption of Ag(I), Cd(II), Cu(II), Pb(II), Ni(II), Co(II) and Zn(II). Under static conditions (batch method), nickel, cobalt, zinc and cadmium were sorbed only in alkaline medium; copper, bismuth and lead were sorbed in both alkaline and acid medium; silver was sorbed only in acid medium. The researchers determined the column method to be more efficient than the batch method, with all elements being sorbed quantitatively at $pH \geq 5$. Sorption rates were influenced by flow rate and sample volume (except for Cu and Pb). All metals except silver were easily desorbed with three portions of 4 M hydrochloric acid. Ag could be desorbed by shaking with three portions of 0.5 M thiosulphate for 10 min each under batch conditions.

A porous polymeric resin loaded with dithizone and two other (unknown) extractants (Uchiumi *et al.,* 1993) was used for the removal of As(III), Sb(III) and Cu(II) ions from industrial wastewater.

Shah & Devi (1997) used dithizone-anchored poly (vinyl pyridine)-based chelating resin to separate quantitatively Pd(II) and Pt(IV) from Au(III) and Ni(II). First, 10 g dithizone was added to a mixture of chloro-methylated poly (vinyl pyridine) in dimethylformamide (DMF). The reaction flask was covered with foil and shaken for 15 days at room temperature to obtain an orange resin.

The orange resin was filtered, washed, and mixed with a solution of 100 mL of 0.5 M ascorbic acid + 50 mL of 1 M NaOH before it was shaken for 30 min to convert the dithizonate to dithizone. The amount of dithizone anchored on the chloro-methylated intermediate support was reported at ~1.1 mmol/g. The impregnation ratio of the final product was not reported but could be presumed to be greater based on the elemental analysis (Table 3.1).

Table 3.1: Elemental analysis of a poly (vinyl pyridine)-based chelating resin before and after impregnation with dithizone

	Content (%)	
	Chloro-methylated	**Dithizone-resin**
C	60.95	72.65
H	6.85	6.94
N	7.27	13.39
Cl	4.97	1.35

Mixtures of 0.1 M HCl/1.0 % thiourea or 0.1 M HCl/5.0 % could elute palladium and platinum quantitatively. The sorbent could be used more than 20 times under static conditions without any decrease in sorption efficiency. The same researchers previously used dithizone anchored poly (vinyl pyridine) support for preconcentration of nanogram levels of mercury (Shah & Devi, 1996).

Amberlite XAD-2 chemically functionalised with dithizone was successfully applied in a field flow preconcentration system (FFPS) for determination of dissolved cadmium in natural seawater (Wu *et al*., 2006). Thermogravimetric analysis (TGA) of the synthesized resin depicted a three-step mass loss up to 540 °C, the last of which was a 63 % mass loss attributed to dithizone. Unfortunately, the mass of the functionalised resin was not recorded; hence, the amount of dithizone loaded onto the resin is not known. Maximum sorption (0.74 mmol Cd per gram of sorbent) occurred within the pH range 6.8 – 8.5 at a flow rate 2.5 mL·min^{-1}. The sorbed cadmium was recovered quantitatively with 3.0 M HNO_3 at an eluent flow rate of 4.7 mL·min^{-1}. The researchers reported that large amounts of foreign ions (Na^+, K^+, Ca^{2+}, Mg^{2+}, Mn^{2+}, Fe^{2+}, Zn^{2+}, Al^{3+} and Cu^{2+}) did not significantly interfere with the preconcentration of cadmium.

Dithizone-modified Amberlite XAD-2 was used for the preconcentration of zinc from water samples (Meena *et al.,* 2014). In the latter case, tolerance levels of interfering heavy metal ions Cu^{2+}, Cd^{2+} and Pb^{2+} were 12, 20 and 25 mg/L, respectively.

Salih *et al.* (1998) immobilised dithizone on polyethylene glycol dimethaacrylate-2-hydroxyethyl methacrylate (EGDMA-HEMA) micro beads via covalent linkage and used the functionalised micro beads to extract the heavy metal ions Cd(II), Hg(II), Cr(III) and Pb(II) from their aqueous nitrate solutions in batch sorption-equilibrium studies. They cite similar studies in which attempts were made to effect preconcentration of mercury from seawater and other aqueous media, but with little success. The prepared micro beads had a hydrophilic structure (in contrast to the hydrophobic nature of ACG300m-H_2Dz) and carried 105.5 μmol dithizone per gram of sorbent. The sorption of metal ions was studied within the pH range 2 – 8. Sorption increased with increasing pH, reaching a plateau value between pH 4 – 6, depending on the metal ions. The sorption capacities of the metal ions based on micromole uptake decreased in the order Cr(III) > Pb(II) > Hg(II) > Cd(II). It differed from the affinity order on a weight basis as follows: Pb(II) > Cr(III) > Hg(II) > Cd(II). The sorption of Cd(II) in particular from its aqueous solution was found to be 18.3 $mg \cdot g^{-1}$ (or 160 $\mu mol \cdot g^{-1}$). In a mixture containing Hg(II), Cr(III) and Pb(II) the sorption capacity of Cd(II) decreased to 9.7 $mg \cdot g^{-1}$ and even further (4.3 $mg \cdot g^{-1}$) in artificial wastewater containing, amongst others, Sn(II) ions. Similarly, sorption of Pb(II) from artificial seawater was almost ten times less compared to an aqueous Pb(II) solution and almost four times less when in competition with the other heavy metals used in the study. Desorption of the heavy metal ions was achieved using 0.1 M HNO_3. The dithizone-anchored micro beads were suitable for repeated use in more than five sorption/desorption cycles without noticeable loss of capacity. The researchers concurred that the S and N atoms of dithizone were available for interaction with the metal ions. However, they could not furnish a plausible argument why the stoichiometry of ion sorption suggested that up to ten metal ions (in the case of Cr(III)) interacted with one dithizone molecule. They surmised that since the micro beads were prone to swelling and were porous, metal ions could be entrapped within the matrix of the swollen micro bead (i.e., in addition to the metal ions that complexed with the dithizone molecules). Moreover, the hydroxyl groups of EGDMA-HEMA could have interacted with the metal ions. This could still not explain the high sorption values of the metal ions under investigation. They postulated that the adsorbed metal ions interacted with heavy metal ions that arrived at the same sorption site during the sorption process; as such, sorption was not monolayer, but multilayer (non-Langmuir type) instead.

In other studies, dithizone was chemically immobilised onto cellulose acetate nanosponges (Zargar *et al.,* 2017), Dowex Optipore L493 (Saxena *et al.,* 2015), nanoporous fructose (Bebhababni *et al*., 2013), silica-gel (Mahmoud *et al.,* 2000), naphthalene (Shabani *et al*., 2007), alumina (Nayebi & Moghimi, 2006) and (EGDMA-HEMA) micro beads (Salih *et al*., 1998).

Instances where dithizone was physically adsorbed (impregnated) onto a support matrix were identified and are presented below.

Dolley & Van der Walt (2014) impregnated Amberlite XAD-8 with dithizone to isolate Cu radionuclides from up to 5 g of ^{nat}Zn. They reported that few applications were found where dithizone was impregnated onto a polymeric matrix, but cited applications where dithizone was loaded onto an active carbon column and a surface-coated microcrystalline naphthalene support. Dolley and van der Walt introduced a novel impregnation procedure to avoid the excessive use of organic solvent. This procedure, which could be considered a modification of the method reported earlier by Shah and Devi (1997), utilised the solubility of dithizone in alkaline medium to form dehydrodithizone (or dithizonate, HDz^-). Dithizone was dissolved in 0.5 M NaOH before impregnation into the dry resin. The sorbed dithizonate anion was then titrated back into its neutral state by slow addition of concentrated HCl. The researchers found that the dithizone loaded resin oxidised slowly over time (even when stored in the dark) but functioned efficiently after three weeks of storage (in 0.05 M HCl). The use of 10 M HNO_3 as eluent caused traces of dithizone to be eluted from the column. A drawback of their research was the failure to optimise the method for dithizone-loading onto Amberlite XAD-8; neither did the researchers report the amount of dithizone loaded onto XAD-8 during impregnation.

Dolley *et al.* (2006) previously developed a two-stage method for the purification of $^{64,67}Cu$ from ^{nat}Zn and other radionuclides. They loaded dithizone onto a methacrylate-based polymeric resin, Amberchrom® CG-71. Dithizone loading was estimated at ~0.33 mg/mL resin. Given that the density of the resin is 0.23 gram of polymer per wet mL (Sigma-Aldrich Co., 1997), the loading reported by Dolley *et al.* was equivalent to ~1.435 mg dithizone per gram of resin, which is almost exactly half the dithizone loading achieved in this study (see Section 5.1). Copper recovery was quantitative (> 97 %) with 5 M HNO_3 warmed to 50 °C. However, concentrated HCl solutions (> 5 M) caused elution of trace amounts of dithizone. The researchers reported that optimising the loading method of dithizone onto the resin proved difficult.

To save cost, Memon *et al.* (2006) replaced costly XAD resins with Styrofoam (packing waste material) impregnated with dithizone to study the sorption of ultra-trace amounts of cadmium ions from aqueous solution. Styrofoam is a mixture of 5 % polystyrene and 95 % air. Impregnation was affected via the dry method, using 30 mL of dithizone (0.02 % dissolved in acetone) mixed with 1 g of Styrofoam.

Characterisation of the sorbent by FTIR spectroscopy confirmed that dithizone was sorbed in its enol form (C-S stretching band at 743 cm^{-1}). The sorption of cadmium ions (in batch equilibrium experiments) was studied as a function of pH, eluent, sorbent dosage and shaking speed. Cadmium sorption increased with increasing pH, attaining a maximum between pH 5 and 8. They established other optimal conditions: 5 mL of 0.2 $mol \cdot L^{-1}$ EDTA (eluent); 100 mg sorbent and 80 rpm shaking speed. Analysis of sorption isotherms based on Freundlich, Langmuir and Dubinin-Radushkevich equations suggested that sorption of cadmium; (i) was slightly suppressed at lower equilibrium concentrations, (ii) occurred mainly via ion exchange and (iii) was highly favourable. Kinetic studies revealed that sorption was achieved within eight minutes ($\geq$ 90 %). Kinetic data was subjected to the Weber-Morris and Lagergren kinetic equations. These equations were satisfied within the first six (6) minutes of agitation only, with correlation coefficients of 0.992 and 0.994, respectively. Thermodynamic studies indicated the endothermic and spontaneous nature of Cd sorption. Lastly, common cations (1:10 concentration) and anions (1:100 concentration) had no significant effect on cadmium sorption, except for Pb(II) that could only be tolerated in 1:2 concentration ratios.

In an earlier study involving polyurethane foam treated with dithizone, Hamza *et al.* (1990) examined the selective detection, quantitative collection, and semi-quantitative determination of trace amounts of bismuth and zinc in aqueous acidic solutions. Their work was predicated on similar studies conducted years earlier in a neutral medium, in which dithizone-impregnated foam was found to not be selective towards zinc. Hamza and his co-workers added a few drops of a saturated sodium sulphite solution to the zinc solution to prevent the oxidation of dithizone to diphenylthiocarbadiazone [$S=C(N=NC_6H_5)_2$]. The latter compound does not react with zinc. To their surprise, they found that in the presence of sulphite ion, zinc was extracted at a much lower pH (1.8), whereas in the absence of sulphite ion extraction of zinc with dithizone occurred in the pH range 4.5 – 6.5. At this low pH, the selectivity of the dithizone foam cubes towards zinc was greatly enhanced. Moreover, the characteristic pink colour of the zinc-dithizonate complex was more pronounced in the presence of sulphite ion. At pH = 1.8 only Cu^{2+} caused interference but could easily be remedied by the addition of a few crystals of sodium thiosulphate.

Diaison resin impregnated with dithizone was used to develop an accurate and precise method for the separation of cadmium, lead and copper in environmental materials and food products (Chwastowska *et al.,* 2008). Tea leaves mixed with Polish herbs and oriental tobacco leaves were reference materials to prove the accuracy of the method.

A selective method was developed for preconcentration and determination of trace amounts of Cu^{2+} from aqueous solution based on the selective sorption-desorption of copper on a column with dithizone immobilised on microcrystalline naphthalene (Shabani *et* al., 2007). Studies were conducted at pH = 1 as copper precipitated as $Cu(OH)_2$ at higher pH values. Many ions did not interfere (even at milligram levels). The sorbed copper was eluted with 4.0 M nitric acid.

Costa *et al.* (2002) also supported dithizone on naphthalene to separate and pre-concentrate five metals – Cd, Cu, Pb, Ni and Zn – from brine samples. All five metals could be quantitatively sorbed at pH ranging from 7.6 to 9.1 and eluted in a single step using 15 mL of 8 M HNO_3 as eluting agent.

Instead of immobilising dithizone on a solid substrate, Rajesh & Manikandan (2008) mixed a known volume of dithizone solution with 10 $mg{\cdot}L^{-1}$ Pb(II) at pH = 9 before loading the sample solution on an Amberlite XAD-1180 column. The reddish-orange lead dithizonate complex was retained on the column and eluted with acetone. The researchers found that heavy metal ions such as Fe^{2+}, Ni^{2+}, Cu^{2+} and Co^{2+} caused significant reduction in the recovery of lead when present at high concentrations ($\geq$ 1000 μg).

Elsewhere dithizone was impregnated onto siliceous mesocellular foam (Zarezade *et al*., 2017), filter paper (Abdullin *et al.,* 1999), admicelles (Hiraide & Shibata, 1998) and polyurethane foam (Rychlovský *et al*., 1993).

Examination of literature reveals few instances where dithizone had been impregnated onto *polymeric resins*. Dithizone-impregnated *polymer resins* have been used mainly for the determination and/or separation of Cu (Dolley & Van der Walt, 2014; Chwastowska *et al.,* 2008; Dolley *et al*., 2006; Rajesh & Manikandan, 2008), Zn (Dolley & Van der Walt, 2014; Chwastowska *et al*., 2008; Dolley *et al.,* 2006) and Pb (Chwastowska *et al.,* 2008; Rajesh & Manikandan, 2008). In only one instance (Chwastowska *et al.,* 2008) was the sorption of Cd onto a dithizone-impregnated polymer reported. Ni and Bi sorption were investigated on naphthalene (Costa *et al.,* 2002) and polyurethane foam (Hamza *et al.,* 1990) respectively. A significant gap in dithizone related studies is the general absence of equilibrium, kinetics, and thermodynamics studies in SPE systems that employ a polymer resin as sorbent. In recent years (post 2010) such studies were conducted on natural zeolite (Mudasir *et al*., 2017), modified zeolite (Shirzadi & Nezamzadeh—Ejhieh, 2017) and chitin (Omar, 2013). An extensive literature survey of dithizone modified SPE systems could not reveal similar studies on Ag, Bi, In or Mn.

CHAPTER 4

Experimental

4.1 Apparatus

Absorbance measurements were performed on a Jenway 7305 spectrophotometer using a quartz cell with path length of 1 cm.

An automatic Orbital Platform Shaker (Labotec model 262) with speed control was used for batch equilibration. For temperature studies, a shaking incubator from Labcon was used.

A Spectro^{TM} ARCOS ICP-OES spectrometer with Smart Analyzer Vision installed software, coupled with a Certac ASX-520 Autosampler was used to determine metal ion concentrations. The operating parameters are listed in Table 4.1:

Table 4.1: Operating parameters of the ICP-OES spectrometer

RF Power	1400 W
Argon Flow	12 L/min
Auxiliary Flow	1.0 L/min
Nebuliser Flow	0.8 L/min
Peristaltic Pump Speed	63 rpm

pH measurements were performed with a Basic 20+ CRISON pH meter calibrated every 20 hours with 4.01, 7.00 and 9.00 standard buffer solutions, respectively.

The mass balance was calibrated weekly using standard weight pieces.

The sorbent was characterised by Fourier-Transform Infrared (FTIR) and Scanning Electron Microscope (SEM) techniques. Vibrational frequencies of functional groups on the unmodified resin (ACG300m) and the modified resin (ACG300m-H_2Dz) were determined with a Spectrum Two® FTIR spectrometer (Perkin-Elmer).

The surface morphology of the sorbent before and after impregnation was studied with a Zeiss Auriga Field Emission Gun Scanning Electron Microscope (FEG-SEM). Sample preparation was done with a Quorum Q150 T ES sputter coater. The sample was coated with an Au-Pd (60:40) film of 10 nm thickness prior to analysis.

A Gilson MINIPULS Evolution peristaltic pump together with a Bio-Rad Model 2110 fraction collector was used in column experiments. The column employed was a customised syringe (Appendix A).

4.2 Reagents and solutions

Amberchrom® CG-300m resin is a styrenic, ester-based polymeric sorbent supplied as white insoluble beads suspended in isopropyl alcohol, purchased from Sigma and Kimix. According to the manufacturer, the resin has a surface area of 700 $m^2 \cdot g^{-1}$, mean pore size 300 Å, porosity 55 – 75 vol. %, bead size (dry particle diameter) 50 – 100 μm and 0.21 grams of dry polymer per wet mL. The percent swelling of Amberchrom® CG-300m in isopropanol is 4 %.

The resin was washed with 0.5 M NaOH before use (as per manufacturer's instruction), followed by multiple washings with deionised water. Washing continued until the pH of the final washing was in the range 6.5 – 7.0. The cleaned resin was dried overnight in an oven at 50 °C and stored in a desiccator before practical use.

All reagents were of analytical or equivalent grade and used without further purification. Deionised water was obtained from a Milli-Q water-purification system.

Diphenylthiocarbazone (dithizone) was a product of Sigma-Aldrich. Purity of dithizone was checked by vigorous agitation with chloroform. The mixture was allowed to separate after agitation – if the chloroform layer remained clear after separation, the dithizone did not require further purification.

Dithizone calibration standards were prepared daily due to the proneness of dithizone to oxidation when exposed to light or air. A 50 mg/L stock solution was prepared by dissolving 2.5 mg dithizone in 100 mL chloroform.

ICP standard solutions (1000 mg/L ± 5) of the various metals in 5 % HNO_3 were used to prepare stock solutions for calibration purposes. These stock solutions were diluted to obtain working solutions of suitable concentration.

Metal ions were obtained from their respective salts, namely $MnSO_4 \cdot H_2O$, $Cu(NO_3)_2 \cdot 3H_2O$, $AgNO_3$, $CoCl_2 \cdot 6H_2O$, In_2O_3, CdO, $NiCl_2 \cdot 6H_2O$, $Bi(NO_3)_3 \cdot 5H_2O$ $SnCl_2 \cdot 2H_2O$, $Pb(NO_3)_2$ and $ZnCl_2$ or $Zn(NO_3)_2 \cdot 6H_2O$. All salts were products of Merck Chemicals (PTY) Ltd., except those of Cd and Bi (BDH Chemicals Ltd.). 1000 $mg \cdot L^{-1}$ stock solutions of each metal ion were prepared in 250 mL volumetric flasks of A-grade quality.

Cd(II) stock solution was prepared by dissolving 0.2856 g of cadmium(II) oxide (CdO) in dilute hydrochloric acid (HCl) or nitric acid (HNO_3) before filling it up to the mark with deionised water. Cu(II) stock solution was prepared by dissolving 0.9505 g of $Cu(NO_3)_2 \cdot 3H_2O$ in deionised water and filled to the 250 mL mark. 0.6045 g In_2O_3 was stirred in warm hydrochloric acid solution until fully dissolved; the solution was quantitatively transferred to a 250 mL flask and filled to the mark with deionised water. 0.5215 g $ZnCl_2$ was dissolved in 250 mL acidified deionised water; alternatively 1.1423 g $Zn(NO_3)_2 \cdot 6H_2O$ was used to prepare 1000 $mg \cdot L^{-1}$ stock solution. Ni(II) stock solution was prepared by dissolving 1.0125 g $NiCl_2 \cdot 6H_2O$ in 250 mL deionised water, while Co(II) stock solution was prepared by dissolving 1.0093 g of its salt in 250 mL deionised water. 0.3996 g of $Pb(NO_3)_2$ was used to prepare its stock solution. 0.9006 g $MnCl_2 \cdot 4H_2O$, 0.3937 g $AgNO_3$ and 0.5803 g $Bi(NO_3)_3 \cdot 5H_2O$ were used to prepare stock solutions of their respective metals.

The pH of the working solutions was adjusted with suitable buffers as follows: 0.2 M KCl/HCl (pH 1 – 2); 0.1 M acetic acid/acetate (pH 3 – 6); KH_2PO_4/K_2HPO_4 (pH 7) and $H_2BO_3/Na_2B_3O_7$ (pH 8 – 10).

All glassware used was soaked in dilute nitric acid and thoroughly rinsed with distilled water before use.

4.3 Procedures

4.3.1 Calibration curves

ICP calibration standards were prepared by suitable dilution of 1000 ppm stock solutions to obtain at least six standard solutions (including blank sample) of appropriate concentrations. Calibration curves were obtained by plotting intensity (cps) against concentration (mg/L). The instrument response for each metal was measured at a minimum of two wavelengths, including the least and most sensitive emission lines.

The calibration curve used for analysis was chosen based on a combination of the following criteria:

- lowest Limit of Detection (LOD);
- lowest background equivalent concentration (BEC);
- accuracy (based on the measurement of a control standard); and
- correlation coefficient (r^2) closest to 1.

In general, for accurate quantitation (i.e., accuracy $\pm$ 2 %), the analyte concentration should be 100 times greater than the LOD (Hou & Jones, 2000). A sample of calibration curves is provided in Appendices B1 – B3 as illustration. Evidently all three curves exhibit excellent linearity, (r^2 > 0.9999), yet have very different LOD and BEC values.

The amount of loaded dithizone was determined by UV-Vis spectroscopy. A 50 mg/L stock solution was suitably diluted with pure chloroform to obtain five calibration standards of concentrations ranging between 2 – 10 mg/L. Pure chloroform was used as blank calibration standard. A calibration curve of absorbance versus concentration (mg/L) was constructed to determine the amount of dithizone loaded onto the modified resin.

4.3.2 Impregnation of Amberchrom® CG-300m

Amberchrom® CG-300m was impregnated with dithizone according to the method proposed by Dolley & Van der Walt (2014). According to this method, the impregnation solution was prepared by dissolving dithizone in sodium hydroxide to obtain an orange-coloured solution (due to the presence of the dithizonate ion, HDz^-). A weighed amount of resin was added to this solution and the resultant slurry was agitated (at 150 rpm) until equilibrium (see Section 5.1.3) was established. The equilibrium mixture was then titrated against concentrated hydrochloric acid until the orange colour turned black/deep purple, at which point the dithizonate ion was converted back to the neutral H_2Dz. The impregnated product was filtered using a funnel fitted with a sintered glass, washed with copious amounts of deionised water, and vacuum-dried in an oven at 50 °C. To determine the loading capacity of the resin, dithizone was stripped off the resin with pure chloroform. The absorbance of dithizone in the eluate was measured at λ = 605 nm. A calibration curve was used to determine the amount of dithizone in the eluate. Optimal impregnation conditions were determined by investigating the following experimental parameters:

- amount of dithizone in the impregnation solution;
- concentration of NaOH;
- agitation time; and
- pH at endpoint.

4.3.2.1 *Dithizone amount*

A 200 mg/L stock solution of dithizone was prepared by dissolving 40 mg of the reagent in 200 mL of 0.5 M NaOH. Varying aliquots of the stock solution were diluted with 0.5 M NaOH to obtain working solutions of various H_2Dz concentrations (10 mg/L – 90 mg/L). Ethanol (and in later experiments, isopropyl alcohol) was added to 'wet' the hydrophobic resin. The concentration of ethanol in 100 mL of working solution was 10 % v/v.

The working solutions were transferred to 250 mL Erlenmeyer flasks where 0.1 g of resin was added to each flask, covered with aluminium foil and the slurry shaken for two hours on a horizontal orbital shaker at a speed of 150 rpm. After two hours, concentrated hydrochloric acid (32 %) was added drop wise to the contents of each flask until one drop turned the orange mixture purplish black. The purplish-black mixture was shaken for a further 15 min and filtered over a sintered glass funnel.

The impregnated resin (green colour) was washed with copious amounts of deionised water and left to dry overnight at ambient room temperature (21 ± 1 °C). The dry, impregnated resin was placed in a sintered glass funnel and washed with 5×10 mL portions of chloroform until no green colour was observed in the last fraction of the eluate (i.e., until the dithizone has been completely desorbed from the impregnated resin).

Eluates were diluted five-fold. The absorbance of each eluate fraction was measured at $\lambda = 605$ nm. The corresponding dithizone concentration was obtained from a calibration curve. Five calibration standards (2, 4, 6, 8 and 10 mg/L respectively) were used to obtain the calibration curve. Chloroform was used as blank.

4.3.2.2 *NaOH concentration*

To determine the effect of NaOH concentration on the impregnation of dithizone, 0.1000 g of resin was mixed with 0.8 mg of dithizone dissolved in 50 mL NaOH/ethanol of various concentrations (0.1, 0.4, 0.5, 0.6 and 1.0 M NaOH respectively). The mixtures were shaken for two hours at 150 rpm, neutralised, and filtered. The impregnated resin was washed and dried as described earlier. The amount of dithizone sorbed onto Amberchrom® CG-300m was determined as described (Section 4.3.2.1) above.

4.3.2.3 *Agitation period*

The time-dependence of dithizone impregnation was studied by equilibrating ~0.1 g resin with 0.8 mg dithizone dissolved in 50 mL of 0.5 M NaOH/ethanol. The slurry was shaken for 30, 45, 60, 75, 90 and 120 min respectively, at 150 rpm. The amount of sorbed dithizone after each time interval was determined as before.

4.3.2.4 *Endpoint pH*

In preliminary experiments the pH of the impregnation solution was adjusted to the same pH value (pH = 2) at the endpoint before it was filtered. To ascertain whether the pH at the endpoint was of any significance, five batches, each containing 0.1000 g of resin with 0.8 mg of dithizone in 0.5 M NaOH/ethanol mixture, were shaken for 60 min at a speed of 150 rpm. After 60 min, each mixture was neutralised and the pH value at the endpoint measured. The amount of sorbed dithizone was determined as described earlier.

4.3.3 Sorption isotherms and kinetics studies

The sorption of metal ions was investigated by the batch technique at ambient temperature (T = 21 ± 1 °C) throughout all experiments. The impregnated resin was prepared freshly prior to each experiment and dried for three to four hours in an oven at 50 °C before use. In all experiments 100 ± 5 mg of the dry impregnated resin was weighed and added to 50 mL of aqueous solution containing a single metal ion. Each aqueous solution contained 5 % v/v isopropyl alcohol to 'wet' the resin for more efficient mixing. The mixture was shaken on the orbital shaker at 150 rpm.

In some experiments where metal sorption seemed to be slow, the resin was used 'wet' as it facilitated more effective sorption of the metal ion onto the modified resin. In these experiments, batches of 100 ± 5 mg Amberchrom® CG-300m in 50 mL dithizone-NaOH solutions were shaken in separate Erlenmeyer flasks. After impregnation, the impregnated resin was filtered, and the funnel flushed with 50 mL of aqueous solution that contained the metal ion. The washings were transferred quantitatively into 50 mL propylene bottles and shaken at 150 rpm.

During equilibrium studies, mixtures were initially solutions shaken overnight (> 12 h), but once the time to reach sorption equilibrium had been firmly established, the agitation period was adjusted accordingly. Shorter periods of shaking were required when 'wet' impregnated resin was used. The effect of the following parameters on sorption equilibrium was investigated:

- initial metal ion concentration;
- pH of the sorption solution;
- temperature; and
- volume-mass ratio (V/m) of impregnation solution to resin.

4.3.3.1 *Initial metal ion concentration*

To study the effect of initial metal ion concentration, solutions varying in concentration were equilibrated with 100 $\pm$ 5 mg of the modified sorbent at known pH. In all experiments (except Cd sorption) the concentration of metal ion was chosen independent of the mole quantity of impregnated dithizone and ranged between 0.25 mg/L – 12 mg/L. Since the amount of H_2Dz impregnated onto Amberchrom® CG-300m was known from previous experiments, [Cd_0] values were chosen to correspond with predetermined Cd^{2+}:H_2Dz mole ratios, *viz*. 1:50, 1:20, 1:10, 1:8, 1:5, 1:4, 1:3, 1:2 and 1:1 respectively. The 1:50 solution, for example, corresponded to a Cd^{2+} concentration of 0.0526 mg/L; the 1:2 solution corresponded to [Cd] = 1.316 mg/L.

Reference solutions of corresponding initial concentrations were prepared. Each reference solution matched the matrix of the working solution, but without sorbent. The concentration of each reference solution was determined by ICP-OES; the value obtained was recorded and used as the initial concentration value (C_0) in subsequent calculations.

After agitation, the sorption mixture was filtered over a sintered glass funnel. The equilibrium concentration (C_e) of metal ion in the filtrate was determined by ICP-OES at suitable wavelengths. For each sample, the mean of three measurements was recorded. The amount of metal ions sorbed at equilibrium (q_e) was calculated using Eq. (2.4).

Sorption data were analysed and fitted to the various isotherms described in Chapter 2. The parameters associated with each isotherm were used for quantitative interpretation of sorption characteristics such as intensity, separation factor, sorption favourability, sorption capacity and to distinguish between physi- and chemisorption mechanisms.

4.3.3.2 *pH of sorption solution*

The effect of pH on metal ion sorption was determined for solutions of known concentration in the pH range 1 – 10, using appropriate buffers. For some metal ions the pH values were limited to ranges cited in literature as favourable for reaction with dithizone. pH studies were conducted at arbitrarily chosen initial concentration values.

4.3.3.3 *Temperature dependence*

The temperature-dependence of sorption of eight (8) metal ions – Ag^{+}, Bi^{3+}, Cd^{2+}, Co^{2+}, Cu^{2+}, Mn^{2+}, Ni^{2+}, Pb^{2+} and Zn^{2+} – was investigated. 100 $\pm$ 0.5 mg resin in 50 mL aqueous solution that contained a known amount of metal ion was agitated in a shaking incubator at 150 rpm. The pH of each solution was kept constant, and temperatures ranged from 10 °C – 25 °C. Experimental data was applied to the van't Hoff Eq. (2.33). Plots of ln K_d versus 1/T (K^{-1}) were constructed and used to derive the values of $\Delta H°$ and $\Delta S°$. The free energy of sorption was calculated by using Eq. (2.36).

4.3.3.4 *V/m ratio*

The effect of *V*/*m* ratio on sorption efficiency was studied for Cd only. Varying quantities of impregnated resin (50 mg, 100 mg, 150 mg, 200 mg, and 250 mg) were contacted with 50 mL Cd^{2+} solutions and shaken for two hours. The pH of each solution was adjusted to pH = 6 with the acetate buffer. The slurry was filtered and the concentration of Cd^{2+} in the filtrate determined by ICP-OES.

Three techniques were employed to study sorption kinetics. In single batch experiments, 200 $\pm$ 5 mg of impregnated resin was added to 100 mL of an aqueous solution containing a metal ion of known concentration. In some experiments 400 ± 5 mg of resin was slurried with 200 mL aqueous solution to ensure a *V*/*m* ratio of 500 was maintained. Depending on the rate of sorption of metal ion, the resin was used in dry or wet condition, and 5 mL aliquots of the supernatant solution were drawn at predetermined time intervals. The length of intervals was contingent upon the rate of sorption of the metal. In some instances, a final aliquot was drawn for analysis after t > 24 h (t_∞). The metal ion concentration in each aliquot was determined by ICP-OES. A drawback of this technique was the difficulty to withdraw homogeneous supernatant aliquots – aliquots contained suspended resin particles and had to be filtered before analysis. Inevitably, the *V*/*m* ratio was altered every time an aliquot was withdrawn.

Each of at least nine Erlenmeyer flasks contained 100 ± 5 mg resin in contact with 50 mL aqueous solution in multi-batch experiments. Aqueous solutions were of identical metal ion concentration and pH. Flasks were removed from the orbital shaker at predetermined intervals, their contents filtered and the residual metal ion concentration in the filtrate determined by ICP-OES.

Given the consistency provided by the dynamic technique, metals with fast kinetics were studied on a column packed with 500 ± 50 mg impregnated resin preconditioned with appropriate buffer. The influent solution contained the metal ion of known concentration. It was pumped through the column at a constant flow rate of 5 mL/min. Eluate fractions were collected every 90 s and their contents analysed.

Kinetic data obtained was applied to various mathematical models, viz. Lagergen pseudo-first order, Ho and McKay pseudo-second order, Weber-Morris, and HPDM.

4.3.4 Separation studies

Binary mixtures of Cd^{2+}-Sn^{4+} and Bi^{3+}-Pb^{2+} and a ternary mixture of Mn^{2+}-Co^{2+}-Ni^{2+} were qualitatively separated on a mini-column (see Appendix A). A customised 10 mL-syringe was packed with 500 ± 50 mg of the impregnated resin. The resin was preconditioned by pumping a buffer solution of appropriate pH through the column. Analyte mixtures that contained known amounts of each metal ion were pumped through the column at a constant flow rate of 5 mL/min using a peristaltic pump. A fractionator was used to collect eluate fractions from the loading step every 90 s. The contents of each fraction were analysed by ICP-OES. A breakthrough curve for each metal ions was constructed by plotting q_t/q_e against the number of eluate fractions.

CHAPTER 5

Results and discussion

This chapter presents the data on the selectivity of the dithizone-impregnated Amberchrom® CG-300m solid-phase extraction system towards ten heavy metals. The optimization of impregnation parameters is reported, followed by the characterisation of the impregnated resin. The sorption of each metal ion onto the modified sorbent is discussed in detail. Graphical illustrations are provided as far as possible. Sorption data of each metal ion is presented and discussed individually – firstly, because single element solutions were used in all studies; secondly, each study presented unique challenges and peculiarities of the metal ion in question. Where possible, challenges have been highlighted, as well as ways in which they were resolved.

5.1 Impregnation of Amberchrom® CG-300m

5.1.1 Dithizone amount

A survey of literature showed the impregnation of various sorbents increased with increasing concentration of extractant until a saturation plateau was reached, at which point the maximum amount of extractant was sorbed on the surface and interior walls of the resin pores. Impregnation of Amberchrom® CG-300m with dithizone showed a similar trend, except no plateau was reached. Instead, with increasing dithizone concentration, a black residue developed in the impregnation solution. After a series of experiments, it was discovered that this soot-like solid was present only when the amount of dithizone in the impregnation solution exceeded 0.8 mg per 100 mg of resin. In other words, this residue was absent at dithizone-resin ratios less than 0.008. Therefore, in all subsequent impregnation experiments, a maximum quantity of 0.8 mg H_2Dz per 100 mg resin was maintained.

5.1.2 NaOH concentration

The concentration of the NaOH sorption solution affected the impregnation capacity of the Amberchrom resin. An inverse relationship was established between the two parameters – impregnation capacity increased with a decrease in concentration of NaOH (Fig. 5.1). However, at [NaOH] < 0.5 M, the formation of a black residue was again prevalent.

Consequently, dithizone was dissolved in 0.5 M NaOH in all subsequent impregnation experiments, similar to the method developed by Dolley & Van der Walt (2014) using Amberlite XAD-8. The amount of dithizone impregnated from a 0.5 M NaOH solution was found to be approximately 2.6 mg/g resin or 32.85 % impregnation (n = 4; RSD = 15.44 %).

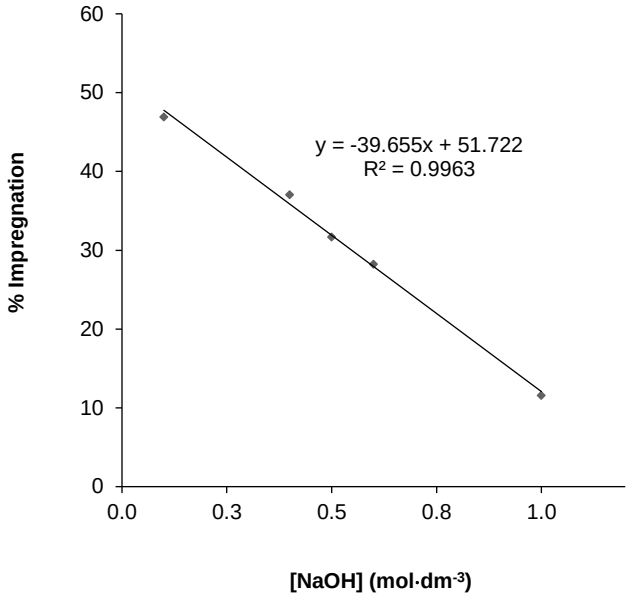

Fig. 5.1: Percent dithizone impregnation decreased with increasing [NaOH]

5.1.3 Agitation period

After 30 min, no significant increase in the amount of sorbed dithizone was evident. An average percentage impregnation of 33.53 % was achieved within this time (Table 5.1).

Table 5.1: Variation of loading capacity of dithizone with agitation period

Time (min)	Absorbance	Concentration (mg/L)	% Impregnation	Mass H_2Dz Impregnated (mg/g resin)
30	0.900	5.241	32.75	2.6
45	0.928	5.405	33.78	2.7
60	0.894	5.205	32.53	2.6
75	0.968	5.641	35.25	2.8
90	0.916	5.335	33.34	2.7
120	1.028	5.994	37.46	3.0

In all subsequent impregnation procedures, the slurry was agitated for a period of no more than 30 min.

5.1.4 Effect of endpoint pH

After titration of the dithizonate ion back to the neutral dithizone form, the pH of the titrant solution at equivalence point was within a narrow range of 2.04 – 2.98 (see Table 5.2). Results showed that the average amount of H_2Dz sorbed (2.6 $\pm$ 0.4 mg/g resin; RSD = 9.10 %) did not vary much within this range. It was therefore not necessary to adjust the pH of sorption solutions once the endpoint had been reached. Two to three more drops of concentrated hydrochloric acid were nonetheless added in all subsequent experiments to ensure the pH at endpoint was sufficiently low.

Table 5.2: Variation of loading capacity of dithizone with endpoint pH

pH	Absorbance	Concentration (mg/L)	% Impregnation	Mass H_2Dz Impregnated (mg/g resin)
2.04	0.922	5.510	34.44	2.8
2.17	0.750	4.466	27.91	2.2
2.49	0.936	5.595	34.97	2.8
2.61	0.820	4.891	30.57	2.5
2.98	0.882	5.267	32.92	2.6

In summary, optimal experimental parameters established for impregnation of Amberchrom® CG-300m with dithizone were as follows:

- 0.8 mg H_2Dz per 100 mg resin;
- 0.5 M NaOH (sorption medium);
- 30 min agitation period; and
- pH < 3 (at endpoint).

Under these conditions, the average amount of dithizone impregnated onto Amberchrom® CG-300m was ~3.2 mg/g resin (n = 14; RSD = 6.97 %). This was more than double the dithizone loading (~1.4 mg/g resin) achieved by Dolley *et al.* (2006) on Amberchrom® CG-71.

5.2 Characterisation of the sorbent

The white beads of Amberchrom-CG300m appeared green after impregnation with dithizone (Appendix H).

SEM images of the Amberchrom resin before and after impregnation are shown in Figs 5.2a and 5.2b, respectively.

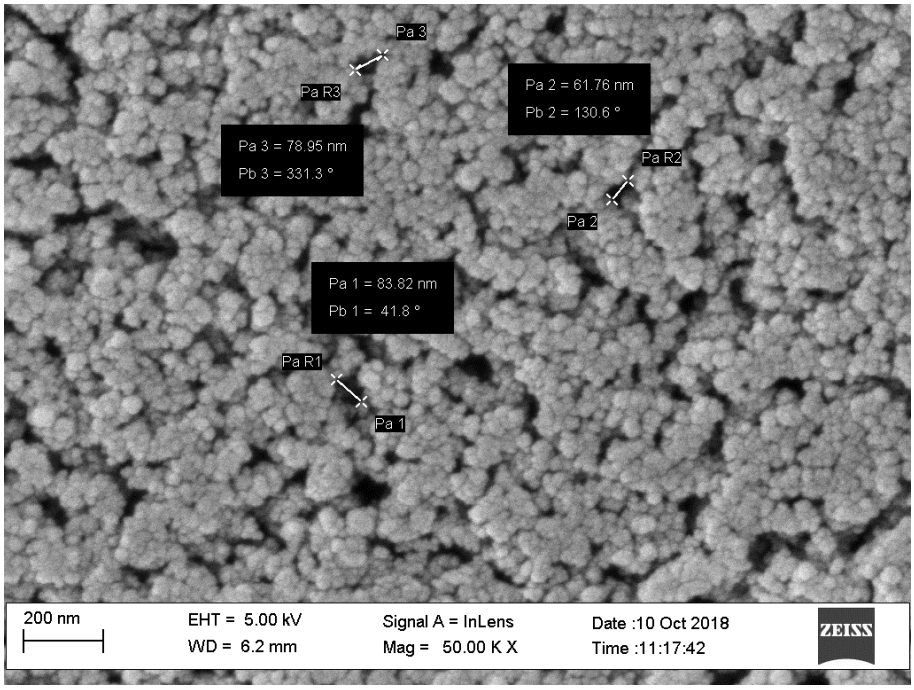

Fig. 5.2a: SEM image of Amberchrom® CG-300m before impregnation

In Fig. 5.2a above the varying pore sizes of the non-activated resin are clearly visible. Measurements derived from multiple images revealed an extensive pore size range, between 35.62 – 94.65 nm. The SEM image of the impregnated resin in Fig. 5.2b shows a significant decrease in pore size; a pore size as small as 11.16 nm was recorded. This decrease in the pore morphology was indicative of the uptake of dithizone within the resin structure.

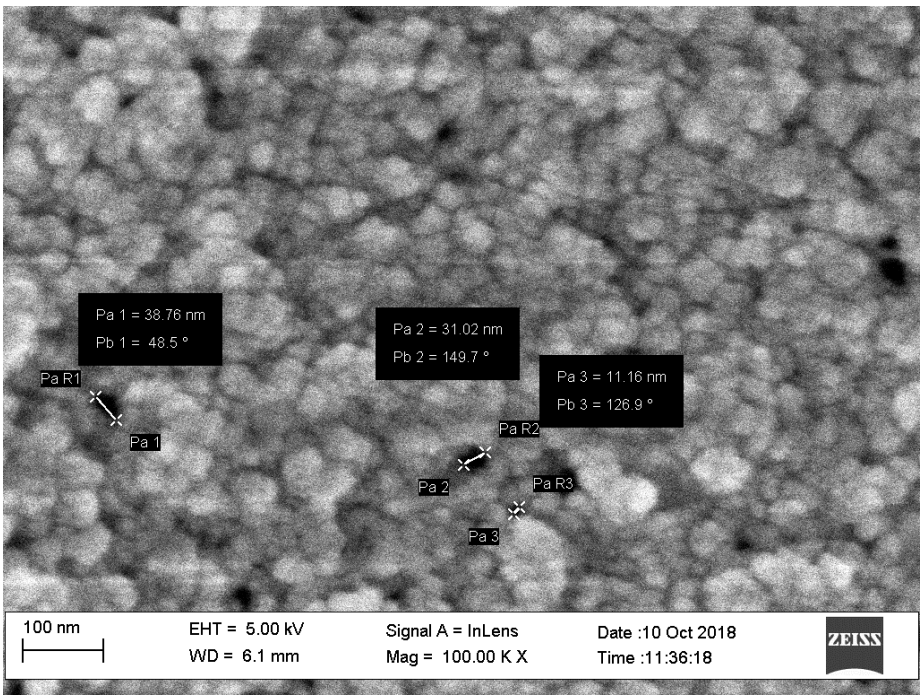

Fig. 5.2b: SEM image of the modified ACG300m-H_2Dz resin

The resin beads were spherical (Fig. 5.3); measured diameters were within the range 50 – 100 Å specified by the manufacturer.

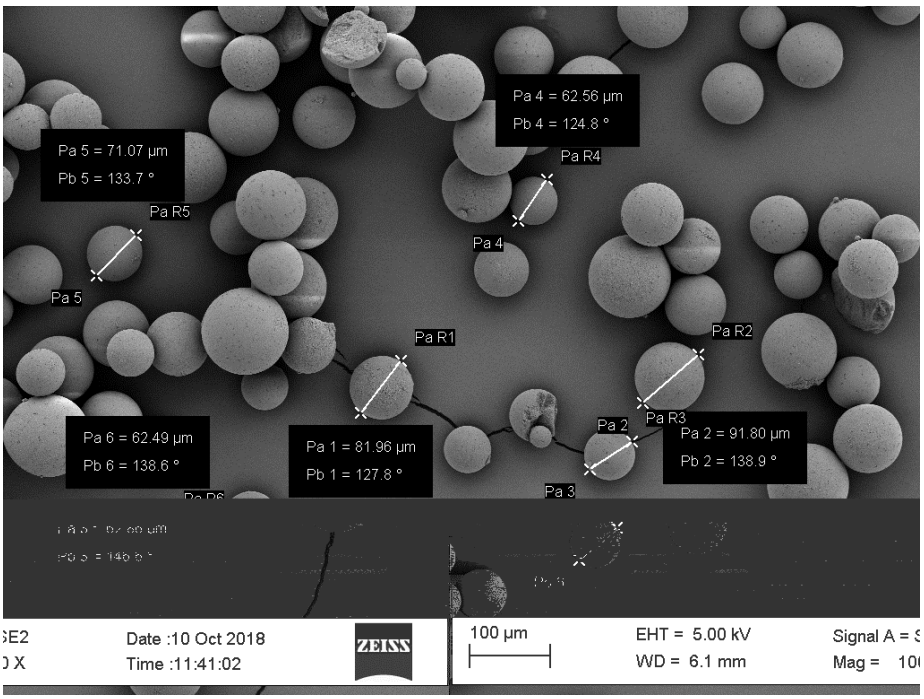

Fig. 5.3: SEM image of ACG300m-H_2Dz showing spherical dimensions of the resin beads

The FTIR spectra of Amberchrom® CG-300m and dithizone in the frequency range 4000 – 400 cm^{-1} are presented in Figs 5.4a and 5.4b respectively. The fingerprint region of dithizone in the sub 1700 cm^{-1} region is complex, mainly because of the many bonds associated with phenyl rings. Labels are assigned to the following characteristic peaks of interest: 1438 cm^{-1} (anhydride N=N stretch), 1215 cm^{-1} (aromatic C-N stretch), 1321 cm^{-1} (aliphatic C-N stretch) and 1139 cm^{-1} (C=S stretch). The intense absorption bands at 1100 – 1400 cm^{-1} are generally characteristic for –SH groups.

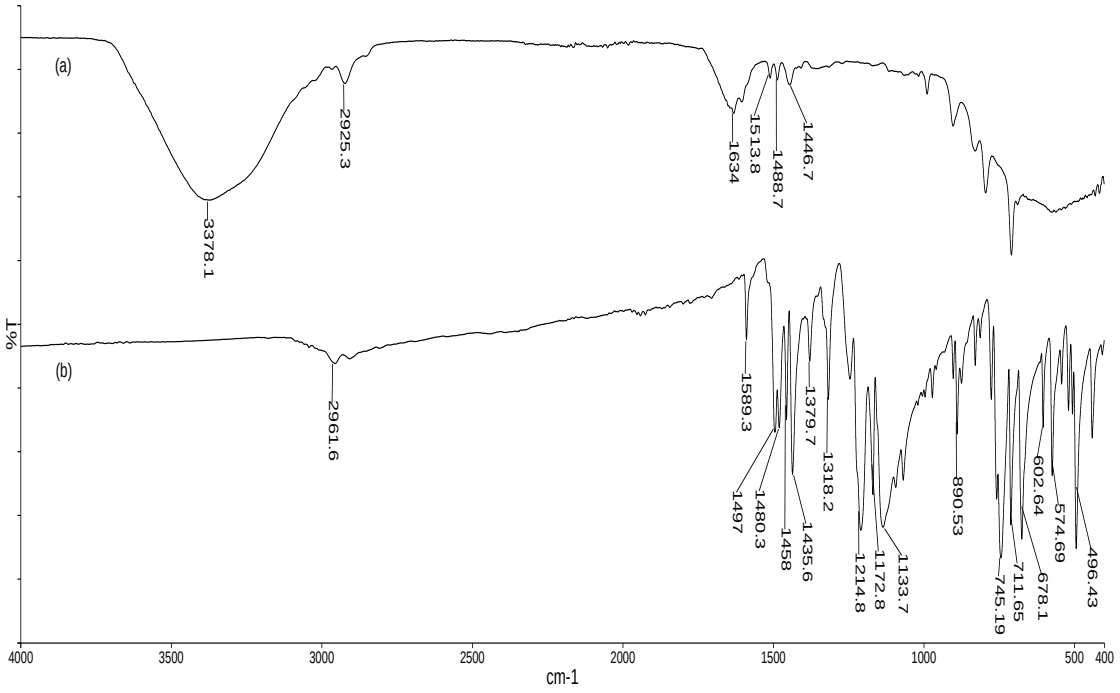

Fig. 5.4: FTIR spectra of (a) unmodified Amberchrom® CG-300m and (b) dithizone in the region 400 – 4000 cm^{-1}

The first significant evidence of modification of the Amberchrom® CG-300m resin with dithizone is the additional peak observed in the higher frequency region of the modified resin around 2975 cm^{-1} (Fig. 5.5b). This peak represents a shift of the characteristic weak band in the dithizone spectrum around 2962 cm^{-1} which is attributable to C–H vibrational absorption. The most noticeable characteristic of the impregnated resin, however, was the broad band that appeared around 1360 cm^{-1}. Generally, absorption bands in the region 1100 – 1400 cm^{-1} represent S–C and S=C–NH stretching vibration modes associated with dithizone (Zargar *et al*.; Salih *et al*., 1998). In particular, peaks that are observed in the spectrum of the modified resin around 1133 cm^{-1} and 1214 cm^{-1} are associated with S=C and C–N stretching, respectively (Ismael, 2014).

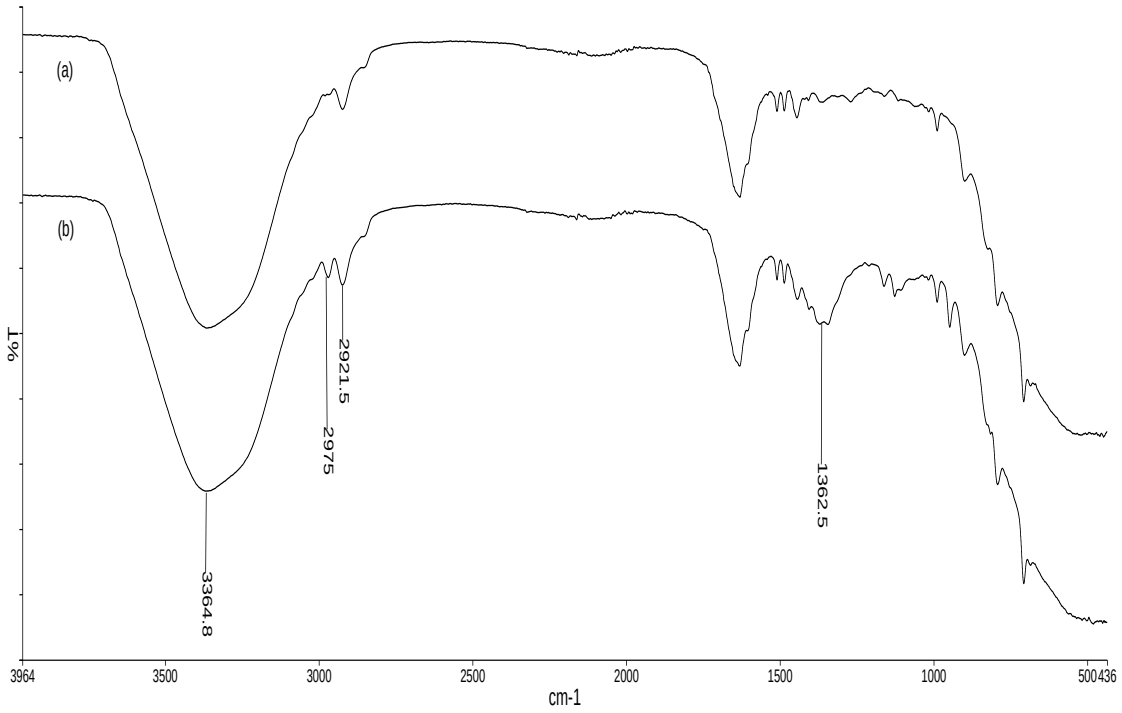

Fig. 5.5: FTIR spectra of (a) ACG300m-dithizone-M (M = metal) and (b) ACG300m-dithizone

The broad band (1100 – 1400 cm^{-1}) was conspicuously absent in FTIR spectra of metal dithizonates (Fig. 5.5a) which suggests coordination was likely to have taken place at the N–C=S functional group of dithizone.

5.3 Sorption equilibrium

The effect of initial ion concentration and pH on the sorption of ten (10) metal ions onto dithizone-impregnated Amberchrom® CG-300m has been studied by batch and column methods. The relationship between the amount of metal ions sorbed at equilibrium (q_e), initial metal ion concentration (C_0) and concentration of the metal ions remaining in the supernatant at equilibrium (C_e) was applied to Langmuir, Freundlich, Temkin and Dubinin-Radushkevich sorption isotherms. The amount of metal sorbed (q_e) onto the functionalized resin was calculated by using Eq. (2.4) (see Section 2.4.1).

5.3.1 Initial metal ion concentration

Concentration-dependence of sorption was studied at appropriate pH values to eliminate the possibility of precipitation. Experimental data obtained for each metal ion is reported individually.

5.3.1.1 *Cadmium*

The effect of initial ion concentration on Cd^{2+} sorption was studied at pH = 6. The amount of Cd^{2+} sorbed increased with increasing initial concentration as shown in Table 5.3.

Table 5.3: Variation of Cd sorption with initial concentration; pH = 6; *T* = 294 K

C_0 (mg/L)	C_e (mg/L)	q_e (mg/g)	% Sorption	K_d	R_L
0.136	0.028	0.054	79.41	1928.6	0.3243
0.250	0.028	0.111	88.80	3964.3	0.2070
0.283	0.028	0.128	90.11	4553.6	0.1874
0.459	0.032	0.214	93.03	6671.9	0.1245
0.565	0.037	0.264	93.45	7135.1	0.1036
0.753	0.051	0.351	93.23	6882.4	0.0798
1.131	0.176	0.478	84.44	2713.1	0.0546
2.293	1.415	0.439	38.29	310.2	0.0277

A plot of q_e versus C_0 (Fig. 5.6) depicts a good linear relationship (r^2 = 0.9998) in the lower concentration range. This is in accordance with Henry's law which states that sorption in a dilute solution is directly proportional to the amount of sorbate species in the solution. At $[Cd^{2+}]_0$ > 1 mg/L, sorption increased at a slower rate until it reached a maximum value of 0.478 mg/g at C_0 = 1.131 mg/L. This value (C_0 = 1.131 mg/L) corresponded well with the predicted value, based on the stoichiometry of Cd^{2+}-dithizone coordination. At $[Cd^{2+}]$ > 1.131 mg/L, sorption ceased as reaction sites were likely becoming more depleted. It can be argued that Cd^{2+} was sorbed in monolayer fashion after which no further interaction occurred between the sorbent and unsorbed ions remaining in the bulk solution. The colour of the Cd-dithizone complex in all experiments that used the resin in dry form, was orange. However, in experiments performed much later using wet resin and higher cadmium concentration, the resin assumed a deep purple colour that was characteristic of the dithizonate complexes formed with Cu^{2+}, Co^{2+}, Ni^{2+} and Pb^{2+}. This anomaly warrants further research.

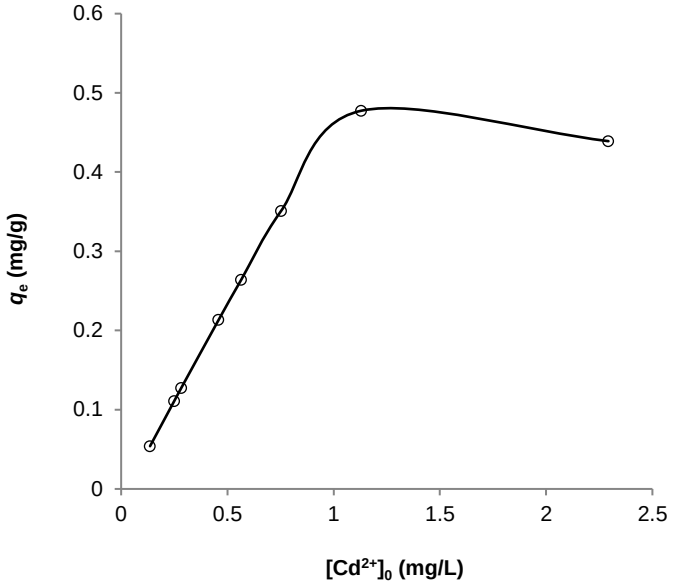

Fig. 5.6: Plot of amount of Cd sorbed (q_e) versus initial concentration (C_0); pH = 6; T = 294 K

Fig. 5.7 illustrates the variation of percent Cd^{2+} sorption with initial concentration. A maximum value of 93.45 % (n = 3; RSD = 3.62 %) was reached at $[Cd^{2+}]$ = 0.565 ppm. Consistent with the argument above, sorption sites became progressively occupied with increasing initial Cd^{2+} concentration so that a smaller percentage of Cd^{2+} ions in the bulk solution found sorption vacancies within the resin structure.

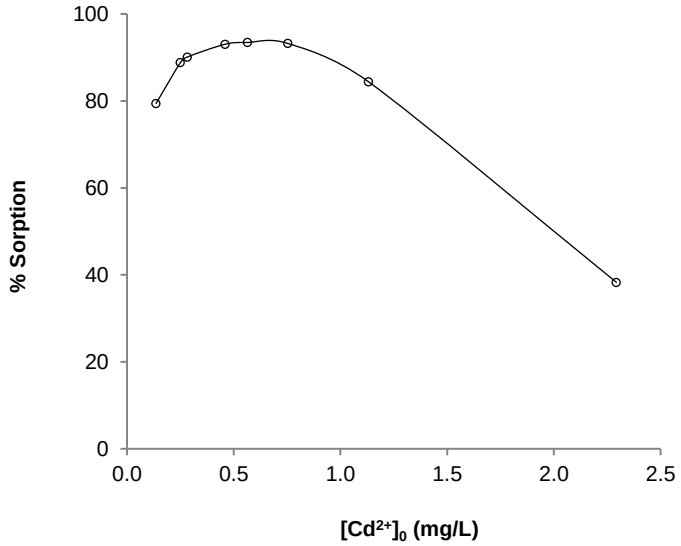

Fig. 5.7: Percent Cd sorbed as a function of initial concentration; pH = 6; T = 294 K

The experimental data was applied to the four isotherms previously identified. Of all the isotherms, the Langmuir isotherm (Fig. 5.8) provided the best fit to the experimental data as the correlation coefficient of its linearly regressed form (r^2 = 0.9810) was the highest, followed by the D-R, Temkin and Freundlich isotherms. This implied Cd^{2+} sorption was driven by a chemical mechanism as opposed to a physical process. In accordance with the basic tenets of Langmuir theory, this confirmed that Cd^{2+} ions sorbed onto the resin beads as a monolayer of ions. Sorption of Cd^{2+} ions occurred at specific homogeneous sites up to a maximum, but once these sites were occupied, no further sorption occurred.

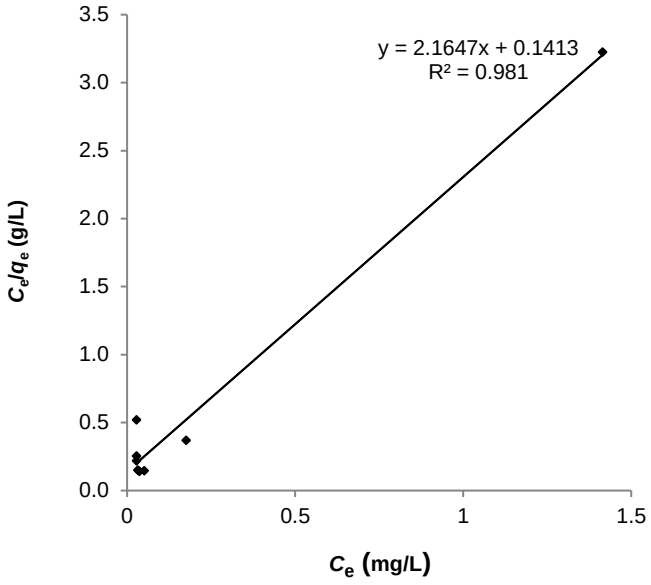

Fig. 5.8: Langmuir isotherm for sorption of Cd onto dithizone-impregnated resin

The Langmuir isotherm is represented by the linear equation:

$$\frac{C_e}{q_e} = 2.1647\, C_e + 0.1413$$

From this equation, the theoretical maximum monolayer sorption capacity (Q_0) and binding strength (K_L) of the impregnated resin were calculated:

$$\frac{1}{Q_0} = 2.1647$$

$$\therefore\ Q_0 = 0.462 \text{ mg/g}$$

This value was in reasonable agreement with the experimental value, $q_{e,\,exp}$ = 0.478 mg/g at the given pH.

$$\frac{1}{Q_0 K_L} = 0.1413$$

$$\therefore K_L = 15.32 \text{ L·mg}^{-1}$$

The Q_0- value had little meaning as there was no point of reference – no other study could be found that reported K_L values associated with Cd sorption onto a dithizone-impregnated sorbent. This value was approximately 47 % larger than the capacity obtained using the unmodified resin. This observation concurred with a previous study (Omar, 2013), in which the mono-layer sorption capacity of ^{60}Co on natural chitin was 12.38, 14.71 and 27.25 mg·g^{-1}, compared to 26.52, 30.20 and 30.58 mg·g^{-1} on dithizone-modified chitin at 27 °C, 35 °C and 45 °C, respectively. Shirzadi & Nezamzadeh-Ejhieh (2017) also found dithizone-modified clinoptilolite nanoparticles showed higher activity for removal of Hg(II) and Pb(II) compared to the raw sorbent, claiming the latter removed metal ions by ion-exchange alone, while the modified resin removed cations by both ion-exchange and complexation processes.

The separation factor, R_L, was calculated using the formula below:

$$R_L = \frac{1}{1 + K_L C_0}$$

Since R_L was in the range 0 – 1 for all $[Cd^{2+}]_0$ values, it followed that sorption onto the modified resin was favourable at all concentrations, accentuating the suitability of the resin for sorption of Cd^{2+} ions from aqueous solution. A summary of the linear regression equations, constants and correlation coefficients of the other isotherms is provided in Table 5.4:

Table 5.4: Summary of linear regression data of Cd sorption isotherms

Isotherm	Regression equation	Correlation coefficient (r^2)	Parameters
Langmuir	$C_e/q_e = 2.1647q_e + 0.1413$	0.9810	Q_0 = 0.462 mg/g K_L = 15.32 L/mg
Temkin	$q_e = 0.088 \ln C_e + 0.4951$	0.6081	K_T = 277.588 L/mg $\frac{RT}{b}$ = 0.088 J/mol
Dubinin-Radushkevich	$\ln q_e = -0.0205\ \varepsilon^2 - 0.439$	0.6065	E = 4.939 kJ/mol X_m = 0.645 mg/g β = 0.0205 mol^2/kJ^2 (6.984 kJ/mol)
Freundlich	$\log q_e = 0.3649 \log C_e - 0.2545$	0.4458	K_F = 0.557 L/mg n = 2.7

5.3.1.2 *Copper*

The concentration dependence of Cu^{2+} sorption was studied in two batch experiments at constant temperature, T = 294 K. pH values were chosen to avoid hydrolysis of Cu^{2+} ions (see Section 5.3.2). In the first experiment, too few data points were obtained for meaningful data analysis, as Cu^{2+} ions were quantitatively sorbed (> 95 %) at pH = 3.86 and $[Cu^{2+}]_0$ < 1.5 mg/L. The experiment was repeated at lower pH and higher concentration range. In both experiments, sorption increased sharply at lower concentrations and tapered off at higher initial concentration (Figs 5.9a and 5.9b) as available reaction sites became saturated.

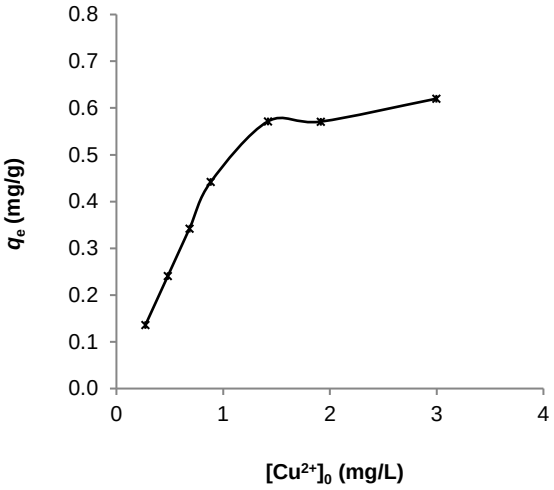

Fig. 5.9a: Isotherm plot of Cu sorption at pH = 3.86

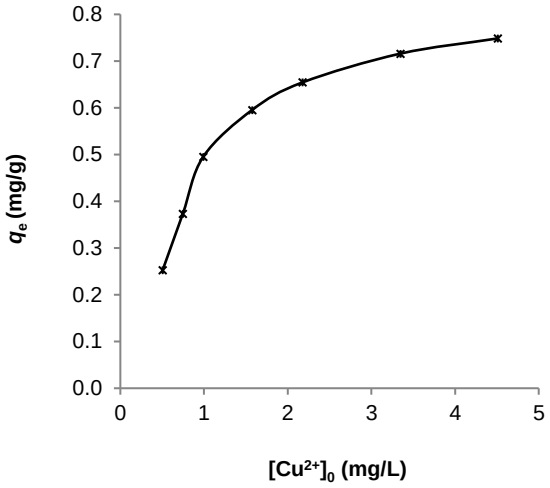

Fig. 5.9b: Isotherm plot of Cu sorption at pH = 2.96

In both experiments, Cu was undetected in the supernatant when initial concentration was less than 1.5 mg/L. Generally, percent sorption decreased with increasing initial concentration. Experimental data is summarised in Table 5.5.

Table 5.5: Experimental data of Cu sorption equilibrium experiments

C_0 (mg/L)	C_e (mg/L)	q_e (mg/g)	% Sorption	R_L	C_0 (mg/L)	C_e (mg/L)	q_e (mg/g)	% Sorption	R_L
0.273	ND[5]	0.137	100.00		0.506	ND	0.253	100.00	
0.482	ND	0.241	100.00		0.747	ND	0.374	100.00	
0.685	ND	0.343	100.00		0.991	ND	0.496	100.00	
0.884	ND	0.442	100.00		1.575	0.384	0.596	75.62	0.0469
1.420	0.277	0.572	80.49	0.0170	2.178	0.869	0.655	60.10	0.0344
1.916	0.774	0.571	59.60	0.0127	3.346	1.914	0.716	42.80	0.0226
2.998	1.758	0.620	41.36	0.0081	4.510	3.013	0.749	33.19	0.0169

A plot of distribution coefficients (K_d) against $[Cu^{2+}]_0$ further illustrates the greater affinity of the sorbent towards Cu^{2+} ions at lower concentration (Fig. 5.10). As a rule, a larger distribution coefficient signifies greater affinity of the resin towards the metal ion.

[5] not detected

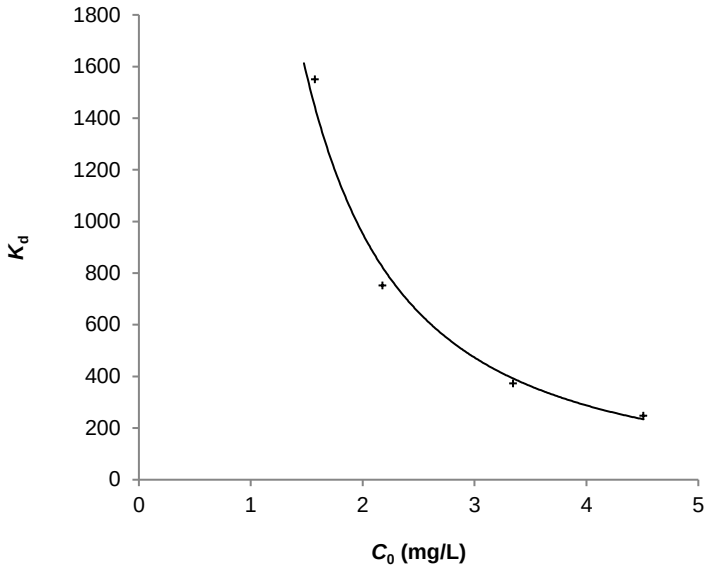

Fig. 5.10: Plot of distribution coefficient (K_d) versus Cu ion initial concentration; pH = 2.96

Data obtained in the second experiment (at pH = 2.96) were fitted to Langmuir, Freundlich, Temkin and D-R isotherms. All isotherms provided excellent approximations of experimental data with correlation coefficients (r^2) greater than 0.9200 in all instances. It is therefore inferred that Cu^{2+} sorption occurred via both physical and chemical sorption processes. The latter was clearly illustrated by observing the distinctive purple colour associated with the $Cu(HDz)_2$ complex.

Table 5.6: Summary of linear regression data of Cu sorption isotherms

Isotherm	Linear regression	Correlation coefficient (r^2)	Parameters
Temkin	$q_e = 0.0747 \ln C_e + 0.6664$	0.9997	RT/b = 0.0747 J/mol K_T = 7.4877 L/mg
Langmuir	$C_e/q_e = 1.2816\ C_e + 0.1877$	0.9995	Q_0 = 0.780 mg/g K_L = 6.83 L/g
Freundlich	$\log q_e = 0.1117 \log C_e - 0.178$	0.9992	K_F = 0.664 L/g n = 9.0
D-R	$\ln q_e = -0.0228\varepsilon^2 - 0.3068$	0.9236	E = 4.683 kJ/mol X_m = 0.736 mg/g β = 0.0228 mol^2/kJ^2 (or 6.623 kJ/mol)

The Temkin isotherm provided the best fit to the recorded data (r^2 = 0.9997), followed by Langmuir (r^2 = 0.9995), Freundlich (r^2 = 0.9992) and D-R (r^2 = 0.9236) isotherms. Statistically there was no difference between the correlation coefficients of the first three isotherms ($p > 0.05$), suggesting there was no clear bias towards either physi- or chemisorption. Fig. 5.11 shows the Temkin isotherm.

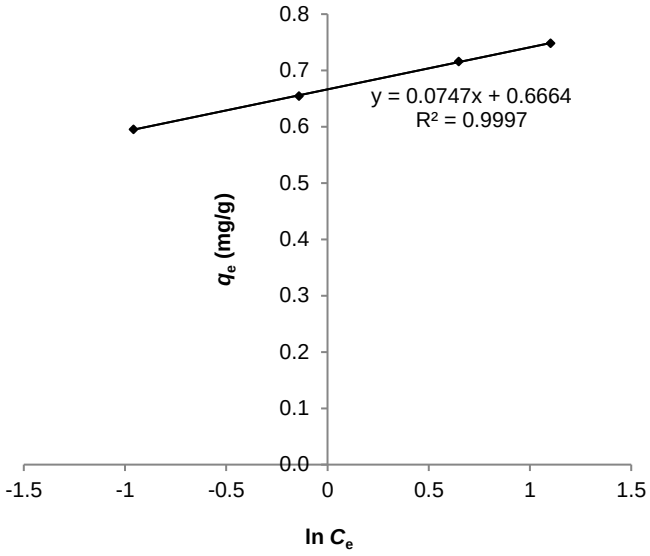

Fig. 5.11: Temkin isotherm of Cu sorption

From the Temkin and D-R isotherms, the values of the sorption energy (β), mean free energy (E) and heat of sorption (RT/b) were less than 20 kJ/mol, typical of sorption characterised by physical processes. Both the Langmuir equation and D-R equations could predict the sorption capacity of the resin with excellent accuracy. From the Langmuir equation, the sorption capacity was determined and found equal to 0.780 mg/g, whereas the D-R equation predicted a theoretical value of 0.736 mg/g. Both these values were reasonably close to the empirical value, Q_0 = 0.749 mg/g. The Langmuir constant (K_L) was equal to 6.830 L/mg. R_L values ranged between 0.2244 (at lowest initial Cu^{2+} concentration) and 0.0314 (at highest initial Cu^{2+} concentration) proving sorption was favourable across the entire concentration range.

It was reasonable to assume that sorption did not occur by a monolayer, but rather multi-layer mechanism as no sorption plateau had yet been reached at [Cu^{2+}] = 4.510 ppm, even though at this concentration the mole amount of Cu^{2+} exceeded the mole quantity of immobilised dithizone by far. The value of n = 9.0 derived from the Freundlich isotherm fell within the range $1 < n < 10$, suggesting that sorption was favourable. In addition, it implied sorption was favourable at low concentration and became less significant at higher concentration, validating experimental evidence that sorption was quantitative at low Cu^{2+} concentration.

5.3.1.3 *Zinc*

0.1 g of resin was contacted with 50 mL aqueous Zn^{2+} solutions in two batch experiments at pH = 5.39 and 5.87, respectively. In the first experiment, eleven batches in the concentration range 0.214 – 8.687 mg/L were used for sorption studies. This experiment revealed that the percent sorption decreased with increasing concentration. At $[Zn^{2+}]_0$ < 0.5 mg/L, Zn^{2+} were sorbed completely. The second experiment was therefore conducted in a smaller range, employing seven batches in the concentration range 0.499 – 3.297 mg/L. In both experiments, the amount of Zn^{2+} sorbed increased sharply at lower initial concentrations, tapering off at higher initial concentrations. Figs. 5.12a and 5.12b represent data of the first experiment only; a similar pattern was observed in the second experiment.

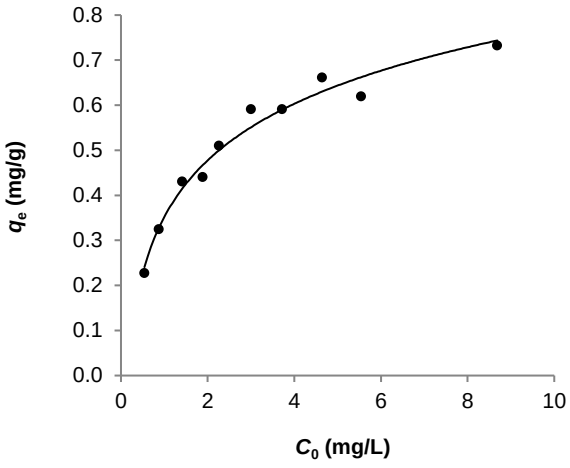

Fig. 5.12a: Isotherm of Zn sorption onto impregnated resin; pH = 5.39

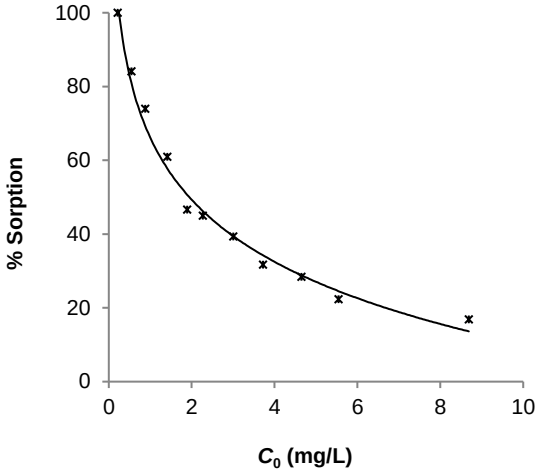

Fig. 5.12b: Percent sorption of Zn as a function of initial concentration; pH = 5.39

Evidently, a sorption plateau has not yet been reached at $[Zn^{2+}]_0$ = 8.867 mg/L, although at this initial concentration, the amount of Zn^{2+} ions in solution exceeded the amount of dithizone loaded onto the resin more than 100-fold. Arguably, sorption occurred via a multi-layered mechanism because of weak attraction forces between hydrated Zn^{2+} complexes and the surfaces of the resin particles. On the other hand, the brilliant dark-pink colour of the resin was evidence of coordination between the Zn^{2+} ions and the impregnated dithizone. Sorption of Zn^{2+} ions was thus likely to occur via a dual mechanism of chemi- as well as physisorption.

Experimental data was fitted to four isotherms. The Langmuir model provided the best fit to the sorption data. Together with its higher correlation coefficient (r^2 = 0.9890), the maximum sorption value obtained from the Langmuir equation (Q_0 = 0.748 mg/g) compared best with the experimetal value, q_e = 0.732 mg/g. Fig. 5.13 shows a plot of the linearised Langmuir isotherm.

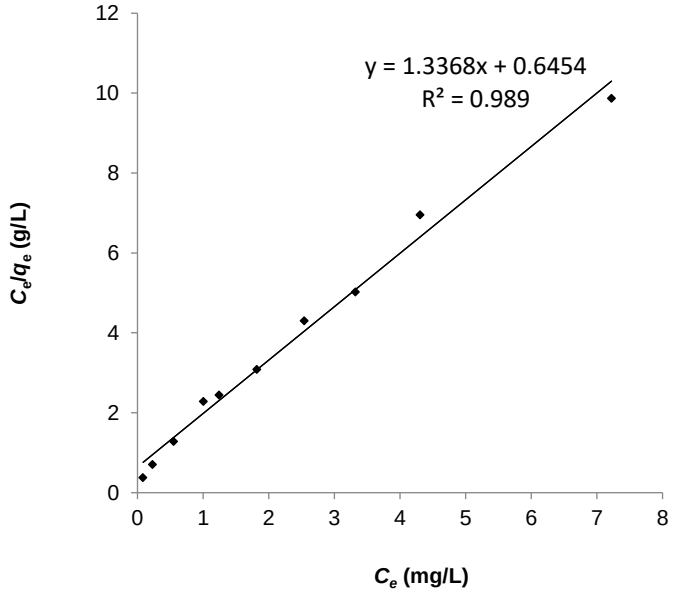

Fig. 5.13: Langmuir isotherm of Zn sorption; pH = 5.39; *T* = 294 K

A summary of the characteristic parameters associated with each of the isotherms is presented in Table 5.7.

Table 5.7: Summary of linear regression data of isotherms of Zn sorption

Isotherm	Linear regression	Correlation coefficient (r^2)	Parameters
Langmuir	$c_e/q_e = 1.3368\ c_e + 0.6454$	0.9890	Q_0 = 0.748 mg/g K_L = 2.0714 L/mg
Temkin	$q_e = 0.1126 \ln c_e + 0.492$	0.9691	RT/b = 0.1126 J/mol K_T = 79.00 L/g
Freundlich	$\log q_e = 0.2571 \log c_e - 0.3332$	0.9674	K_F = 0.4643 L/g n = 3.9
D-R	$\ln q_e = -0.0272\varepsilon^2 - 0.5308$	0.8546	E = 4.287 kJ/mol X_m = 0.588 mg/g β = 0.0272 mol^2/kJ^2 (or 6.063 kJ/mol)

Clearly, the Temkin and Freundlich isotherms also showed good correlation (r^2 > 0.9670) between experimental parameters, supporting the argument that Zn^{2+} ions were sorbed onto the modified resin by physical means. The fitting of the data to the Freundlich isotherm suggested the sorption process was favourable and not restricted to one specific class of sites (El Sofany, 2008).

The value of "*n*" derived from the slope of the Freundlich isotherm was between 1 and 10, meaning sorption of Zn onto the dithizone-modified resin was favourable. Sorption energies derived from Temkin (0.1126 J/mol) and D-R isotherms (4.287 kJ/mol) were less than 20 kJ/mol, supporting the claim that physisorption also contributed significantly to the overall sorption process.

5.3.1.4 *Indium*

The limit of detection (LOD) and background equivalent concentration (BEC) of In^{3+} obtained from its calibration data in earlier experiments were relatively high (LOD > 0.136 mg/L and BEC > 5.02 mg/L). The precision of measurements in the concentration range of working solutions was therefore often problematic (RSD > 5 %).

At times, the problem of unacceptable RSD values was circumvented by running a second triplicate measurements. Accuracy of results was also questionable as values were often significantly suppressed, likely due to hydrolysis of In^{3+}. This will be discussed in greater detail in Section 5.3.2.

Sorption experiments were conducted at least six (6) times using dry impregnated resin, four times at pH ~ 3 and twice at pH ~ 6. In all experiments, the impregnated resin remained green in the lower pH range, but a distinct orange colour was observed in the resin in the pH range 4 – 6.

At lower pH, no clear sorption pattern emerged. At higher pH, sorption increased linearly with increasing initial ion concentration, with no saturation plateau reached (Fig. 5.14). However, it is not clear whether increased "sorption" at pH > 3.3 was because of interaction between the metal ion and sorbent, precipitation in the bulk solution as well as the interior of the resin particles, or both. Nonetheless, the distinct colour observed between pH 4 – 6 confirmed formation of the In(III)-dithizonate complex.

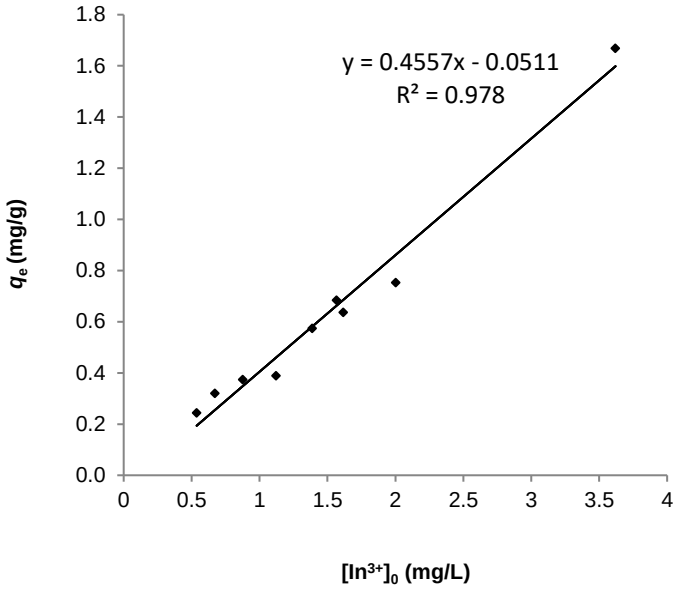

Fig. 5.14: Isotherm of In sorption; pH ~ 6

Curious to see if the same trend would prevail when using the wet impregnated resin, concentration-dependent studies were repeated months later at pH = 3.05 and pH = 4.34, respectively. In the first of these experiments, initial concentration ranged between 4 mg/L – 10 mg/L. In the latter experiment, a range of 3 – 7 mg/L was chosen. Again, no trend emerged at pH < 3.3 (Fig. 5.15).

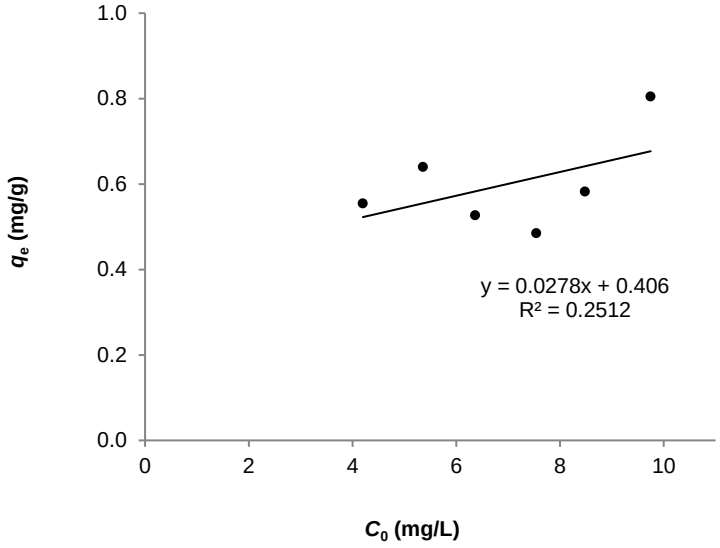

Fig. 5.15: No clear trend prevailed in In sorption; pH = 3.05

In the last experiment (at pH = 4.34), results were consistent with earlier experiments conducted on dry impregnated resin (Fig. 5.16). [One data point (1.409; 0.535) was considered an outlier and excluded from the graph.]

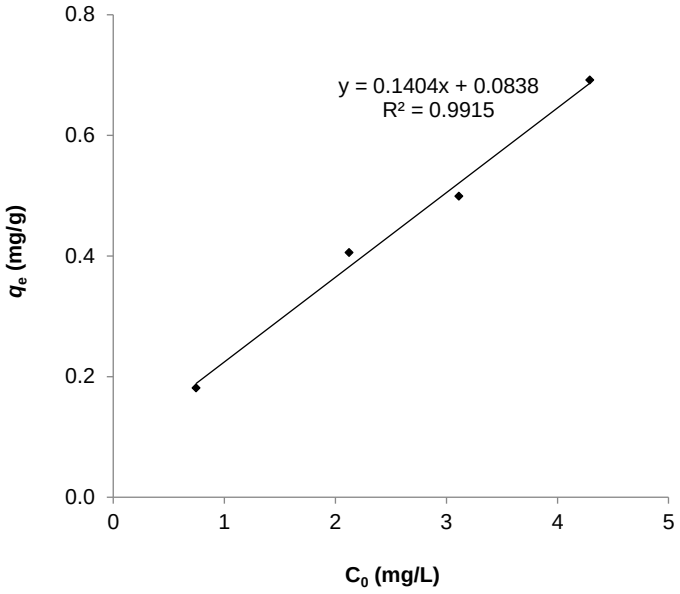

Fig. 5.16: Isotherm of In sorption at pH = 4.34

Notably, the colour of the resin in each batch was purple blue (as opposed to the orange colour that presented in the dry resin), underscoring the real possibility of complex formation. The FTIR spectrum of the ACG-H_2Dz-In complex (Appendix C) confirmed coordination between In^{3+} and the resin. Such coordination was confirmed by Harrowfield *et al.* (1983) when they determined the crystal structure of Indium(III) dithizonate [$In(HDz)_3$] by single-crystal *X*-ray diffraction methods at 295 ± 1 K. Their results indicated the molecular geometry of the complex was trigonal bipyramidal with one ligand unidentate, co-ordinated equatorially through the sulphur [In–S 2.468(3) Å]; the other two were bidentate via *N*,*S* atoms, spanning axial and equatorial positions.

5.3.1.5 *Nickel*

Four batch experiments were conducted under varying conditions. In the first experiment the effect of concentration was investigated at pH = 5.49 and concentration range 0.25 – 4.0 mg/L, using 0.1 g of dry resin. In this instance, 100 % of Ni^{2+} ions were extracted from the 0.25 mg/L solution. Sorption data fitted the Langmuir isotherm best (r^2 = 0.9567), with Q_0 = 0.400 mg/g comparing remarkably well with the experimental value ($q_{e,\,cal}$ = 0.400 mg/g).

The second experiment was conducted at lower pH of 4 and in a slightly higher range (0.5 – 5.0 mg/L), using 0.1 g of wet resin. The colour observed in the resin was a characteristic purple. The amount of Ni^{2+} ions sorbed at the lower pH was less, with maximum sorption (q_e) achieved only 0.331 mg/g. Again, sorption data was best modelled by the Langmuir isotherm (r^2 = 0.8569) and the calculated sorption capacity (Q_0) was equal to 0.400 mg/g. The third experiment was performed at higher pH (8.90) in the presence of 2 % (v/v) tartrate and in the concentration range 1.5 – 4.0 mg/L. Under these conditions, the amount of Ni^{2+} ions sorbed was considerably higher than in the first two experiments, with maximum sorption (0.753 mg/g) obtained at $[Ni^{2+}]_0$ = 4.0 mg/L. This was to be expected since sorption was more efficient at higher pH (see Section 5.3.2). Sorption data fitted the Langmuir isotherm best (r^2 = 0.9854), followed by Temkin (r^2 = 0.8843), Dubinin-Radushkevich (r^2= 0.8737), and Freundlich (r^2 = 0.8574). The maximum sorption capacity was best approximated by the D-R isotherm ($q_{e,\,cal}$ = 0.739 mg/g).

As stated before (see Chapter 3), dithizone has an affinity towards most heavy metals in an alkaline medium containing tartrate ion. Curious to determine the effect of increased tartrate ion on the sorption of Ni^{2+}, the third experiment (pH = 8.90) was repeated, but with 10 % v/v tartrate ion in the sorbate medium. The initial Ni^{2+} ion concentration range was 0.5 – 5.0 mg/L. Sorption at lower concentrations, $[Ni^{2+}]_0$ < 1.2 mg/L, was quantitative (100 %). However, the increased amount of tartrate ion did not significantly alter maximum sorption capacity, found to be 0.666 mg/g. Notably, initial concentration values were significantly suppressed at pH > 4 (even in the presence of tartrate), from which it could be inferred that Ni^{2+} hydrolysed at pH > 4. Fig. 5.17 illustrates how the amount of Ni sorbed varied with initial concentration in the last experiment.

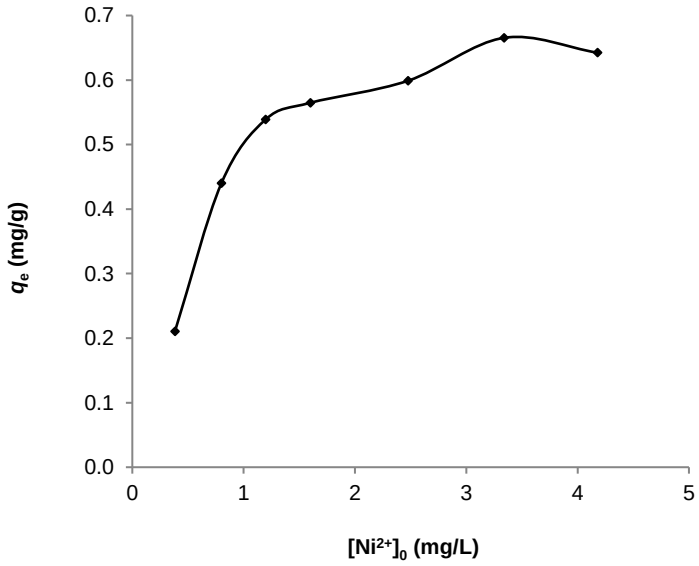

Fig. 5.17: Isotherm of Ni sorption; pH = 8.90

The characteristic parameters associated with the Langmuir, Freundlich, Temkin and D-R isotherms are given in Table 5.8.

Table 5.8: Linear regression data of isotherms of Ni sorption

Isotherm	Linear regression	Correlation coefficient (r^2)	Parameters
Langmuir	$C_e/q_e = 1.5035\ C_e + 0.1238$	0.9972	Q_0 = 0.6651 mg/g K_L = 12.1467 L/mg
Freundlich	$\log q_e = 0.0773 \log C_e - 0.2223$	0.8840	K_F = 0.5994 L/g n = 13
D-R	$\ln q_e = -0.0103\varepsilon^2 - 0.4547$	0.7242	E = 6.9673 kJ/mol X_m = 0.6346 mg/g β = 0.0103 mol^2/kJ^2 (or 9.8533 kJ/mol)
Temkin	$q_e = 0.0533 \ln C_e + 0.6101$	0.6984	RT/b = 0.1126 J/mol K_T = 93.573 kL/mol

The maximum sorption value (Q_0 = 0.665 mg/g) obtained from the Langmuir graph (Fig. 5.18) was in excellent agreement with the experimental value (0.666 mg/g) obtained at $[Ni^{2+}]_0$ = 3.340 mg/L.

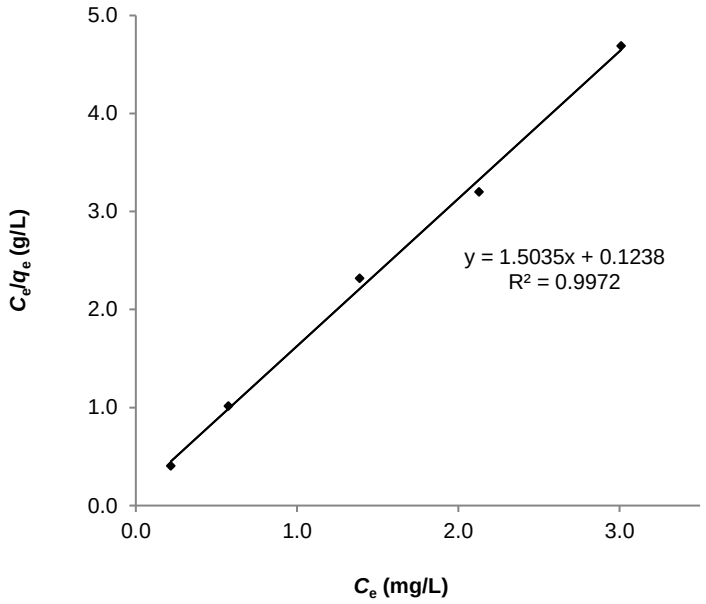

Fig. 5.18: Langmuir isotherm of Ni sorption

The reasonable fit of the linearised Freundlich isotherm (r^2 = 0.8840) suggested sorption occurred via physical processes as well.

5.3.1.6 *Cobalt*

Following initial pH studies, the variation of Co^{2+} sorption with initial concentration was studied at pH = 8.14 (Table 5.9) and pH = 5.79 (Table 5.10), respectively.

Table 5.9: Experimental data of Co sorption; pH = 8.14

C_0 (mg/L)	C_e (mg/L)	q_e (mg/g)	% Sorption
0.489	0.059	0.215	87.93
1.110	0.577	0.267	48.02
1.762	1.291	0.236	26.73
2.327	1.920	0.204	17.49
3.002	2.464	0.269	17.92
3.663	3.150	0.257	14.00
4.937	4.214	0.362	14.64

Table 5.10: Experimental data of Co sorption; pH = 5.79

C_0 (mg/L)	C_e (mg/L)	q_e (mg/g)	% Sorption
0.573	0.480	0.047	16.23
0.946	0.669	0.139	29.28
1.283	0.956	0.164	25.49
1.942	1.598	0.172	17.71
3.421	3.065	0.178	10.41
4.115	3.776	0.170	8.24

Sorption increased with increasing initial Co^{2+} ion concentration in both experiments. In the first experiment, a plot of sorbed amount (q_e) versus initial concentration (C_0) did not produce the graph typically associated with sorption studies. Data of both experiments were nonetheless fitted to the various isotherms, with the Langmuir isotherm providing the best fit in both cases (Fig. 5.19).

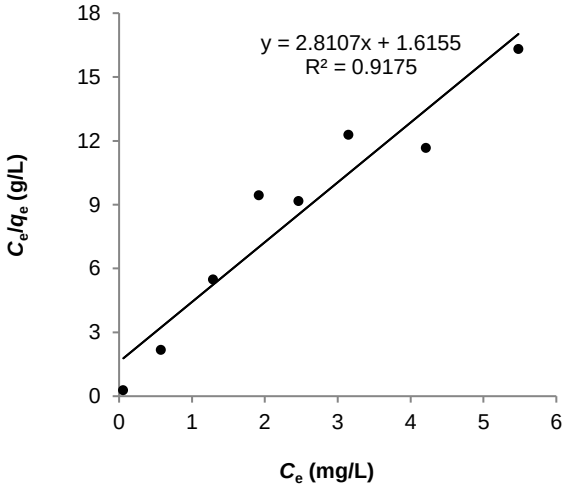

Fig. 5.19a: Langmuir isotherm of Co sorption; pH = 8.14

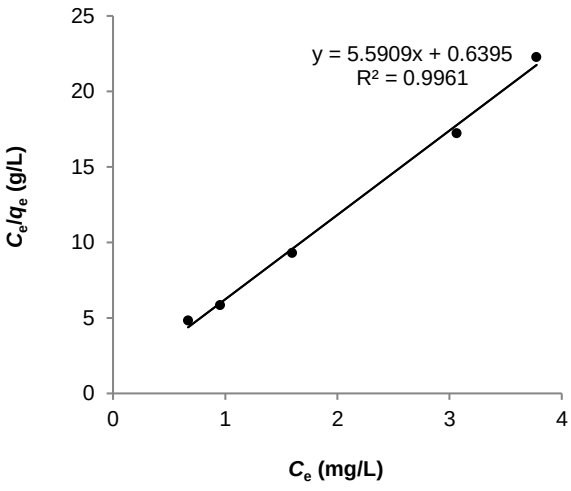

Fig. 5.19b: Langmuir isotherm of Co sorption; pH = 5.79

The maximum sorption capacity (Q_0) obtained from the slope of the Langmuir graph (Fig. 5.19a) was found equal to 0.356 mg/g, in close agreement with the experimental value (q_e = 0.362 mg/g) obtained at $[Co^{2+}]_0$ = 4.937 ppm. In the second experiment, the calculated sorption capacity was equal to Q_0 = 0.169 mg/g, also comparing well with the experimental value (q_e = 0.172 mg/g) attained at $[Co^{2+}]_0$ = 1.942 mg/L.

On surmise that the low sorption rate could be attributable to the dry condition of the resin, a third experiment was conducted with similar experimental parameters (m = 0.1 g, pH = 5.79 and V = 47.5 mL), but using wet resin. Table 5.11 shows the experimental results.

Table 5.11: Experimental data of Co sorption using wet resin

C_0 (mg/L)	C_e (mg/L)	Q (mg/g)	% Sorption
0.653	ND	0.312	100.00
1.078	ND	0.514	100.00
1.463	0.053	0.672	96.38
2.214	0.651	0.745	70.59
3.015	1.228	0.853	59.27
3.900	2.035	0.890	47.82
4.691	2.567	1.013	45.28

Clearly, Co^{2+} ions were more effectively sorbed onto the wet resin. In addition, in the latter experiment, the characteristic purplish-blue of the cobalt dithizonate complex was observed; this was not the case in previous experiments with dry resin. A plot of sorbed amount (q_e) versus initial concentration (C_0) is shown in Fig. 5.20.

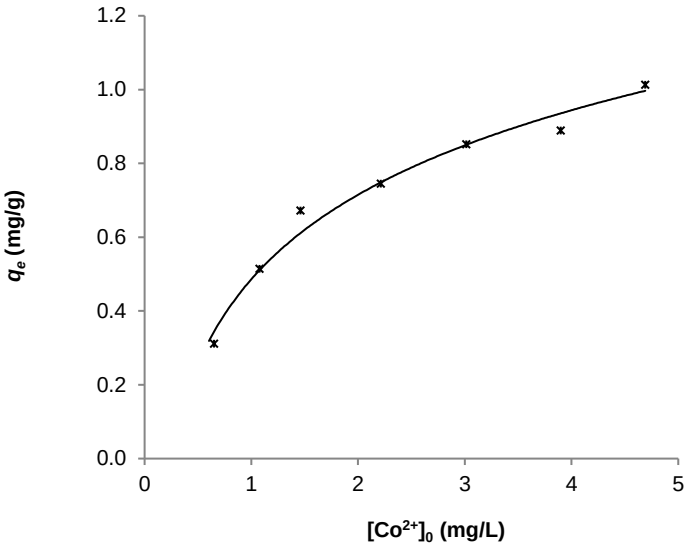

Fig. 5.20: Co sorption as a function of initial concentration onto wet, impregnated resin; pH = 5.79

The Langmuir isotherm modelled the sorption data best (Fig. 5.21).

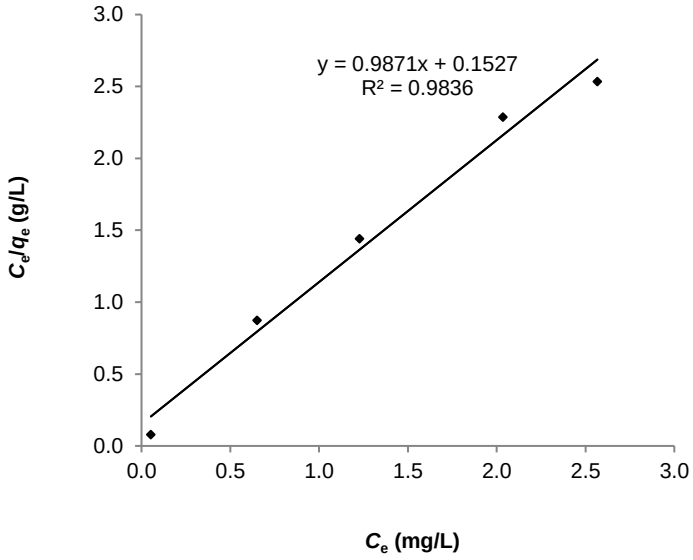

Fig. 5.21: Langmuir isotherm of Co sorption onto wet, impregnated resin

The maximum sorption capacity (Q_0) was obtained from the slope of the Langmuir graph. The calculated value (Q_0 = 1.013 mg/g) was in perfect agreement with the experimental value (Table 5.12).

Table 5.12: Summary of linear regression data of Co sorption; wet, impregnated resin

Isotherm	Linear regression	Correlation coefficient (r^2)	Parameters
Langmuir	$c_e/q_e = 0.9871\ c_e + 0.1572$	0.9836	Q_0 = 1.013 mg/g K_L = 6.465 L/mg
Freundlich	$\log q_e = 0.092 \log c_e - 0.0708$	0.8195	K_F = 0.8496 L/g n = 11
Temkin	$q_e = 0.0741 \ln c_e + 0.857$	0.7742	RT/b = 0.0741 J/mol b = 32.987 K_T = 105.345 kL/mol
D-R	$\ln q_e = -0.0053\ \varepsilon^2 - 0.127$	0.5909	E = 9.713 kJ/mol X_m = 0.881 mg/g β = 0.0053 mol^2/kJ^2

5.3.1.7 *Lead*

In the first of five experiments, 0.1 g of dry resin was equilibrated with 50 mL Pb^{2+} solutions of varying concentration. Reactions proceeded slowly and the characteristic blue-red colour of the lead dithizonate complex was not observed in any of the batches, except for a notable orange tint at concentrations greater than 1.5 mg/L. Subsequently, four experiments were conducted at pH ~ 5.5 using wet resin. The purple-red colour of the formed lead dithizonate became more pronounced with an increasing Pb^{2+} ion concentration. The measured concentration values (C_0) of reference solutions were significantly supressed, intimating the likelihood of precipitation. Furthermore, despite an increase in sorption amount with increasing concentration, no clear trend was observed (Table 5.13).

Table 5.13: Experimental data of Pb sorption on wet, impregnated resin at pH = 5.5

Ref (mg/L)	C_0 (mg/L)	C_e (mg/L)	q_e (mg/g)	% Sorption
0.5	0.072	ND	0.036	100.00
1.0	0.524	ND	0.262	100.00
1.5	1.035	0.342	0.347	66.96
2.0	1.509	0.852	0.329	43.54
2.5	1.933	1.039	0.447	46.25
3.0	2.415	1.288	0.564	46.67
3.5	2.815	2.094	0.361	25.61
4.0	3.354	2.430	0.462	27.55
4.5	3.504	2.672	0.416	23.74

Assuming the low concentrations of the reference solutions were due to hydrolysis of Pb^{2+}, the experiment was repeated at the same pH, but with 10 % (v/v) tartrate ion in the analyte solution. Measurements were more accurate. RSD-values exceeded 5 % but improved at higher concentrations. Again, no clear trend was established (Table 5.14).

Table 5.14: Experimental data of Pb sorption on wet, impregnated resin in the presence of 10 % (v/v) tartrate; pH = 5.5

Ref (mg/L)	C_0 (mg/L)	C_e (mg/L)	q_e (mg/g)	% Sorption
0.5	0.530	0.169	0.181	68.11
1.0	0.938	0.340	0.299	63.75
1.5	1.356	0.712	0.322	47.49
2.0	1.812	0.927	0.443	48.84
2.5	2.247	1.622	0.313	27.81
3.0	2.656	1.884	0.386	29.07
3.5	3.015	2.328	0.344	22.79
4.0	3.474	2.679	0.398	22.88
4.5	3.889	3.030	0.430	22.09

At a fifth attempt, all sample inlet-tubing of the ICP-OES spectrometer were replaced with new ones, as perhaps residue in the tubes interfered with the uptake of Pb^{2+} into the plasma flame. While the same conditions were maintained as in previous experiments, the concentration range was adjusted to 1.510 mg/L – 5.027 mg/L as the equilibrium concentrations at the lower end of the range were too close to the BEC (0.587 mg/L). Samples were shaken for 120 min only. The results of the fifth experiment are presented in Table 5.15. The accuracy of the C_0 values is evident.

Table 5.15: Experimental data of Pb sorption on wet, impregnated resin at pH = 5.5

Ref (mg/L)	C_0 (mg/L)	C_e (mg/L)	q_e (mg/g)	% Sorption	K_d	R_L
1.5	1.510	0.301	0.605	80.07	2008.3	0.1530
2.0	1.999	0.606	0.697	69.68	1149.3	0.1201
2.5	2.547	0.918	0.815	63.96	887.3	0.0967
3.0	3.066	1.336	0.865	56.43	647	0.0817
3.5	3.596	1.778	0.909	50.56	511.2	0.0705
4.0	4.158	2.264	0.947	45.55	418.3	0.0616
5.0	5.027	2.952	1.038	41.28	351.5	0.0515

A plot of q_e versus $[Pb^{2+}]_0$ produced the characteristic curve depicted in Fig. 5.22.

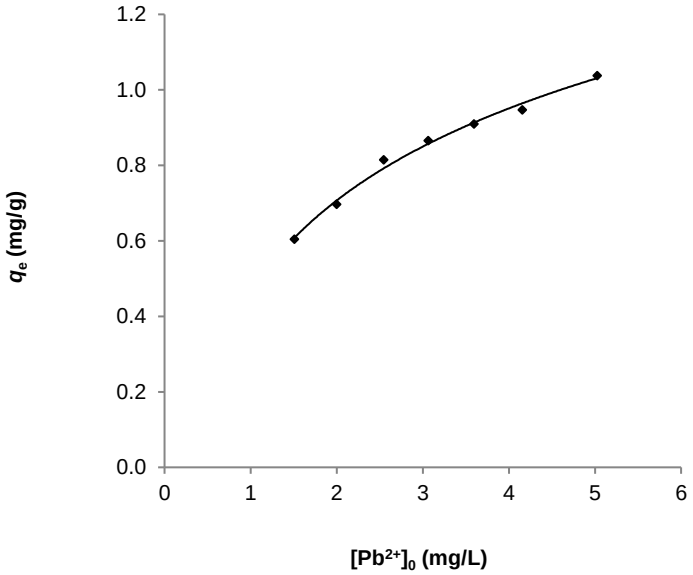

Fig. 5.22: Isotherm of Pb sorption

The Langmuir isotherm provided the best fit to the experimental data (Fig. 5.23).

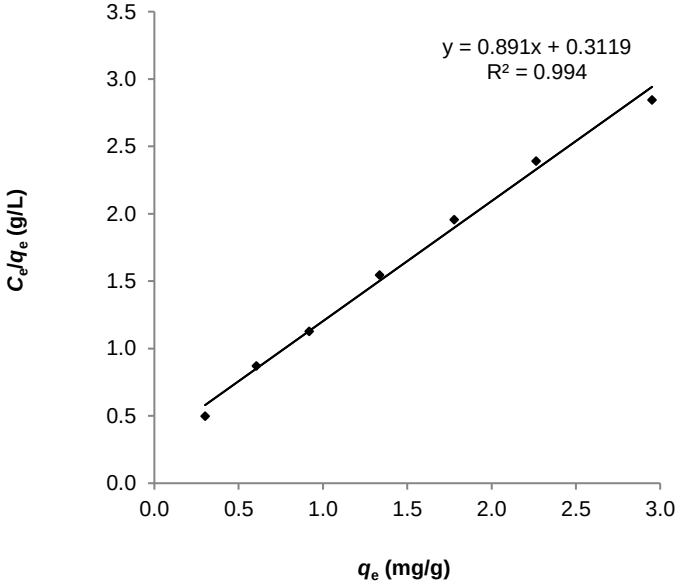

Fig. 5.23: Langmuir isotherm of Pb sorption

The slope ($\frac{1}{Q_0} = 0.891$) of the linearly regressed Langmuir equation indicated that the sorption capacity Q_0 (or $q_{e,\,calc}$) was equal to 1.122 mg/g (*cf.* $q_{e,\,exp}$ = 1.038 mg/g). The Temkin and Freundlich isotherms provided equally reasonable fits to the sorption data (r^2 = 0.9845 and r^2 = 0.9876, respectively). Pb^{2+} sorption could therefore be explained best by monolayer coverage onto an energetically homogeneous surface (Langmuir), but possible interaction between sorbed Pb^{2+} ions and Pb^{2+} ions in the bulk solution could not be ruled out entirely. The complete set of Langmuir, Temkin, Freundlich and D-R isotherms parameters are tabled (Table 5.16).

Table 5.16: Summary of linear regression data of Pb sorption

Isotherm	Linear regression	Correlation coefficient (r^2)	Parameters
Langmuir	$C_e/q_e = 0.891C_e + 0.3119$	0.9940	Q_0 = 1.122 mg/g K_L = 2.8575 L/mg
Freundlich	$\log q_e = 0.2323 \log C_e - 0.0965$	0.9876	K_F = 0.8008 L/g n = 4.3
Temkin	$q_e = 0.1849 \ln C_e + 0.8133$	0.9845	RT/b = 0.1849 J/mol b = 13.22 kJ/mol K_T = 81.3364 L/mol
D-R	$\ln q_e = -0.0396\,\varepsilon^2 - 0.045$	0.8802	E = 3.5533 kJ/mol X_m = 0.9560 mg/g β = 0.0396 mol^2/kJ^2 (or 5.0252 kJ/mol)

5.3.1.8 *Manganese*

The concentration dependence of Mn^{2+} sorption was initially studied using 0.1 g wet resin per 50 mL batch at pH = 8.54 in the presence of 10 % v/v tartrate ion. The Mn^{2+} concentration ranged between 0.5 – 4.0 mg/L. The concentrations of reference solutions were severely depressed, indicating the possibility of precipitate formation. High RSD values (> 7.2 %) at pH > 7 also implied likelihood of hydrolysis, despite the presence of tartrate ions. This was confirmed much later when a few drops of Mn^{2+} solution were added to a buffer solution of pH 8, containing tartrate ions. The solution remained clear initially but turned cloudy after a few minutes.

Preliminary pH studies have shown much better precision in the pH range 3 – 6, thus the experiment was repeated at pH = 4.57. Results of this experiment are shown in Table 5.17. Concentration values of reference solutions were accurate and precise (RSD < 0.9 %). Clearly, Mn remained virtually unsorbed, and no visible colour change could be seen in the impregnated resin over the entire concentration range.

Table 5.17: Experimental data of Mn sorption on wet, impregnated resin at pH = 4.57

Ref (mg/L)	C_0 (mg/L)	C_e (mg/L)	% Sorption
0.5	0.487	0.635	0
1.0	1.009	1.244	0
1.5	1.446	1.494	0
2.0	2.005	1.974	1.55
2.5	2.519	2.411	4.29
3.0	3.075	3.168	0
4.0	3.917	4.403	0

Expecting sorption to be more efficient using the column method (Chwastowska & Kosiarska, 1988), a third experiment was performed. A 2 mg/L solution was pumped through a column packed with 0.5 g resin at a flow rate of 5.0 mL/min. The resin was conditioned with the same buffer that was used in previous batch experiments (pH = 4.57). Eluate fractions were collected every 90 seconds and the amounts of Mn^{2+} ions in each fraction were determined by ICP-OES. Mn^{2+} ions passed through the column "unsorbed". The experiment was repeated at higher pH (pH = 5.92) and once again Mn^{2+} ions were seemingly not sorbed onto the column. When separating Mn^{2+} from a mixture of Co^{2+} and Ni^{2+} ions at pH = 6, breakthrough of Mn^{2+} ions occurred after the third fraction (see Fig. 6.2).

Mindful of work done by Fischer (1933) that revealed manganese reacted with dithizone in its lowest valency only, SO_2 was bubbled through the influent as reducing agent; this did not alter the sorption behaviour of Mn^{2+} either. The lack of affinity of the resin towards Mn contradicted claims by Costa *et al.* (2002) that dithizone does coordinate with Mn(II). The FTIR spectrum of the ACG-H_2Dz-Mn complex (Appendix D) shows no additional peaks or band shifts, confirming the absence of Mn-H_2Dz coordination.

5.3.1.9 *Silver*

Ag^+ is sensitive to dithizone in acid medium (White, 1935). Chwastowska and Kosiarska (1988) successfully extracted Ag^+ in acid medium onto a DVB substrate chemically modified with dithizone under static conditions. Considering these facts, a preliminary batch experiment was conducted at pH = 3. Initial concentrations varied between 0.5 – 5.0 mg/L. At $[Ag^+] \leq 2.5$ mg/L, no Ag^+ was detected in the supernatant at λ = 328.068 nm, which happened to be the most suitable emission line (r^2 = 0.9999; DL = 0.002 mg/L; BEC = 0.315 mg/L). To obtain more data points, the concentration range was subsequently adjusted upward between 4.104 – 11.324 mg/L. RSD values were excellent (< 2 %), as all values in the chosen concentration range were sufficiently higher than the BEC. The results of the latter experiment are presented in Table 5.18.

Table 5.18: Experimental data of Ag sorption

C_0 (mg/L)	C_e (mg/L)	q_e (mg/g)	% Sorption	K_d	R_L
4.104	0.136	1.984	96.69	14588.2	0.0310
5.274	0.782	2.246	85.17	2872.1	0.0243
6.653	1.383	2.635	79.21	1905.3	0.0193
7.608	2.061	2.774	72.91	1346	0.0169
8.827	3.247	2.790	63.22	859.3	0.0146
9.967	4.681	2.643	53.04	565	0.0130
11.324	6.774	2.275	40.18	336	0.0115

$0 < R_L < 1$ proved that sorption was favourable over the entire range. Noteworthy was the exceptionally high values of the distribution coefficient (K_d) at lower concentrations, indicative of the high selectivity of dithizone for Ag^+ in acid medium. It is a known fact that metal ions with low charge, such as Ag^+, can form strong covalent bonds (Persson, 2010). The affinity towards Ag^+ was later confirmed in dynamic studies in which Ag^+ was so strongly retained on the column that a 5.0 M nitric acid solution could not desorb it, in accordance with similar findings by Chwastowska and Kosiarska (1988). Judging by the yellow-brown colour of the resin in batch and column methods, there was chemical interaction between Ag^+ and dithizone.

A plot of sorbed quantity (q_e) versus time (t) (Fig. 5.24) showed a maximum value attained at $[Ag^+]_0$ = 8.827 mg/L before decreasing towards the upper end of the concentration range.

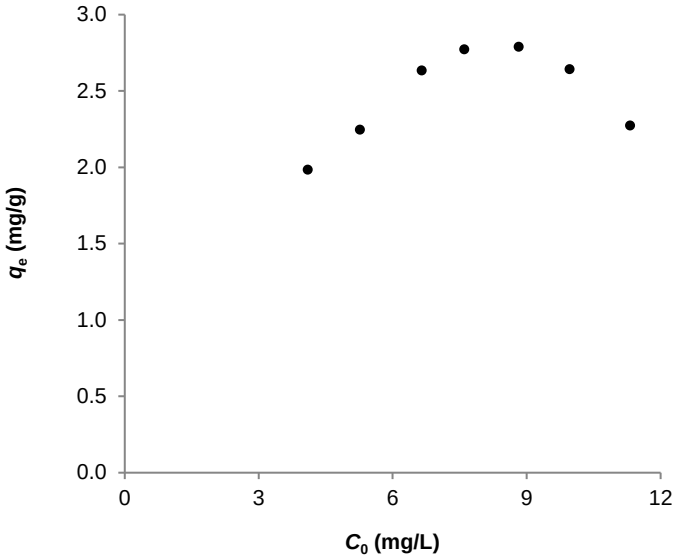

Fig. 5.24: Isotherm of Ag sorption

Reaction sites apparently became exhausted at $[Ag^+]_0$ = 8.827 mg/L. At this concentration, the molar amount of Ag^+ exceeded the molar quantity of dithizone molecules by more than 3.4 times, after which the large number of metal ions in solution obscured further access to the already depleted sites. Given that Ag^+ was known to form secondary dithizonate complexes of the form Ag_2Dz, the anomaly regarding reaction stoichiometry implied Ag^+ sorption was not solely due to chemical reaction, but a significant extent of physisorption as well. This was corroborated by the Freundlich isotherm (r^2 = 0.9270) providing a reasonable fit to experimental data, second to the Langmuir isotherm (r^2 = 0.9973) (Fig. 5.25).

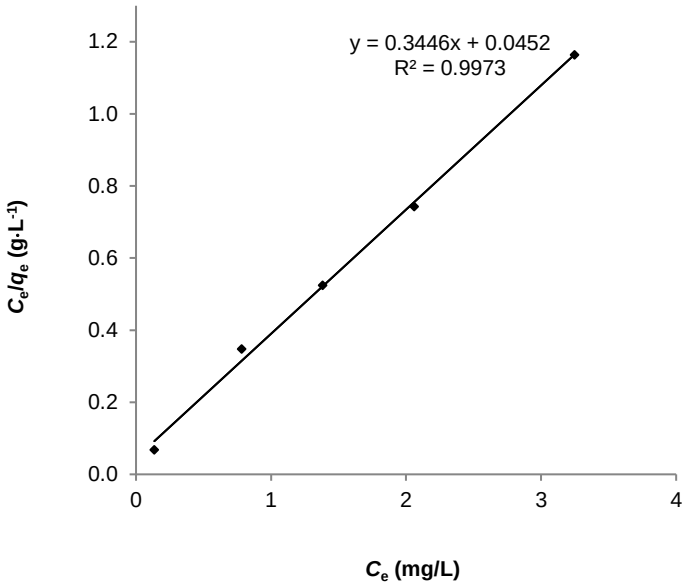

Fig. 5.25: Langmuir isotherm of Ag sorption

From the slope of the Langmuir isotherm, $\frac{1}{Q_0}$ = 0.3446. Thus, the calculated value of the sorption capacity, Q_0 = 2.902 mg/g. This value corresponded well with the experimental value, $q_{e,\,exp}$ = 2.790 mg/g. The Langmuir constant (K_L), together with parameters associated with other isotherms, are presented in Table 5.19.

Table 5.19: Linear regression data of Ag sorption

Isotherm	Linear regression	Correlation coefficient (r^2)	Parameters
Langmuir	$c_e/Q_e = 0.3446c_e + 0.0452$	0.9973	Q_0 = 2.902 mg/g K_L = 7.6237 L/mg
Freundlich	$\log q_e = 0.117 \log c_e - 0.3918$	0.9270	K_F = 2.4649 L/g n = 8.5
Temkin	$q_e = 0.2766 \ln c_e + 2.4866$	0.9138	RT/b = 0.2766 J/mol b = 8.837 kJ/mol K_T = 8.0215 kL/mol
D-R	$\ln q_e = -0.0116\ \varepsilon^2 + 0.9807$	0.7662	E = 6.5653 kJ/mol X_m = 2.6663 mg/g β = 0.0116 mol^2/kJ^2 (or 9.2848 kJ/mol)

5.3.1.10 *Bismuth*

The static method was used to study the sorption of Bi^{3+} over the concentration range 0.355 mg/L – 5.342 mg/L. From results obtained in preliminary experiments, a pH-value of 4.39 was arbitrarily chosen for concentration-dependent studies. At this pH, no clear trend was observed in the sorption behaviour of Bi^{3+}; in fact, the spread of data points was erratic. In addition, no Bi^{3+} could be detected in the supernatant at $[Bi^{3+}]_0 < 3.022$ mg/L. This observation could be wholly attributed to the hydrolysis of Bi at this pH. The experiment was repeated under dynamic conditions using influent solution of concentration 2.785 mg/L, pumped through a column packed with 0.5 g resin preconditioned at pH = 3.85. Under these conditions Bi^{3+} was quantitatively held onto the column, undetected in all of 23 eluent fractions of 7.5 mL each. The resin bed had a rusty brown colour.

A third experiment was conducted under static conditions in even more acidic medium (0.01 M HNO_3, pH = 1.92) and higher concentration range (1.135 mg/L – 9.067 mg/L). Sorption was quantitative at $[Bi^{3+}]_0 < 3$ mg/L; results are presented in Table 5.20.

Table 5.20: Experimental data of Bi sorption using the static technique

C_0 (mg/L)	C_e (mg/L)	q_e (mg/g)	% Sorption	K_d	R_L
1.135	ND		100.00		0.2035
1.835	ND		100.00		0.1365
2.802	0.041*	1.381	98.54	33671	0.0938
3.320	0.770	1.275	76.81	1656	0.0803
4.210	1.309	1.451	68.91	1108.1	0.0644
5.705	2.274	1.716	60.14	754.4	0.0484
7.744	4.374	1.685	43.52	385.2	0.0361
9.067	5.592	1.738	38.33	311	0.0310

(*Large RSD value indicated uncertainty of measurement)

The linearly regressed Langmuir isotherm (Fig. 5.26) provided an excellent fit to experimental data.

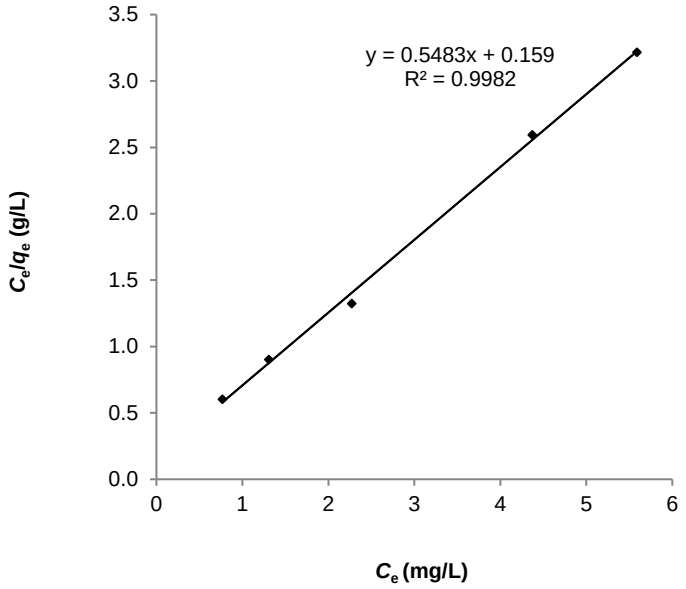

Fig. 5.26: Langmuir isotherm of Bi sorption

The maximum sorption capacity was determined as before, Q_0 = 1.824 mg/g, comparing well with the experimental value, $q_{e,\,exp}$ = 1.738 mg/g. As in some other experiments in this study, the D-R isotherm (Fig. 5.27) provided an even better prediction of the sorption capacity, viz. $q_{e,\,calc}$ = 1.752 mg/L.

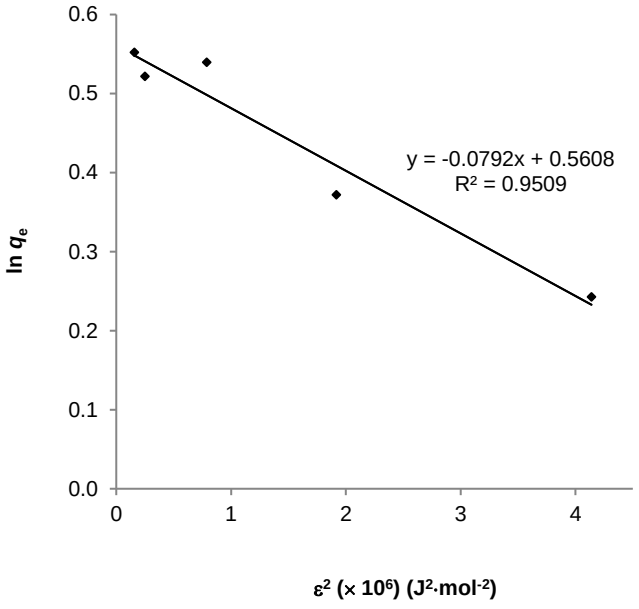

Fig. 5.27: D-R isotherm of Bi sorption

All parameters associated with the relevant isotherms are presented in Table 5.21.

Table 5.21: Linear regression data of Bi sorption

Isotherm	Linear regression	Correlation coefficient (r^2)	Parameters
Langmuir	$C_e/q_e = 0.5483C_e + 0.159$	0.9982	Q_0 = 1.824 mg/g K_L = 3.4485 L/mg
D-R	$\ln q_e = -0.0792\ \varepsilon^2 + 0.5608$	0.9509	E = 2.5126 kJ/mol X_m = 1.752 mg/g β = 0.0792 mol^2/kJ^2 (or 3.5533 kJ/mol)
Temkin	$q_e = 0.2254 \ln C_e + 1.3912$	0.8419	RT/b = 0.2254 J/mol b = 10.884 kJ/mol K_T = 0.4792 kL/mol
Freundlich	$\log q_e = 0.1496 \log C_e + 0.1413$	0.8375	K_F = 1.3845 L/g n = 6.7

In summary, maximum sorption capacity of Ag and Bi were the highest among the metals studied (2.790 mg/g and 1.738 mg/g, respectively). The order of sorption capacity of metals in this study was as follows:

Ag^+ (2.790 mg/g) > Bi^{3+} (1.738 mg/g) > Pb^{2+} (1.038 mg/g) > Co^{2+} (1.013 mg/g) > Cu^{2+} (0.7490 mg/g) > Zn^{2+} (0.7320 mg/g) > Ni^{2+} (0.6660 mg/g) > Cd^{2+} (0.4780 mg/g) > Mn^{2+} (unsorbed)

Sorption capacity of metals was determined at varying initial metal ion concentration and pH. In view of this, the sorption capacities of metals at the same pH are compared below (initial concentrations are shown):

pH ≅ 3: Cu^{2+} (4.51 mg/L; 0.73 Å) < Bi^{3+} (9.067 mg/L; 1.03 Å) < Ag^+ (8.827 mg/L; 1.15 Å)

pH ≅ 6: Mn^{2+} (unsorbed; 0.67 Å *ls*; 0.83 Å *hs*) < Cd^{2+} (1.131 mg/L; 0.95 Å) < Zn^{2+} (8.867 mg/L; 0.74 Å) < Co^{2+} (4.937 mg/L; 0.65 Å *ls*; 0.75 Å *hs)* < Pb^{2+} (5.027 mg/L; 1.19 Å)

pH > 8: Cd^{2+} (1.131 mg/L; 0.95 Å) < Ni^{2+} (3.340 mg/L; 0.69 Å *ls*)

No clear correlation between sorption capacity and ionic radius is evident.

Except for Cu, the Langmuir isotherm fitted sorption data of all metals best. It should be noted for Cu that correlation coefficients (r^2) for linearly regressed Temkin, Langmuir and Freundlich isotherms were greater than 0.9990 For Cd sorption, the Langmuir isotherm was the only isotherm that fitted the experimental data.

The Freundlich isotherm proved a credible model for sorption of all metals except Cd; lowest r^2-values (> 0.8200) were recorded for Ni and Co. A summary of the percent sorption of the metals investigated is presented in Table 5.22.

Table 5.22: Summary of percent sorption of heavy metals studied

	% Sorption
Ag	100 % at C_0 < 2.5 ppm; 96.69 % at C_0 = 4.104 ppm, pH =3
Bi	100 % at C_0 < 2.8 ppm; 98.54 % at C_0 = 2.802 ppm, pH = 1.92
Cd	97.61 % at C_0 = 1.131 ppm, pH = 8
Co	100 % at C_0 < 1.4 ppm; 96.38 % at C_0 = 1.463 ppm, pH = 5.79
Cu	100 % at C_0 < 1.0 ppm; 80.49 % at C_0 = 1.420 ppm, pH = 2.96
Mn	4.29 % at C_0 = 2.519 ppm; pH = 4.57
Ni	100 % at C_0 < 1.2 ppm; 81.80 % at C_0 = 1.198 ppm, pH = 8.90
Pb	80.07 % at C_0 = 1.510 ppm, pH = 5.5
Zn	100 % at C_0 < 0.5 ppm; 96.21 % at C_0 = 0.791 ppm, pH = 5.39

5.3.2 pH dependence

The pH-value of the sorbate solution affects the surface charge and metal binding sites of the sorbent (Fu *et al*., 2018). In addition, changes in the pH of the sorbate solution affect the degree of ionisation of functional groups and chemical speciation of the sorbate during sorption. Bilba *et al.* (1997) postulated that the sorption capacity for different ions changes with the ionic strength and pH of the solution. Dithizone is not a selective reagent at moderate to high pH values. However, its selectivity at lower pH values can be increased by adding a complex forming agent or masking agent to the aqueous solution (Hamza *et al*., 1990). In alkali medium, it is advisable to conduct experiments in the presence of citrates or tartrates to prevent the precipitation of many metals (May & Hoffman, 1948). Hydrolysis of metal ions becomes significant at a pH range of approximately 7.5 – 8.5.

Important results of pH-dependence of sorption of each metal ion are discussed in detail in the sections hereafter.

5.3.2.1 *Cadmium*

Sorption from a solution of lower Cd^{2+} concentration (C_0 = 0.141 mg/L) increased with an increase in pH until it reached a maximum capacity of 0.057 mg/g at pH = 4. Sorption from a solution of higher Cd^{2+} concentration (C_0 = 1.131 mg/L) increased rapidly at lower pH before reaching a maximum capacity of 0.551 mg/g at pH = 8. The results are presented in Fig. 5.28.

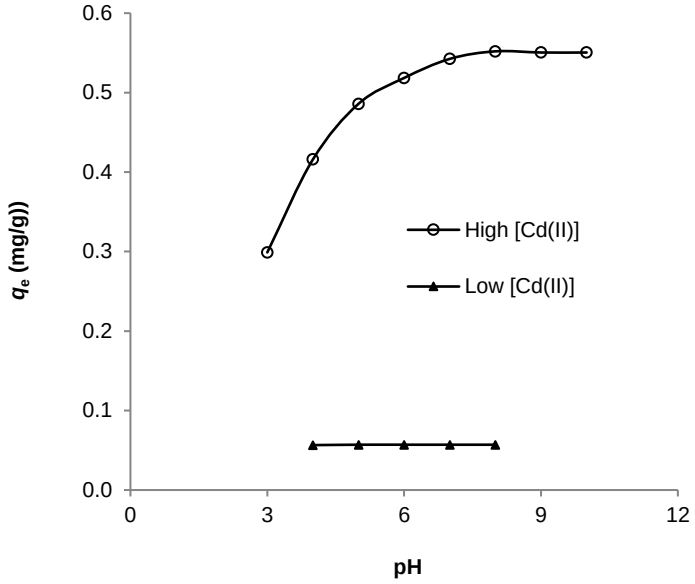

Fig. 5.28: Cd uptake as a function of pH from low and high concentration metal ion solutions

The percent sorption (80.85 %) from the dilute Cd^{2+} solution was lower as compared to the percent sorption (97.61 %) from the more concentrated solution (Fig. 5.29). The pH at which quantitative sorption occurs is therefore ostensibly affected by the metal ion concentration.

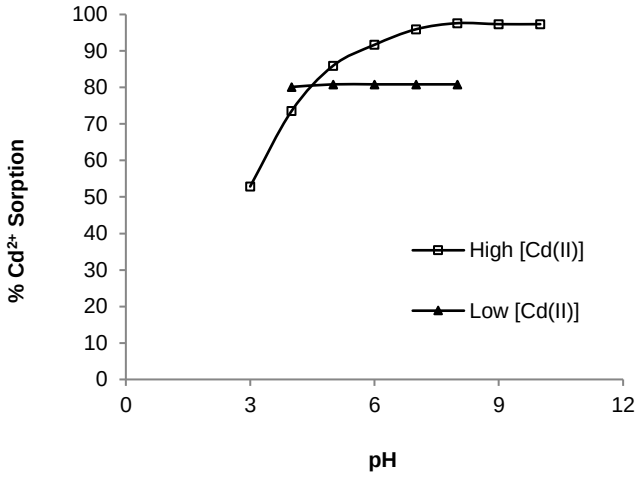

Fig. 5.29: Sorption efficiency of Cd as a function of pH and initial metal ion concentration

This difference in sorption efficiency could be explained in terms of the equilibrium described in Chapter 3 (Section 3.2), according to which the enol form of the Cd-dithizonate complex is favoured by conditions of high pH and high [Cd^{2+}], whereas conditions of low pH and low [Cd^{2+}] favour formation of the keto analogue.

Quantitative sorption (> 95 %) of Cd^{2+} has been reported for dithizone-anchored poly (EGDMA-HEMA) micro beads at pH 4 – 8 (Salih *et al.* 1997); XAD-dithizone resin between pH 5 – 6 (Chwastowka & Kosiarska, 1988); dithizone co-crystallized with microcrystalline naphthalene at pH 3 – 10 (Costa *et al.,* 2002); dithizone-impregnated styrofoam at pH 6 – 8 (Memon e*t al*., 2006); XAD-2 chemically modified with dithizone at pH 6 – 8 (Wu *et al.,* 2006); and dithizone-modified cellulose nanosponges at pH 5.4 – 8.0 (Zargar *et al.,* 2017).

The variation of the distribution coefficient (K_d) with pH of the sorption solution was determined and is shown in Tables 5.23 and 5.24.

Tables 5.23 & 5.24: Variation of K_d with pH; $[Cd]_0$ = 1.131 mg/L and 0.141 mg/L respectively

pH	C_0 (mg/L)	C_e (mg/L)	% Sorption	q_e (mg/g)	K_d	log K_d
3	1.131	0.533	52.87	0.299	561	2.75
4	1.131	0.299	73.56	0.416	1391	3.14
5	1.131	0.159	85.94	0.486	3057	3.49
6	1.131	0.094	91.69	0.519	5516	3.74
7	1.131	0.046	95.93	0.543	11793	4.07
8	1.131	0.027	97.61	0.552	20444	4.31
9	1.131	0.030	97.35	0.551	18350	4.26
10	1.131	0.030	97.35	0.551	18350	4.26
pH	**C_0 (mg/L)**	**C_e (mg/L)**	**% Sorption**	**q_e (mg/g)**	**K_d**	**log K_d**
4	0.141	0.028	80.14	0.057	2018	3.30
5	0.141	0.027	80.85	0.057	2111	3.32
6	0.141	0.027	80.85	0.057	2111	3.32
7	0.141	0.027	80.85	0.057	2111	3.32
8	0.141	0.027	80.85	0.057	2111	3.32

The large K_d values highlighted the affinity of the dithizone impregnated resin towards Cd^{2+}, especially at pH > 5 and higher initial metal ion concentration.

5.3.2.2 *Indium*

Sorption studies of In^{3+} proved somewhat more difficult than other metals, wholly attributable to the tendency of indium to precipitate at pH > 3.3, even in the presence of 10 % (v/v) tartrate ions. Fig. 5.30 shows the repartition profile of In^{3+} in pure water at 25 °C.

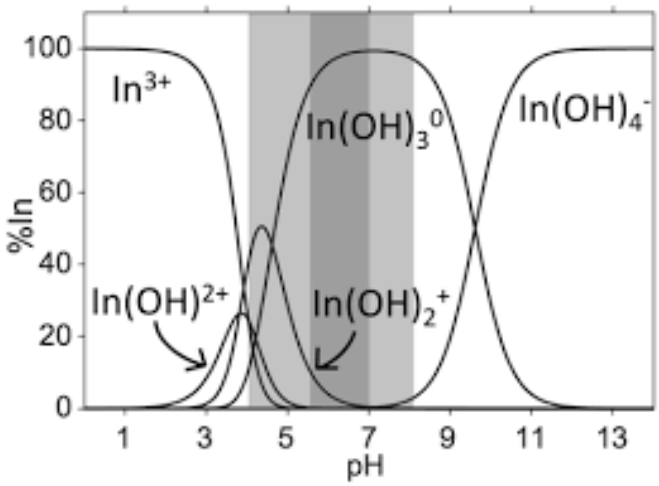

Fig. 5.30: Speciation of In(III) as a function of pH (Woods & Allen, 2006)

Due to its tendency to hydrolyse, precision of In^{3+} determination at pH > 3 was less than satisfactory. In many instances, RSD values were as high as 10 %. In earlier experiments, this problem was exacerbated by the high instrument detection limits, 0.20 mg/L (λ = 303.936 nm) and 0.14 mg/L (λ = 325.609 nm) respectively. Background equivalent concentration (BEC) values were also high, 7.85 mg/L and 5.02 mg/L, respectively. Months later a new calibration was performed, using ultrapure 65 % nitric acid to prepare the blank and calibration standards. For this calibration method, the respective LOD and BEC values were 016 mg/L and 1.6 mg/L (λ = 325.609 nm) respectively. Further evidence of precipitation presented when sample inlet tubes became “dislodged” due to pressure build-up. Replacing the nebulizer and connecting new inlet tubes did not solve the problem. The problem was eventually fixed when ultrapure 65 % nitric acid was used to rinse the tubes in between sample readings.

Precipitation not only caused lack of precision, but accuracy was also compromised. This was proved by measuring the concentration of In^{3+} at pH < 3 and pH = 6, respectively. Table 5.25 shows the variance in accuracy and precision of [In^{3+}] measurements at the various pH values. The same phenomenon presented at pH ~ 4. Generally, suppression was more pronounced at lower concentrations.

Table 5.25: Accuracy of [In^{3+}] measurements at different pH values (λ = 325.609 nm)

Actual Concentration (mg/L)	Measured Concentration (mg/L)	
	At pH ≤ 3	At pH = 6
1.0	$\bar{x}$ = 1.049 (n = 4; rsd = 7.93%)	$\bar{x}$ = 0.5027 (n = 3; rsd = 7.50%)
2.0	$\bar{x}$ = 1.892 (n = 7; rsd = 7.51%)	$\bar{x}$ = 1.280 (n = 4; rsd = 9.60%)

Notwithstanding substantial hydrolysis, sorption increased with increasing pH. This could be a result of dual processes of precipitation and chemical reaction between In^{3+} and dithizone. The distinctive orange colour of the sorbent observed between pH 3 – 6 (Appendix G) attested to the possibility of chemical reaction. Fig. 5.31 shows the sorption profile of a 2 mg/L In^{3+} solution. At lower pH (≤ 2) virtually no In^{3+} ions were sorbed, but sorption increased sharply at pH > 3 to a maximum of 0.651 mg/g at pH = 6. This was equivalent to a sorption efficiency of 91.23 %. A similar pattern emerged from an experiment using 1 mg/L In^{3+} solution.

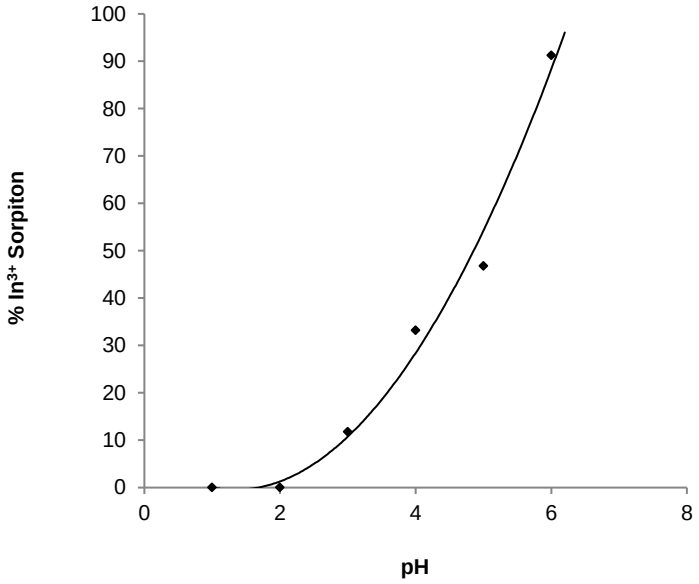

Fig. 5.31: Efficiency of In(III) sorption as a function of pH

In studies using bis(4-cyclohexylcylohexyl) phosphoric acid (or D4DCHPA) as extractant, In^{3+} extraction reached a maximum at pH = 2.4 (Nakamura *et al*., 2009). However, Phetphaisit *et al.* (2017) found that In^{3+} extraction with 2-acrylamido-2-methylpropane sulphonic acid increased with increasing pH to a maximum value (88.1 %) at pH = 5. They ascribed the variation in sorption of In^{3+} with pH to ion exchange mechanisms.

Sorption of In^{3+} onto thiosemicarbazone-modified cellulose was more favourable in the pH range 2 – 2.5 (Mansour & Elmenshawy, 2017) and decreased sharply at higher pH values. Researchers involved in the latter study attributed the decrease in sorption at pH > 2.5 to the formation of insoluble metal hydroxides, thus upholding views expressed in this study.

In an extensive examination of literature, only one study (May & Hoffman, 1948) was found that reported on dithizone as a reagent with indium. However, the extraction of indium was based upon a chloroform extraction of indium. Reportedly, upon shaking, solutions of trivalent indium salts imparted a red colouration to carbon tetrachloride containing dithizone when a narrow pH range (4 – 6) is maintained. Investigating the reaction of indium with chloroform solutions, May & Hoffman found that the indium dithizonate complex formed in the presence of moderate concentrations of cyanide and at higher alkalinity (pH 8.3 – 9.6). In the present study, the possibility of using cyanide ion as complexing agent was ruled out as it caused leaching of dithizone from the impregnated resin. In their studies, May & Hoffman also found the presence of citrates and tartrates prevented the extraction of indium by dithizone, but extraction proceeded rapidly in the presence of hydroxylamine-hydrochloride.

5.3.2.3 *Copper*

Dithizone is one of a few chelating agents that permits separation of Cu^{2+} at low pH (Shabani *et al.,* 2007) where it forms a stable primary dithizonate complex according to the equation:

$$2\ H_2Dz\ (s) + Cu^{2+}\ (aq) \rightarrow Cu(HDz)_2\ (s) + 2\ H^+\ (aq)$$

Two solutions of different concentrations were employed to study the pH dependence of Cu^{2+} sorption. Unfortunately, experiments at higher pH values were conducted in the absence of tartrate ion, which is known to prevent the hydrolysis of Cu^{2+} ions. Sorption increased gradually with increasing pH, before accelerating rapidly at pH > 5, especially at higher metal ion concentration. However, at pH > 5, RSD values also increased significantly (5 < RSD < 10), indicative of chemical interference due to precipitation. Sorption from a 2.972 mg/L solution reached a maximum of 0.977 mg/g at pH = 6; sorption from a 5.713 mg/L solution reached a maximum of 2.789 mg/g at pH = 8. Results are shown in Fig. 5.32.

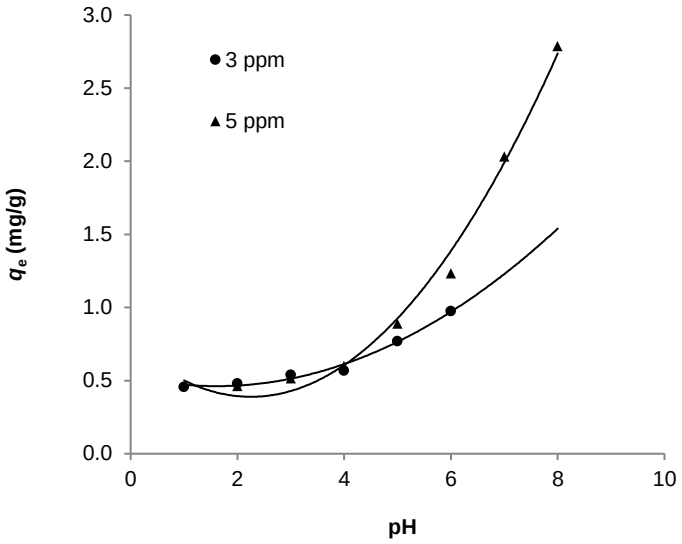

Fig. 5.32: Cu(II) uptake as a function of pH

Shabani & co-workers, choosing pH = 1 for high efficiency and good selectivity of dithizone-naphthalene towards copper in column experiments, found the sorbed amount of Cu^{2+} decreased with increasing pH and ascribed it to the precipitation of Cu^{2+} as copper hydroxide. Costa & co-workers (2002), to the contrary, reported maximum extraction (over 95 %) of Cu^{2+} in brine samples was achieved in the pH range 7.6 – 9.1 on a naphthalene-dithizone solid phase. Chwastowska and Kosiarska (1988) did not report on the possible hydrolysis of Cu^{2+} in moderate to high pH media either, stating that a chelating resin loaded with dithizone could be applied to the isolation of a group of metals (including copper) at pH 5.0 – 6.5. They went further to state the optimum pH for sorption of Cu and Pb was lower (4.0 – 6.5) in the column method than for the other metals under investigation.

5.3.2.4 *Zinc*

Sorption of Zn^{2+} from a 3 mg/L solution increased with increasing pH and was quantitatively sorbed (98.66 %) at pH = 8, in the absence of tartrate. Seemingly, the absence of tartrate did not have a significant effect on the sorption of Zn^{2+} as RSD values were within acceptable limits (< 2 %).

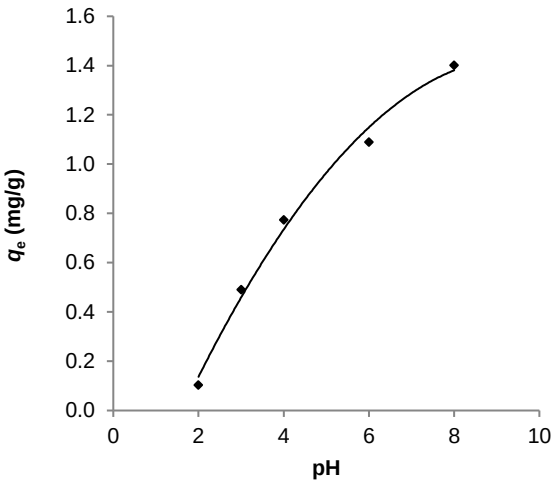

Fig. 5.33: Variation of Zn uptake with pH

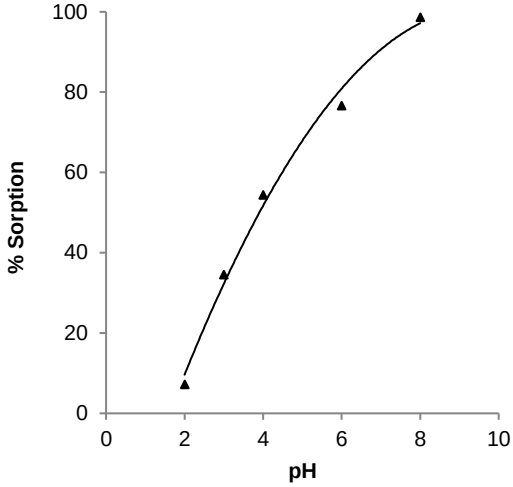

Fig. 5.34: Sorption efficiency of Zn versus pH

The maximum amount of Zn^{2+} ions sorbed at pH = 8 was 1.402 mg/g. Meena *et al.* (2014) reported pH = 8 as optimum condition for sorption of Zn^{2+} onto dithizone-impregnated XAD-2, whereas Costa *et al.* (2002) studied sorption of metal ions (including zinc) onto co-crystallized naphthalene dithizone in the pH range 8.5 – 9.1. As mentioned in Chapter 3 (Section 3.3), Hamza & colleagues found that in the presence of sulphite ion, zinc was extracted at a much lower pH (1.8), whereas in the absence of sulphite ion, extraction of zinc occurred in the pH range 4.5 – 6.5. They proposed a reason for this anomaly, arguing the sulphite ion might participate in a mixed coordination sphere (triple complex), enhancing the stability of the zinc dithizonate complex.

5.3.2.5 *Nickel*

In an earlier experiment, it was established that Ni^{2+} was sorbed completely (100 %) from a solution at pH = 9 and $[Ni^{2+}]_0$ < 1.5 mg/L. Thus, the pH dependence of sorption from a 0.896 mg/L Ni^{2+} solution was studied in the pH range 4 – 10. Sorption was complete at pH ≥ 8 and the maximum amount sorbed was 0.435 mg/g. The results of the latter experiment are shown in Fig. 5.35.

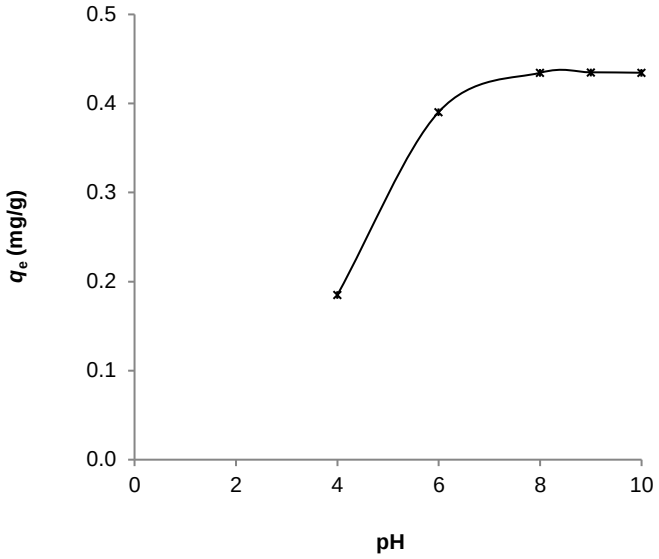

Fig. 5.35: Ni uptake as a function of pH

In only two other studies reporting on Ni^{2+} sorption onto dithizone-functionalised sorbents, Chwastowska & Kosiarska (1988) reported quantitative sorption of nickel in alkaline medium, while Costa & co-workers reported maximum extraction in the pH range 7.6 – 9.1. However, they reported 100 % sorption of nickel in the pH range 5 – 6.5, corroborating evidence found in this study that maximum sorption occurs at lower pH in the column method, as reported briefly later (Chapter 6).

5.3.2.6 *Cobalt*

In a batch experiment using 0.1 g of dry resin contacted with 6 × 50 mL aqueous solutions at varying pH and concentration 2.327 mg/L, sorption of Co^{2+} was limited, with only 22.99 % sorption achieved at pH = 6. The resin showed no significant colour change, indicative of restricted sorption. The experiment was repeated, this time employing 0.1 g wet resin. A distinct purplish-blue colour presented, like that seen in experiments with Ni and Cu. Yet, sorption was still not quantitative, with only 50.50 % achieved at pH = 8. However, during column studies in which the separation of Co, Mn and Ni was attempted, Co^{2+} was completely sorbed onto the column from a 0.379 mg/L solution at pH = 5.93.

5.3.2.7 *Lead*

Chwastowska & Kosiarska (1988) reported that the sorption of Pb onto a dithizone functionalised polymer occurred in both alkaline and acidic media. In this study, 75.45 μg Pb^{2+} was completely sorbed at pH > 8 (Table 5.26). The instrument detection limit was significantly low (0.018 mg/L at λ = 168.215 nm; 0.0043 mg/L at λ = 220.353 nm), providing reasonable certainty that most Pb^{2+} ions were sorbed at pH 8 – 9.

Table 5.26: Experimental data of Pb sorption as a function of pH

pH	C_0 (mg/L)	C_e (mg/L)	% Sorption	q_e (mg/g)
3	1.509	> 1.509		
4	1.509	1.376	8.81	0.067
5	1.509	1.016	32.67	0.247
6	1.509	0.567	62.43	0.471
8	1.509	ND	100.00	0.755
9	1.509	ND	100.00	0.755

In strongly acidic medium (pH < 4), sorption was poor. For this reason, when a Pb^{2+} solution of concentration 1.931 mg/L was passed through a column conditioned at pH = 1.60, Pb^{2+} was not retained and breakthrough was achieved in less than nine (9) minutes.

5.3.2.8 *Manganese*

50 mL of a 1.993 mg/L Mn^{2+} solution was contacted with 0.1 g resin at pH ranging between 2 and 9. RSD values of measurements in alkali medium were greater than 7 %, indicative of probable hydrolysis. The pronounced decrease in Mn^{2+} concentration in alkali medium could therefore be attributed to precipitation rather than sorption and is confirmed by the ion speciation profile (Fig. 5.36, dotted line) of Mn^{2+} in 0.01 M NaCl solution and 0.00045 M EDTA.

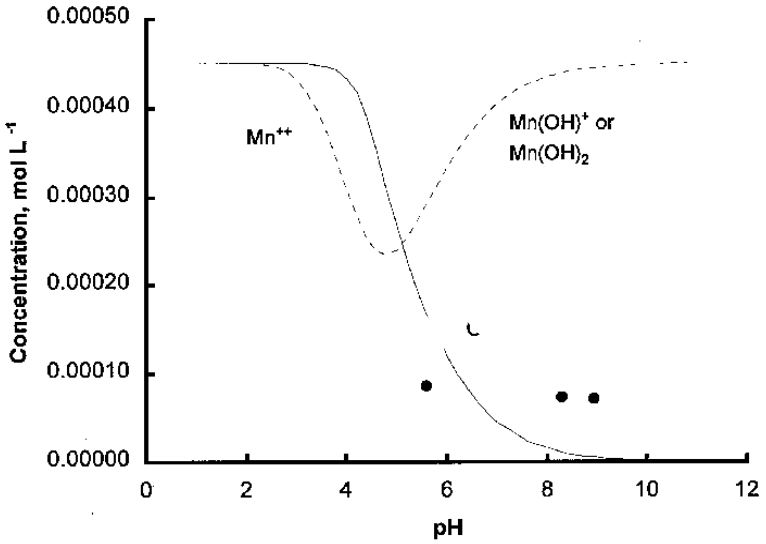

Fig. 5.36: Manganese ion speciation profile (Räsänen *et al*., 2001)

Removal capacity (*R* %) in acidic medium remained low, despite the prevalence of free Mn^{2+}, as illustrated in Fig. 5.37.

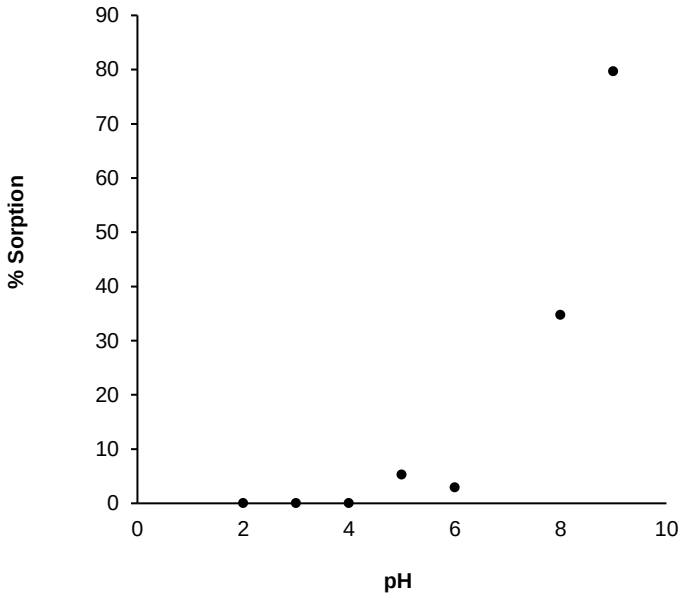

Fig. 5.37: Removal capacity of Mn with pH

5.3.2.9 *Silver & Bismuth*

In studies involving sorption of Ag^{+} and Bi^{3+} onto dithizone-modified substrates, Chwastowska & Kosiarska (1988) reported that Ag^{+} was quantitatively sorbed in acidic medium (1 M HNO_3) while Hamza *et al.* (1990) studied Bi^{3+} sorption at pH ~ 1.2. For this reason, the effect of pH on Ag^{+} and Bi^{3+} sorption was not studied. Sorption of these ions was nonetheless investigated in column studies at pH < 2; both ions were quantitatively sorbed (see Section 6.3).

5.3.3 Volume-to-mass ratio

The amount (*m*) of sorbent affects the sorption of metal ions – an increase in sorbent dose implies larger surface area and therefore more available reaction sites, provided all other parameters remain constant. One parameter often used to investigate sorbent dose is the *V*/*m* ratio, where *V* is the volume of aqueous solution and *m* is the sorbent mass. In this study, the effect of sorbent dose was limited to Cd^{2+} sorption studies, assuming results could be extrapolated to other metal ions.

Sorption data of a solution of initial concentration $[Cd^{2+}]_0$ = 1.131 mg/L (pH = 6; $T = 293 \pm 1$ K) showed that the percent Cd(II) sorption increased with decreasing *V/m* ratio, i.e., with increasing amount of sorbent (Fig. 5.38).

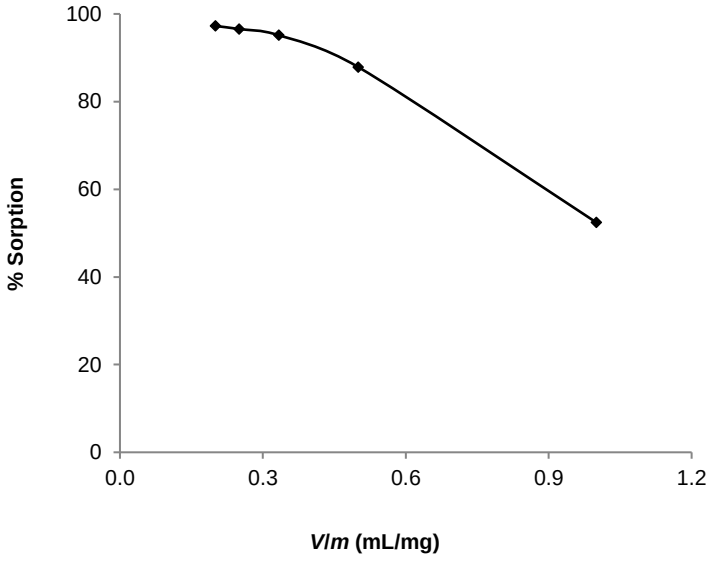

Fig. 5.38: Effect of *V*/*m* ratio on Cd sorption efficiency

Sorption was at a maximum (95.26 %) when the sorbent dosage was 250 mg per 50 mL solution, i.e., $\frac{V}{m} = 0.2$ mL/mg. The amount of Cd^{2+} ions sorbed at this *V*/*m* ratio was 0.550 mg/g (see Table 5.27), almost the same as the value (0.551 mg/g) attained at pH = 8 but using 100 mg of sorbent (*V*/*m* = 0.5 mL/mg). For cost-efficiency, it would therefore be expedient to adjust the pH of the sorption medium instead of increasing sorbent dosage. All experiments in this study were therefore performed at *V*/*m* = 0.5 mL/mg (i.e., 100 mg sorbent per 50 mL solution).

Table 5.27: Effect of *V*/*m* ratio on Cd sorption parameters

m **(mg)**	***V*** **(mL)**	***V*/*m*** **(mL/mg)**	C_0 **(mg/L)**	C_e **(mg/L)**	**% Sorption**	q_e **(mg/g)**	K_d
50	50	1.00	1.131	0.538	52.43	0.297	551
100	50	0.50	1.131	0.137	87.89	0.497	3628
150	50	0.33	1.131	0.055	95.14	0.538	9782
200	50	0.25	1.131	0.039	96.55	0.546	14000
250	50	0.20	1.131	0.031	97.26	0.550	17742

5.4 Sorption kinetics

As discussed in Chapter 2, mathematical models used to describe the kinetic process of sorption can generally be categorised as sorption *reaction* models and sorption *diffusion* models. In this study, pseudo-first order and pseudo-second order models were employed to gain insight into reaction kinetics; Weber-Morris and HPD models were used to describe diffusion kinetics. Chapter 2 entertains divergent interpretations of the HPDM; the discussion below incorporates the various opinions expressed in literature. The mean pore size of Amberchrom CG-300 resins is 300 Å (Sigma-Aldrich, 1997) which is almost three hundred times the ionic radius of the largest ion used in this study, Bi^{3+} = 1.07 Å. It can therefore be assumed that the SPM will *not* represent a good approach to the sorption diffusion kinetics of metals on dithizone-impregnated Amberchrom® CG-300m. Batch experiments were performed at moderate agitation (150 rpm), so the effect of film diffusion could not be disregarded.

As before, sorption kinetics of each element is discussed individually since each metal presented its own peculiarities. Kinetics analysis of manganese sorption data is excluded due to its poor sorption capacity.

5.4.1 Reaction kinetics

5.4.1.1 *Cadmium*

The variation of Cd^{2+} sorption was studied over a period of 120 min using two solutions of initial concentration 0.141 mg/L and 1.131 mg/L, respectively, at pH = 6. As shown in Fig. 5.39, sorption from the 1.131 mg/L solution increased with time but has not yet attained equilibrium after 120 min. Sorption from the 0.141 mg/L solution, on the other hand, remained almost constant. Sorptive uptake of this solution at 150 min was within 1 % of the uptake after 210 min, so equilibrium was assumedly attained at t = 150 min.

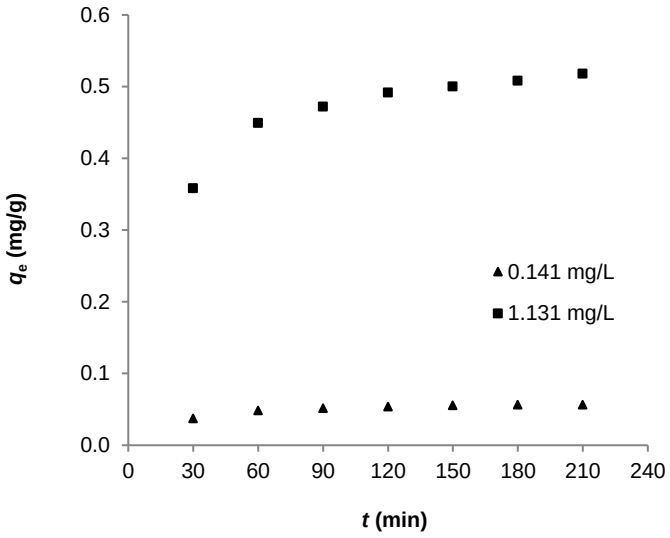

Fig. 5.39: Time dependence of Cd sorption; two sorption solutions of different metal ion concentration

Experimental data are presented in Table 5.28.

Table 5.28: Experimental data of time-dependent studies of Cd sorption from a 0.141 mg/L solution and a 1.131 mg/L solution

t (min)	C_e (mg/L)	q_e (mg/g)
0	0.141	0.000
30	0.066	0.038
60	0.044	0.049
90	0.038	0.052
120	0.033	0.054
150	0.030	0.056
180	0.028	0.057
210	0.028	0.057

t (min)	C_e (mg/L)	q_e (mg/g)
0	1.131	0.000
30	0.415	0.358
60	0.233	0.449
90	0.187	0.472
120	0.148	0.492
150	0.131	0.500
180	0.115	0.508
210	0.095	0.518

The transient behaviour of the batch sorption process of Cd^{2+} from each solution was analysed using Lagergren pseudo-first order and the Ho and McKay pseudo-second order models, respectively. Plots of log ($q_e - q_t$) vs. t are shown in Fig. 5.40.

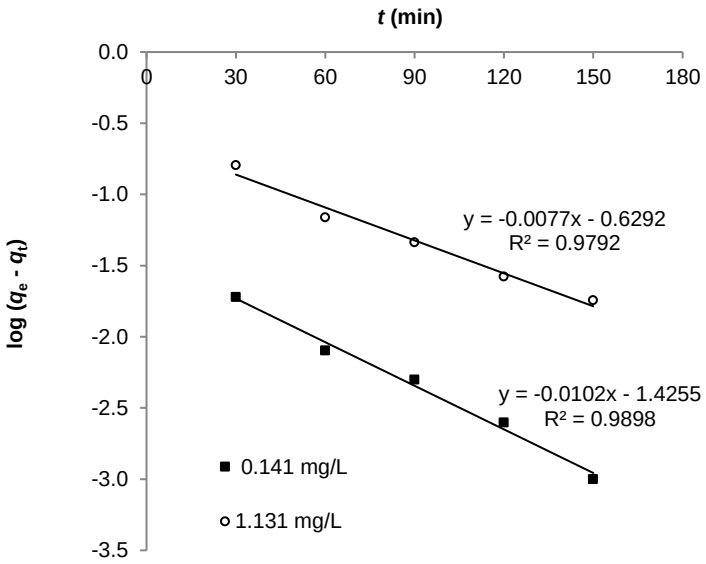

Fig. 5.40: Lagergren pseudo-first order plots for the kinetic modelling of Cd sorption; T = 294 K

The slope of each curve was used to determine the respective first order rate constant, k_1. From the intercept of each curve, the sorption capacity was calculated and compared with experimental values. A summary of results is given in Table 5.29.

Table 5.29: Parameters of pseudo-first order kinetics of Cd sorption

$[Cd^{2+}]_0$ (mg/L)	Pseudo-first order rate constant, k_1 (min^{-1})	Sorption capacity, q_e (mg/g)
0.141	0.024	0.038
1.131	0.018	0.235

Despite the relatively high correlation coefficients of both pseudo-first order graphs, the calculated values of sorption capacity were not in acceptable agreement with the experimental values of 0.057 mg/g and 0.518 mg/g, respectively. This “anomaly” was discussed in Chapter 2 (Section 2.3.2.1) and will present itself without further discussion throughout this chapter.

The relatively high correlation coefficients of the pseudo-first order graphs implied physisorption could be considered as sorption mechanism, a possibility that was refuted earlier (Section 5.3.1.1). Applying the Ho and McKay pseudo-second order equation to data of both experiments produced the graphs in Fig. 5.41.

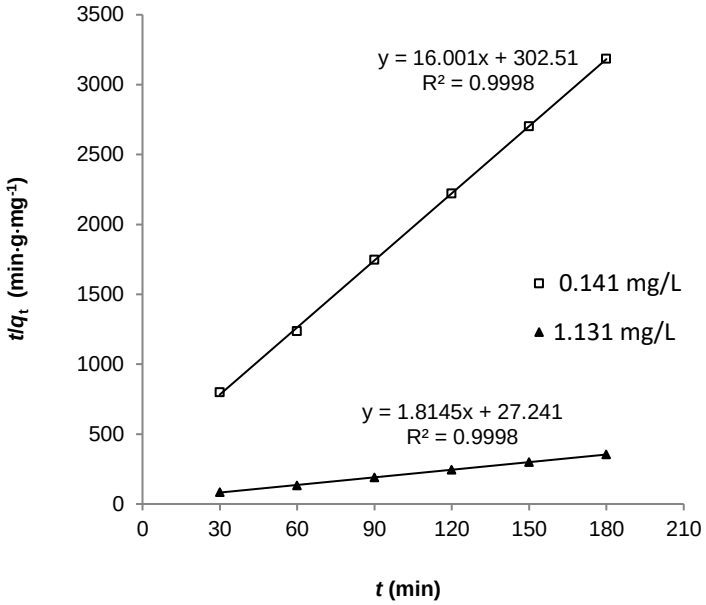

Fig. 5.41: Pseudo-second order plots for kinetic modelling of Cd sorption at *T* = 294 K

The pseudo-second order rate constants (k_2) and sorption capacities (q_e) were derived from the intercepts and slopes of the graphs respecitively and are presented in Table 5.30:

Table 5.30: Parameters of pseudo-second order kinetics of Cd sorption

$[Cd^{2+}]_0$ (mg/L)	Pseudo-second order rate constant, k_2 (g/mg·min^{-1})	Sorption capacity, q_e (mg/g)
0.141	0.846	0.063
1.131	0.121	0.551

Significantly high correlation coefficients (r^2 = 0.9998) and much better agreement between calculated and experimental values confirmed pseudo-second order kinetics as the preferred model over pseudo-first order kinetics, suggesting the overall sorption rate of Cd^{2+} was controlled by chemisorption (Ho & McKay, 1999).

The higher second order rate constant (k_2 = 0.846 g/mg·min^{-1}) implied sorption occurred much faster in the more dilute solution, almost in direct proportion with initial concentration, presumably because fewer ions in the bulk solution competed for finite active sites on the surface and interior of the resin pores. The calculated q_e-value (0.551 mg/g) showed remarkable resemblance with the experimental value (0.552 mg/g) obtained during pH-dependent studies, as well as the maximum sorption value (0.550 mg/g) obtained in *V*/*m* studies.

Finally, it has been shown in the beginning of this Chapter that the amount of dithizone impregnated onto Amberchrom® CG-300m was approximately 3.2 mg H_2Dz per gram resin (or 12.37 μmol/g). Experimental data has shown at [Cd^{2+}] = 0.141 mg/L and pH = 6, the maximum sorption capacity (*Q*) of the modified resin was 0.057 mg Cd^{2+} per gram resin (or 0.507 μmol/g). Assuming chelation between the divalent Cd ion and H_2Dz proceeded via predicted stoichiometric ratios, this implied that for every 100 sites available for reaction, only ~8 sites were occupied by Cd^{2+} ions. Similarly, at [Cd^{2+}] = 1.131 mg/L and pH = 8, maximum sorption capacity was 0.552 mg Cd^{2+} per gram resin (or 4.910 μmol Cd^{2+}/g), implying nearly 80 % of all available reaction sites were occupied by Cd^{2+} ions, a tenfold increase in sorptive uptake.

5.4.1.2 *Copper*

The sorption kinetics of Cu(II) on the dithizone-modified Amberchrom resin was studied in a number of single batch experiments in the time range 10 – 330 min. In one experiment, 0.4 g of dry resin was contacted with 200 mL of a 5.986 mg/L Cu^{2+} solution at constant pH = 2.88. The results of this experiment are shown in Table 5.30 with a plot of sorbed amount (*q*) versus time (*t*) alongside (Fig. 5.42).

Table 5.31: Experimental data of Cu sorption kinetics studies

t (min)	C_e (mg/L)	q_e (mg/g)	X
10	5.773	0.107	0.12
20	5.744	0.121	0.14
30	5.720	0.133	0.15
45	5.619	0.184	0.21
60	5.589	0.199	0.22
75	5.588	0.199	0.22
90	5.442	0.272	0.31
120	5.353	0.317	0.36
180	5.178	0.404	0.46
240	5.064	0.461	0.52
t_∞	4.213	0.887	

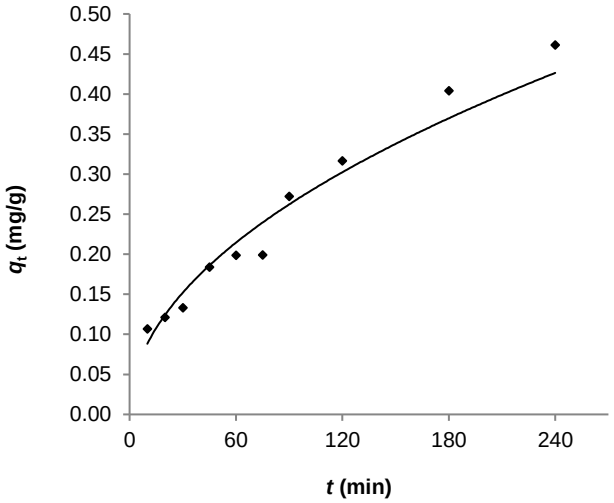

Fig. 5.42: Rate of Cu sorption onto impregnated resin

It is clear from Fig. 5.42 that saturation has not been reached after four hours and that infinite surface coverage presumably occurred, indicative of multilayer sorption. Such a hypothesis agreed with an earlier observation that Cu sorption could be modelled quite adequately by the Temkin, Freundlich and Langmuir isotherms alike. For confirmation, the Ho & McKay pseudo-second order as well as Lagergren pseudo-first order reaction kinetic models were tested, represented by Figs. 5.43 and 5.44, respectively.

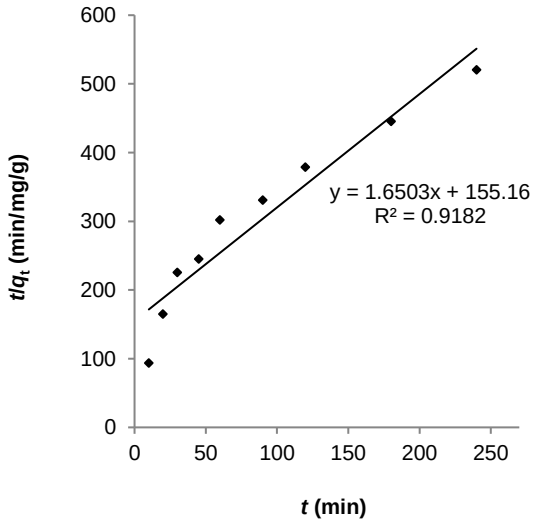

Fig. 5.43: Pseudo-second order plot for kinetic modelling of Cu sorption

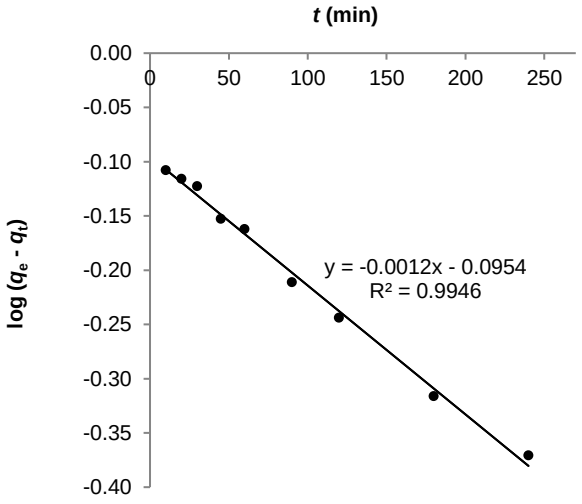

Fig. 5.44: Pseudo-first order plot for kinetic modelling of Cu sorption

The higher correlation coefficient (r^2 = 0.9946) implied sorption followed pseudo-first order kinetics. Since pseudo-first order kinetics is normally associated with a physisorption regime, it provided further evidence that Cu^{2+} ions covered the resin surface in multi-layer fashion (Section 5.3.1.2). This hypothesis was endorsed by the fact that the calculated sorption capacity $q_{e,\,calc}$ = 0.803 mg/g derived from the intercept of the graph (Fig. 5.44) agreed better with the experimental value (0.887 mg/g) achieved at t_∞ = 27 hours. The theoretical value of q_e derived from the slope of the pseudo-second order plot (Fig. 5.43) was $q_{e,\,calc}$ = 0.606 mg/g. In a follow-up experiment, sorption kinetics of a more dilute Cu^{2+} solution (1.709 $mg{\cdot}L^{-1}$) was studied at the same pH (2.88). Results of this experiment were erratic, save to say maximum sorption achieved after 27 hours was 0.842 mg/g.

The apparent slow kinetics of Cu^{2+} sorption necessitated another experiment, still using the batch technique, but this time using the resin wet (i.e., immediately after filtration without drying). In this experiment 0.4 g resin was agitated with 200 mL of a 1.709 $mg{\cdot}L^{-1}$ Cu^{2+} solution at pH = 3.04. In what was to become a turning point in the entire study, the increase in kinetics was spectacular, with the resin turning purplish-blue almost immediately upon contact with the analyte solution. A similar observation was made when Se(IV) was sorbed onto sulphuric acid-treated peanut shell (El-Shafey, 2007). Table 5.32 shows the results of the last experiment.

Table 5.32: Experimental data of Cu sorption kinetics studies

t **(min)**	C_e **(mg/L)**		
	λ (nm)		
	324.754	**327.754**	**224.700**
15	0.015	N/D	N/D
30	0.017	N/D	N/D
45	0.031	N/D	N/D
60	0.046	N/D	N/D
90	0.027	N/D	N/D
120	N/D	N/D	N/D

At less sensitive emission lines (λ = 224.700 nm and λ = 327.754 nm), Cu^{2+} ions were not detected in the sorbate solution despite low instrument detection limits (0.002 mg/L and 0.007 mg/L respectively). It should be noted that the RSD-values of measurements recorded at λ = 324.754 nm were relatively high (> 7 %) indicating that measurements were too close to the limit of quantification (LOQ = 0.006 mg/L). The accuracy of these results is thus questionable. Yet, data almost perfectly fitted the pseudo-second order kinetic equation (Fig. 5.45).

The saturation value (0.842 mg/g) attained in the experiment using dry resin was almost exactly the average sorption capacity (0.841 mg/g) of the wet resin. However, maximum sorption onto the wet resin was achieved within 15 min only. A hypothesis could be formulated – the condition of the resin (wet or dry) did not affect Cu sorption capacity, only the rate at which maximum sorption was achieved (provided the pH was kept constant).

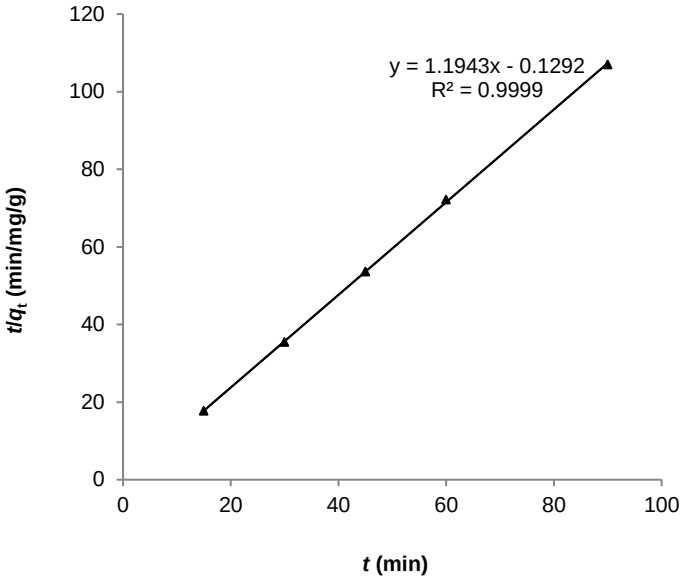

Fig. 5.45: Pseudo-second order plot for kinetic modelling of Cu sorption onto wet resin

To confirm pseudo-second order kinetics, the maximum amount of Cu^{2+} ions sorbed onto the wet resin was calculated and compared with the experimental value. The agreement was remarkable, q_e = 0.837 mg·g^{-1}. The negative value of the intercept was absurd as $h = k_2 q_e^2$ is always greater than zero. If the absolute value were used, the pseudo-second order rate constant could be calculated as follows:

$$|h| = k_2 \times (0.837) = 0.1292$$

$$\therefore\ k_2 = 11.048\ \text{g/mg·min}^{-1}$$

Cu^{2+} sorption seemed to follow pseudo-first order kinetics on dry resin, whereas pseudo-second order kinetics prevailed on wet resin. This observation implied sorption on the dry resin was a result of weak interaction between Cu^{2+} ions and the resin, whereas the wet resin facilitated stronger chemical bonding between Cu^{2+} ions and the impregnated dithizone. Aqueous solution trapped inside the resin pores probably promoted migration of the metal ions towards active sites that are otherwise hindered by air that fills the dry resin beads.

This observation is supported by evidence discussed in Section 5.2.1, that Cu^{2+} sorption on dry resin could best be modelled by the Temkin isotherm, followed closely by Langmuir and Freundlich isotherms. It will become evident in later discussions that Cu was the only metal whose sorption followed pseudo-first order kinetics.

5.4.1.3 *Zinc*

Zinc exhibited extremely fast kinetics, making it difficult to study its sorption kinetics in batch experiments. Even on dry resin, the characteristic pink-red colour of the zinc dithizonate complex presented almost immediately. Initially, multiple batch experiments (single and multiple batches) were conducted in the pH range 6 – 8, over various time ranges and intervals. In all experiments, the resin was contacted with analyte solutions of concentrations ranging between 1.536 mg/L and 4.177 mg/L. Although the distinctive, deep pink-red colour of the solid phase clearly implied the formation of the Zn-dithizonate complex over the studied pH range and ion concentration, results indicated that sorption seemingly decreased with time (suggesting desorption), in some instances within less than two minutes. In addition, results showed no clear trend, making meaningful data analysis virtually impossible. The only logical arguable case was that some steady-state approximation was established quickly, at which point minor changes in experimental conditions such as ambient room temperature could alter the delicate “equilibrium”. It will be proved later (Section 5.5) that sorption of Zn^{2+} was reversible; this could be a plausible argument for the transitory nature of Zn sorption equilibrium.

After numerous “failed” attempts (having since continued with other experiments), a switch was made to the column method for kinetic studies as it is generally known to be more efficient (Chwastowska & Kosiarska, 1988). The column method made it easier to control experimental parameters. A peristaltic pump with variable settings ensured a steady flow rate while an automated fractionator collected constant fraction volumes over pre-set time-intervals. In the first of two experiments conducted on a column, a 3.949 mg/L feed solution at arbitrary pH = 3.5 was pumped at 5.0 mL/min through a column packed with 0.5 g impregnated resin. The column was conditioned with buffer of pH = 3.5 before the influent was passed through. Based on earlier pH studies, Zn^{2+} was not expected to be held onto the resin at pH = 3.5. Yet, no Zn^{2+} ions were detected in the first four eluate fractions. Only after seven min had passed (5^{th} fraction) Zn presented in the effluent and breakthrough was achieved after 27 min (Fig. 5.46).

To obtain additional data points to render kinetic studies more feasible, the experiment was repeated at higher pH (8.48) to avoid early breakthrough and to ensure Zn was retained on the column for a longer period. The concentration of the feed solution was 1.768 mg/L. The Zn^{2+} content in each eluate fraction was determined at three emission lines. No Zn^{2+} was detected at the line of mid intensity (λ = 213.856 nm) after only five fractions. More data points were obtained at the lowest intensity line (λ = 206.200 nm) and were thus used for analysis. The breakthrough curves of both experiments are shown below:

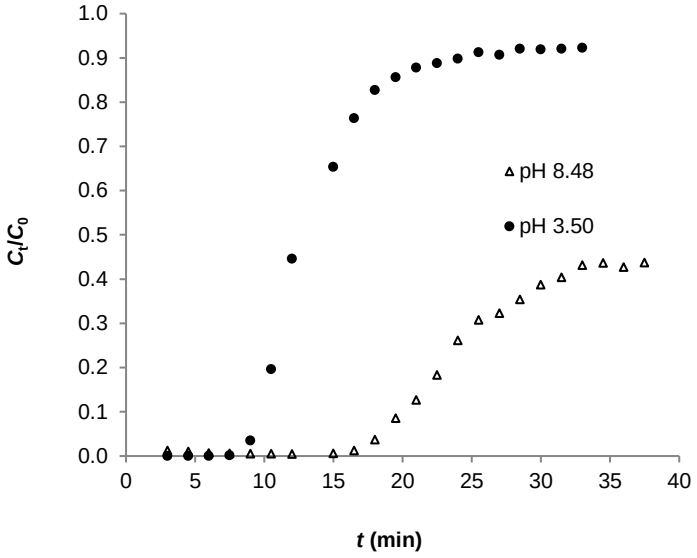

Fig. 5.46: Breakthrough curve of ACG300m-H_2Dz for sorption of Zn at different pH; flow rate = 5.0 mL·min^{-1}; influent concentration = 1.768 mg/L

Breakthrough was achieved later (*t* = 34.5 min) at the higher pH. Results of the first 12 min of the experiment are presented in Table 5.33.

Table 5.33: Results of Zn kinetic studies; flow rate = 1.5 mg/mL; pH = 8.48

t (min)	C_e (mg/L)	q_t (mg/g)	*X*
3.0	0.051	0.2060	0.982
4.5	0.041	0.2072	0.987
6.0	0.028	0.2088	0.995
7.5	0.023	0.2094	0.998
9.0	0.021	0.2096	0.999
10.5	0.020	0.2098	0.999
12.0	0.019	0.2099	1.000

Clearly, a steady-state approximation has already been attained at t = 3 min as q-values after this period were within 1 % off each other. Fractional attainment of equilibrium was significantly high at t = 3 min, reaching unity after only 12 min. This narrow range of X values attested to the rapid rate at which Zn^{2+} ions were sorbed onto the resin. A graph of the amount of Zn^{2+} ions sorbed (q_t) versus *time* (t) is shown in Fig. 5.47.

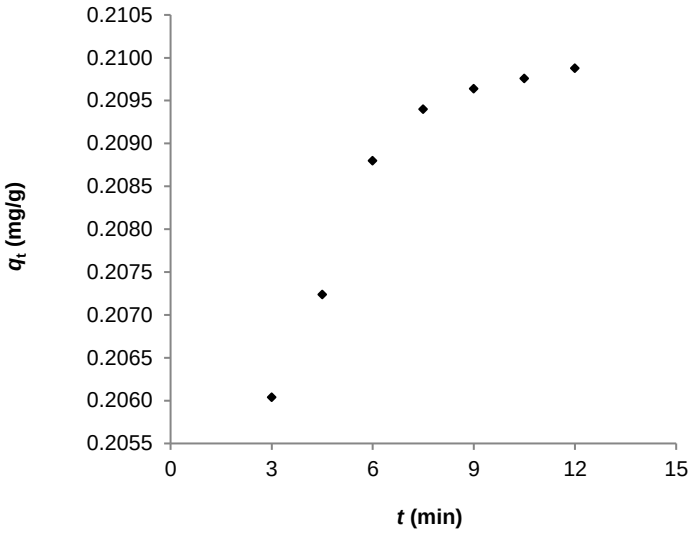

Fig. 5.47: Amount of Zn^{2+} ions sorbed with time in column method; flow rate = 5.0 mL·min^{-1}; [Zn^{2+}] = 1.768 mg/L; pH = 8.48

Kinetic data was applied to pseudo-first order and pseudo-second order equations, with respective graphs shown in Figs. 5.48 and 5.49.

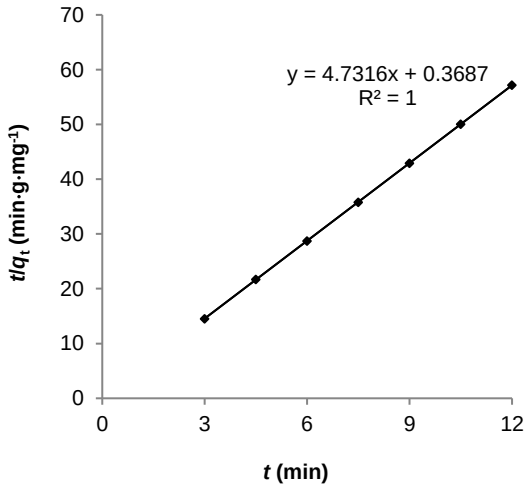

Fig. 5.48: Pseudo-second order plot for kinetic modelling of Zn sorption; dynamic technique

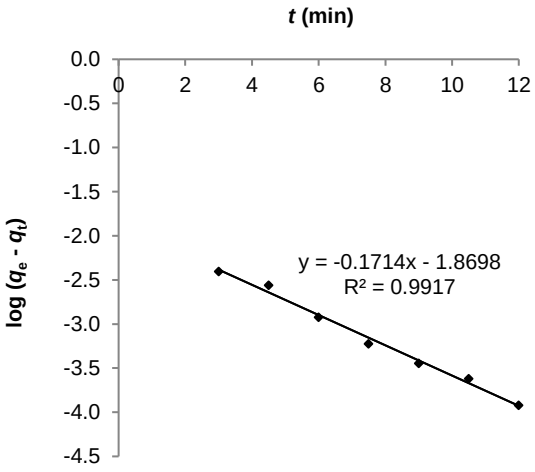

Fig. 5.49: Pseudo-first order plot for kinetic modelling of Zn sorption; dynamic technique

Both models provided excellent approaches to the reaction kinetics of Zn sorption ($r^2 > 0.99$). However, the perfect correlation coefficient ($r^2 = 1$) of the pseudo-second order graph is a result of the near constant q_e values associated with a steady-state approximation. This phenomenon presented in all subsequent kinetic studies performed using the column method. Hence, analysis of the pseudo-second order kinetic model based on data obtained in column experiments hereafter will be superfluous. Notwithstanding, the sorption capacity or saturation value ($q_{e,\,calc}$) derived from the pseudo-second order graph closely resembled the experimental value of 0.210 mg/g.

$$\frac{1}{q_{e,calc}} = 4.7316$$

$$\therefore\ q_{e,\,calc} = 0.211 \text{ mg/g}$$

From the calculated value, the pseudo-second order rate constant k_2 was calculated and determined to be equal to $k_2 = 60.74$ g/mg·min^{-1}. The value of the pseudo-first order constant was $k_1 = 0.395$ min^{-1}. The exceptionally high k_2-value bore further testimony to the fast reaction kinetics of Zn on the dithizone-modified substrate.

5.4.1.4 *Nickel*

Sorption kinetic studies of Ni^{2+} ions were carried out using the batch technique. Results recorded in Table 5.34 were obtained in a fourth experiment where 0.4 g of wet resin was slurried with 208 mL of 1.671 mg/L solution at pH = 9 in the presence of 10 % (v/v) tartrate ion. Earlier attempts were not successful, probably due to the long time-intervals (30 min) of aliquot withdrawals, and in other cases, likely due to the absence of tartrate ion.

Table 5.34: Experimental data of Ni sorption kinetics; batch-experiment

t (min)	C_e (mg/L)	Q (mg/g)	*X*
3	0.658	0.527	0.793
5	0.620	0.547	0.823
10	0.605	0.554	0.835
15	0.556	0.580	0.873
20	0.516	0.601	0.905
30	0.499	0.609	0.918
45	0.472	0.623	0.939
60	0.444	0.638	0.961
75	0.422	0.649	0.978
90	0.397	0.662	0.998
150	0.395	0.664	0.999

The fractional attainment of equilibrium (X) was greater than 0.3 and approached unity at t = 150 min. The sorption rate of Ni increased until it plateaued at t = 90 min (Fig. 5.50).

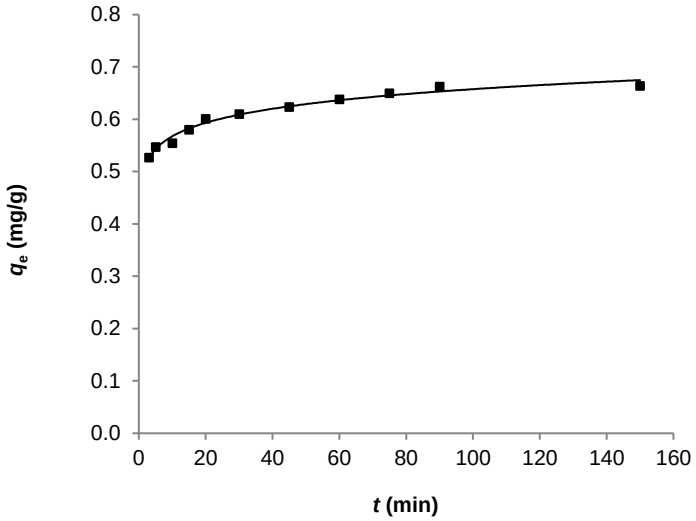

Fig. 5.50: Rate of Ni uptake; pH = 9; 10 % (v/v) tartrate ion

Reaction kinetics was best described by the pseudo-second order model (Fig. 5.51).

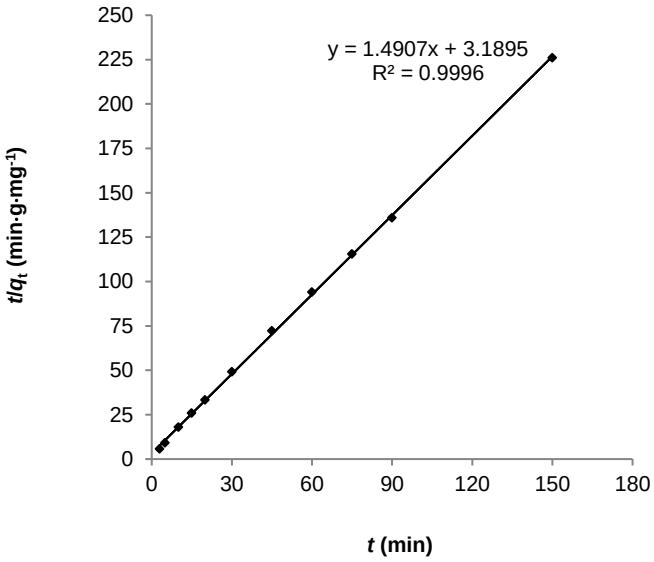

Fig. 5.51: Pseudo-second order plot of kinetic modelling of Ni sorption

The theoretical sorption capacity ($q_{e,\,calc}$) was determined from the slope of the graph as before. Its value, q_e = 0.671 mg/g, was in excellent agreement with the experimental value (0.664 mg/g). The pseudo-second order rate constant was calculated from the intercept of the graph, k_2 = 0.697 g/mg·min^{-1}.

The relatively high r^2-value (0.9840) of the pseudo-first order plot (Fig. 5.52) indicated the feasibility of pseudo-first order kinetics (normally associated with physi-sorption). The pseudo-first order rate constant, k_1 = 0.029 min^{-1}, was much smaller compared to k_2.

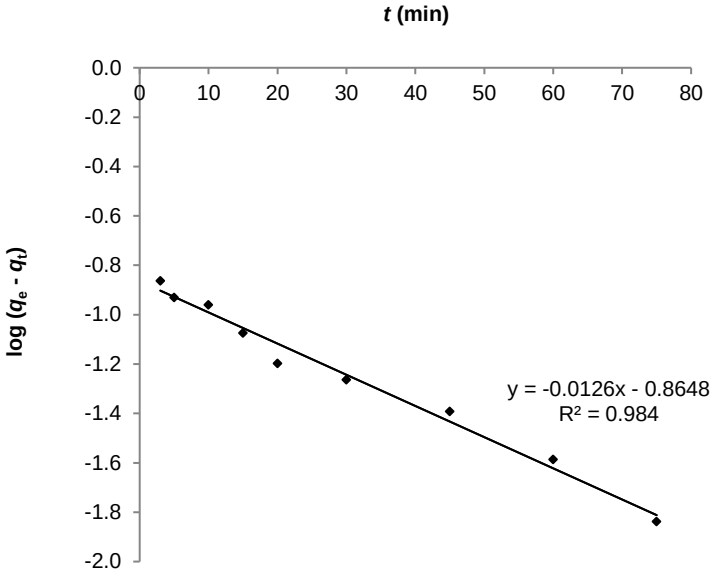

Fig. 5.52: Pseudo-first order plot of kinetic modelling of Ni sorption

5.4.1.5 *Cobalt*

Kinetic studies of Co^{2+} were the first to be performed in multiple batch experiments. In the first of two experiments, nine solutions each containing 51 mL of 1.261 mg/L sample solution in contact with 0.1 g of wet resin were shaken in Erlenmeyer flasks at 150 rpm. The pH of each solution was maintained at pH = 5.76. Sample solutions were removed from the shaker at predetermined times within a 5 – 15 min interval, filtered, and the metal content in the filtrate determined by ICP-OES. Results showed that metal ion uptake occurred rapidly within 15 min. After 15 min, sorption capacity was apparently reached, and fewer ions were sorbed onto activated sites on the surface and inside the resin pores (Table 5.35).

Due to the rapid uptake of Co^{2+} ions and few data points, the first experiment was repeated under similar conditions, but samples were removed after shorter time intervals (Table 5.36). The initial concentration of sample solutions in the second experiment was 0.743 mg/L. Results of both experiments showed that Co^{2+} ion uptake reached equilibrium within 15 min. The sorption capacities achieved in both experiments were 0.598 mg/g and 0.334 mg/g respectively.

Table 5.35: Kinetics data of Co sorption over longer time intervals

t (min)	C_e (mg/L)	q_e (mg/g)
5	0.580	0.347
10	0.172	0.555
15	0.088	0.598
20	0.121	0.581
25	0.127	0.578
30	0.151	0.566
35	0.132	0.576
40	0.093	0.596
45	0.113	0.585
105	0.139	0.572

Table 5.36: Kinetics data of Co sorption over shorter time intervals

t (min)	C_e (mg/L)	q_e (mg/g)	*X*
2	0.250	0.251	0.75
5	0.190	0.282	0.84
8	0.150	0.302	0.91
11	0.131	0.312	0.93
14	0.089	0.334	1.00
20	0.089	0.334	
26	0.089	0.334	

Fig. 5.53 illustrates the time-dependence of Co sorption.

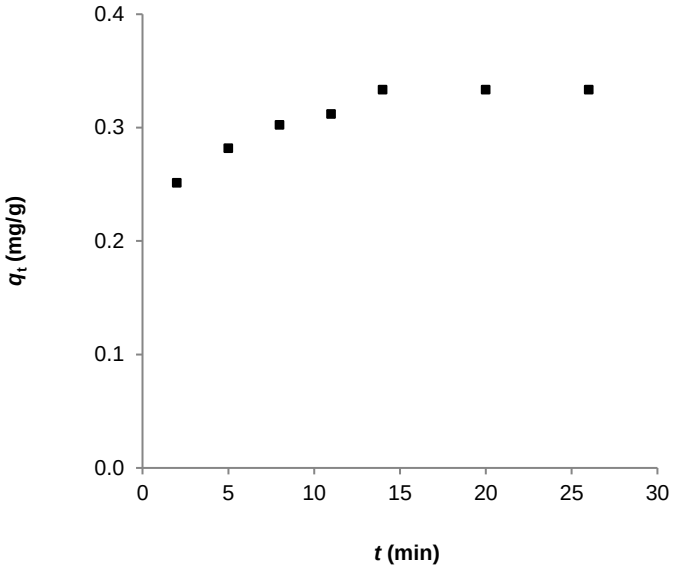

Fig. 5.53: Rate of Co uptake; pH = 5.76

Reaction kinetics data were modelled on pseudo-second order and pseudo-first order equations (Figs. 5.54 and 5.55) respectively. Both graphs revealed excellent correlation between experimental parameters (r^2 > 0.9940), suggesting sorption onto the modified resin occurred via both chemisorption and physi-sorption processes.

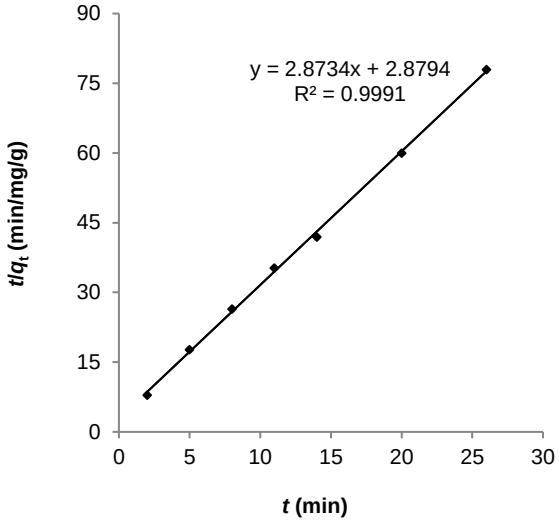

Fig. 5.54: Pseudo-second order plot for kinetic modelling of Co sorption

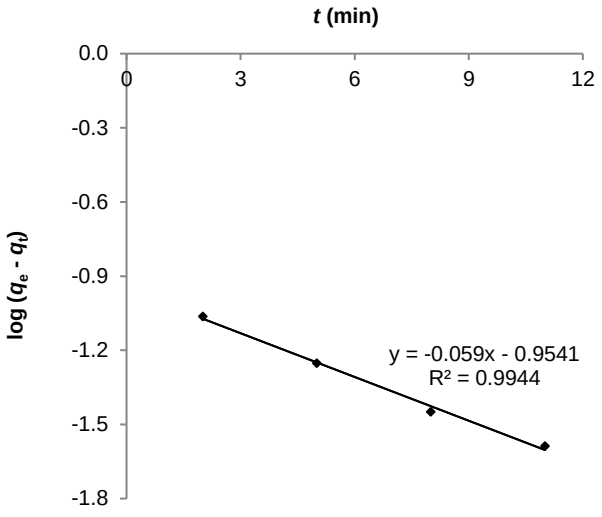

Fig. 5.55: Pseudo-first order plot for kinetic modelling of Co sorption

The calculated sorption capacity was obtained from the slope of the graph depicted in Fig. 5.54.

$$\frac{1}{q_e} = 2.8734$$

$$\therefore q_e = 0.348 \text{ mg/g}$$

The rate constant, k_2, was calculated as follows:

$$h = k_2 q_e^{\,2} = \frac{1}{2.8794}$$

$$\therefore k_2 = 2.868 \text{ g/mg·min}^{-1}$$

5.4.1.6 *Lead*

Sorption kinetics of Pb^{2+} ions was studied in batch and column experiments. Using the batch technique, 0.4 g resin was slurried with 216 mL of a 3.343 mg/L solution in the presence of 10 % (v/v) tartrate. The pH of the aqueous solution was maintained at pH = 5.79. The mixture was shaken at 150 rpm and 5 mL aliquots of the supernatant were drawn at predetermined intervals, with the Pb^{2+} ion content in each aliquot determined by ICP-OES. The results of this experiment are presented in Table 5.37.

Table 5.37: Experimental data of Pb sorption kinetics

t (min)	C_e (mg/L)	q_t (mg/g)
2	1.115	1.203
5	1.123	1.199
8	1.041	1.243
11	1.020	1.254
14	0.988	1.272
17	0.978	1.277
20	0.917	1.310
23	0.872	1.334
26	0.857	1.342
29	0.787	1.380
32	0.741	1.405
35	0.717	1.418
38	0.735	1.408
41	0.724	1.414
44	0.731	1.410
47	0.715	1.419
∞	0.732	1.410
	$Ave_{t > 35\ min}$:	1.413
	$RSD_{t > 35\ min}$:	0.6356

It could be assumed with reasonable confidence that equilibrium was established after 35 min and that maximum sorption achieved was 1.413 mg/g.

Kinetics data was applied to both the pseudo-second order and pseudo-first order equations, with the two respective graphs displayed in Figs 5.56 and 5.57:

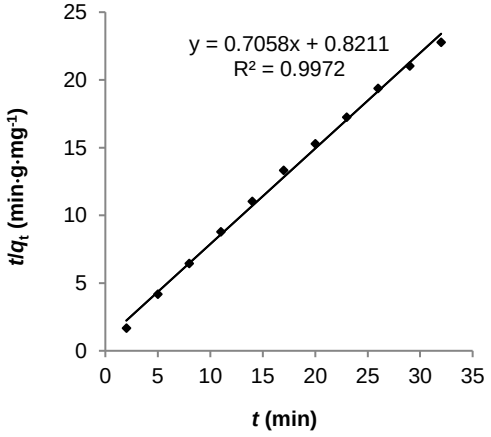

Fig. 5.56: Pseudo-second order plot of kinetic modelling of Pb sorption

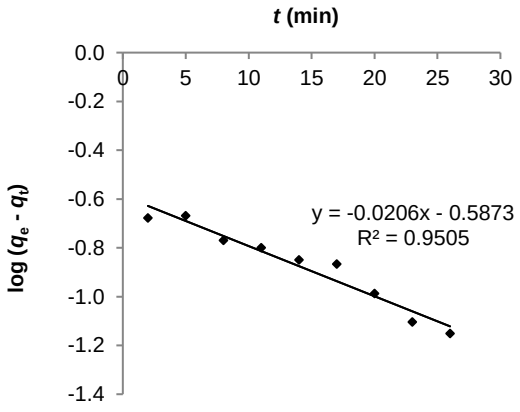

Fig. 5.57: Pseudo-first order plot of kinetic modelling of Pb sorption

A higher correlation coefficient (r^2 = 0.9972) predicted the favourability of pseudo-second order kinetics, and the calculated sorption capacity, $q_{e,\,calc}$, derived from the slope of the graph (Fig. 5.56) was in excellent agreement with the experimental value ($q_{e,\,exp}$ = 1.413 mg/g):

$$\frac{1}{q_{e,calc}} = 0.7058$$

$$\therefore\ q_{e,\,calc} = 1.417\ \text{mg/g}$$

Deriving the saturation value from the intercept of the pseudo-first order graph yielded a value of $q_{e,\,calc}$ = 0.258 mg/g that differed vastly from the experimental value. The value of the second order rate constant, k_2, was derived from the intercept of the appropriate graph, calculated as follows:

$$\frac{1}{h} = \frac{1}{k_2 q_e^{\,2}} = 0.8211$$

$$\therefore\ k_2 = 0.607\ \text{g/mg·min}^{-1}$$

The value of the pseudo-first order rate constant, k_1, was derived from the slope of the corresponding graph:

$$\frac{k_1}{2.303} = 0.0206$$

$$\therefore\ k_1 = 0.047\ \text{min}^{-1}$$

5.4.1.7 *Bismuth*

Earlier experiments of pH dependence revealed that Bi^{3+} ions could be sorbed quantitatively from a slight to high acidic medium (pH = 2 – 5). The time-dependence of Bi sorption was therefore investigated by the dynamic method at pH = 3.85. A solution of initial concentration $[Bi^{3+}]_0$ = 2.785 mg/L was pumped through a column at a flow rate of 5.0 mL/min and eluate fractions were collected every 90 seconds. The characteristic rust-brown colour of the bismuth-dithizonate complex was observed in the column as Bi^{3+} ions migrated through the resin bed. The Bi^{3+} content in each fraction was determined by ICP-OES. Results are presented in Appendix E, showing that no Bi could be detected in the effluent.

To avoid complete sorption of Bi, a binary solution of 4.175 mg/L Bi and 1.931 mg/L Pb at pH 1.6 was subsequently pumped through a fixed bed column at 5.0 mL/min. It was assumed that Pb^{2+} ions competing for activated sites would suppress the sorption of Bi^{3+} ions. Also, previous experiments showed that Pb^{2+} ions were not sorbed at low pH. Fractions were collected at 90 second intervals (Table 5.38) and the metal ion content determined by ICP-OES (also see Appendix F).

Table 5.38: Time-dependence of Bi sorption

t (min)	C_e (mg/L)	q_t (mg/g)	X
1.50	0.108	0.4270	0.9840
3.00	0.072	0.4308	0.9927
4.50	0.057	0.4324	0.9963
6.00	0.053	0.4328	0.9973
7.50	0.049	0.4332	0.9982
9.00	0.044	0.4338	0.9994
10.50	0.042[6]	0.4340	0.9999
12.00	0.046	0.4335	
15.00	0.044	0.4338	
16.50	0.043	0.4339	
18.00	0.039	0.4343	
19.50	0.044	0.4338	
21.00	0.036	0.4346	
22.50	0.039	0.4343	
24.00	0.042	0.4340	
Ave	0.042		
SD	0.003		
RSD	8.006		

Sorption occurred at a very high rate during the first three minutes before tapering off as available reaction sites became depleted (Fig. 5.58). The plateau of the graph corresponded with the experimental value of the sorption capacity, $q_{e,\,exp}$ = 0.434 mg/g. As with Zn and Pb, kinetics was so fast that quasi-steady state approximation could be assumed at t = 1.5 min already; the q_t value at t = 3 min was within 1 % of the q_t value at time t = 1.5 min. Sorption equilibrium was attained within 10.5 min. Further evidence of a quasi-steady state approximation was the high values of fractional attainment of equilibrium, reaching unity in less than 11 min. Kinetic studies could therefore be based on short-time data.

[6] The value after 10 min is the average of the eight readings recorded between t = 12 – 24 min.

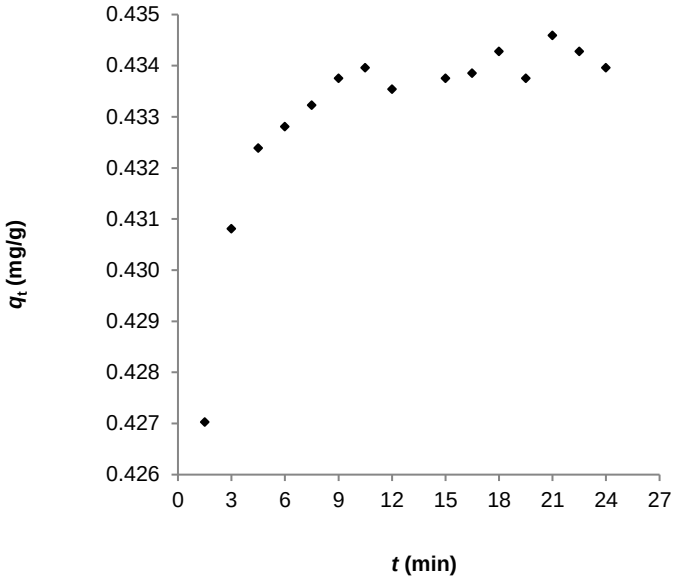

Fig. 5.58: Bi uptake as a function of time

The calculated sorption capacity was derived from the slope of a graph of t/q_t versus time (t) ($y = 2.2982x + 0.0683$).

$$\frac{1}{q_{e,calc}} = 2.2982$$

$$\therefore q_{e,\,calc} = 0.435 \text{ mg/g}$$

The good correlation between experimental and calculated sorption capacity meant pseudo-second order kinetics provided an excellent mathematical model to sorption kinetics. Sorption thus occurred predominantly via chemical reaction. The initial sorption rate was derived from the intercept of the graph, $\frac{1}{h} = 0.0683$. Thus, $h = 14.64$ mg/g·min^{-1}. This large value of h was congruent with the initial shape of the graph of q_t versus t; it was even higher than the initial sorption rate of Zn (2.712 mg/g·min^{-1}). The second order rate constant was calculated as before and found $k_2 = 77.34$ g/mg·min^{-1}. Bismuth therefore exhibited slower kinetics than Lead, despite its smaller ionic radius (1.07 Å). This anomaly could be explained by the fact that both Bi(III) and Pb(II) have $d^{10}s^2$ electron configuration. The lone s^2 electron pair may affect the stereochemistry of their complexes. However, in lead the lone electron pair occupies nearly half of the sphere of the ion, whereas in the hydrated Bi(III) complex with its distorted square anti-prism geometry, the stereochemical effects of the lone s^2 electron pair are suppressed probably due to the high charge density, yielding no gap for the lone electron pair. The hydrated Bi(III) complex therefore has a holo-directed configuration retarding its kinetics (Perrson, 2010).

A plot of log (q_e – q_t) against *time* (Fig. 5.59) was linear. This meant physical processes influenced Bi sorption. The pseudo-first order rate constant was k_1 = 0.406 min^{-1}.

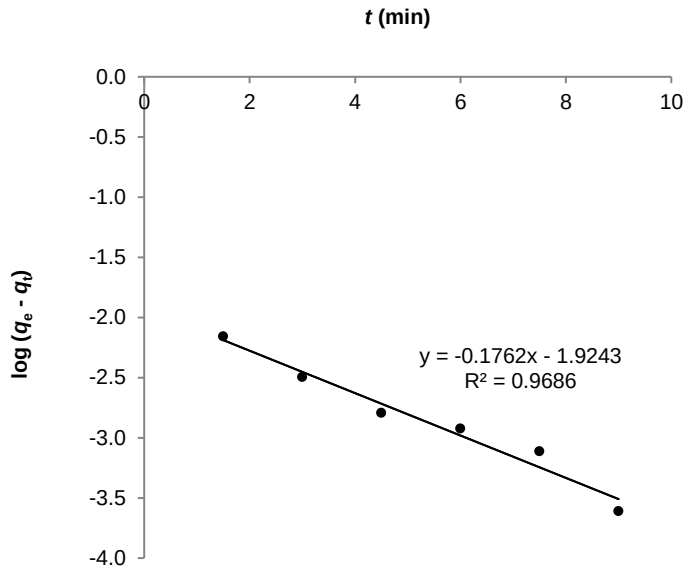

Fig. 5.59: Pseudo-first order plot of reaction kinetics modelling of Bi sorption

5.4.1.8 *Silver*

The kinetics of silver sorption was investigated in dynamic studies, where a feed solution of [Ag^+] = 6.857 mg/L was pumped through a column at 5.0 mL/min. 500 ± 5 mg of resin was packed in a 10 mL column with diameter 10 mm. The resin was conditioned with the same buffer (pH = 1.88) with which the sample solution was prepared. A yellow-orange band was observed in the resin as Ag^+ ions migrated through the column. The Ag^+ content in each eluate fraction was determined by ICP-OES. Table 5.39 represents a reduced sample of results.

Table 5.39: Experimental data of sorption reaction kinetics of Ag

t **(min)**	C_e **(mg/L)**	q_t **(mg/g)**	***X***
1.50	0.104	0.405	0.9849
3.00	0.088	0.406	0.9872
4.50	0.059	0.408	0.9914
6.00	0.029	0.410	0.9958
7.50	ND	0.411	1.0000
9.00	ND		
10.50	ND		

Ag was undetected (ND) in the eluate at t = 9.00 min and remained undetected thereafter. Maximum sorption capacity (q_e) was 0.411mg/g.

Kinetics was best modelled by pseudo-second order kinetics. From the plot described by the linear equation, $t/q_t = 2.4209t + 0.1051$ (r^2 =1), the amount of Ag^+ ions sorbed at equilibrium was calculated and found in good agreement with the experimental value.

$$\frac{1}{q_{e,calc}} = 2.4209$$

$$\therefore q_{e,\,calc} = 0.413 \text{ mg/g}$$

The pseudo-second order rate constant, k_2 was equal to 55.76 g/mg·min^{-1}.

Chemisorption was probably accompanied by physisorption as suggested by sorption energy values derived from the Freundlich, Temkin and D-R isotherms (Section 5.2.2), as well as the reasonably good correlation coefficient (r^2 = 0.9712) of a pseudo-first order graph (Fig. 5.60).

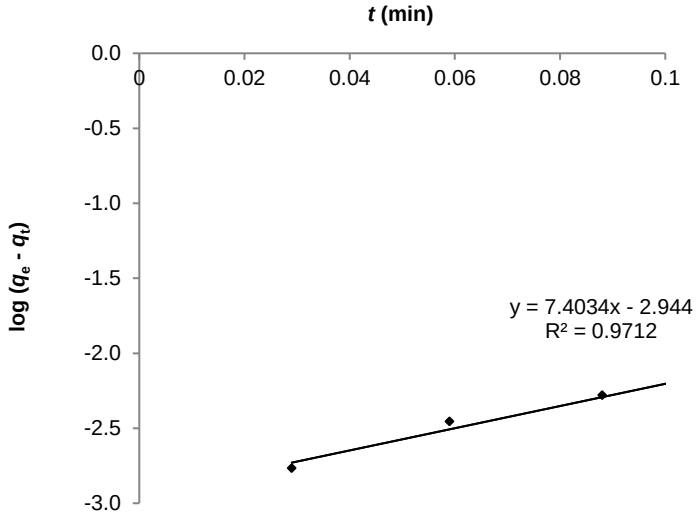

Fig. 5.60: Pseudo-first order plot of reaction kinetics modelling of Ag sorption

In summary, sorption of Ag, Bi, Cd, Co, Ni, Pb and Zn followed pseudo-second order reaction kinetics. Sorption of Cu onto dry, impregnated resin followed pseudo-first order kinetics though. Reaction kinetics of the metal ions was compared based on the values of their calculated rate constants. However, since studies were conducted using different experimental designs, data obtained under similar experimental conditions (batch versus column) were compared. Reaction kinetics of metals studied in batch experiments using wet resin decreased in the order: Cu^{2+}, Co^{2+}, Ni^{2+}, Pb^{2+}. Reaction kinetics of metals studied in column experiments decreased in the order: Pb^{2+}, Bi^{3+}, Zn^{2+}, Ag^+.

5.4.2 Diffusion kinetics

5.4.2.1 *Cadmium*

To determine the kinetics of diffusion, experimental data obtained in the two experiments discussed above were firstly applied to the Weber-Morris model. Plots of q_t versus $t^{½}$ (Fig. 5.61) produced straight lines, suggesting that sorption was controlled by intra-particle diffusion.

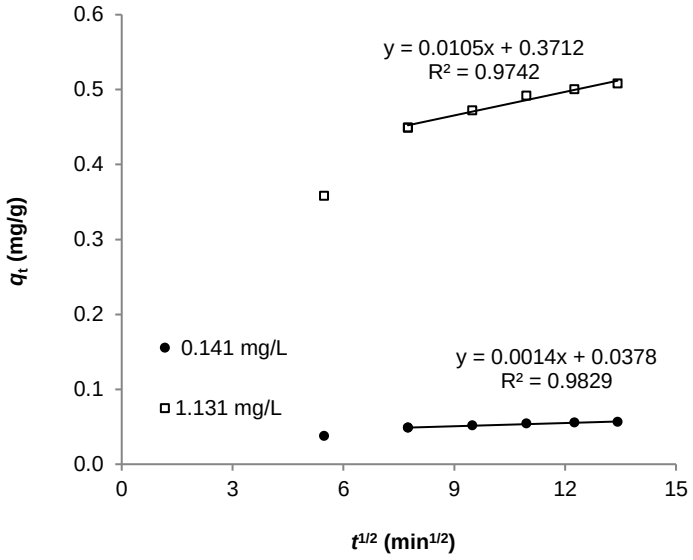

Fig. 5.61: Weber-Morris plots for modelling of Cd diffusion kinetics

The first data point (5.48; 0.358) of the 1.131 mg/L solution could not necessarily be deemed an outlier; instead, more data could have been collected in the time-interval 30 – 60 min to prove multi-linearity. Nonetheless, the fact that the plots did not pass through the origin suggested intra-particle diffusion was not the only diffusion mechanism that influenced the sorption process.

Arguably, at $t^{½} > 6$ min^{½} pore diffusion controlled the sorption of Cd^{2+} ions. Notwithstanding the scale used for the vertical axis, the bilinearity of the graph representing data of the 0.141 mg/L solution was less pronounced. It could be argued that the lower ion concentration gradient across the boundary layer impeded less on the initial pore diffusion, supporting a view expressed by Ho *et al.* (2000) that the concentration-dependence of a diffusion-sorption process will yield K_{ads} values that vary with the square root of concentration.

Experimental data was subsequently applied to the Homogeneous Particle Diffusion Model (HPDM) based on Nernst-Planck equations (2.13) and (2.14) as described by Cortina *et al.* (1998). Plots of *ln* $(1 - X^2)$ and *ln* $(1 - X)$ against *time* that passed through the origin would confirm pore and film diffusion as rate controlling mechanisms, respectively. For brevity, only experimental data of the 0.141 mg/L Cd^{2+} solution was plotted. Fairly linear graphs were obtained for both plots (Fig. 5.62), meaning both pore and film diffusion influenced the overall diffusion process.

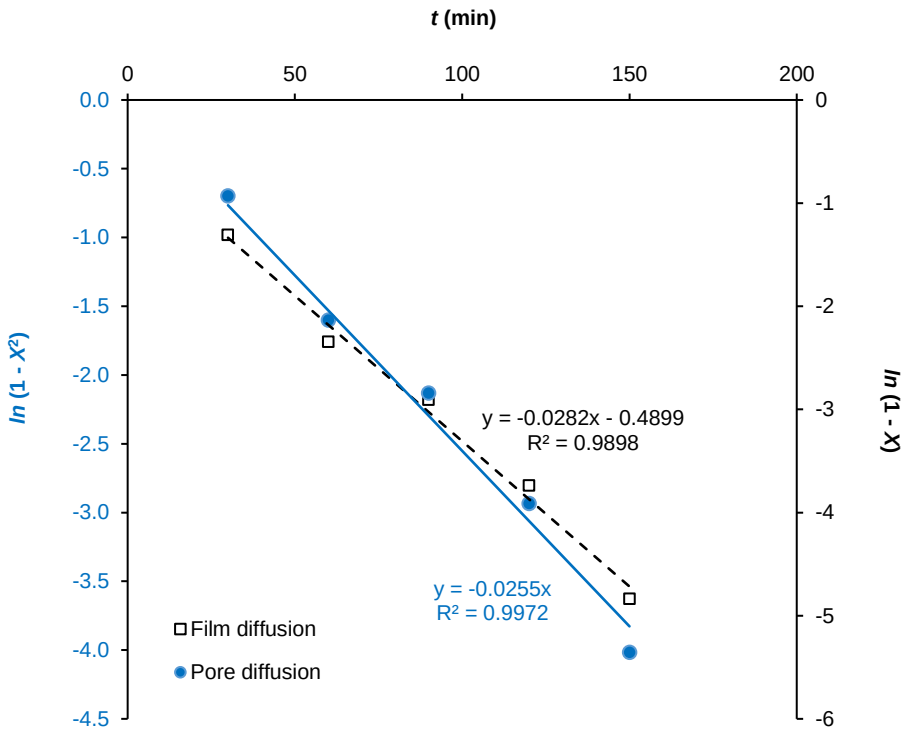

Fig. 5.62: Adsorption plots of pore and film diffusion mechanisms of Cd sorption; $[Cd^{2+}]_0$ = 0.141 mg/L

The film diffusion graph did not pass through the origin, from which it can be inferred pore diffusion was more likely the rate-limiting mechanism. The pore diffusion constant (k_{pore}) was obtained from the slope of the corresponding graph (k_{pore} = 0.013 min^{-1}) and used to determine the pore diffusion coefficient, D_r:

$$D_r = \frac{k_p {r_0}^2}{\pi^2} = \frac{0.013\ min^{-1} \times (37.5 \times 10^{-4} cm)^2}{\pi^2} = 3.1 \times 10^{-10} cm^2 \cdot s^{-1}$$

This value confirmed the inference that one could not differentiate between pore or film diffusion as rate controlling step. In earlier studies (Saha *et al.*, 2000 and Bilba *et al.*, 1999) sorption of cadmium ions onto thiol containing chelating resins and Purolite S-930 was controlled by pore diffusion. Elsewhere (Cortina *et al.*, 2006) it was postulated that liquid-film diffusion controlled the metal extraction rate at low concentrations of metal ions.

Sorption data of the 0.141 mg/L Cd^{2+} solution was applied to the HPD model based on Fick's laws as proposed by Qiu *et al.* (2009) and Nibou *et al.* (2010). Since the values of *X* were in the range 0.6637 – 1.000, a graph of *ln* (1 – *X*) versus *time* (Fig. 5.63) was accordingly constructed as described by Eq. (2.19)[7]:

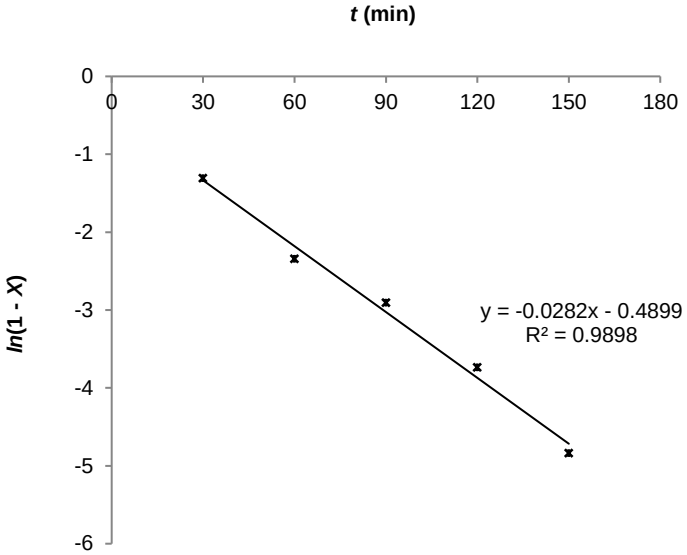

Fig. 5.63: Test of HPDM for modelling Cd diffusion kinetics; $[Cd^{2+}]_0$ = 0.141 mg/L

This graph provided an excellent fit to experimental data (r^2 = 0.9898). The value of the pore diffusion coefficient, D_r, was determined from the slope of the graph. The calculated value agreed favourably with the value found earlier:

$$D_r = -\frac{S_r r_0^2}{\pi^2} = -\frac{-0.0282\times(37.5\times10^{-4})^2}{\pi^2} = 6.7\times10^{-10} cm^2\cdot s^{-1}$$

A similar graph (Fig. 5.64) was plotted based on data obtained for the 1.131 mg/L Cd^{2+} solution. *X* values were resembled those of the 0.141 mg/L solution, proving that attainment of fractional equilibrium was independent of initial ion concentration. It was therefore *not* unexpected for the graph to resemble that in Fig. 5.63.

[7] The value of r_0 was taken as the mean radius of the resin beads (37.5×10^{-4} cm)

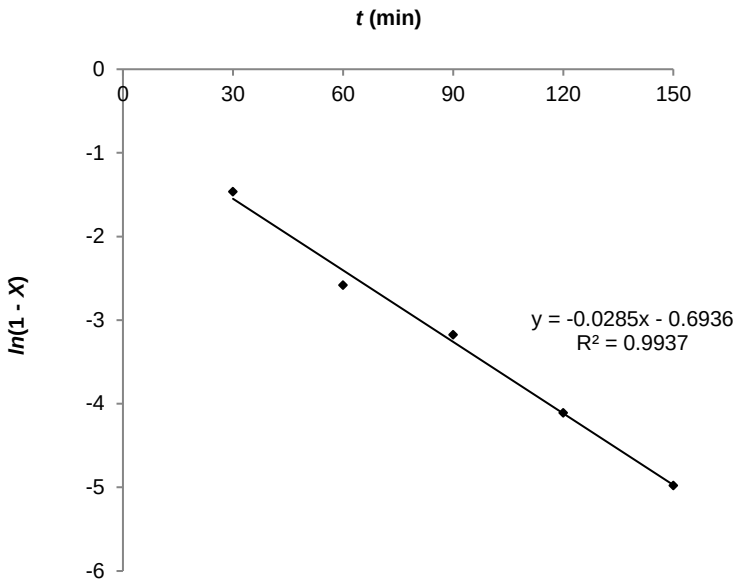

Fig. 5.64: Test of HPDM for modelling Cd diffusion kinetics; $[Cd^{2+}]_0$ = 1.131 mg/L

As expected, the value of the pore diffusion coefficient, D_r, was similar to that obtained at lower concentration:

$$D_r = -\frac{S_r r_0^2}{\pi^2} = -\frac{-0.0285\times(37.5\times10^{-4})^2}{\pi^2} = 6.8\times10^{-10} cm^2\cdot s^{-1}$$

Both values of the pore diffusion coefficient were not in either of the ranges described by Doke & Khan (2017), meaning Eq. (2.20) could not reliably predict pore diffusion as controlling diffusion mechanism. Instead, these values attested to the duality of pore and film diffusion as contributors to the overall sorption process.

Finally, graphs of X versus $t^{½}$ (Fig. 5.65) were drawn for initial concentrations 0.141 mg/L (low) and 1.131 mg/L (high) respectively. The similarity of the graphs proved the earlier assertion that fractional attainment of equilibrium (X) was independent of concentration. Graphs deviated from linearity and did not pass through the origin. Similar deviations from linearity were observed by Bilba *et al.* (1999) and Cortina *et al.* (1998) who ascribed the phenomenon to film diffusion effects.

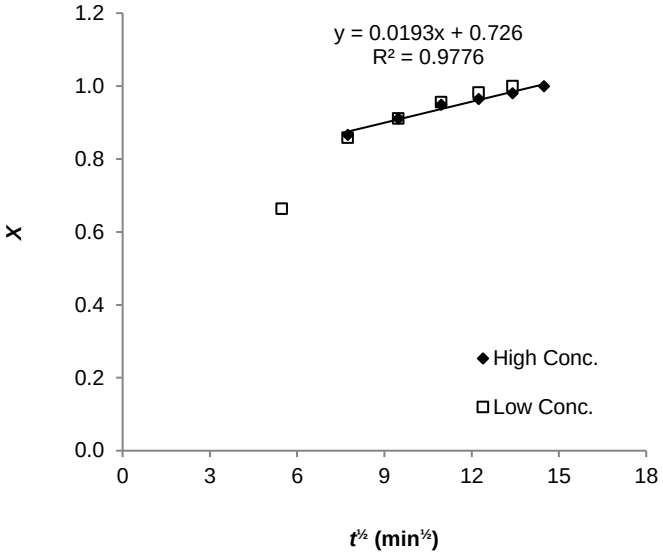

Fig. 5.65: Rates of fractional attainment of equilibrium of Cd sorption

The pore diffusion coefficient was derived from the second portion of the curve only and confirmed the predominance of pore diffusion after $t^{½}$ > 7.75 $min^{½}$.

$$D_{rr} = \frac{S_{rr}^2 \pi r^2}{36} = \frac{(0.0193)^2 \times \pi \times (37.5 \times 10^{-4})^2}{36} = 7.6 \times 10^{-12} cm^2 \cdot s^{-1}$$

In summary, all kinetic diffusion models applied to Cd^{2+} sorption attested to the duality of pore and film diffusion. However, film diffusion only controlled the initial stage of the sorption process – this could be credited to the mild degree of agitation in the bulk solution.

5.4.2.2 *Copper*

Due to insufficient data obtained in the last experiment, data from an earlier experiment was applied to the Weber-Morris and HPD models to gain insight into the diffusion regime of Cu^{2+} sorption. In this experiment, 0.4 g of resin was shaken in a 5.986 mg/L Cu^{2+} solution at pH = 2.88.

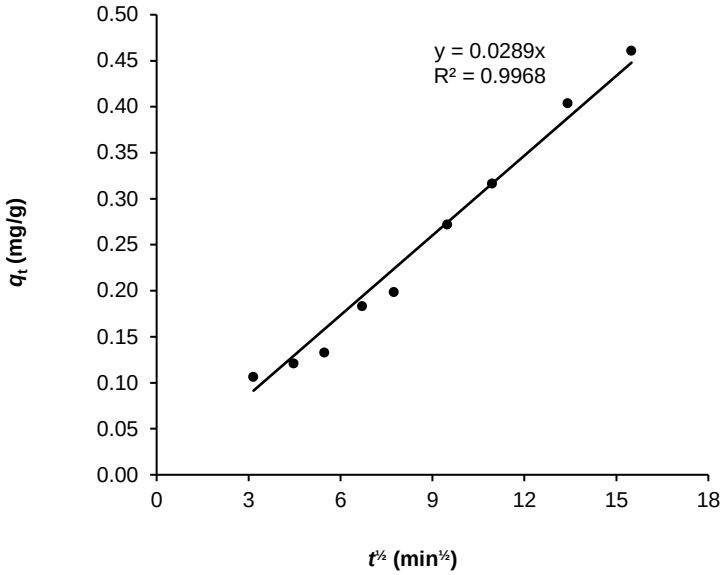

Fig. 5.66: Weber-Morris plot for modelling of pore diffusion mechanism of Cu sorption

A linear graph (Fig. 5.66) with good correlation coefficient (r^2 = 0.9837) that passed through the origin meant pore diffusion controlled the sorption process and was the only rate-determining step. In a repeat experiment at the same pH but lower metal ion concentration (1.709 mg/L), a plot of q_t versus $t^{½}$ produced a similar linear graph passing through the origin, with K_{ads} = 0.0298 mg/g/min^{½} and correlation coefficient, r^2 = 0.9761.

Among the metals studied, Cu(II) was the only metal with d^9 configuration and whose hydrated complex displayed Jahn-Teller distorted octahedral configuration (two longer axial and four shorter equatorial bond distances). Jahn-Teller distortions are more pronounced in systems with an odd number of electrons in the e_g orbitals, such as Cu^{2+} and Cr^{3+}. The distorted Cu^{2+} system is more stable than the undistorted complex by 0.5 δ_1 (Persson, 2010). The distortion can be pronounced, to the extent that the geometry of the hydrated Cu(II) ion can be regarded as effectively square planar. Disruption of the hydrated sphere of the square planar hydrated Cu^{2+} ion is probably faster compared to the octahedral hydrated complexes of other metals in this study, explaining its faster film diffusion.

Plots of *ln* (1 – X^2) versus *time* (*t*) and *ln* (1 – *X*) versus *time* (*t*) representing Nernst-Planck pore and film diffusion equations, respectively, are shown in Fig. 5.67. Experimental data of the 5.986 mg/L solution were used.

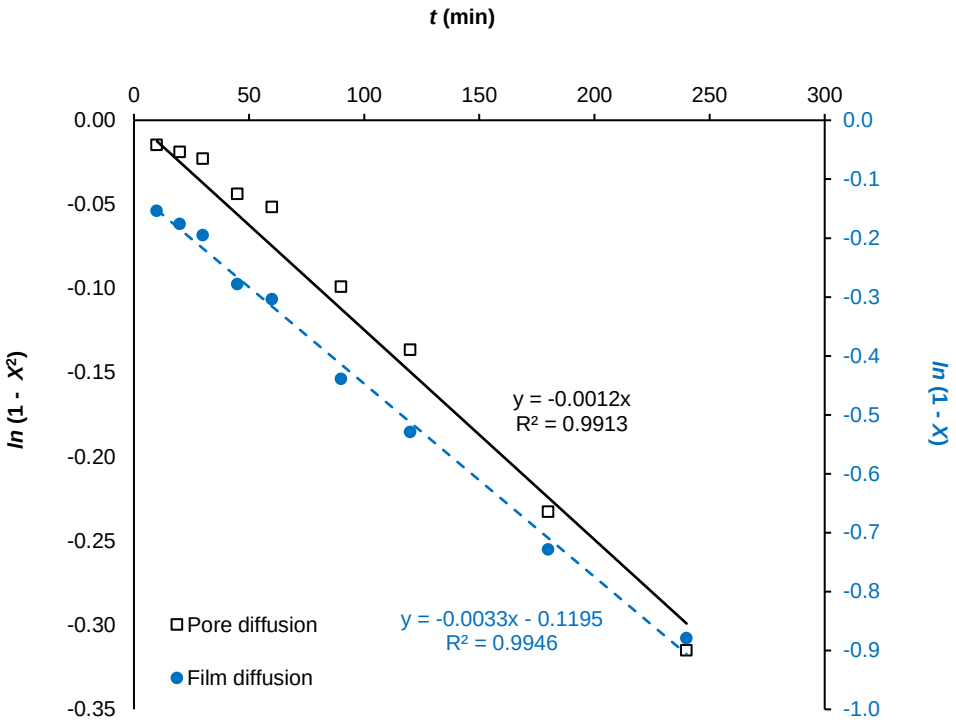

Fig. 5.67: Adsorption plots of pore and film diffusion mechanisms of Cu sorption

Although the correlation coefficient associated with film diffusion (r^2 = 0.9946) was higher, the graph did not pass through the origin. The pore diffusion rate constant and the corresponding diffusion coefficient, D_r, were calculated.

$$2\,k = 0.0012$$

$$\therefore\ k_p = 0.0006\ \text{min}^{-1}$$

$$D_r = \frac{k_p {r_0}^2}{\pi^2} = \frac{0.0006\ min^{-1} \times (37.5 \times 10^{-4} cm)^2}{\pi^2} = 1.4 \times 10^{-11} cm^2 \cdot s^{-1}$$

Since D_r was within the range 10^{-11} – 10^{-13} $cm^2 \cdot s^{-1}$, it suggests diffusion was controlled by pore diffusion.

Fractional attainment of equilibrium (X) was generally low ($0.12 < X < 0.52$) over a period of 240 min. A plot of X against $t^{½}$ (Fig. 5.68) was nonetheless considered a realistic proposition.

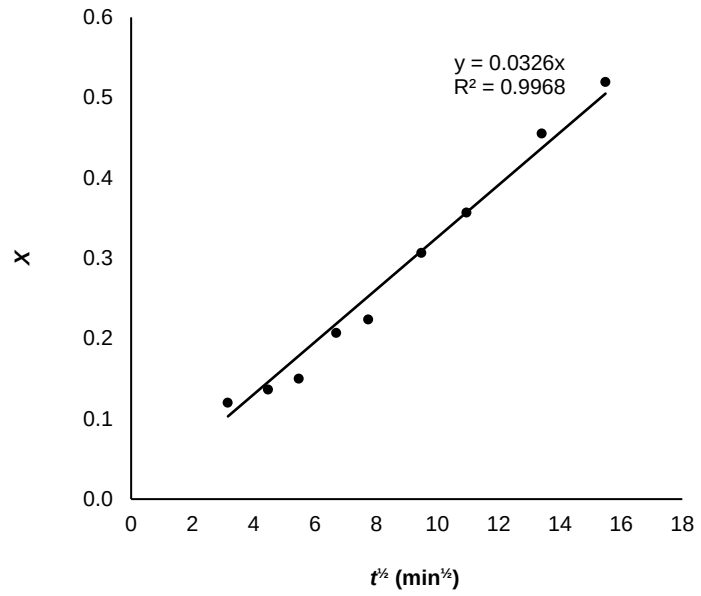

Fig. 5.68: Rate of fractional attainment of equilibrium of Cu sorption

The pore diffusion coefficient was derived from the graph depicted in Fig. 5.68.

$$D_r = \frac{{S_r}^2 \pi r^2}{36} = \frac{(0.0326)^2 \times \pi \times (37.5 \times 10^{-4})^2}{36} = 2.2 \times 10^{-11} cm^2 \cdot s^{-1}$$

Since the above value of the pore diffusion coefficient was in the range 10^{-11} – 10^{-13} $cm^2 \cdot s^{-1}$, it proved unambiguously that the diffusion process was controlled by pore diffusion. The HPD model was nonetheless tested further using Eq. (2.20) on the basis that sorption occurred over a long time (240 min). A plot of *ln* (1 – *X)* versus *time* produced a characteristic linear graph (Fig. 5.69).

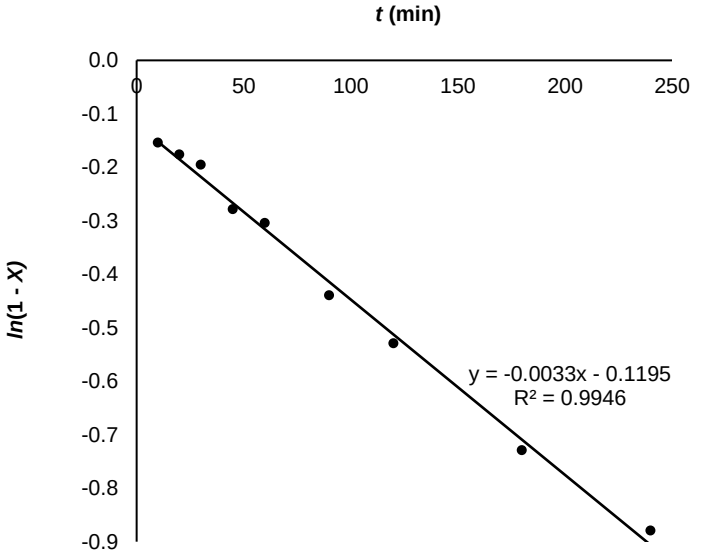

Fig. 5.69: Test of HPD model to predict diffusion kinetics of Cu sorption

The slope of this graph was used to calculate the pore diffusion coefficient (D_r). Since $D_r \in [10^{-11} – 10^{-13}\ cm^2 \cdot s^{-1}]$, it corroborated earlier conclusions that pore diffusion was the rate-controlling mechanism.

$$D_r = \frac{k_p {r_0}^2}{\pi^2} = \frac{0.0033\ min^{-1} \times (37.5 \times 10^{-4} cm)^2}{\pi^2} = 7.8 \times 10^{-11} cm^2 \cdot s^{-1}$$

5.4.2.3 *Zinc*

Diffusion kinetics was evaluated by applying experimental data to the Weber-Morris equation. The bi-linear plot[8] shown in Fig. 5.70 proved pore diffusion was the rate-determining mechanism. The graph did not pass through the origin: both linear portions cut the vertical axis at values *I* = 0.200 mg/g and 0.208 mg/g, respectively. Pore diffusion was therefore preceded by film diffusion. The relatively high I-values suggested film diffusion significantly controlled the initial stages of the sorption process.

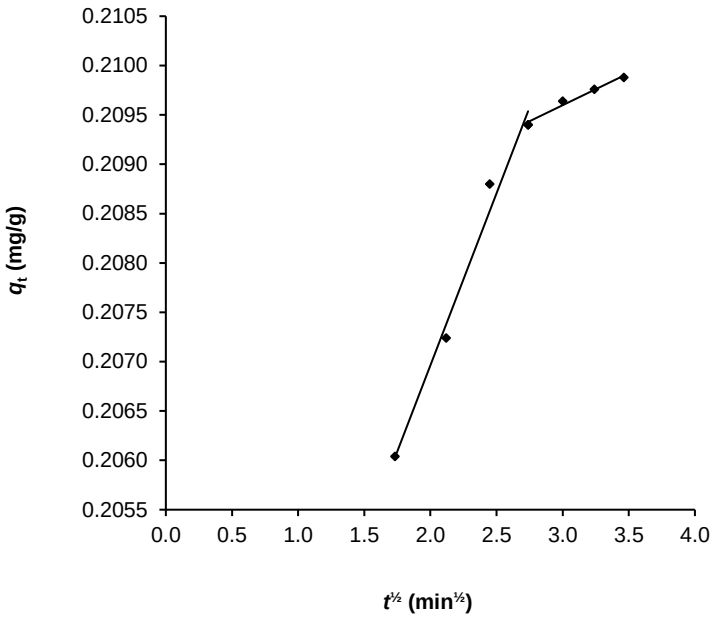

Fig. 5.70: Weber-Morris plot for the diffusion kinetic modelling of Zn sorption

The fractional attainment of equilibrium (*X*) converged to 1.000 at 12 min and exceeded the 0.3-value proposed by Qiu and co-workers (2006) by far. A linear plot of *ln* (1 – *X*) versus *time* (r^2 = 0.9924) meant pore diffusion was the rate-determining step in the overall diffusion of Zn.

[8] The bilinearity of the graph is accentuated by the scale of the vertical axis.

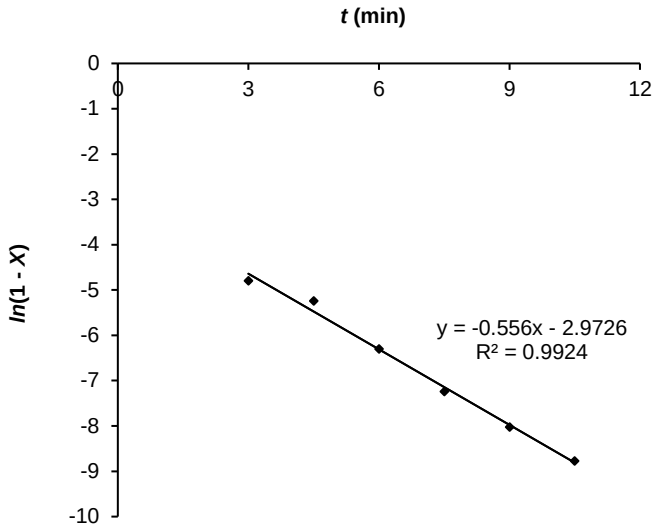

Fig. 5.71: Test of a mathematical model proposed for homogeneous particle diffusion of Zn^{2+}

The value of the pore diffusion coefficient was calculated:

$$D_r = \frac{k_p {r_0}^2}{\pi^2} = \frac{0.556\ min^{-1} \times (37.5 \times 10^{-4} cm)^2}{\pi^2} = 1.3 \times 10^{-8} cm^2 \cdot s^{-1}$$

This value suggested that Zn sorption was controlled by film diffusion over the entire sorption period. However, since a quasi-steady state approximation was established in short time, a plot of X versus $t^{½}$ would probably provide more reliable and realistic information about the rate-determining diffusion mechanism, despite the high value of fractional attainment of equilibrium. Such an assumption showed a predisposition towards the time factor rather than fractional attainment of equilibrium. Fig. 5.72 shows the plot of X versus $t^{½}$.

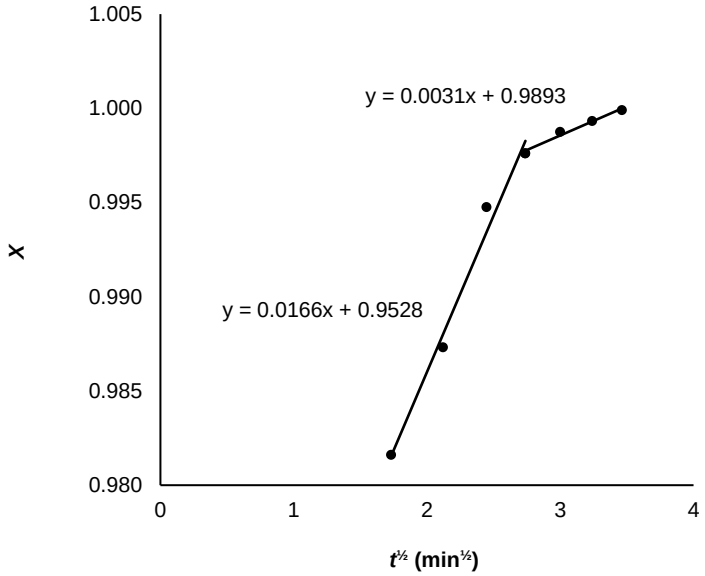

Fig. 5.72: HPDM plot for diffusion modelling of Zn^{2+} sorption, assuming short-time data

The initial pore diffusion coefficient D_i was derived from the earlier portion of the graph as follows:

$$D_i = \frac{{S_i}^2 \pi r^2}{36} = \frac{(0.0166)^2 \times \pi \times (37.5 \times 10^{-4})^2}{36} = 5.6 \times 10^{-12} cm^2 \cdot s^{-1}$$

Similarly, from the second portion of the graph, the value of D_f was calculated:

$$D_f = \frac{{S_f}^2 \pi r^2}{36} = \frac{(0.0031)^2 \times \pi \times (37.5 \times 10^{-4})^2}{36} = 2.0 \times 10^{-13} cm^2 \cdot s^{-1}$$

Both values confirmed pore diffusion as rate-controlling mechanism as they were in the interval 10^{-11} – 10^{-13} $cm^2 \cdot s^{-1}$. Diffusion coefficients were thus lower in the order 10^5. A similar trend emerged in other experiments where quasi-steady state approximation was assumed (see Sections 5.4.1.6 – 5.4.1.8).

5.4.2.4 *Nickel*

Diffusion kinetics of Ni^{2+} ions was controlled by pore diffusion as demonstrated by the two distinct linear portions of the graph of q_t versus $t^{½}$ (Fig. 5.73).

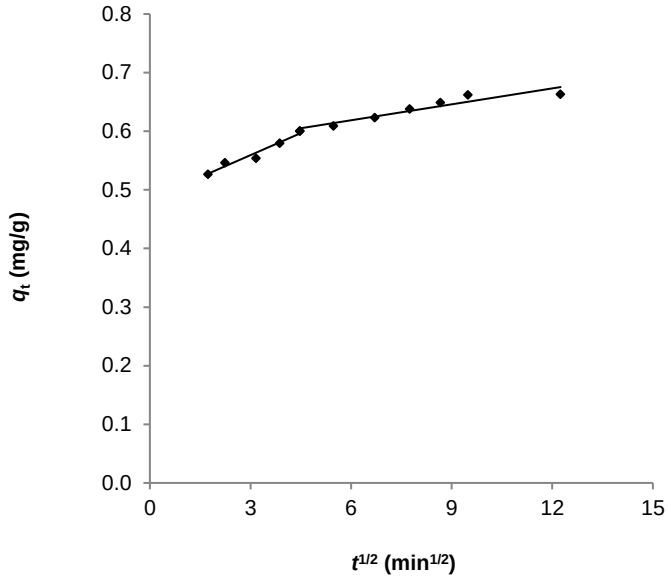

Fig. 5.73: Weber-Morris plot of intra-particle diffusion of Ni

Kinetics data was subjected to the HPD model. The fractional attainment at equilibrium (X) was greater than 0.3. A plot of *ln* (1 – X) versus *time* produced a straight line described by the equation *ln* (1 – X) = -0.0349t – 1.896 (Fig. 5.74).

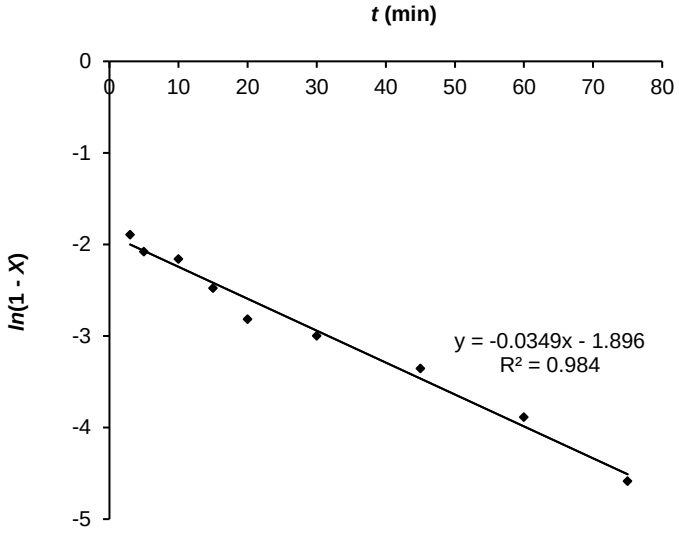

Fig. 5.74: HPDM plot of diffusion kinetic modelling of Ni sorption; X > 0.3

Despite a reasonable correlation coefficient, the above graph presented an illogicality – at the boundary condition t = 0, the value of X approached the improbable value of X = 0.850. Aside from this, the value of the diffusion constant, D_r, suggests neither film nor pore diffusion was rate controlling:

$$\frac{D_r \pi^2}{r_0^2} = 0.0349$$

$\therefore D_r = 8.3 \times 10^{-10}$ cm^2·s^{-1}

Since fractional attainment of equilibrium approached unity after a relatively long time, it could be argued that Eq. (2.20) would no longer hold true, in which case a linear plot of X versus $t^{½}$ would be a more realistic model to predict the rate-determining diffusion mechanism. Indeed, a linear graph was obtained (Fig. 5.75) that failed to pass through the origin.

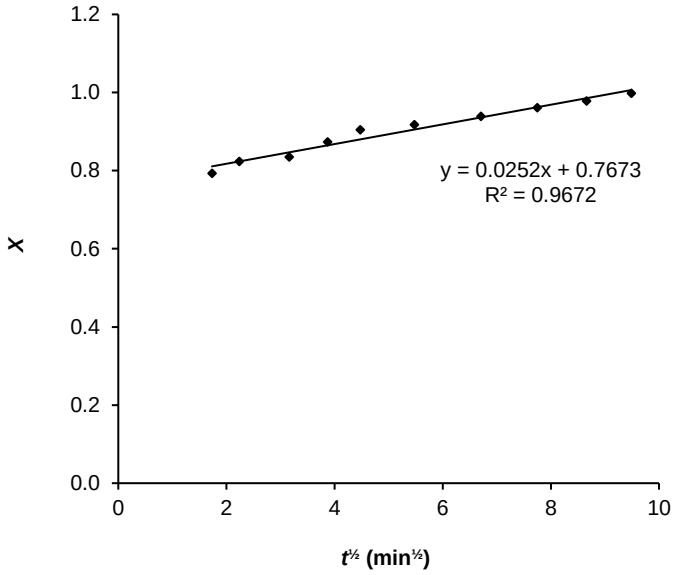

Fig. 5.75: An HPDM plot of diffusion kinetic modelling of Ni sorption based on short-time data

The pore diffusion coefficient D_r was calculated from the slope of the graph, its value suggesting pore diffusion was the rate-controlling process:

$$D_r = \frac{{S_r}^2 \pi r^2}{36} = \frac{(0.0252)^2 \times \pi \times (37.5 \times 10^{-4})^2}{36} = 1.3 \times 10^{-11} cm^2 \cdot s^{-1}$$

Diffusion kinetics was subjected to HPDM defined by the Nernst-Planck equation. Fig. 5.76 shows the results of studies over the first 75 min of the experiment.

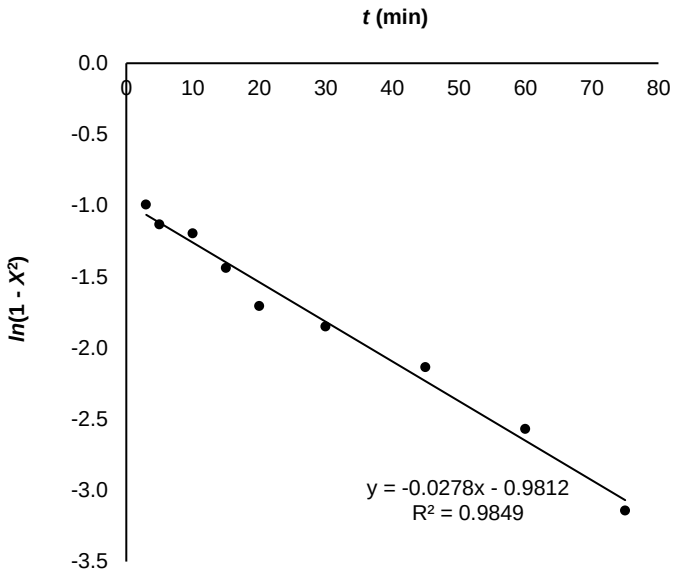

Fig. 5.76: HPDM plot of pore diffusion of Ni; *t* < 75 min

The pore diffusion coefficient was calculated accordingly, its value suggesting both pore and film diffusion-controlled sorption.

$$D_r = \frac{k_r {r_0}^2}{\pi^2} = \frac{0.0278\ min^{-1} \times (37.5 \times 10^{-4} cm)^2}{\pi^2} = 6.6 \times 10^{-10} cm^2 \cdot s^{-1}$$

5.4.2.5 *Cobalt*

A plot of q versus $t^{½}$ produced a mono-linear graph (Fig. 5.77) that did not pass through the origin. Pore diffusion was therefore not the only diffusion mechanism. Since the graph was uni-linear, the rate of intra-particle diffusion was seemingly independent of pore size.

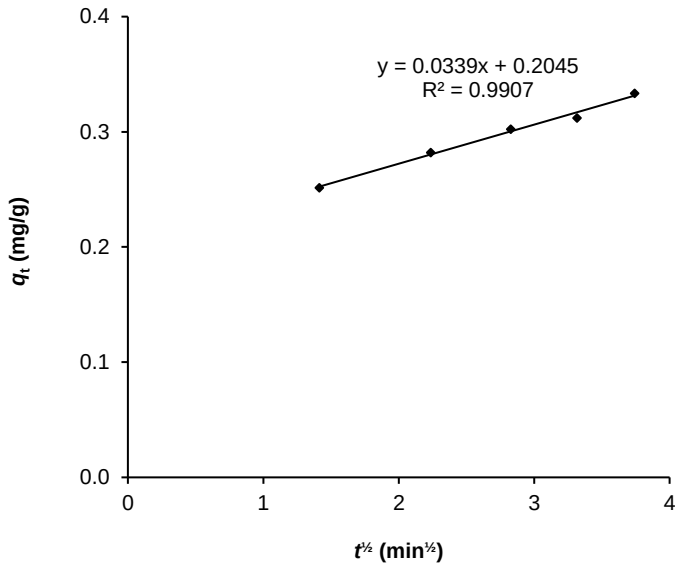

Fig. 5.77: Weber-Morris plot of Co intra-particle diffusion

The rate constant of intra-particle diffusion (K_{ads}) was equal to 0.034 mg/g·min^{½} and I = 0.205 mg/g. The K_{ads} value deviated considerably from the pseudo-second order rate constant (and to a lesser extent from the pseudo-first order rate constant) which suggested diffusion kinetics was not comparable to reaction kinetics. In other words, the overall sorption rate of Co^{2+} was determined primarily by the rate of formation of the Co-dithizonate complex.

Co diffusion kinetics exhibited the same incongruity as Zn, viz. fractional attainment at equilibrium (X) was greater than 0.3, but unity was attained in short time. Steady state approximation could not be assumed as with Zn, because q-values were not within 1 % of each other. Data was therefore applied to the HPDM according to the interpretation of Qiu *et al.* (2010). Fig. 5.78 below depicts the graph of *ln* (1 – X) versus *time*.

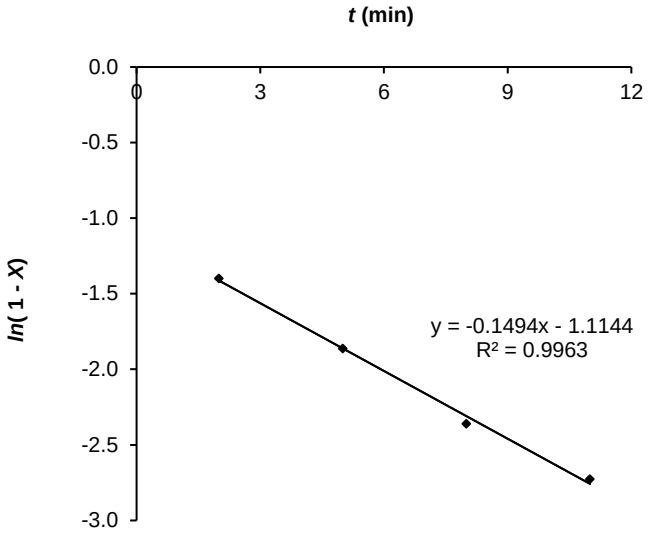

Fig. 5.78: HPDM plot for diffusion kinetics modelling of Co sorption

As $t \rightarrow 0$, $ln\ (1 - X) \rightarrow$ -1.1144 and the value of resin conversion approached a realistic value of X = 0.6719. From the slope of the graph, the value of the diffusion coefficient, D_r, was determined. The calculated value of D_r endorsed the contribution of film diffusion to the sorption process.

$$\frac{D_r \pi^2}{r_0^2} = 0.1494$$

$$\therefore D_r = 3.6 \times 10^{-9}\ cm^2 \cdot s^{-1}$$

Despite the large values of X, data was nonetheless applied to the equation assuming short-time data. The graph of X plotted against $t^{½}$ was used to derive the pore-diffusion coefficient D_i (Fig. 5.79).

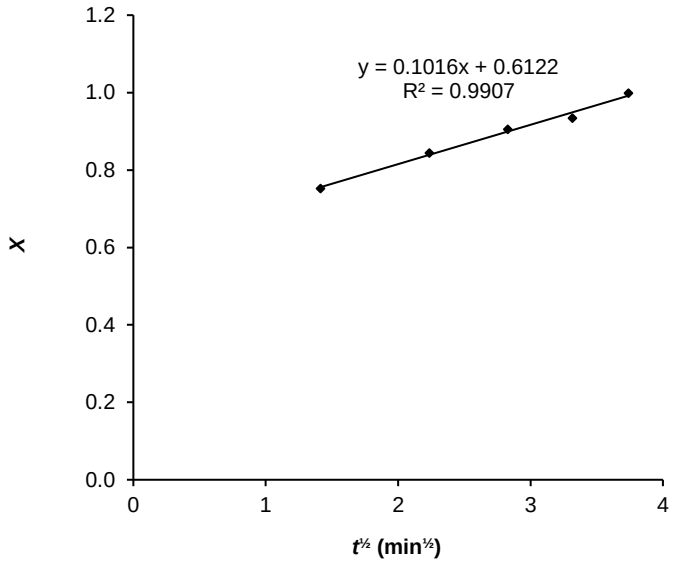

Fig. 5.79: HPDM plot for modelling diffusion kinetics of Co sorption, assuming short-time data

From the slope (S_i) of the graph,

$$D_i = \frac{S_i^2 \pi r^2}{36} = \frac{(0.1016)^2 \times \pi \times (37.5 \times 10^{-4})^2}{36} = 2.1 \times 10^{-10} cm^2 \cdot s^{-1}$$

The latter value, combined with the fact that the graph did not pass through the origin, also ruled out the possibility of pore diffusion as the exclusive mechanism.

Lastly, the HPDM model based on the Nernst-Planck equations was assessed. Both functions *ln* $(1 - X^2)$ and *ln* $(1 - X)$ exhibited excellent linear relationships with *t* yet failed to pass through the origin (Figs. 5.80 and 5.81).

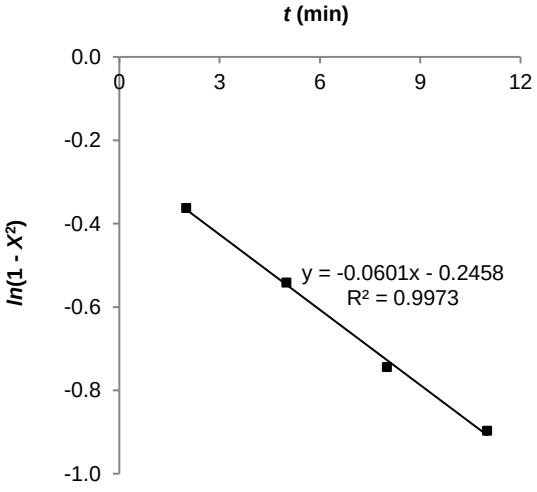

Fig. 5.80: HPDM plot for pore diffusion of Co

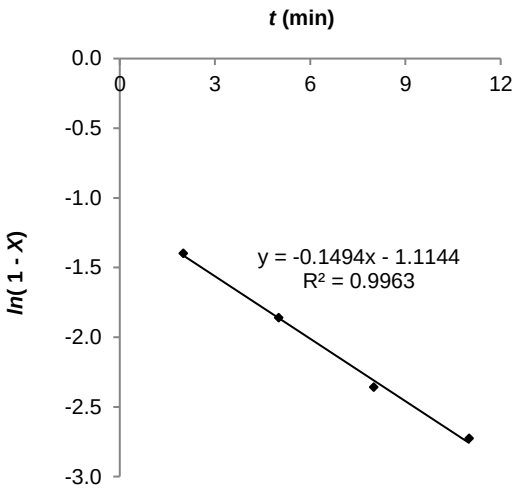

Fig. 5.81: HPDM plot for film diffusion of Co

From the graph of *ln* (1 – X^2) versus *t*, the pore diffusion coefficient was calculated:

$$\frac{D_r \pi^2}{r_0^{\ 2}} = 0.0301$$

$$\therefore D_r = 7.2 \times 10^{-10}\ \text{cm}^2 \cdot \text{s}^{-1}$$

All calculated values of diffusion coefficients fell outside either range as specified earlier, confirming that pore and film diffusion both contributed to diffusion kinetics. Pore diffusion coefficients had lower values (in the order 10^{-10} $\text{cm}^2 \cdot \text{s}^{-1}$) than the film diffusion coefficient ($\times 10^{-9}$ $\text{cm}^2 \cdot \text{s}^{-1}$), suggesting that pore diffusion occurred at a slower rate than film diffusion as earlier inferred and was therefore the rate-determining mechanism.

5.4.2.6 *Lead*

Experimental data of Pb(II) sorption was applied to the Weber-Morris model (Fig. 5.82). A mono-linear graph was obtained that did not pass through the origin, implying diffusion was controlled by both pore and film diffusion.

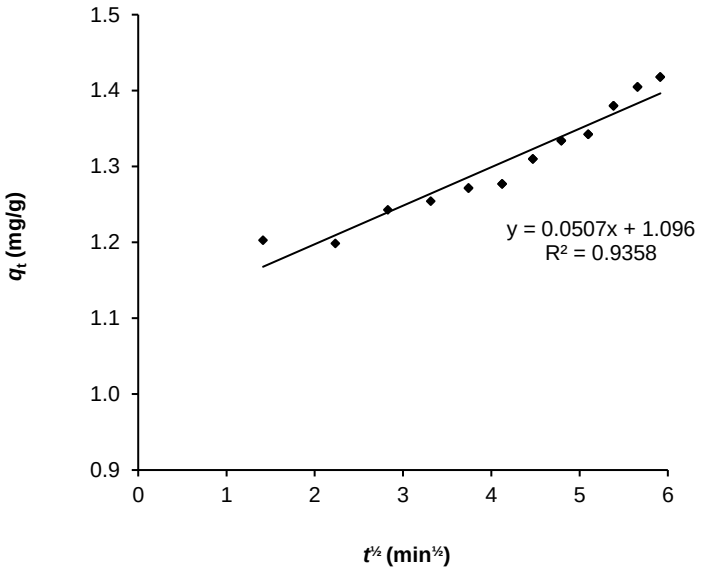

Fig. 5.82: Weber-Morris plot for intra-particle diffusion of Pb^{2+} ions

Since *X* > 0.3, a graph of *ln* (1 – *X*) against *time* (Fig. 5.83) was constructed from which the value of the pore diffusion constant was derived.

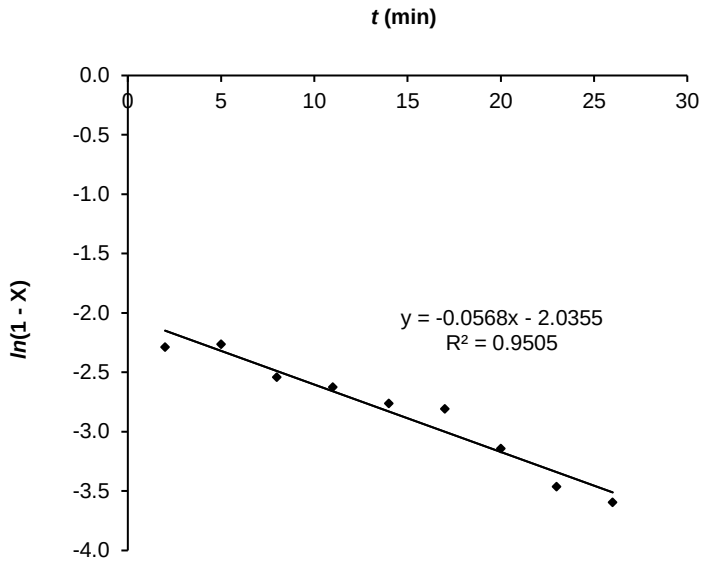

Fig. 5.83: HPDM plot for diffusion kinetics of Pb sorption

$$\frac{D_r \pi^2}{r_0^2} = 0.0568$$

$$\therefore D_r = 1.4 \times 10^{-9}\ \text{cm}^2 \cdot \text{s}^{-1}$$

The D_r-value suggested HPDM could not discriminate between film diffusion and pore diffusion as the rate-determining mechanism. The HPDM was subsequently tested by constructing a plot of X against $t^{½}$ (Fig. 5.84).

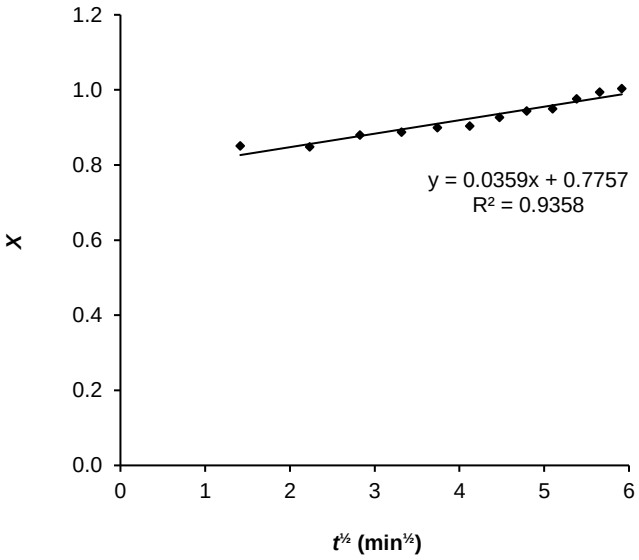

Fig. 5.84: A test of the HPDM for modelling diffusion kinetics of Pb

The slope of the graph was used to calculate the pore diffusion constant, D_i as shown below.

$$D_i = \frac{S_i^2 \pi r^2}{36} = \frac{(0.0359)^2 \times \pi \times (37.5 \times 10^{-4})^2}{36} = 2.6 \times 10^{-11} cm^2 \cdot s^{-1}$$

The calculated value implied sorption was controlled by pore diffusion.

To validate the assertion that the column method was more efficient than the batch method (Chwastowska & Kosiarska, 1988), the kinetics of Pb sorption was investigated utilising a column packed with 0.5 g resin. The resin was equilibrated at pH = 5.76 before a 2.765 mg/L Pb^{2+} solution was passed through at a constant flow rate of 5 mL/min. Eluate fractions were collected every 90 seconds. The Pb content of each eluate fraction was determined by ICP-OES (see Table 5.40).

Table 5.40: Sorption kinetics data of Pb; column method; [Pb^{2+}] = 2.765 mg/L

t (min)	C_e (mg/L)	% Sorption	q_t (mg/g)	X
1.5	0.102	96.311	0.280	0.981
3.0	0.073	97.360	0.283	0.992
4.5	0.059	97.866	0.284	0.997
6.0	0.058	97.902	0.284	0.997
7.5	0.055	98.011	0.285	0.998
9.0	0.053	98.083	0.285	0.999
10.5	0.051	98.156	0.285	1.000
12.0	0.054	98.047	0.285	
13.5	0.053	98.083	0.285	
15.0	0.051	98.156	0.285	
16.5	0.053	98.083	0.285	
18.0	0.057	97.939	0.284	
19.5	0.051	98.156	0.285	
21.0	0.051	98.156	0.285	
28.5	0.050	98.192	0.285	
$Ave_{t>9}$	0.052			
SD	0.002			
RSD	3.942			

The percentage sorption achieved by the column method exceeded that of the batch method by more than 20 %. Sorption was quantitative and reached saturation (q_e = 0.285 mg/g) in less than eight minutes. Moreover, the efficiency of the column method could be assessed in terms of the rate of fractional attainment of equilibrium (Fig. 5.85). In the column method, X approached unity faster compared to the batch method.

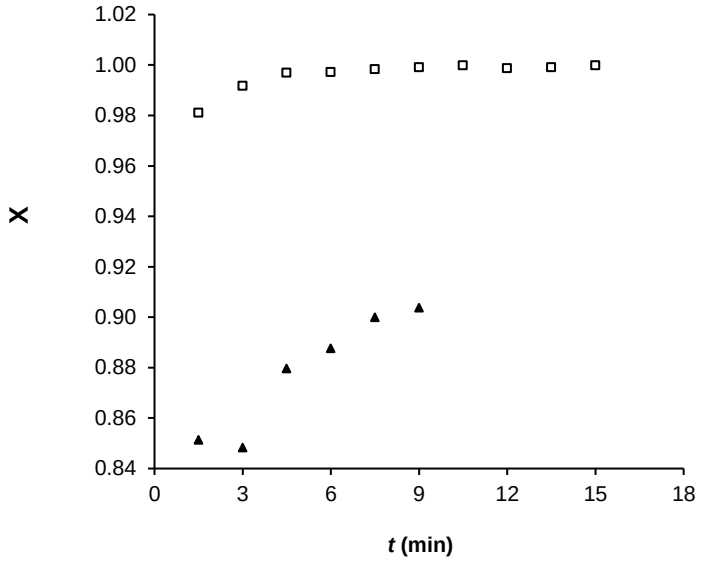

Fig. 5.85: Comparing rates of attainment of fractional equilibrium of Pb in batch (□) and column (▲) experiments

Kinetics of dynamic sorption was best fitted to the pseudo-second order equation (t/q_t = 3.4988 t + 0.1123). The calculated sorption capacity ($q_{e,\,calc}$ = 0.286 mg/g) was in close agreement with the experimental value (0.285 mg/g). The perfect correlation (r^2 = 1) could, however, be attributed to the steady-state approximation; t/q_t increased linearly with time because the values of q_t remained virtually constant over the entire time-period. The pseudo-second order rate constant, k_2, was calculated and found equal to 108.87 g/mg·min^{-1}. The large k_2-value bore further testimony to the efficiency of the dynamic technique. A graph (Fig. 5.86) representing Lagergren pseudo-first order kinetics also showed good correlation between log ($q_e - q_t$) and *time*. The pseudo-first order rate constant, k_1, was equal to 0.393 min^{-1}.

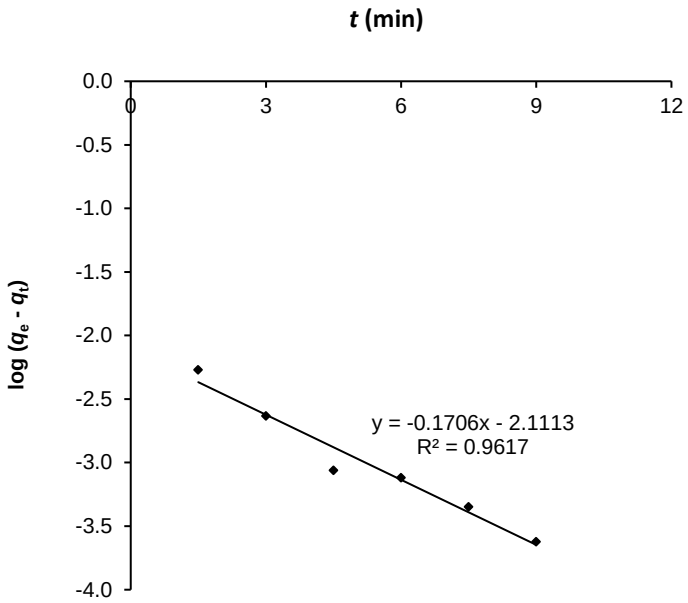

Fig. 5.86: Pseudo-first order plot of reaction kinetics modelling of Pb sorption

The fast kinetics of Pb^{2+} was incongruent with its large ionic radius (1.20 Å). According to Persson (2010), heavy metal ions with ionic radius greater than 0.98 Å are expected to have coordination number higher than eight in a square antiprism configuration. However, the structure of the hydrated Pb^{2+} ion ($d^{10}s^2$) is strongly affected by the lone pair, resulting in a hemi-directed structure with low symmetry. In the hemi-directed structure (Fig. 5.87), a “gap” in the molecular structure houses the lone pair, making it more accessible for coordinate bonding as opposed to the holo-directed structure (Fig. 5.88). Extended X-ray absorption fine structure (EXAFS) studies revealed the mean Pb–O bond distance in the hydrated Pb(II) ion in aqueous solution was 2.54 Å, strongly indicating a hemi-directed six-coordinate complex.

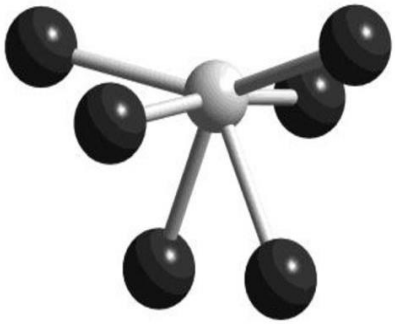

Fig. 5.87: Hemi-directed configuration of the Pb^{2+} ion

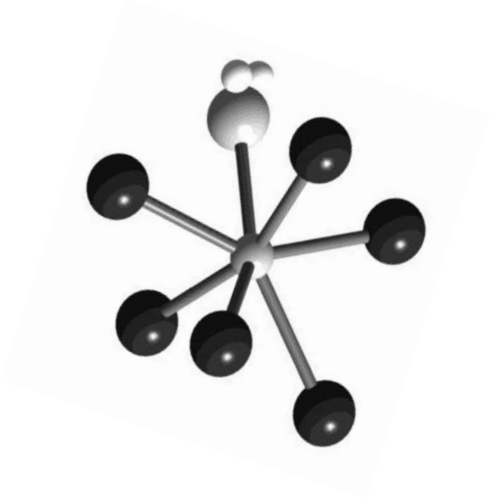

Fig. 5.88: Holo-directed configuration of the Pb^{2+} ion

Diffusion kinetics was controlled by pore diffusion as illustrated by the linear curves[9] shown in Fig. 5.89. The bilinearity of the graph meant pore diffusion was dependent of pore size. Film diffusion also contributed to the overall diffusion of Pb^{2+} ions, explaining why the curves did not pass through the origin.

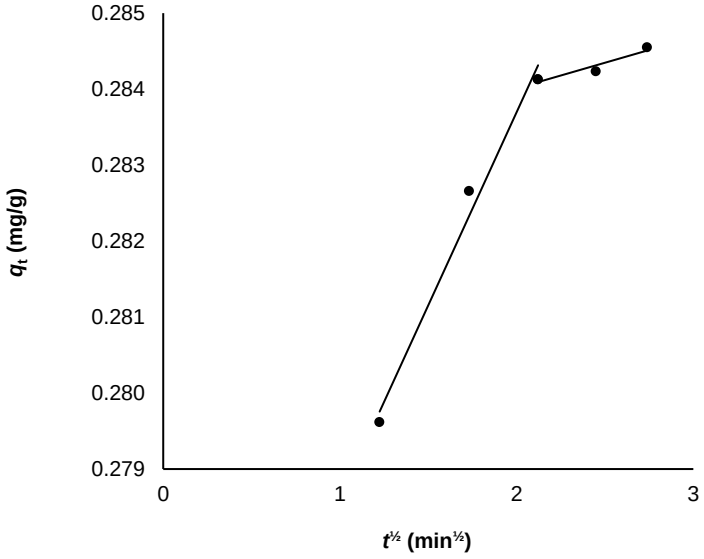

Fig. 5.89: Weber-Morris plot of intra-particle diffusion of Pb^{2+} ions

[9] The short range of q_t values could be construed as steady-state approximation; alternatively, sorption equilibrium was established at t = 3 min.

The above hypothesis was tested against the HPDM. A plot of X versus $t^{½}$ (Fig. 5.90) was regarded as more appropriate because of the short time in which equilibrium had been attained.

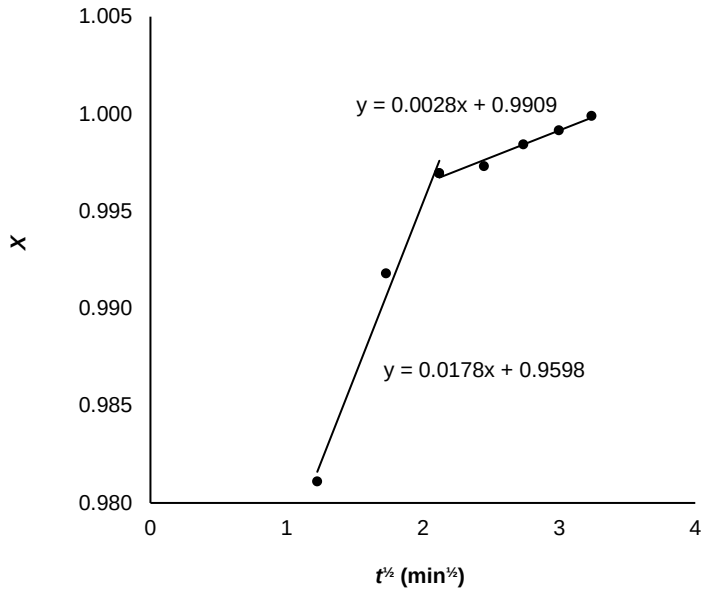

Fig. 5.90: HPDM plot of diffusion kinetics modelling Pb sorption

From the initial linear portion of the graph, the value of the initial pore diffusion coefficient was calculated:

$$D_i = \frac{{S_i}^2 \pi r^2}{36} = \frac{(0.0178)^2 \times \pi \times (37.5 \times 10^{-4})^2}{36} = 6.5 \times 10^{-12} cm^2 \cdot s^{-1}$$

Similarly, the value of the final pore diffusion coefficient was calculated:

$$D_f = \frac{{S_f}^2 \pi r^2}{36} = \frac{(0.0028)^2 \times \pi \times (37.5 \times 10^{-4})^2}{36} = 1.6 \times 10^{-13} cm^2 \cdot s^{-1}$$

Both values suggested pore diffusion was the rate-controlling mechanism after $t^{½}$ = 2.121 $min^{½}$ and that pore diffusion was characterised by a faster initial step followed by a slower final step.

5.4.2.7 *Bismuth*

A plot of q_t vs. $t^{½}$ (Fig. 5.91) revealed that diffusion of bismuth ions was controlled by intra-particle diffusion.

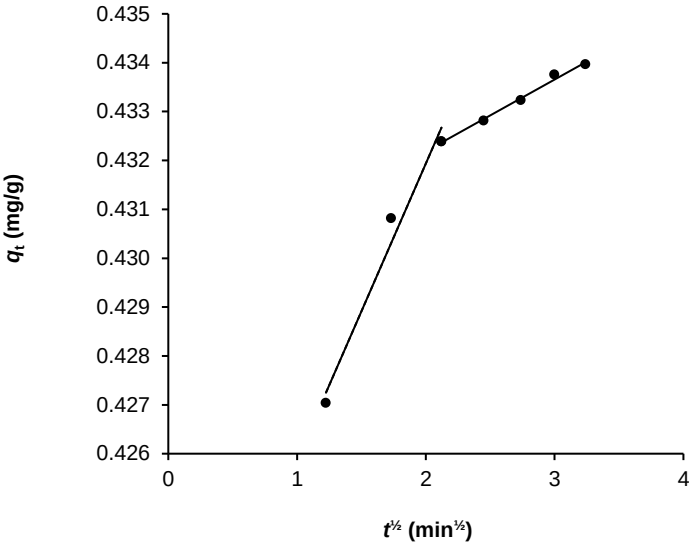

Fig. 5.91: Weber-Morris plot of intra-particle diffusion of Bi^{3+} ions

Data was subsequently also subjected to the HPDM by plotting *ln* (1 – *X*) against *time* (Fig. 5.92).

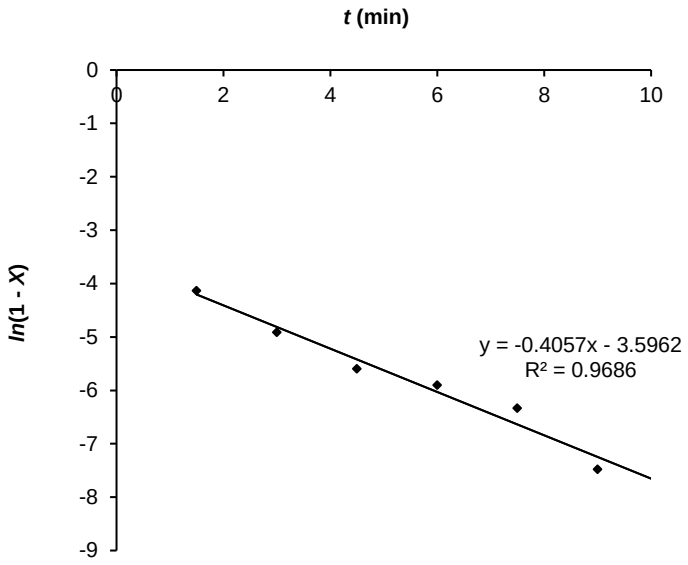

Fig. 5.92: HPDM plot of diffusion kinetics of Bi sorption

From the graph,

$$\frac{D_r \pi^2}{r_0^2} = 0.4057$$

$$\therefore D_r = 9.6 \times 10^{-9}\ cm^2 \cdot s^{-1}$$

Since X >> 0.3 and sorption data was assumed to be based on short time, a plot of X versus $t^{½}$ (Fig. 5.93) would be expected to provide more realistic insight into the diffusion mechanism.

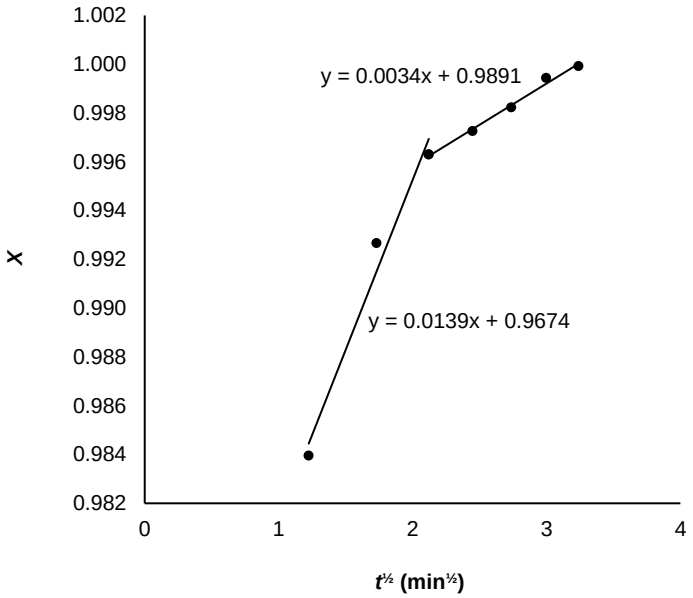

Fig. 5.93: HPDM plot of diffusion kinetics of Bi based on short-time data

Values of the pore diffusion coefficient associated with each of the graph were determined.

$$D_i = \frac{{S_i}^2 \pi r^2}{36} = \frac{(0.0139)^2 \times \pi \times (37.5 \times 10^{-4})^2}{36} = 4.0 \times 10^{-12} cm^2 \cdot s^{-1}$$

and,

$$D_f = \frac{{S_f}^2 \pi r^2}{36} = \frac{(0.0034)^2 \times \pi \times (37.5 \times 10^{-4})^2}{36} = 2.4 \times 10^{-13} cm^2 \cdot s^{-1}$$

These values were well within the 10^{-11} – 10^{-13} $cm^2 \cdot s^{-1}$ range, suggesting that sorption was controlled by pore diffusion.

5.4.2.8 *Silver*

The diffusion mechanism that controlled Ag sorption was determined by applying experimental data to the Weber-Morris and Homogeneous Particle Diffusion models (Figs. 5.94 and 5.95, respectively). Linearity of the graph meant pore diffusion was the rate-determining step.

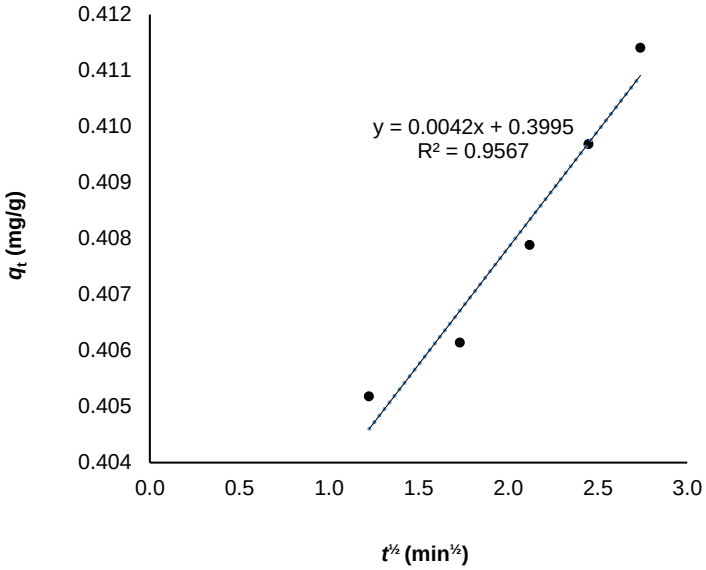

Fig. 5.94: Weber-Morris plot of intra-particle diffusion of Ag

The fractional attainment of equilibrium (X) exceeded 0.3 by far, so the feasibility of HPDM was tested using Eq. (2.20). Fig. 5.95 depicts a plot of ln (1 – X) versus t:

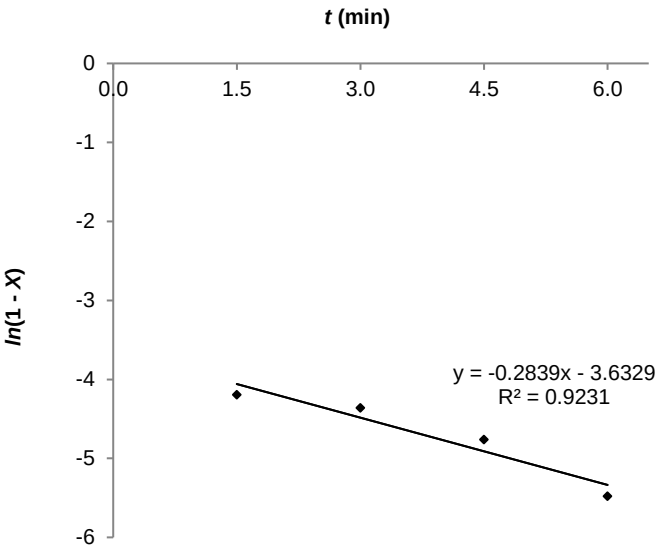

Fig. 5.95: HPDM plot for diffusion kinetics of Ag sorption

From the graph,

$$\frac{D_r \pi^2}{r_0^{\ 2}} = \text{slope} = 0.2839$$

$$\therefore D_r = 6.7 \times 10^{-9}\ \text{cm}^2 \cdot \text{s}^{-1}$$

This value was not entirely within the range $10^{-6} – 10^{-8}$ $\text{cm}^2 \cdot \text{s}^{-1}$, but supported the argument that film diffusion played a role in the overall sorption mechanism of Ag nonetheless. Besides, a plot of *ln* (1 – *X*) vs. *t* assumed fractional attainment of equilibrium reached unity after a relatively long time-interval. This was not the case, so a plot of *X* versus $t^{½}$ was constructed instead (Fig. 5.96).

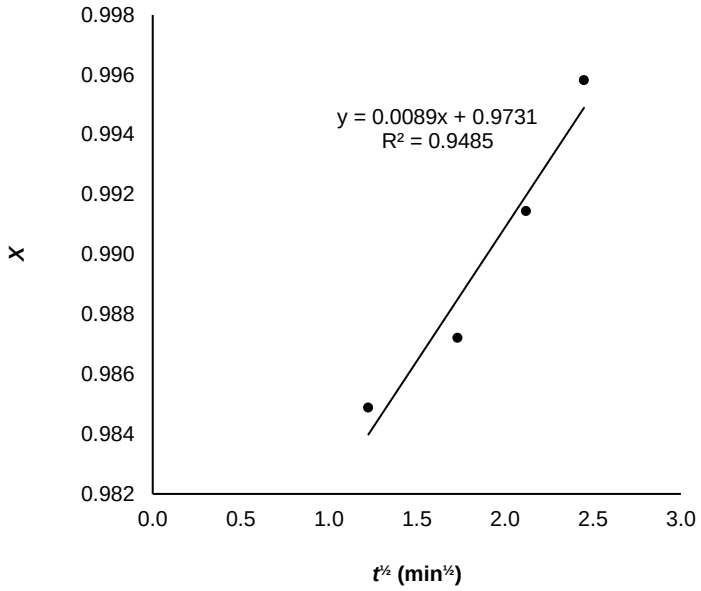

Fig. 5.96: HPDM plot of diffusion kinetics of Ag based on short-time data

The pore diffusion coefficient was calculated as before, underscoring the significance of pore diffusion as rate-determining step:

$$D_r = \frac{S_r^2 \pi r^2}{36} = \frac{(0.0089)^2 \times \pi \times (37.5 \times 10^{-4})^2}{36} = 1.6 \times 10^{-12} cm^2 \cdot s^{-1}$$

In summary, diffusion was controlled by intra-particle processes, although film diffusion also contributed to the overall sorption process. This was to be expected as the agitation rate in all experiments was low (150 rpm) as compared to other studies in which the effect of film diffusion was diminished by vigorous shaking. Diffusion kinetics of Cu was controlled by intra-particle diffusion only. Diffusion rates of Co^{2+}, Pb^{2+}, Cu^{2+}, Ni^{2+} were compared based on their respective rates of fractional attainment of equilibrium (*X*) during batch experiments. The observed trend (in decreasing order) was: Co^{2+}, Pb^{2+}, Cu^{2+}, Ni^{2+}.

Fig. 5.97 (https://chem.libretexts.org) shows the variation of ionic radii of divalent ions of fourth-period metals.

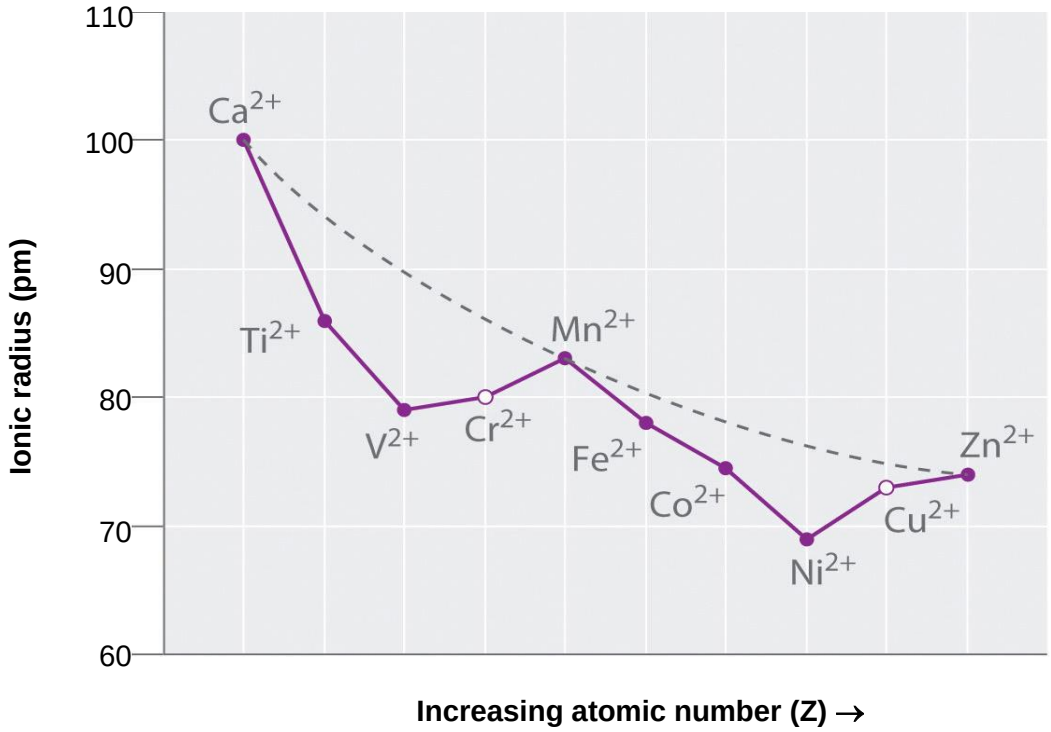

Fig. 5.97: Variation of ionic radii of fourth-period divalent metal ions with atomic number (https://chem.libretexts.org)

The dashed line shows the trend in ionic radii based solely on electrostatic interactions. Typically, cations with spherically symmetrical distributions of *d*-orbital electrons such as Ca^{2+} (d^0), Mn^{2+} (d^6) and Zn^{2+} (d^{10}) lie on this line. The radii of metal ions with asymmetrical distribution of *d*-electrons are smaller than expected and therefore deviate from the dashed line. This deviation is because of *d*-orbital splitting in octahedral complexes. The ionic radii of Cr^{2+} and Cu^{2+} are shown by open circles because they are not truly octahedral, but rather square planar due to Jahn-Teller distortion. Notably, the ionic radius of Ni^{2+} deviates most, so that in terms of size, $Co^{2+} > Cu^{2+} > Ni^{2+}$.

Thus, the trend in diffusion rates of first-row transition metals showed an inverse relationship with the trend in ionic radii. To understand the trend in diffusion rates of metal ions in aqueous medium, one must compare the sizes of the hydration spheres of the respective ions. An inverse relationship exists between non-hydrated ion radius and hydrated ion radius (Dove & Nix, 1997) (Fig. 5.98).

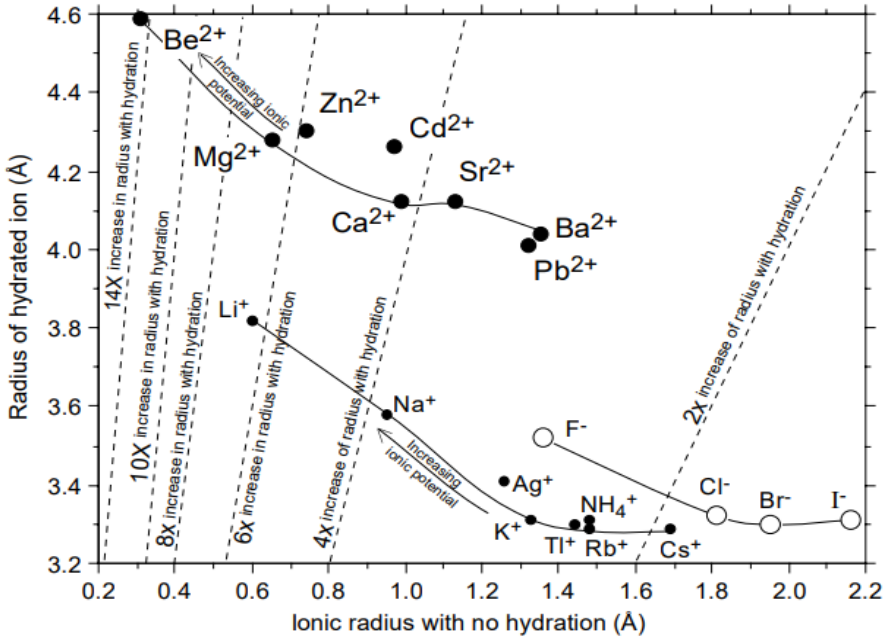

Fig. 5.98: Variation in hydrated and non-hydrated radii of solvated metal ions (Dove & Nix, 1997).

Generally, a smaller ion has a higher charge density that increases the electrostatic attraction between the ion and surrounding water molecules (see Fig. 5.99).

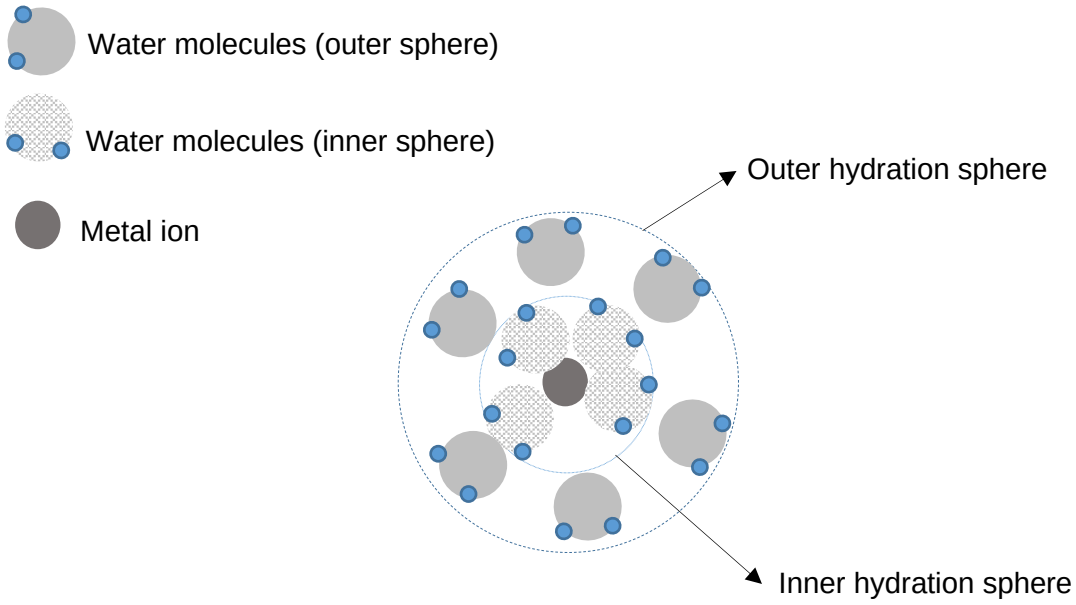

Fig. 5.99: Inner and outer hydration spheres around a metal ion with high charge density

The smaller Ni^{2+} ion is therefore expected to have a larger hydration sphere than metal ions of larger ionic radius. The large hydration sphere surrounding the Ni^{2+} ion may hinder its migration through the resin pores, resulting in a slow diffusion rate. According to the plot in Fig. 5.98, the hydrated radii of Co^{2+}, Cu^{2+} and Ni^{2+} are almost six times the size of their non-hydrated ions; the radius of the hydrated Pb^{2+} radius is roughly three times the size of the non-hydrated Pb^{2+} ion. By extrapolation, the hydrated Pb^{2+} ion has the smallest hydration sphere and is expected to exhibit faster diffusion kinetics; however, Co^{2+} diffused more than ten times faster than Pb^{2+}. This is an anomaly that warrants further investigation.

Diffusion rates in the column method decreased in the order: Zn^{2+} (0.74 Å) > Bi^{3+} (1.03 Å) > Ag^{+} (1.15 Å), showing an inverse relationship between the non-hydrated ionic radii and diffusion rates of metal ions.

5.5 Thermodynamics studies

Sorption of Ag, Bi, Cd, Co, Cu, Mn, Ni, Pb and Zn was studied in two experiments in the temperature range 283 – 303 K. In the first experiment, Ag and Bi samples were prepared in 0.01 M HNO_3 solution; all other metal solutions were buffered at pH = 6 to avoid hydrolysis. In this experiment, Ag and Bi were completed sorbed and was undetected in the supernatant solution.

Pb was also undetected in the first experiment. In a second experiment, all metal solutions (including Ag and Bi) were buffered at pH = 3.73; this was done mainly to reduce the sorption capacity of Ag, Bi and Pb. The initial concentrations of these metal ions were also increased to inhibit the extent of their sorption. In the second experiment, the Pb concentration in the supernatant remained virtually constant (RSD = 1.58 %) across the temperature range, implying that Pb sorption was independent of temperature. However, Ag and Bi were again completely sorbed and undetected in the supernatant. Mn sorption was minimal.

Data were applied to the van't Hoff equation. Plots of ln K_d versus 1/T (Fig. 5.100) were constructed and used to derive the values of ΔH^0 and ΔS^0. Eq. (2.38) was subsequently used to calculate $\Delta G°$.

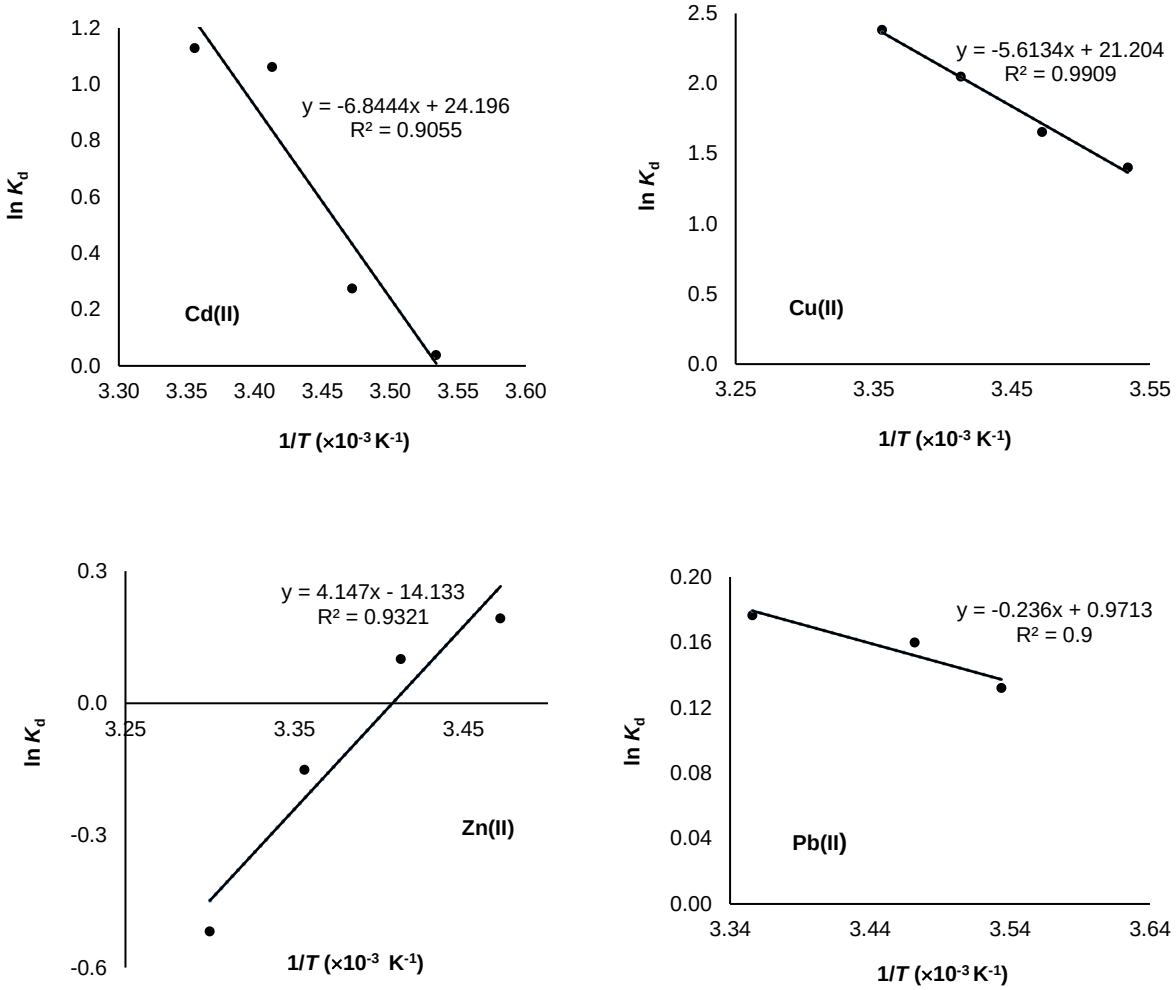

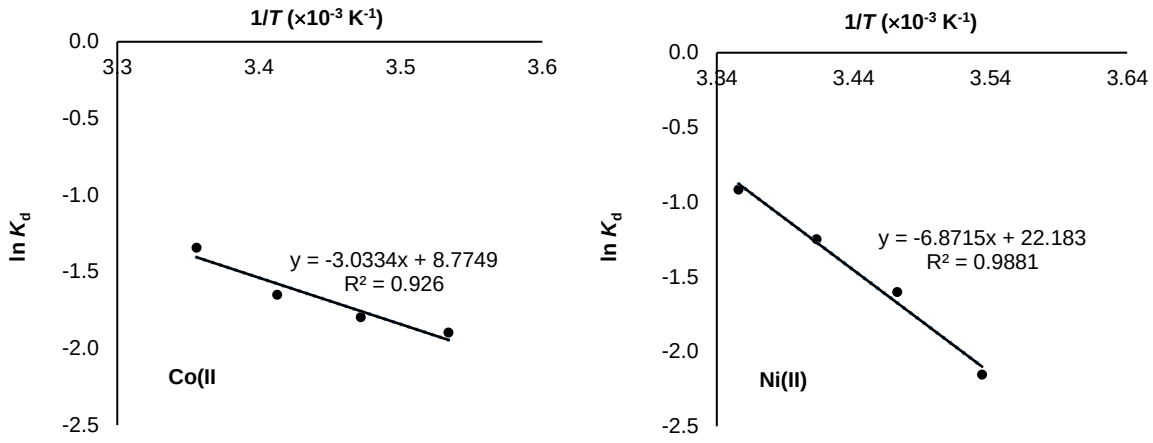

Fig. 5.100: Graphs of ln K_d versus 1/T for Cd, Co, Cu, Ni, Pb and Zn

The values of all thermodynamic parameters are presented in Table 5.41.

Table 5.41: Thermodynamics parameters of sorption of Cd, Co, Cu, Ni, Pb and Zn

	ΔH^0	ΔS^0	ΔG^0 (kJ/mol)				
	(kJ/mol)	(kJ/mol/K)	283 K	288 K	293 K	298 K	303 K
Cd	56.901	0.201	0.018	-0.987	-1.992	-2.997	
Co	25.216	0.073	4.557	4.192	3.827	3.462	
Cu	46.666	0.176	-3.142	-4.022	-4.902	-5.782	
Pb	1.962	0.008	-0.302	-0.342	-0.382		
Ni	57.134	0.184	5.062	4.142	3.222	2.302	
Zn	-34.478	-0.118		-0.494	0.096	0.686	1.276

Sorption of Cd, Co, Cu, Pb and Ni was endothermic ($\Delta H^0 > 0$), whereas Zn was the only metal whose sorption was exothermic ($\Delta H^0 < 0$). Increasing negative values of the Gibbs's free energy (ΔG^0) of Cd, Cu and Pb implies their sorption was favourable, and more so with increasing temperature. Zn sorption was favourable at temperature less than 293 K. ΔG^0 values suggest Co and Ni sorption were not favourable over the temperature range studied – this somehow contradicted evidence of sorption at room temperature (T < 298 K), demonstrated by the purple colour of the resin as soon as it encountered the metal ions. Despite their similar ΔH^0 and ΔS^0 values, Ni and Cd differed vastly with respect to ΔG^0 – this discrepancy vanishes if the said values are reported to fewer significant figures.

ΔH values in the range 25 – 60 kJ/mol (except for Pb) are indicative of coordination (Huang *et al*., 2007) between the metal ions and the dithizone ligand. The small value of ΔH associated with Pb sorption is more likely attributable to its constant sorption capacity over the temperature, rather than its coordinating ability with the dithizone ligand. As stated earlier (Section 2.6, p. 31) the heat of physisorption is normally in the range 2.1 – 20.9 kJ·mol^{-1}, whereas sorption associated with chemical processes generally falls in the range 80 – 200 kJ·mol^{-1}. Therefore, ΔH-values obtained in this study confirmed earlier observations that sorption of metal ions onto the impregnated resin could be attributed to a physico-chemical sorption process, rather than pure physi- or chemisorption. The positive ΔS^0 values associated with sorption of all metals (except Zn) reflect the affinity of the sorbent for towards the sorbed species (Saha & Chowdury, n.d.). It suggests increased randomness at the resin/solution interface and structural changes in the sorbent and sorbate.

In the case of Zn sorption on the other hand, $\Delta S^0 < 0$ implied decreased disorder at the solid/liquid interface, causing ions to escape from the solid phase into the bulk solution. This was congruent with the perceived behaviour of Zn explained in Section 5.4.3.

5.6 Error Analysis

Linear regression analysis is frequently applied to analysis of experimental data and is among the most pronounced and viable tools used in the verification of the consistency of adsorption models, and the theoretical assumptions that underpin them (Ayawei *et al*., 2017). However, the error structure of experimental data is usually distorted during the transformation of adsorption isotherms into their linearized forms. According to Kumar (2006), linear regression assumes the scatter of points about a line follows a Gaussian distribution, and that the standard deviation is the same for every point along the horizontal axis-value. These assumptions are rarely true.

Non-linear regression analysis uses the original (non-transformed) form of the sorption isotherm or kinetics equation, thus minimizing the error distribution between the experimental data and the mathematical model. Unlike linear regression, experimental parameters remain fixed on the same axes when plotting the original, non-linear equations.

One of the most used error functions is the *sum square of errors* (SSE), defined as:

$$SSE = \sum_{i=1}^{N} (q_{e,1,calc} - q_{e,i,meas})^2 \quad (5.1)$$

($q_{e,calc}$ and $q_{e,meas}$ are the equilibrium capacities (mg/g) obtained from the model and experiment, respectively.)

The lower the value of SSE, the better the goodness-of-fit. Another error function which is important in the determination of the best-fit of an adsorption system, is the *non-linear Chi-square test* (χ^2). It can be obtained by judging the sum of square difference between experimental and calculated data, with each square difference divided by its corresponding experimental value:

$$\chi^2 = \sum_{i=1}^{N} \frac{(q_{e,calc} - q_{e,meas})^2}{q_{e,meas}} \quad (5.2)$$

The smaller the value of χ^2, the better the goodness-of-fit.

Error functions of the non-linear isotherm and kinetics sorption models of eight metal ions are shown in Table 5.42. Correlation coefficients (r^2) of the linear forms are included in the table. Sorption parameters associated with the various isotherm and kinetics equations were optimised using the solver add-in function in MS Excel®. In most cases, results obtained by the non-linear regression method agreed with linear regression. The non-linear method showed Bi sorption was better modelled by the Freundlich isotherm. The Langmuir isotherm also showed good correlation with experimental data, but the calculated sorption capacity deviated significantly from the experimental value. This observation applied to Cd sorption as well; however, the capacities obtained from the D-R and Langmuir isotherms were similar. The error functions further show Bi, Pb, and Zn sorption are better explained by pseudo-first order kinetics. Neither regression method could unambiguously predict which kinetic model best described sorption of Cu and Ni, as the difference in error functions of both metals was insignificant. $SSE_{Cu,\ PFO}$ and $SSE_{Cu,\ PSO}$ were equal to 6.6×10^{-3} and 5.2×10^{-3}, respectively. The χ^2-values of the pseudo-first order and pseudo-second order models of Ni were 0.0227 and 0.0234, respectively.

Non-linear forms of pseudo-first order and pseudo-second order kinetics correlated much better with experimental data than the linear forms. In all cases, except Cu, the calculated values of the sorption capacities were in excellent agreement with the measured values.

Table 5.42: Error functions of non-linear isotherms and kinetic models

Metal	Langmuir	Freundlich	Temkin	D-R	PFO	PSO
Ag	r^2 = 0.9973 SSE = 0.1547 χ^2 = 0.0717	r^2 = 0.9270 SSE = 7.909 χ^2 = 3.436	r^2 = 0.9138 SSE = 31.40 χ^2 = 12.43	r^2 = 0.7662 SSE = 0.1691 χ^2 = 0.0778	r^2 = 0.9712 SSE = 6.9×10^{-5} χ^2 = 1.7×10^{-4}	r^2 = 1.000 SSE = 9.4×10^{-6} χ^2 = 2.3×10^{-5}
Bi	r^2 = 0.9982 SSE = 2.09×10^{-3} χ^2 = 1.4×10^{-3}	r^2 = 0.8375 SSE = 0 χ^2 = 0	r^2 = 0.8419 N/A N/A	r^2 = 0.9509 SSE = 0.2995 χ^2 = 0.5071	r^2 = 0.9686 SSE = 6.7×10^{-6} χ^2 = 1.6×10^{-5}	r^2 = 1.000 SSE = 3.6×10^{-5} χ^2 = 8.3×10^{-5}
Cd	r^2 = 0.9810 SSE = 0.0215 χ^2 = 0.0505	r^2 = 0.4458 N/A N/A	r^2 = 0.6081 SSE = 0.0178 χ^2 = 0.0459	r^2 = 0.6065 SSE = 0.0203 χ^2 = 0.0568	r^2 = 0.9792 SSE = 3.8×10^{-4} χ^2 = 8.4×10^{-4}	r^2 = 0.9998 SSE = 1.4×10^{-4} χ^2 = 3.1×10^{-4}
Co	r^2 = 0.9836 SSE = 0.0607 χ^2 = 0.0824	r^2 = 0.8195 SSE = 0.7847 χ^2 = 1.050	r^2 = 0.7742 SSE = 0.0203 χ^2 = 0.0266	r^2 = 0.5909 SSE = 0.0582 χ^2 = 0.0779	r^2 = 0.9944 SSE = 1.6×10^{-3} χ^2 = 5.7×10^{-3}	r^2 = 0.9991 SSE = 4.4×10^{-4} χ^2 = 1.5×10^{-3}
Cu	r^2 = 0.9995 SSE = 6.7×10^{-4} χ^2 = 1.0×10^{-3}	r^2 = 0.9992 SSE = 0.4542 χ^2 = 0.6981	r^2 = 0.9997 SSE = 7.3×10^{-6} χ^2 = 5.5×10^{-6}	r^2 = 0.9236 SSE = 7.6×10^{-3} χ^2 = 5.5×10^{-3}	r^2 = 0.9946 SSE = 6.6×10^{-3} χ^2 = 0.0534	r^2 = 0.9182 SSE = 5.2×10^{-3} χ^2 = 0.0426
Ni	r^2 = 0.9972 SSE = 4.9×10^{-3} χ^2 = 8.8×10^{-3}	r^2 = 0.8840 SSE = 1.4×10^{-3} χ^2 = 2.2×10^{-3}	r^2 = 0.6984 SSE = 0.6464 χ^2 = 1.081	r^2 = 0.7242 SSE = 3.5×10^{-3} χ^2 = 3.5×10^{-3}	r^2 = 0.9840 SSE = 0.0227 χ^2 = 0.0395	r^2 = 0.9996 SSE = 0.0234 χ^2 = 0.0347
Pb	r^2 = 0.9940 SSE = 6.1×10^{-3} χ^2 = 9.2×10^{-3}	r^2 = 0.9876 SSE = 0.5086 χ^2 = 0.7401	r^2 = 0.9845 SSE = 0.0203 χ^2 = 0.0314	r^2 = 0.8802 SSE = 0.0150 χ^2 = 0.0221	r^2 = 0.9505 SSE = 0.0370 χ^2 = 0.0145	r^2 = 0.9972 SSE = 0.0456 χ^2 = 0.0342
Zn	r^2 = 0.9890 SSE = 0.0130 χ^2 = 0.0525	r^2 = 0.9674 SSE = 0.2345 χ^2 = 0.6987	r^2 = 0.9691 SSE = 0.0006 χ^2 = 0.0024	r^2 = 0.8546 SSE = 0.0258 χ^2 = 0.1067	r^2 = 0.9917 SSE = 4.7×10^{-6} χ^2 = 2.2×10^{-5}	r^2 = 1.000 SSE = 3.9×10^{-5} χ^2 = 1.7×10^{-4}

*N/A means the non-linear method could not prove any correlation exists between the mathematical model and experimental data.

CHAPTER 6

Application – separation of heavy metals

As stated in Chapter 1, paramount to the efficiency of a separation system are efficiency and selectivity. Selectivity is predominantly associated with the sorption mechanism. The sorption mechanisms of various heavy metals have been studied and discussed in detail in Chapter 5. Based on the findings outlined in the previous chapter, the separation of various cations from binary or ternary mixtures was attempted according to their sorption characteristics. The selection of mixtures was mainly arbitrary. The ternary mixture of Co-Mn-Ni as well as the binary Bi-Pb mixture were chosen based on the proximity of these metals in the periodic table. The separation of Cd from Sn, however, is key to the isolation of the Sn-117m isotope which has promising application in the palliative treatment of painful metastases in bone cancers (Stevenson & Gonzales, 2016).

While most metals could be separated based on differentiating sorption capacity in relation to pH and initial concentration, the affinity (or lack thereof) of others towards dithizone was used to separate them. In the latter category, Sn^{4+} and Mn^{2+} ions were most conspicuous.

Separations were conducted by the column method because of its greater efficiency. However, there was no intention to optimise the separation capability of the impregnated resin; hence, this part of the study was more qualitative in nature, leaving room for further research. Neither was the intention to separate all metals studied in this project.

6.1 Cd^{2+}-Sn^{4+} ions separation

The high selectivity of dithizone towards Cd in particular, made separation of Cd^{2+} and Sn^{4+} ions very easy. When present in equal concentration (5 mg/L), no Cd could be detected in the first few eluate fractions. However, after a few minutes, Cd began to break through the column. At high Sn^{4+} ion concentration, there was greater competition for sorption sites, causing Cd^{2+} ions to break through. The experiment was therefore repeated but with Cd and Sn in a 2:1 concentration ratio, viz. 1.073 mg/L Cd and 0.497 mg/L Sn. In the latter experiment, Cd^{2+} ions were retained on the column while most of the Sn^{4+} ions passed through, as illustrated in their respective breakthrough curves (Fig. 6.1).

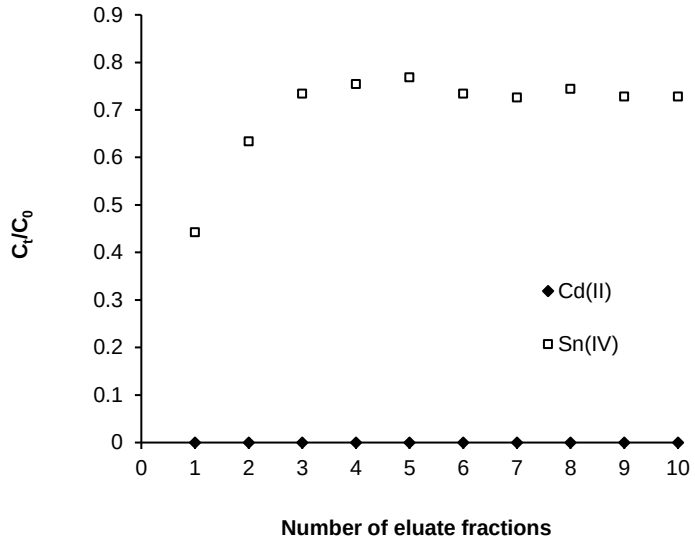

Fig. 6.1: Breakthrough curve for ACG300m-H_2Dz for Cd and Sn sorption; [Cd^{2+}] = 1.073 mg/L; [Sn^{4+}] = 0.497 mg/L; pH = 5.97; flow rate = 5.0 mL/min

6.2 Mn^{2+}-Co^{2+}-Ni^{2+} ions separation

Since Mn was not retained on the resin in earlier experiments (under static and dynamic conditions), while Ni and Co were retained with fair to good success (under static conditions and pH > 6), an attempt was made to separate Mn from Ni and Co. The concentration of each element in the mixture was 1.976 mg/L (Co^{2+}), 0.378 mg/L (Ni^{2+}) and 0.979 mg/L (Mn^{2+}). The pH of the influent solution was maintained at pH = 5.93. The breakthrough curve of each element is presented in Fig. 6.2.

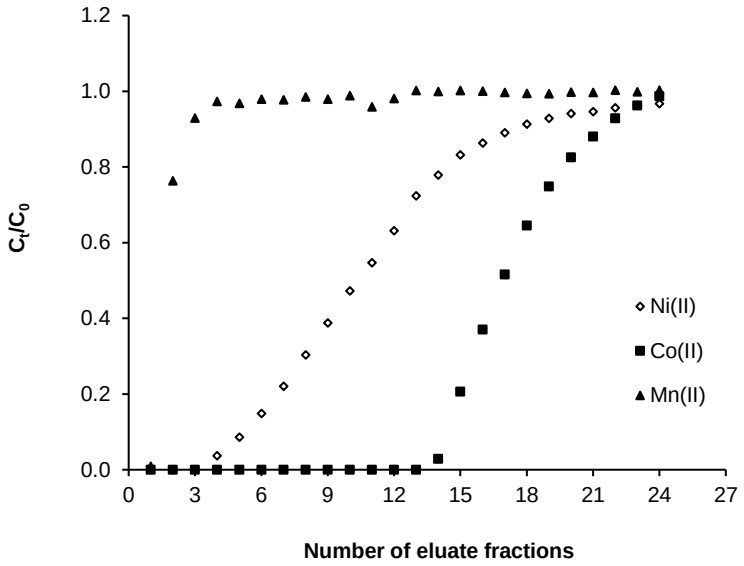

Fig. 6.2: Breakthrough curve for ACG300m-H_2Dz for Mn, Co and Ni sorption; [Mn^{2+}] = 0.979 mg/L; [Co^{2+}] = 1.976 mg/L; [Ni^{2+}] = 0.378 mg/L; pH = 5.93; flow rate = 5.0 mL/min

From Fig. 6.2 it follows that Co and Ni could be separated with great efficiency from Mn as breakthrough of Mn was achieved after only six minutes, followed by Ni and Co (after approximately 40 min). With careful manipulation of experimental parameters such as pH, initial concentrations and flow rate, the separation efficiency could be accelerated even further. Such investigations, however, fell outside the scope of this project.

6.3 Bi^{3+}-Pb^{2+} ions separation

Bi was separated from Pb in strongly acidic medium (pH < 2). The influent solution was made up to 4.175 mg/L Bi^{3+} and 1.931 mg/L Pb^{2+}. Bi was qualitatively sorbed within the first 90 seconds, reaching equilibrium within 10 min, approximately the same time in which breakthrough of Pb was achieved (Fig. 6.3). Notably, the Bi content in the effluent gradually began to increase after approximately 23 min. At this point, the resin was completely saturated with Bi as was evident from the total conversion of the green impregnated resin to a rust-brown mass. (Data recorded after the 23rd min was not included in the curves shown in Fig. 6.3 but is shown in Appendix F).

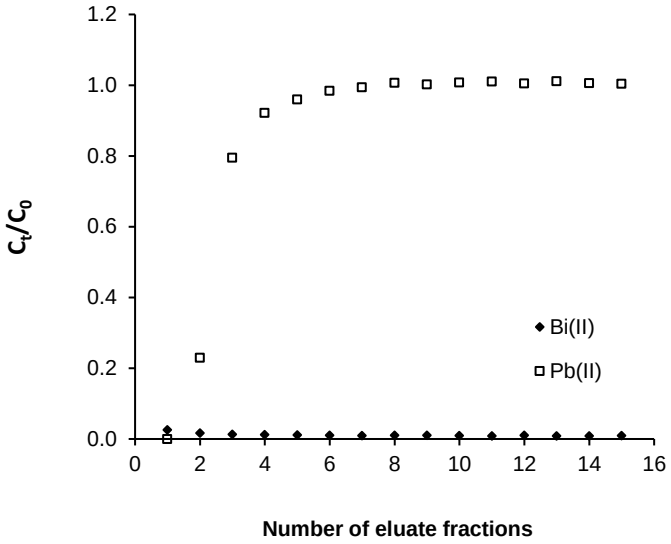

Fig. 6.3: Breakthrough curve for ACG300m-H_2Dz for Bi and Pb sorption; [Bi^{3+}] = 4.175 mg/L; [Pb^{2+}] = 1.931 mg/L; pH < 2; flow rate = 5.0 mL/min

CHAPTER 7

Conclusions and recommendations

7.1 Concluding remarks

A systematic investigation of the sorption mechanisms of ten heavy metal ions onto a dithizone-impregnated polymer resin was undertaken for the first time. Amberchrom CG-300m polymer resin was employed as novel sorbent for extraction of the metal ions from aqueous solutions. The inert resin was successfully modified by impregnation with dithizone in alkaline medium (NaOH). Amberchrom CG-300m is supplied as white, opaque beads, but after impregnation it took on the characteristic green color of dithizone. Characterization (FT-IR) and surface morphology studies (SEM) of the resin before and after impregnation confirmed successful impregnation. SEM images revealed an ostensible decrease in free pore volume, while a broad absorption peak around 1360 cm^{-1} in the FT-IR spectrum of the impregnated resin confirmed the presence of the S=C−N functional group of dithizone.

The loading capacity of the resin did not reach a saturation value as is usually the case in other similar studies. Leaching of dithizone occurred at higher ligand concentrations when the ratio of resin to ligand exceeded 100:0.8 (mg/mg). Leaching also occurred when the concentration of impregnation solution [NaOH] < 0.5 M. As a result of these impediments, the maximum loading achieved was 3.2 mg dithizone per gram of sorbent, achieved in less than 30 min. The impregnated resin could be preserved in a dark bottle under SO_2 for no longer than 7 days. This limits the application of the SPE system as the modified resin will have to be freshly prepared every week.

The functionality of dithizone as modifier was central to this study because of its known selectivity towards certain heavy metal ions. Yet, a case had to be argued for the modification of the Amberchrom resin. Consequently, the sorption capacities of Cd on both the modified and unmodified resins were compared. It was established that Cd sorption on the modified resin was approximately 47 % more efficient compared to the unmodified resin.

Most metal ions in the study were quantitatively sorbed under varying conditions of pH, metal ion concentration, time, and temperature. Sorption generally increased with increasing pH. As exceptions to this observation Ag^{+}, Bi^{3+} and Cu^{2+} were sorbed at low to moderate pH (1 – 5). Maximum extraction of Co^{2+} accurred in mildly acidic medium (pH ~ 6), while strongly alkaline conditions (pH > 8) facilitated quantitativey sorption of Cd^{2+}, Ni^{2+}, Pb^{2+} and Zn^{2+}.

Metal extraction at higher pH could not solely be attributed to sorption mechanisms as many heavy metal ions form insoluble hydroxide complexes in alkaline media.

Indium sorption at pH < 3.3 was poor and increased in the pH range 4 – 6, although in the latter range sorption could be attributed to dual mechanisms of chemical coordination and precipitation. Based on pH-dependence, the Amberchrom-dithizone system therefore holds promise for the extraction and separation of some of the metal ions investigated in this study.

Most metals were quantitatively (> 95 %) sorbed at low initial concentration. Ag(I) and Bi(III), however were the only metals sorbed quantitatively at relatively high initial concentration (4.104 mg/L and 3.30 mg/L respectively).

The modified resin had no affinity for Sn^{4+} and Mn^{2+} under any of the conditions studied. While it is generally known that the higher valency Sn(IV) does not coordinate with dithizone, the lack of affinity towards manganese was surprising and contrary to findings reported in solvent extraction studies elsewhere. Based on these findings, the dithizone-impregnated resin shows good promise for future use in the isolation and/or separation of Mn(II) and Sn(IV) ions from aqueous solutions.

The condition of the resin (wet or dry) played a significant role in the rate of metal ion sorption. In the early stages of the study, a large batch (> 1000 mg) of resin was impregnated and allowed to dry in an oven or room temperature. Smaller batches (100 mg each) were then weighed for use in batch experiments. It was later found the impregnated resin exhibited faster kinetics when used without drying. This was proven by a comparative study of the sorption behaviour of Co and Cu on dry and wet resin. In all subsequent experiments, batches of 100 mg were impregnated separately, filtered, and immediately contacted with the metal ion solution.

The rate of metal ion sorption was found to be much faster in column experiments. Kinetic studies involving Pb(II) revealed sorption in dynamic mode was so fast that steady-state approximation was established within the first 3 min. Pb(II) sorption in batch mode was ten times slower, maximum capacity achieved after approximately 35 min only. In addition, the dynamic method was found to be more reliable as experimental parameters such as flow rate and resin dosage could be better controlled, especially in kinetics studies. However, in some cases the fast rate of sorption prohibited the collection of enough data points for kinetic analysis.

Sorption of most metals (except for Cd) was driven by both chemical and physical processes. The physico-chemical duality of metal ion sorption was confirmed by thermodynamics and kinetics studies. Cd sorption was driven solely by chemical processes. Sorption equilibrium of all metals was best modelled by the Langmuir isotherm; it is only Cu sorption (on dry resin) that showed no clear bias toward Langmuir type sorption. The predominance of chemisorption underscored the significance and impact of resin modification. Sorption capacity at optimal conditions of initial metal ion concentration and pH decreased in the following order: $Ag^{+} > Bi^{3+} > Pb^{2+} > Co^{2+} > Ni^{2+} > Cu^{2+} > Zn^{2+} > Cd^{2+} > Mn^{2+}$

Sorption of Ag, Bi, Cd (on dry resin), Co, Ni, Pb and Zn followed pseudo-second order reaction kinetics, whereas Cu sorption onto dry, impregnated resin followed pseudo-first order kinetics. Second order kinetics is normally associated with chemisorption, validating the data obtained in equilibrium studies. Reaction kinetics of metals studied in batch experiments decreased in the order: Cu^{2+}, Co^{2+}, Ni^{2+}, Pb^{2+} (kinetics of Cd^{2+} sorption was studied on dry resin and is therefore not included). Reaction kinetics of metals studied in column experiments decreased in the order: Pb^{2+}, Bi^{3+}, Zn^{2+}, Ag^{+}.

In all instances (except Cu), mathematical models employed could not distinguish between pore and film diffusion as rate-controlling regime. Diffusion kinetics of Cu was controlled by intra-particle diffusion only. Diffusion rates of Co^{2+}, Pb^{2+}, Cu^{2+}, Ni^{2+} were compared based on their respective rates of fractional attainment of equilibrium (X) during batch experiments; the observed trend (in decreasing order) was: Co^{2+}, Pb^{2+}, Cu^{2+}, Ni^{2+}. Diffusion rates in the column method decreased in the order Zn^{2+} (0.74 Å) > Bi^{3+} (1.03 Å) > Ag^{+} (1.15 Å), showing an inverse relationship between the non-hydrated ionic radii and diffusion rates of metal ions.

Equilibrium, kinetics and thermodynamics studies suggest the dithizone-impregnated resin can be used for the extraction and separation of a selection of heavy metal ions. It was effectively employed for separation of Cd^{2+} and Sn^{4+} ions from a binary mixture containing the metals in 2:1 ratio. Mn could be separated from Co within 6 min; results of the same experiment showed that, with further investigation, optimal experimental conditions could be designed for the separation of Ni and Co. Bi was easily separated from Pb, indicating Ag and Pb could also be separated with ease at low pH. Generally, Ag and Bi, could be separated from all metal ions employed in this study at low pH (< 2). Optimisation of separation parameters (flow rate, column height, choice of eluent) is recommended for further studies.

7.2 Recommendations

Emanating from this study, the following aspects warrant further research:

- The anomaly of poor Mn sorption on the dithizone-impregnated Amberchrom CG-300m resin should be further investigated. While it may be possible for manganese(II) to have been extracted from aqueous media into an organic layer that contains dithizone during solvent-extraction, an extensive literature survey does not reveal any incidence of Mn(II) extraction during solid-phase exctraction.
- This project aimed to document in a systematic manner the sorption mechanisms of some of the twenty odd heavy metals known to coordinate with dithizone. A similar investigation into other heavy metals previously shown to form dithonates is recommended.
- A study of the quantitative separation of metal ions, using the ACG300m-H_2Dz separation system, was outside the scope of this study and is recommended.

References:

Abdullin, I.F., Turova, E.N. and Budnikov, G.K. 1999. Determination of copper and cadmium by Atomic Absorption Spectrometry with electrochemical and sorption preconcentration. *Journal of Analytical Chemistry*, 55(6), pp. 567 – 569.

Andrews, J. and Stringer, W.J. 1951. Colorimetric determination of trace metals in beer and in brewing materials. *Unknown Journal*. pp. 438 – 441.

Ansari, S.A., Pathak, P.N., Husain, M., Prasad, A.K., Parmar, V.S. and Manchanda, V.K. 2006. Extraction chromatographic studies of metal ions using *N*,*N*,*N*',*N*'-tetraoctyl diglycolamide as the stationary phase. *Talanta*, 68, pp. 1273 – 1280.

Atkins, F.W. 1999. Inorganic Chemistry. 3rd Edition. Oxford University Press. Oxford.

Ayawei, N., Ebelegi, A.N. and Wankasi, D. 2017. Modelling and interpretation of adsorption isotherms. *Journal of Chemistry*. Open access. Accessed on 5 September 2017.

Behbahani, M., Najafi, M., Amini, M.M., Sadeghi, O., Bagheri, A. and Salarian, M. 2013. Dithizone-modified nanoporous fructose as a novel sorbent for solid-phase extraction of ultra-trace levels of heavy metals. *Microchimic Acta*. 180. pp. 911 – 920.

Bilba, D., Bejan, D. and Tofan, L. 1997. Chelating Sorbents in Inorganic Chemical Analysis. *Croatica Chemica Acta*, 71 (1), pp. 155 – 178.

Bilba, D., Bilba, N. and Albu, M. 1999. Kinetics of cadmium ion sorption on ion exchange and chelating resins. *Solvent Extraction and Ion Exchange*, 17(6), pp. 1557 – 1569.

Chwastowska, J., Skwara, W., Sterlińska, E., Dudek, J., Dąbrowska and Pszonicki, L. 2008. GFAAS determination of cadmium, lead and copper in environmental materials and food products after separation on dithizone sorbent. *Chem. Anal. (Warsaw)*, 53(887), pp. 887 – 894.

Chilton, N., Jack, N. Losso, N., Wayne, E. and Marshall, R. 2002. Freundlich adsorption isotherm of agricultural byproduct-based powdered activated carbon in a geosmin-water system. *Bioresource Technology*. 85(2). pp. 131 – 135.

Chwastowska, J. and Kosiarska, E. 1988. Synthesis and analytical characterisation of a chelating resin loaded with dithizone. *Talanta*, 35(6), pp. 439 – 442.

Chwastowska, J., Skwara, W., Sterlińska, E., Dudek, J., Dąbrowska, M. and Pszonicki, L. 2008. GFAAS Determination of cadmium, lead and copper in environmental samples and food products after separation on dithizone sorbent. *Chem. Anal. (Warsaw)*, 53, pp. 887 – 894.

Cortina J.L., Arad-Yellin R., Miralles N., Sastre A.M. and Warshawsky A. 1998. Kinetic studies on heavy metal ions extraction by Amberlite XAD-2 impregnated resins containing a bifunctional organophosphorous extractant. *React. Func. Polym.,* 38, pp. 269 – 278.

Cortina, J.L. and Warshawsky, A. 1997. In Marinsky, J.A., Marcus, Y. (eds). I*on-exchange and Solvent Extraction*. 13. New York: Marcel Dekker, p. 195.

Cortina, J.L., Miralles, N., Sastre, A.M. and Aguilar, M. 1997. Solid-liquid extraction studies of divalent metals with impregnated resins containing mixtures of organophosporous extractants. *Reactive & Functional Polymers*, 32, pp. 221 – 229.

Costa, A., Lopes, L., Korn, M. and Portela, J. 2002. Separation and preconcentration of cadmium, copper, lead, nickel and zinc by solid-liquid extraction of their co-crystallized naphthalene dithizone chelate in saline matrices. *J. Braz. Chem. Soc.*, 13(5), pp. 674 – 678.

Dave, S.R., Kaur, H. and Menon, S. 2010. Selective solid-phase extraction of rare earth elements by the chemically modified Amberlite XAD-4 resin with azacrown ether. *Reactive & Functional Polymers,* (70), pp. 692 – 698.

Despotopulos, J.D., Kmak, K.N., Moody, K.J., and Shaughnessy, D.A. 2018. *Development of a ^{212}Pb and ^{212}Bi generator for homolog studies of flerovium and moscovium*. United States: N. p. Web. doi:10.1007/s10967-018-5848-7.

Doke, K.M. and Khan, E.M. 2017. Equilibrium, kinetic and diffusion mechanism of Cr(VI) adsorption onto activated carbon from wood apple shell. *Arabian Journal of Chemistry*. S252 – S260.

Dolley, S.G. and van der Walt, T.N., 2014. Isolation of Cu radionuclides with dithizone impregnated XAD-8. *Radiochimica Acta*., 102(3), pp. 263 – 269.

Dolley, S.G., Van Der Walt, T.N., Steyn, G.F., Szelecsényi, F. and Kovács, Z., 2006. The production and isolation of Cu-64 and Cu-67 from zinc target material and other radionuclides. *Czechoslovak Journal of Physics*, 56(4), pp. D539 – D544.

Dove, P.M. and Nix, C.J. 1997. The influence of the alkaline earth cations, magnesium, calcium, and barium on the dissolution kinetics of quartz. *Geochimica et Cosmochimica Acta*. 61(16). pp. 3329 – 3340.

El-Naggar, I.M., Zakaria, E.S., Ali, I.M., Khalil, M. and El-Shahat, M.F. 2012. Kinetic modelling analysis for the removal of cesium ions from aqueous solutions using polyaniline titanotungstate. *Arabian Journal of Chemistry,* 5, pp. 109 – 119.

El-Shafey, E.I. 2007. Removal of Se(IV) from aqueous solution using sulphuric-acid treated peanut shell. *Journal of Environmental Management*. 84(4). pp. 620 – 627.

Fu, Y., Huang, Y. and Hu, J. 2018. Preparation of chitosan/MCM-41-PAA nano-composites and the sorption behaviour of Hg(II) ions. DOI: 10.1098/rsos.171927 [Accessed 5 June 2018].

Grinstead, R.R. 1971. *Report by the Dow Chemical Company.* Contract No. 14-12-808 to the Water Quality Office of US Environmental Protection Administration.

Gulipalli, C.S., Prasad, B. and Wasewar, K.L. 2011. Batch study, equilibrium and kinetics of sorption of selenium using rice husk ash (RHA). *Journal of Engineering Science and Technology*, 6(5), pp. 586 – 605.

Hamza, A.G., Farag, A.B., Amireh, T.A., El-Basyouni, Z.E. and Al-Nowaiser, F.M., 1990. Detection, quantitative collection and semiquantitative determination of bismuth (III) and zinc (II) in aqueous media using polyurethane foam treated with dithizone. *Analytical Sciences,* 6(6), pp. 889 – 892.

Harrowfield, J., Pakawatchai, C. and White, A. H. 1983. Crystal structure of indium(III) dithizonate. *Journal of the Chemical Society, Dalton Transactions*. 6. pp. 1109 – 1113.

Hiraide, M. and Shibata, W. 1998. Collection of trace heavy metals on dithizone-impregnated admicelles for water analysis. *Analytical Sciences*. 14. pp. 1084 – 1088.

Ho, Y.S., Ng, J.C.Y. and McKay, G. 1998. Kinetic models for the sorption of dye from aqueous solution by wood. *Process Safety and Environmental Protection*. 76(2). pp. 183 – 191.

Ho, Y.S. 2006. Second order kinetic model for the sorption of cadmium onto tree fern: a comparison of linear and non-linear methods. Water Research. 40. pp. 119 – 125.

Ho, Y.S., Ng, J.C.Y. and McKay, G. 2000. Kinetics of pollutants sorption by biosorbents: Review. *Separation and Purification methods*. 29(2). pp. 189 – 232.

Horwitt, M.K and Cowgill G.R. 1937. A titrimetric method for the quantitative estimation of lead in biological samples. *J. Biol. Chem*..119. pp. 553 – 564.

Hou, X. and Jones, B.T. 2000. Inductively coupled plasma/optical emission spectroscopy. *Encyclopedia of Analytical Chemistry*. Chicchester: John Wiley & Sons Ltd. pp. 9468 – 9485.

Huang, X., Gao, N. and Zhang, Q. 2007. Thermodynamics and kinetics of cadmium adsorption onto oxidised granular activated carbon. *Journal of Environmental Sciences*. 19(2007). pp. 1287 – 1292.

Hutton, A.T. 1980. Structural and Spectroscopic Studies with dithizone and its derivatives. PhD dissertation, University of Cape Town, Rondebosch.

Igwe, J.C. and Abia, A.A. 2007. Sorption isotherm studies of Cd(II), Pb(II) and Zn(II) ions bioremediation from aqueous solution using unmodified and EDTA-modified maize cob. *Ecl. Quím.,* 32(1), pp. 33 – 42.

Ismael, F.J. 2014. Surfacted mediated cadmium determination with dithizone in aqueous solution. MSc Thesis. Eastern Mediterranean University. Gazimağusa, North Cyprus.

Jeřábek, K., Hanková, L., Strikovsky, A.G. and Warshawsky, A. 1996. Solvent impregnated resins: relation between impregnation process and polymer support morphology I. Di-(2-ethylhexyl) dithiophosphoric acid. *Reactive & Functional Polymers,* 28, pp. 201 – 207.

Juang, R. and Chen, M. 1997. Application of the Elovich equation to the kinetics of metal sorption with solvent-impregnated resins. *Ind. Eng. Chem. Res*., 36, pp. 813 – 820.

Juang, R. and Su, J. 1992. Sorption of copper and zinc from aqueous sulfate solutions with bis(2-ethylhexyl) phosphoric acid impregnated macroporous resin. *Ind. Eng. Chem. Res.*, 31, pp. 2774 – 2779.

Kabay, N., Cortina, J.L., Trochimczuk, A. and Streat, M. 2010. Solvent-impregnated resins (SIRs) – methods of preparation and their applications. *Reactive & Functional Polymers,* 70, pp. 484 – 496.

Kabay, N., Gizli, N., Demircioğlu, M., Yuksel, M., Sağlam, M., Arda, M., Yuksel, U., Saha, B. and Streat, M. 2003. Removal of cadmium from phosphoric acid solution by solvent-impregnated resins (SIRs) – sorption kinetics and equilibria studies. *Chem. Eng. Comm.,* 190, pp. 936 – 947.

Kantipuly, C., Katragadda, S., Chow, A. and Gesser, H.D. 1990. Chelating polymers and related supports for separation and preconcentration of trace metals. *Talanta*. 37. pp. 491 – 497.

Koroleff, F. 1950. Determination of traces of heavy metals in seawater by means of dithizone; metal-dithizone equilibria. Unpublished article.

Kumar, K.V. 2006. Linear and non-linear regression analysis for the sorption kinetics of methylene blue onto activated carbon. *Journal of Hazardous Materials*. pp 1538 – 1544.

Lagergren, S. 1898. Zur theorie der sogennanten adsorption gelöster stoffe. *Kungliga Svenska Vetenskapakademiens*. Handlingar. 24(4). pp. 1 – 39.

Mahmoud, M.E., Osman, M.M. and Amer, M.E. 2000. Selective preconcentration and solid phase extraction of mercury(II) from natural water by silica gel-loaded dithizone phases. *Analytica Chimica Acta*, 415(1), pp. 33 – 40.

Mansour, R.A. and Elmenshawy, A.M. 2017. Removal of heavy metals from aqueous solutions by sorption onto modified cellulose: equilibrium, kinetics, and thermodynamics study. *International Water Technology Journal*, 7(2), pp. 116 – 132.

Maslov, O.D., Starodub, G.Y., Vostokin, G.K., Gustova, M.V., Dmitriev, S.N., Shvetsov, V.N., Szucs, Z., Jansen, D. and Zeevaart, J.R. 2011. Production of ^{117m}Sn with high specific activity by cyclotron. *Applied Radiation and Isotopes*, 69(7), pp. 965-968.

May, I. and Hoffman, J.I. 1948. A study of dithizone as a reagent for Indium. *Journal of the Washington Academy of Sciences*, 38(10), pp. 329 – 336.

Meena, P.L., Saxena, R. and Sharma, N., 2014. A rapid analytical method using flow injection preconcentration of zinc on dithizone impregnated on Amberlite XAD-2 and its determination in water samples by FAAS. *Int. J. Agric. Food Sci. Technol.*, 5, pp. 287 – 296.

Memon, S.Q., Bhanger, M.I., Hasany, S.M. and Khuhawar, M.Y., 2006. Sorption behavior of impregnated styrofoam for the removal of Cd (II) ions. *Colloids and Surfaces A: Physicochemical and Engineering Aspects*, 279(1), pp. 142 – 148.

Mendoza, R.N., Medina, T.I.S., Vera, A., Rodriguez, M.A. and Guibal, E. 2000. Study of the sorption of Cr(III) with XAD-2 resin impregnated with di-(2,4,4 trimethylpentyl) phosphinic acid (Cyanex 272). *Solvent Extraction and Ion-exchange*. 18(2). pp. 319 – 343.

Metwally, E. 2006. Kinetic studies for sorption of some metal ions from aqueous acid solutions onto TDA impregnated resin. *Journal of Radioanalytical and Nuclear Chemistry*, 270(3), pp. 559 – 566.

Mudasir, M., Karelius, K., Aprilita, N. H. and Wahyuni, E. T. 2016. Adsorption of mercury(II) on dithizone-immobilised natural zeolite. *Journal of Environmental Chemical Engineering*. 4. pp. 1839 – 1849.

Nakamura, T., Ikawa, T., Nishihama, S. and Yoshizuka, K. 2009. Selective recovery of indium from acid sulphate media with solvent impregnated resin of bis(4-cyclohexylcyclohexyl) phosphoric acid as an extractant. *Ion Exchange Letters*, 2, pp. 22 – 26.

Nayebi, P. and Moghimi, A. 2006. Selective preconcentration and solid phase extraction of mercury(II) from natural water by alumina-loaded dithizone phases. *Materials Science Research India*. 3(2a). pp. 179 – 186.

Nesterenko, P.N., Jones, P. and Paull, B. 2011. *High Performance Chelation Ion Chromatography*. Cambridge: RSC.

Nibou, D., Mekatel, H. Amokrane, S., Barkat, M. and Trari, M. 2010. Adsorption of Zn^{2+} ions onto NaA and NaX zeolites; kinetic, equilibrium and thermodynamic studies. *Journal of Hazardous Materials*. 173(1-3). pp. 637 – 646.

Omar, H. A. 2013. Adsorption of ^{60}Co on natural and dithizone-modified chitin. *Radiochemistry*. 55(1), pp. 101 – 107.

Paradkar, R.P. and Williams, R.R. 1994. Micellar colorimetric determination of dithizone metal chelates. *Anal. Chem.* 66(17). pp. 2752 – 2756.

Paul, V. and Jones, P. 1996. Chromatographia. 42(9-10). P. 528.

Persson, I. 2010. Hydrated metal ions in aqueous solution. How regular are their structures? *Pure Appl. Chem.*, 82(10), pp. 1901 – 1917.

Phetphaisit, C.W., Wapanyakul, W., Chaiyasith, W.C. and Sriprang, N. 2017. Selective sorption of indium ions on polyacrylamido-2-methyl propane sulphonic acid-grafted natural rubber. *Songklanakarin Journal of Science and Technology*. Unpublished article. DOI: SJST-2016-0441.R1.

Piccin, J.S., Dotto, G.L. and Pinto, A.A. 2011. Sorption isotherms and thermochemical data of FD&C Red n° 40 binding by chitosan. *Brazilian Journal of Chemical Engineering*, 28(2), pp. 295 – 304.

Qiu, H., Pan, B., Zhang, Q., Zhang, W. and Zhang, Q. 2009. Critical review in sorption kinetic models. *L Zheijang Univ Sci A*.,10(5), pp. 716 – 724.

Rajesh, N. and Manikandan, S. 2008. Spectrophotometric determination of Lead after preconcentration of its diphenylthiacarbazone complex on an Amberlite XAD-1180 column. *Spectrochimica Acta Part A: Molecular and Biomolecular Spectroscopy*, 70(4), pp. 754 – 757.

Rice, C.R., Faulkner, R.A., Jewsbury, R.A., Bullock, S. and Dunmore, R. 2017. A structural study of dithizone coordination chemistry. *CrystEngComm*. 19. 3414.

Rychlovský, P., Bílý, J. and Denková, P. 1993. The use of dithizone-polyurethane foam sorbent in a solid-liquid preconcentration step of the determination of lead in drinking and surface waters and in soils. *Chem. Papers*. 47(4). pp. 233 – 236.

Saha, B., Gill, R.J., Bailey, D.G., Kabay, N. and Arda, M. 2004. Sorption of Cr(VI) from aqueous solution by Amberlite XAD-7 resin impregnated with Aliquat 336. *Reactive & Functional Polymers*, 60, pp. 223 – 244.

Saha, B., Iglesias, M., Cumming, I.W. and Streat, M. 2000. Sorption of trace heavy metals by thiol containing chelating resins. *Solvent Extraction and Ion Exchange*, 18(1), New York. Marcel Dekker. pp. 133 – 167.

Saha, P. and Chowdury. n.d. Insight into adsorption thermodynamics. www.intechopen.com [accessed 14 June 2019].

Salih, B., Denizli, A., Kavakh, C., Say, R. and Pişkin, E. 1998. Sorption of heavy metal ions onto dithizone-anchored poly (EGDMA-HEMA) microbeads. *Talanta*, 46, pp. 1205 – 1213.

Saxena, R., Tiwari, S. and Sharma, N. 2015. Flow-injection solid phase extraction using Dowex Optipore L493 loaded with dithizone for preconcentration of Chromium species from industrial waters and determination by FAAS. *RSC Adv.*, 5, pp. 69196 – 69204.

Shabani, A.M.H., Dadfarnia, S., Nasirizadeh, N. and Shishehbore, M.R. 2007. Preconcentration of Copper with dithizone-naphthalene for subsequent determination by Atomic Absorption Spectrometry. *Journal of Analytical Chemistry*, 62(1), pp. 46 – 50.

Shah, R. and Devi, S. 1996. Preconcentration of Mercury (II) on dithizone anchored poly (vinylpyridine) support. *Reactive & Functional Polymers*, 31, pp. 1 – 9.

Shah, R. and Devi, S. 1997. Preconcentration and separation of Palladium(II) and Platinum(IV) on a dithizone anchored poly (vinylpyridine)-based chelating resin. *Analytica Chimica Acta.*, 341(2-3), pp. 217 – 224.

Shahida, S., Ali, A. and Khan, M.H. 2013. On-line spectrophotometric determination of scandium after preconcentration on XAD-4 resin impregnated with nalidixic acid. *J. Iran. Chem. Soc.*, 10, pp. 461 – 470.

Shaw, M.J., Cowan, J. and Jones, P. 2003. Fabrication of an aurin tricarboxylic acid immobilised chelating polymer for the ion chromatographic determination of trace metal ions in highly mineralized waters. *Analytical Letters.*, 36(2), New York: Marcel Dekker. pp. 423 – 439.

Shirzadi, H. and Nezamzadeh-Ejhieh, A. 2017. An efficient modified zeolite for simultaneous removal of Pb(II) and Hg(II) from aqueous solution. *Journal of Molecular Liquids*. 230, pp. 221 – 229.

Sigma-Aldrich Co. 1997. *Separate and purify pharmaceuticals and small biomolecules, using polymeric RPLC resins*. Bulletin 863C.

Skoog, D.A., West, D.M., Holler, F.J. and Crouch, S.R. 2004. *Fundamentals of Analytical Chemistry*. 8th Edition. Belmont: Brooks/Cole. pp. 914.

Stevenson, N.R. and Gonzales, G. 2016. Manufacturing and Nuclear Medicine Applications of the Novel Isotope Sn-117m. *Proceedings of the 2016 International Conference on Translational Research in Radiation Oncology and Physics for Health (ICTR-PHE)*, Geneva, Switzerland, 16th February 2016.

Strikovsky, A.G., Jeřábek, K., Cortina, J.L., Sastre, A.M. and Warshawsky, A. 1996. Solvent impregnated resin (SIR) containing dialkyl dithiophosphoric acid on Amberlite XAD-2: extraction of copper and comparison to the liquid-liquid extraction. *Reactive & Functional Polymers*, 28, pp. 149 – 158.

Tiwari, S., Ruhil, J. and Saxena, R. 2016. *A solid phase extraction method for determination of cadmium in industrial water samples using flame atomic absorption spectrometry*. International Journal of Engineering Technology Science and Research. 3(2). pp. 64 – 70.

Uchiumi A., Tokunaga S., Eyama T. and Shibayama H. 1993. Removal of heavy metals from industrial wastewaters: development of new chelating resins for arsenic(II), antimony(II) and copper(II) ions. *Int. Conf. Process, Mater. Prop.*, 1, pp. 101 – 104.

Von Eschwege, K.G., Conradie, J. and Kuhn, A. 2011. Dithizone and its oxidation products: A DFT, spectroscopic and X-ray structural study. *J. Phys. Chem.*, 115, pp. 14637 – 14646.

Warshawksy, A. 1971. South African Patent Application 71/5637.

Warshawsky, A., Marinsky, J.A. and Marcus, Y. (Eds.). 1981. *Ion Exchange and Solvent Extraction*. Volume 8. Marcel Dekker, NY. pp. 229.

Wewers, F. 2012. Transition metal complexes of bis(diphenylphosphino)methane, dithizone and dithiolenes: structural, spectroscopic, electrochemical and computational studies. PhD thesis, University of Cape Town, Rondebosch.

White, W.E. 1935. Dithizone as an analytical reagent. *Proceedings of the 1935 12th Ohio-Michigan Regional Meeting of the American Chemical Society*, Toledo, Ohio, 19th October 1935. pp. 369 – 373.

Wu, D., Wang, A. and Guo, L. 2006. Synthesis and application of Amberlite XAD-2 functionalized with dithizone for field preconcentration and separation of trace Cadmium in seawater. *Analytical Sciences: the International Journal of the Japan Society for Analytical Chemistry*, 22, pp. 1245 – 1248.

Yu, H.M., Song, H. and Chen, M.L. 2011. Dithizone immobilised silica gel on-line preconcentration of trace copper with detection by flame atomic absorption spectrometry. *Talanta*, 85(1), pp. 625 – 630.

Zarezade, V., Aliakbari, A. Es'haghi, M., Amini, M.M., Behbahani, M., Omidi, F. and Hesam, G. 2017. Application of a new nanoporous sorbent for extraction and preconcentration of lead and copper ions. *International Journal of Environmental Analytical Chemistry*, 97(4), pp. 383 – 397.

Zargar, B., Parham, H. and Shiralipour, R. 2017. Removal of Pb and Cd ions from contaminated water by dithizone-modified cellulose acetate nanosponges. *Journal of Materials and Environmental Sciences*, 8(3), pp. 1039 – 1045.

APPENDIX A: Picture of a customised syringe (column)

APPENDIX B-1: Calibration curve of Cu: λ = 224.700 nm

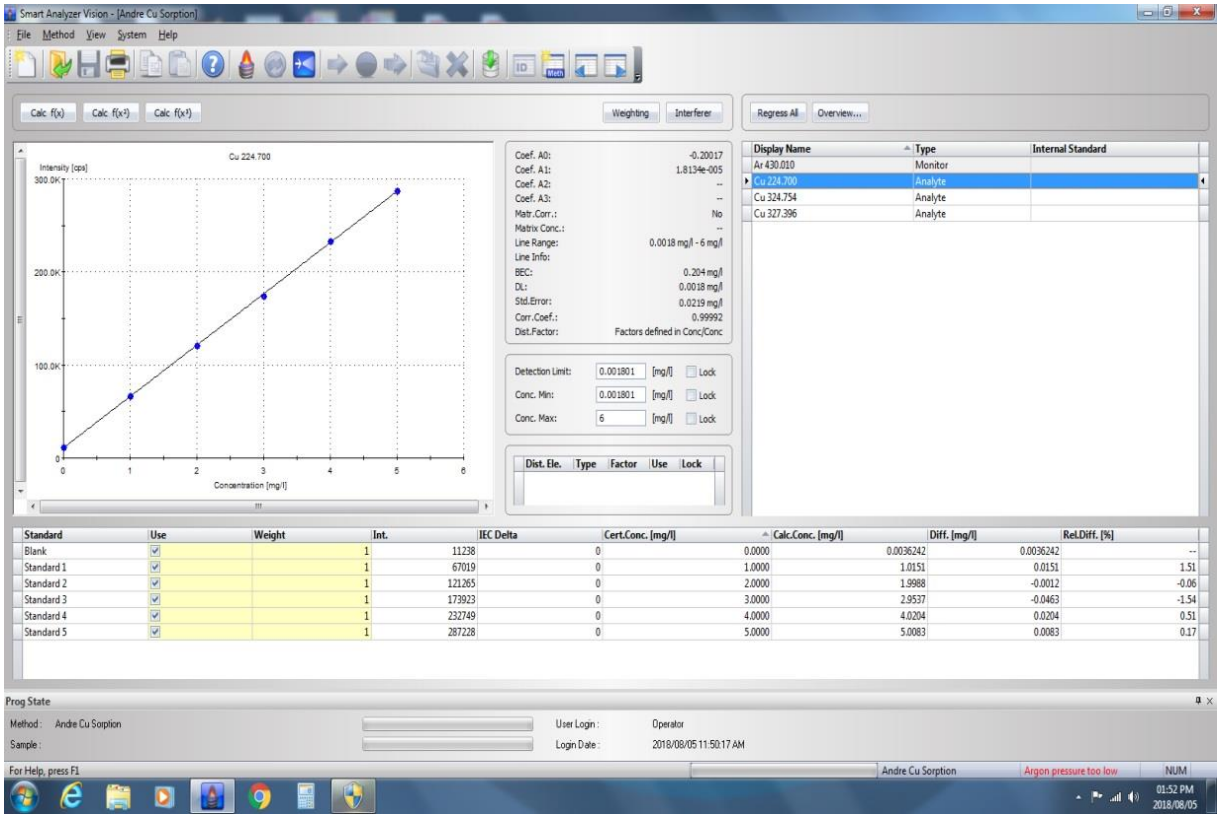

APPENDIX B-2: Calibration curve of Cu: λ = 324.754 nm

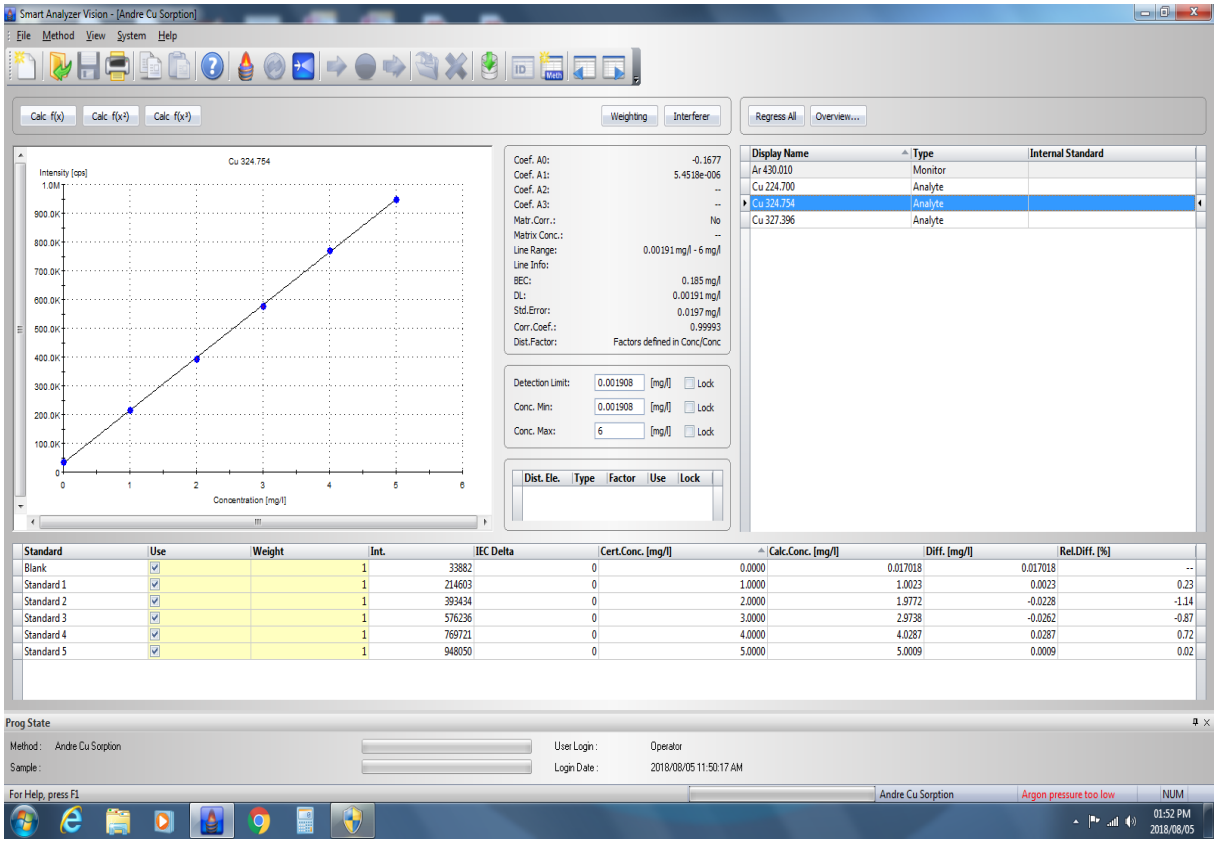

APPENDIX B-3: Calibration curve of Cu: λ = 327.396 nm

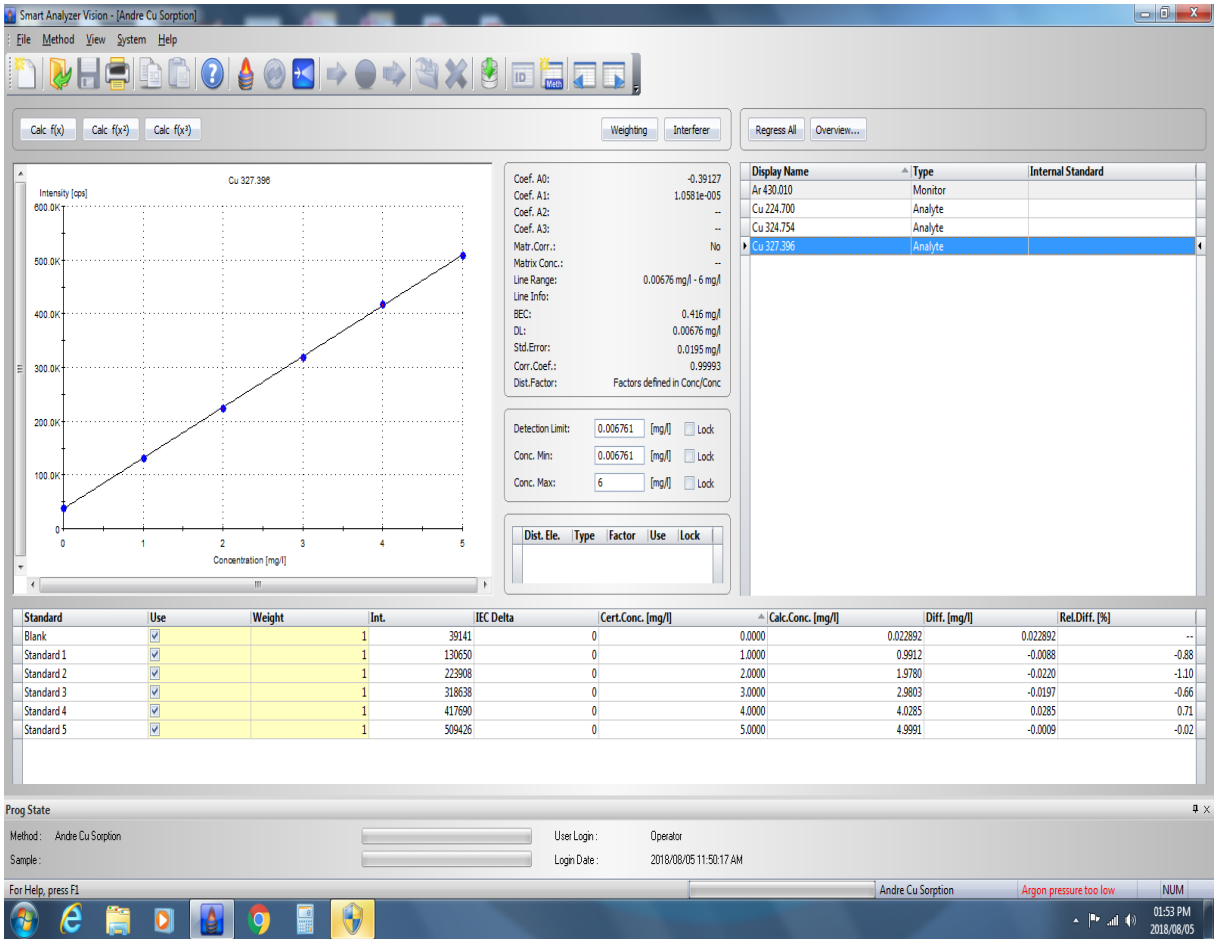

APPENDIX C: FTIR spectra of ACG300m-H_2Dz-In and ACG300m-H_2Dz

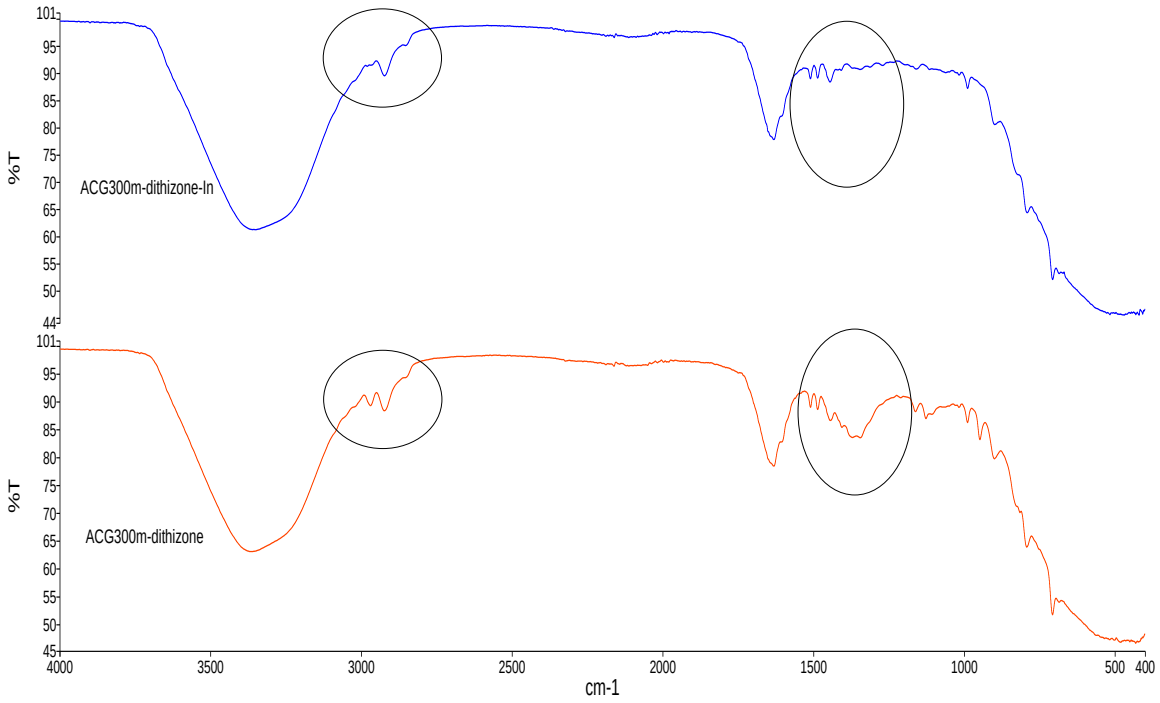

APPENDIX D: FTIR spectrum of ACG300m-H_2Dz-Mn

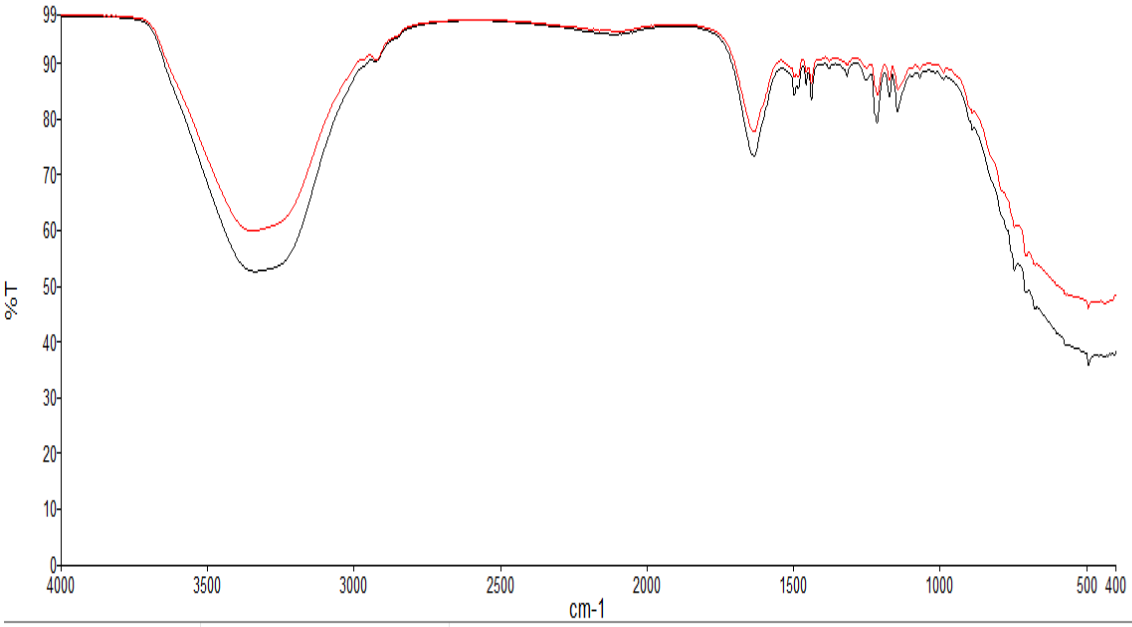

Name	Description
D only	Sample 002 By Administrator Date Thursda...
M & D	Sample 003 By Administrator Date Thursda...

APPENDIX E: Time dependence of Bi sorption; C_0 = 2.785 mg/L; pH = 3.85; column method

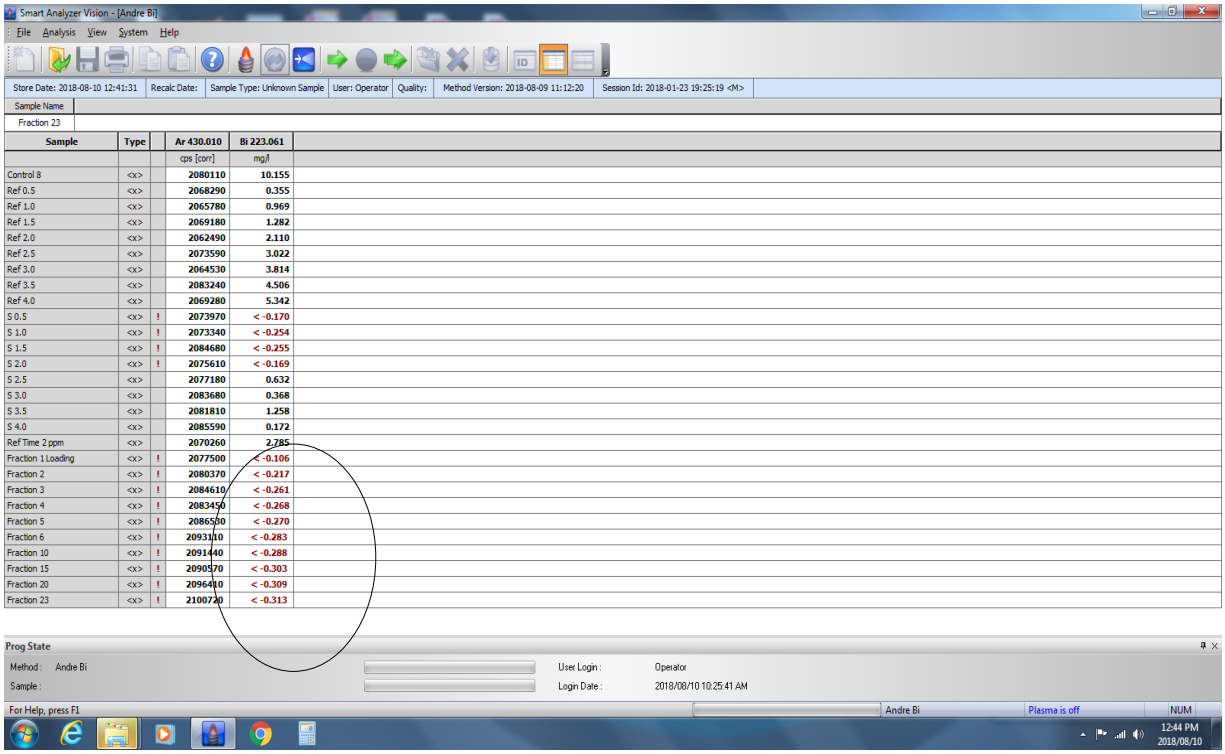

APPENDIX F: Time dependence of Bi sorption using a binary solution; $[Bi^{3+}]_0$ = 4.175 mg/L; $[Pb^{2+}]_0$ = 1.931 mg/L; pH = 1.60; column method

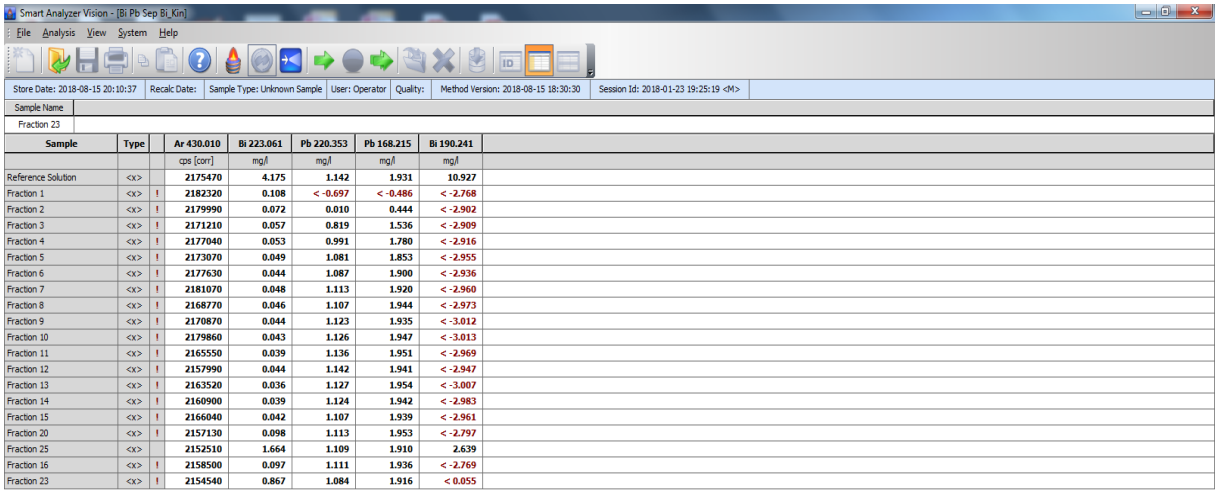

Sample	Type		Ar 430.010	Bi 223.061	Pb 220.353	Pb 168.215	Bi 190.241
			cps [corr]	mg/l	mg/l	mg/l	mg/l
Reference Solution	<x>		2175470	4.175	1.142	1.931	10.927
Fraction 1	<x>	!	2182320	0.108	< -0.697	< -0.486	< -2.768
Fraction 2	<x>	!	2179990	0.072	0.010	0.444	< -2.902
Fraction 3	<x>	!	2171210	0.057	0.819	1.536	< -2.909
Fraction 4	<x>	!	2177040	0.053	0.991	1.780	< -2.916
Fraction 5	<x>	!	2173070	0.049	1.081	1.853	< -2.955
Fraction 6	<x>	!	2177630	0.044	1.087	1.900	< -2.936
Fraction 7	<x>	!	2181070	0.048	1.113	1.920	< -2.960
Fraction 8	<x>	!	2168770	0.046	1.107	1.944	< -2.973
Fraction 9	<x>	!	2170870	0.044	1.123	1.935	< -3.012
Fraction 10	<x>	!	2179860	0.043	1.126	1.947	< -3.013
Fraction 11	<x>	!	2165550	0.039	1.136	1.951	< -2.969
Fraction 12	<x>	!	2157990	0.044	1.142	1.941	< -2.947
Fraction 13	<x>	!	2163520	0.036	1.127	1.954	< -3.007
Fraction 14	<x>	!	2160900	0.039	1.124	1.942	< -2.983
Fraction 15	<x>	!	2166040	0.042	1.107	1.939	< -2.961
Fraction 20	<x>	!	2157130	0.098	1.113	1.953	< -2.797
Fraction 25	<x>		2152510	1.664	1.109	1.910	2.639
Fraction 16	<x>	!	2158500	0.097	1.111	1.936	< -2.769
Fraction 23	<x>	!	2154540	0.867	1.084	1.916	< 0.055

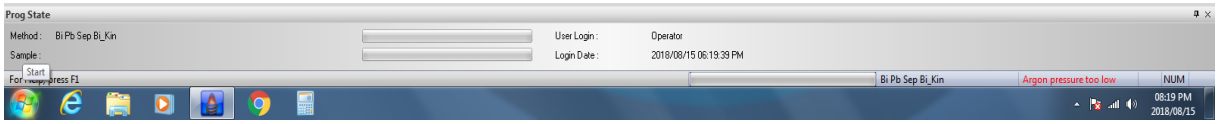

APPENDIX G: pH dependence of In sorption

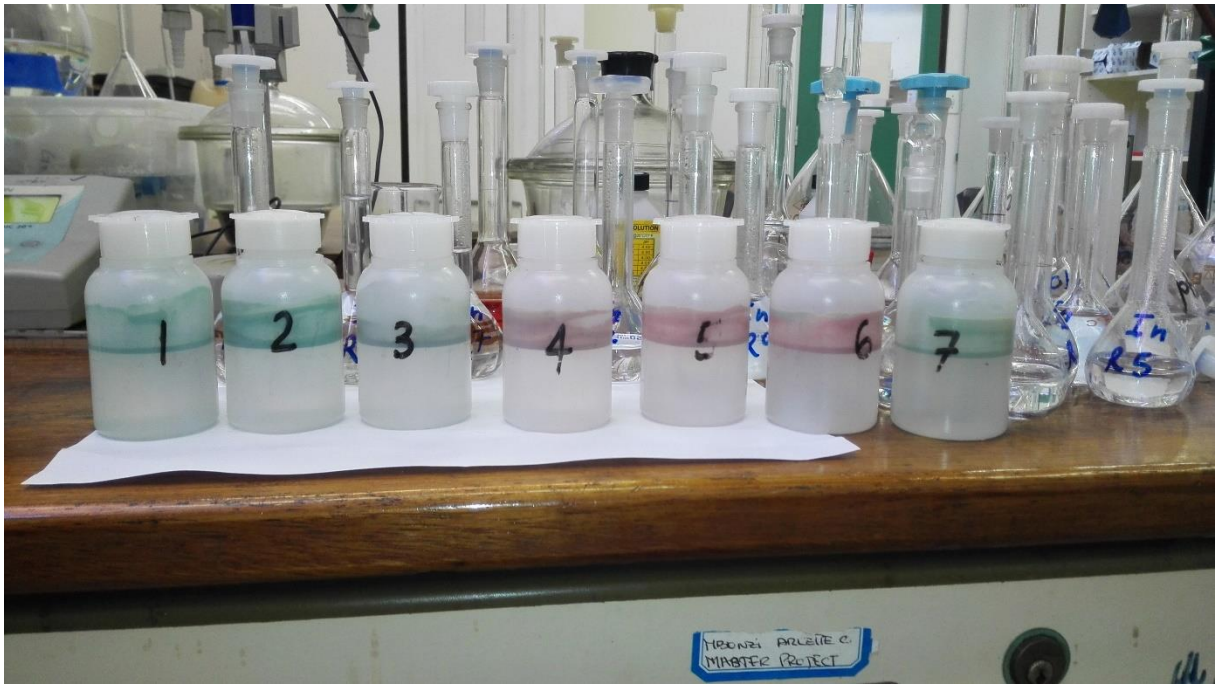

APPENDIX H: Amberchom CG-300m after impregnation